The Pennsylvania State University

The Graduate School

Eberly College of Science

OXYGEN ACTIVATION AND ELECTRON TRANSFER IN CLASS I RIBONUCLEOTIDE REDUCTASE

A Thesis in

Biochemistry, Microbiology, and Molecular Biology

by

Lana Saleh

Submitted in Partial Fulfillment

of the Requirements

for the Degree of

Doctor of Philosophy

August 2005

The thesis of Lana Saleh has been reviewed and approved by the following:

J. Martin Bollinger, Jr.
Associate Professor of Biochemistry, Molecular Biology, and Chemistry
Thesis Advisor
Chair of Committee

Squire J. Booker
Associate Professor of Biochemistry and Molecular Biology

John H. Golbeck
Professor of Biochemistry, Molecular Biology, and Chemistry

Carsten Krebs
Assistant Professor of Biochemistry and Molecular Biology

Sharon Hammes-Schiffer
Professor of Chemistry

Robert A. Schlegel
Professor and Head of the Department of Biochemistry and Molecular Biology

Abstract

Activation of oxygen at the carboxylate-bridged diiron cluster of ribonucleotide reductase (RNR) protein R2 from *Escherichia coli* leads to the formation of the catalytically essential tyrosyl radical by one-electron oxidation of tyrosine 122. The Y122 radical (Y122•) generates, by electron transfer over a remarkably long distance, a cysteinyl radical in its partner subunit, R1. The cysteinyl radical (C439•) initiates the catalytic reaction by removal of a hydrogen atom from the substrate. The long-distance R1-->R2 electron transfer step seems to be mediated by 5 amino acids in R2 and two others in R1, but the mechanism of this remarkable process is not well understood. The mechanism of Y122• formation involves transient oxidation of a near-surface residue tryptophan 48 (W48) by a kinetically masked diiron(II)-O_2 adduct. This step produces an intermediate state containing W48 cation radical ($W48^{+\bullet}$) and the formally Fe_2(III/IV) cluster **X**. The last step of the reaction is the slow oxidation of Y122 by **X** to produce the catalytically essential Y122•.

Oxygen activation by R2 is mechanistically similar to oxidation reactions catalyzed by other members of the diiron-carboxylate family of oxidases and oxygenases, most notably methane monooxygenase hydroxylase (MMOH) and stearoyl acyl carrier protein Δ-9 desaturase. R2 and MMOH share similar tertiary structures and contain almost indistinguishable diiron clusters. Despite these similarities, the outcomes of their reactions with O_2 are quite different: alkane hydroxylation in MMOH and formation of a stable tyrosyl radical by one-electron oxidation of Y122 in R2. Two intermediates, **P** and **Q**, have been detected in the MMOH reaction and are thought to have μ-[1, 2-peroxo]diiron(III) and *bis*-μ-[oxo]diiron(IV) structures, respectively. In the R2 reaction,

only **X** has been unequivocally demonstrated, because the one-electron-more-oxidized precursor to **X** undergoes rapid reduction by the indole sidechain of W48. Identification of the precursor to **X** has been a challenging yet crucial step in understanding the mechanism of oxygen activation by R2. This task has been adopted by several investigators in the field who proposed that the subtle differences in coordination that are observed in these two proteins are of secondary functional significance, and that both proteins direct reactions that begin with one or more common intermediate down divergent mechanistic pathways. In Chapter 3, we have achieved the long-sought goal of characterizing this species by application of chemical, kinetic, and spectroscopic methods, including protein mutagenesis combined with chemical rescue (Chapter 2), and stopped-flow absorption and rapid freeze-quench electron paramagnetic resonance (EPR) and Mössbauer spectroscopies. In this chapter, evidence that the "kinetically masked" intermediate in the reaction of R2 has a geometry and electronic structure distinct from those of intermediates **P** and **Q** of MMOH is presented. The results show that the state, trapped in the reaction of the variant R2-W48A/Y122F (with the wild-type ligand set), comprises at least two complexes that are in rapid equilibrium. Each is diamagnetic and exhibits a Mössbauer quadrupole doublet with parameters characteristic of high-spin Fe(III). Each is probably a peroxodiiron(III) structural isomer of the **P**-like μ-[1,2-peroxo]diiron(III) species, previously characterized in the reactions of D84E variants of R2 (the Asp to Glu substitution renders the ligand set of R2 identical to that of MMOH). At present it is postulated that the complexes detected in the chemical rescue experiments with R2-W48A/Y122F are two rapidly inter-converting successors to the μ-[1,2-

peroxo]diiron(III) complex that is extremely fleeting in R2 proteins with the wild-type ligand set but longer lived in D84E-containing variants.

The mechanism of rapid transfer of the electron to the "kinetically masked" intermediate resulting in the formation of **X** involves transient oxidation of the near-surface residue W48 to its cation radical ($W48^{+\bullet}$). $W48^{+\bullet}$ is readily reduced by facile one-electron reductants such as ascorbate, $Fe(II)_{aq}$, or thiols. A detailed examination of pathways for decay of the $W48^{+\bullet}$ in the absence of a reductant in the wild-type protein, R2-Y122F, R2-Y356F, and R2-Y122F/Y356F is presented in Chapter 4. This study uncovered what we believe is a previously unforeseen mechanism of gating of electron transfer to the diiron cluster during O_2 activation by R2 involving binding of a divalent metal cation between the flexible, carboxylate-rich C-terminus of the protein and the region that includes the electron-shuttling residue, W48. This discovery emerged from noting that $W48^{+\bullet}$ decays via three simultaneous pathways in the absence of a reductant. One pathway for $W48^{+\bullet}$ decay involves reduction by Y356, the catalytically essential tyrosine in the flexible C-terminus. Mediation of $W48^{+\bullet}$ reduction by Y356 was shown to be dependent on the presence of salt and most efficient in the presence of divalent cations such as Mg^{2+}. This result lead to the hypothesis that Y356, which is located at the surface of the R2 subunit on the flexible C-terminus, becomes more ordered and at closer proximity with the W48 residue at higher salt concentrations, allowing for facile electron transfer between it and W48. The concentration of divalent metal ion required to exert this effect is sufficiently low that we suspect that this phenomenon may be important in the physiological function of the protein. Chapter 5 investigates potential Mg^{2+} ligands on the C-terminus and the surface of R2 (close to W48) that could drive this

conformational effect that places Y356 into proximity to and electronic communication with the $W48^{+\bullet}$. It is likely that the divalent metal ion requirement reflects its role in redox mediation not only in steps during O_2 activation by R2 but also at the R1-R2 interface during RNR catalysis.

In the last chapter (**6**), we transition from examining O_2 activation in the isolated R2 subunit from *E. coli* to examining the reaction in the recently identified class Ic R2 proteins, specifically R2 from *Chlamydia trachomatis* ($R2_{Ct}$). Class Ic R2 proteins (found mostly in pathogenic eubacteria) lack the conserved tyrosine that forms the radical in class Ia and Ib R2s. A recent study proposed a novel radical-generation strategy in these RNRs, in which the cluster **X**-like complex in *C. trachomatis* R2 ($\mathbf{X_{Ct}}$) generates the cysteine radical in R1, by-passing the intermediate Y• radical that serves this function in class Ia and Ib RNRs. In other words, the study suggested that O_2 activation at the diiron(II) center in $R2_{Ct}$ is coupled directly to production of the catalytically essential radical in R1. A primary objective in our study of these novel RNRs is to test the hypothesis that O_2 activation in $R2_{Ct}$ directly generates the Cys radical in R1, and ultimately to understand the mechanism of this step and how it fits into the overall catalytic cycle. To do so, we set out to dissect the mechanism of the $R2_{Ct}$ reaction by kinetic (stopped-flow and freeze-quench) and spectroscopic (optical absorption, EPR, and Mössbauer) methods. Our studies elucidated an *alternative* electron-injection pathway in which a tyrosine residue, and *not* W51 (the cogante residue of W48), acts as an electron shuttle to the diiron center of $R2_{ct}$, resulting in the formation of a transient Y• detected by stopped-flow spectroscopy and EPR spectroscopy. It was first assumed that this role might be adopted by Y338 (the cogante residue of Y356) and that the transient Y• formed

might, directly or through an electron transfer pathway constituted of tyrosine residues in R1, oxidize the catalytic cysteine in R1. Although Y338 was shown (by mutagenesis) not to play this role, it was revealed that it communicates with the tyrosine of interest in a fashion similar to that observed to occur between W48 and Y356 in *E. coli* R2 in the presence of Mg^{2+}. On the basis of these results and other observations discussed in Chapter 6, we posit that electron transfer to the diiron center of $R2_{Ct}$ does not occur to Fe1, as is the reactions of *E. coli* and mouse R2s, but is mediated by a chain of hydrogen-bonded residues comprising Y112, a water molecule, a second sphere aspartate, E119, (E119 is only E in the class Ic proteins and is conserved therein), and the H123 ligand to Fe2. In other words, we propose a remodeling by evolution to employ an **Fe2-side specific electron transfer pathway**, a remarkable diversion from the mechanism for and pathway of electron transfer employed by the class Ia R2 proteins.

TABLE OF CONTENTS

List of Figures

List of Tables

List of Schemes

ACKNOWLEDGEMENTS

First and by far the most I would like to extend my sincerest thanks to my good friend and advisor Marty Bollinger for his guidance and support throughout my graduate career. I will forever be indebted to his wisdom and deep insight, which helped me in times of hardships and difficulties. He believed in me and encouraged me every step of the way and I am proud to say that he was not only my mentor in science but also in life. From him I learned to be critical, analytical, kind, loving, and understanding. I will always value our "intense" discussions in science, politics, religion, and relationships. I am also very grateful for the rich scientific environment and opportunities that he made sure are available to all members of his group including "state of the art" instruments, extensive scientific collaborations, and international conferences. He allowed us to think freely and treated us like colleagues and not like employees. His teachings are engraved in my mind and my heart forever.

I would like to thank the members of my comprehensive and thesis committees, Prof. Carsten Krebs, Prof. Squire J. Booker, Prof. John H. Golbeck, Prof Craig E. Cameron, Prof. Sharon Hammes-Schiffer, and Prof. Timothy E. Glass, for their time and efforts. I am also thankful for the people who contributed to the work presented in this thesis. I thank Brian A. Kelch, Betsy A. Pathickal, Jeffrey Baldwin, and Brenda A. Ley for laying the foundation for the chemical rescue work presented in Chapters 2 and 3. I also thank Young An, Gang Xing, Corinne Floyd, Alexis Herman, and Brandon Chicalese for their contribution in the cloning and purification of several of the carboxylate variants discussed in Chapter 5. I thank Danny Yun for cloning *Chlamydia trachomatis* R2-Y338F (discussed in Chapter 6) and for his scientific insight that helped

me solve many of the experimental problems that I faced along the way. I thank Wei Jiang for working side by side on the *Chlamydia trachomatis* R2 project. I thank Lee Hoffart for his involvement in the discussions of the Mössbauer spectra presented in Chapter 6. I thank Prof. Vincent Huynh for analyzing the Mössbauer spectra presented in Chapters 2 and 3. Last but not least, I thank Carsten Krebs for the analysis and preparation of the Mössbauer spectra presented in Chapter 6, for his contribution in the analysis of the Mössbauer spectra presented in Chapter 3, and for the time he spent explaining Mössbauer spectroscopy to me.

My work in the Bollinger group resulted in eleven publications, which were the synergistic products of many minds. For this reason, I would like to thank our collaborators who allowed us to tackle the R2 project from many angles. Mössbauer spectroscopic studies were carried by Prof. Vincent Huynh, Prof. Carsten Krebs, and Dr. Sunail Naik at the Department of Physics in Emory University. CD/MCD spectroscopic studies were carried by Prof. Edward I. Solomon, Dr. Natasa Mitic, Pin Pin Wei, Andrew Skulan, and co-workers at the Chemistry Department in Stanford University. X-ray crystallographic studies were carried by Prof. Amy C. Rosenzweig, Walter C. Voegtli, and Dr. Monica Sommerhalter at the Chemistry Department in Northwestern University. EXAFS spectroscopic studies were carried by Prof. Pamela Riggs-Gelasco and co-workers at the Department of Chemistry and Biochemistry in the College of Charleston. Resonance Raman spectroscopic studies were carried by Prof. Pierre Moënne-Loccoz and co-workers at the Department of Environmental and Biomolecular Systems in Oregon Health and Science University.

I feel a deep sense of gratitude for all the people who made my experience at Penn State extremely enjoyable. My lab-mates were my family away from home: Danny, Bhramara, Gang, Elham, J. C., Eric, Gretchen, Irene, Jeff, Wei, Yinghui, Brenda, Young, Corinne, Alexis, Brandon, Anthony, Chris, Alex, and Kristen. I would especially like to thank Dan for being "the technical consultant" of the group and for maintaining all the instruments and the computers in the lab; Jeff for holding my hand during the first months in the lab; Irene for taking care of ordering; Wei for working very hard on the *Chlamydia trachomatis* R2 project; Young for teaching me tennis; Corinne for accompanying me on my shopping trips; and all the others for making my experience culturally rich. I want to also thank the people who made my stay here more fun. I will always remember the shopping trips with Victoria, the "get-togethers" with Rob, Carsten, Eva, Squire, Dave, and Cindy. I will also remember Carsten's German chocolate and his famous Pina Colada

Most importantly, I want to thank the person who was always there for me in the good times and the bad times. Danny was my shoulder to cry on and the person to share my laughs with. He knew me for who I am and loved me in spite of all my faults, my bad temper, and moody behavior. For this I will forever love him.

Ofcourse, I will not forget the people who made me who I am, my Mom and Dad. I am forever grateful for their love and support. I will always value the sacrifices they made so that I will attain my goals. I am also very thankful to God who gave me the best sisters ever, Lucine, Maysaa, and Nadine, who always listened to my complaints and shared my happy moments. I love you very much.

Dedication

To my mother and father,
Nazmieh and Youssef
for their infinite love and never-ending sacrifices

To my sisters,
Lucine, Maysaa, and Nadine
for ALWAYS being there for me

This thesis is also dedicated in memoriam to my beloved grandmother,
Aaisha

Chapter 1

Introduction

I. Ribonucleotide Reductase

Ribonucleotide reductases (RNRs) catalyze all *de novo* synthesis of deoxyribonucleotides by reducing the corresponding ribonucleotides. They thus provide the building blocks for DNA biosynthesis, which is indispensable for the survival of all organisms (*1-4*). These enzymes utilize a free radical-based mechanism to effect the chemically very challenging replacement of the ribose 2'-OH in the substrate by hydrogen. The first step of the reaction includes the production of a radical by the use of a metallo-cofactor (*1*). This radical is subsequently used by the "reductase" part of the protein to oxidize the substrate to a radical form using an active site transient thiyl radical (S•) (*5*). Interestingly, the metallo-cofactor seems to vary between different organisms, whereas the reductase remains similar. Therefore, RNRs were divided into three classes (I-III) based on the nature of their metallo-cofactors (Table 1-1) (*1, 6, 7*).

A. Three Classes of Ribonucleotide Reductases

Class I RNR is a dimer of dimers ($\alpha_2\beta_2$). It utilizes a dinuclear-iron(III) cluster and a tyrosyl radical (Y•) as its metallo-cofactor. It was discovered by Reichard and co-workers in the early 1950s (*8, 9*) and is present in all eukaryotes, many prokaryotes, and several viruses. Several *Enterobacteracae* contain two sub-classes of class I RNRs that differ in their reductant sources and the conditions under which they are expressed, while exhibiting similar allosteric regulation. Consequently, this class has been subdivided into classes Ia (*nrdAB* genes) and Ib (*nrdEF* genes) (*10-15*). Recently, a third subclass, Ic (*nrdAB* genes), has been identified by Nordlund and co-workers (*16*). The R2 subunits of class Ic RNRs possess the diferric cluster but lack the essential radical-forming tyrosine of classes Ia and Ib (the corresponding residue is a phenylalanine). The few organisms

Table 1-1: Classes of ribonucleotides reductases. Adapted from references 6 and 16.

	Class Ia	Class Ib	Class Ic	Class II	Class III
Prototype	*E. coli*	*L. typhimurium*	*C. trachomatis*	*L. leishmanii*	*E. coli*
Oxygen Dependence	Aerobic	Aerobic	Aerobic	Aerobic /Anaerobic	Anaerobic
Metal Center	Fe-O-Fe	Fe-O-Fe	Fe-O-Fe	Co	4Fe-4S
Radical	Cys...Tyr	Cys...Tyr	Cys?...?	Cys... AdoCbl	Cys...Gly
Genes	nrdAB	nrdEF	nrdAB	nrdJ	nrdDG
Structure	$\alpha_2\beta_2$	$\alpha_2\beta_2$	$\alpha_2\beta_2$	α or α_2	$\alpha_2\beta_2$

known to possess class Ic RNRs are intracellular pathogenic bacteria or thermophilic archaea (*16*).

In classes Ia and Ib, the larger homodimer, R1 (α_2; 171 kDa for the *E. coli* protein), contributes binding sites for the substrates and allosteric effectors and multiple cysteine residues that cooperate in substrate reduction (*17*). Each monomer of the R2 subunit (β_2; 87 kDa for the *E. coli* protein) contains one copy of the enzyme's catalytically essential cofactor, an oxo- and carboxylate-bridged diiron(III) cluster and an adjacent Y• (*18*). The radical is produced by one-electron oxidation of the conserved tyrosine residue (Y122 in *E. coli* R2) (*19*). The R2 cofactor functions by generating (via electron transfer that may be coupled to proton transfer) a reactive S• in the R1 subunit (*17, 18, 20*) (from Cys439 in *E. coli* R1), which initiates reduction of the substrate by homolytic scission of the 3' C-H bond (*21*). In this way, the Y• of R2 stores a latent oxidizing equivalent for use in catalysis by R1, and is therefore essential for nucleotide reduction.

Class II RNR, discovered by Blakley (*22*), Beck (*23*), and co-workers, is found in both aerobic and anaerobic bacteria. It is encoded by one gene (*nrdJ*) and is either monomeric (α) or dimeric (α_2) in structure (*24-26*). Radical generation in a class II RNR is effected by the cobalt(III) metallo-cofactor, 5'-deoxy-adenosylcobalamin (AdoCbl). Unlike the other classes, the S• in a class II RNR is generated from the deoxy-adenosyl radical and not from an amino acid radical (e.g. Y• in class I and glycyl radical in class III (discussed below)) (*27*).

Class III RNR was first reported by Barlow and co-workers (*28*). It is present in certain strictly and facultatively anaerobic bacteria and some bacteriophages. This class

is encoded by the *nrdDG* genes. It is homodimeric (α_2) with a stable glycyl radical (G•) . A second protein (β_2), also known as activase, employs an 4Fe-4S cluster and S-adenosyl methionine (SAM) to generate the G• in the α_2 subunit (*29*), which in turn is suggested to abstract a hydrogen atom from a neighboring cysteine residue to form the thiyl radical initiator of NTP reduction (*30*).

B. The Catalytic Mechanism of Ribonucleotide Reductase

In all classes of RNR, the function of the different cofactors is to initiate the radical-dependent nucleotide reduction process, which is mechanistically quite similar for all the enzymes thus far examined. Scheme 1-1 summarizes the working hypothesis for the mechanism of this reaction (*31*). The first step of this mechanism is the generation of a transient S•. The S• abstracts a hydrogen atom from the 3' position of the nucleotide substrate to form a 3'-nucleotide radical **(1)**. Protonation of the 2'-hydroxyl group results in the subsequent elimination of this group as a water molecule, thus resulting in the generation of the 3'-keto-2'-deoxynucleotide radical **(2)**. In the class I and II RNRs, reduction of **(2)** via a pair of cysteines occurs in two proton-coupled electron transfer steps. The first step, which includes action by the sulfur pair and a glutamate residue, generates a disulfide-radical-anion intermediate and a 3'-keto-2'-deoxynucleotide **(3)**. The second step is believed to generate a 3'-deoxynucleotide radical **(4)** and the disulfide. In the last step of the reaction, **(4)** re-abstracts the originally removed hydrogen atom from the cysteine, providing the product and regenerating the S•. In the class III RNRs, reduction of **(2)** is effected by formate. Once again, two electron-transfer steps are proposed to generate **(4)** and carbon dioxide prior to the re-generation of the cysteine radical. This working hypothesis has been supported by results from studies with normal

Scheme 1-1: A proposed mechanism for all three classes of ribonucleotide reductases.

Adapted from reference 31.

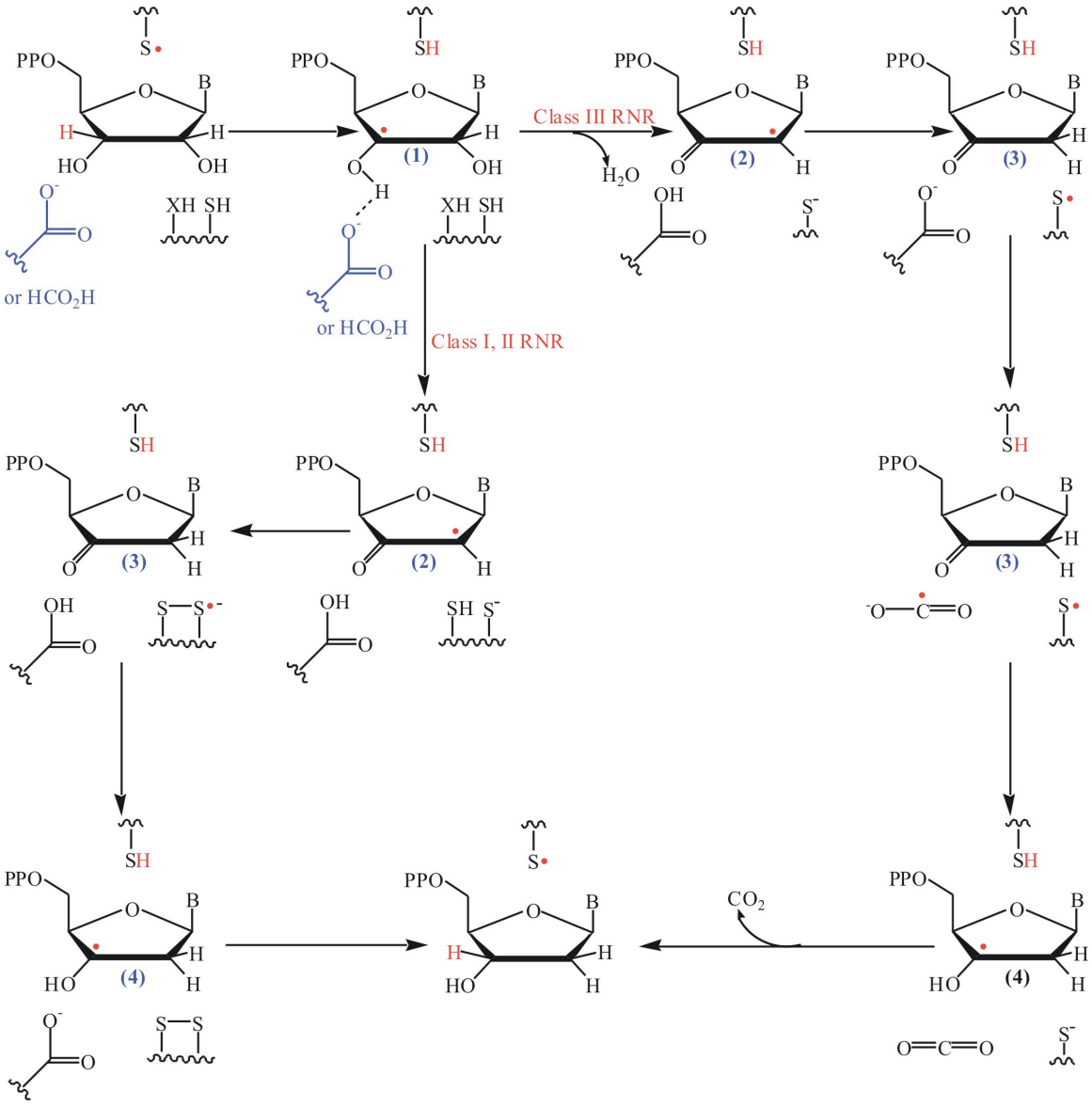

substrates, a variety of mechanism-based inhibitors, site-directed variant proteins, and crystallographic studies conducted primarily on class I and II, and to a lesser extent class III, RNRs (*31, 32*).

C. Radical Initiation in the Class I Ribonucleotide Reductase

Understanding of the catalytic reaction carried out by the R1 and R2 subunits of the class Ia and Ib RNRs is fairly advanced as a result of extensive studies on the RNRs from *E. coli* and mouse. However, one very important question remains unanswered: how does the cofactor (diferric-Y•) in the R2 subunit initiate the formation of a transient S• in the R1 subunit? The C-terminus of R2 is believed to provide the driving force for the binding of R1 and R2 (*33*). Removal of the C-terminus prohibits R1-R2 interactions in various class I RNRs. Also, peptides corresponding to the terminal 20-30 amino acid residues of R2 inhibit class I RNRs due to their ability to compete for binding of R1 (*33-36*). In RNR from *E. coli*, the active form is thought to be in a 1:1 complex between R1 and R2 (*1*). The 35 residues of the C-terminus are thermally labile and are not detected by X-ray crystallography (*37*). Also, the crystallization of R1 was successful only in the presence of a peptide corresponding to the last 20 amino acid residues of the R2 C-terminus (*1*). Based on the above information, the interfacial complementarities between the R1 and R2 structures, and the absolute conservation of amino acids residues from 40 sequences of RNRs, Eklund and Uhlin proposed a docking model for *E. coli* RNR in which the catalytic cysteine (C439) in R1 and the cofactor tyrosine (Y122) in R2 are separated by a distance of ~ 35 Å (*1*). According to the Marcus-Levich equation for electron transfer (ET) between two cofactors at fixed distance and orientation, ET between C439 and Y122 at the distance of 35 Å (assuming an exponential decrease for

the rate constant of ET with distance and a β value (the tunneling barrier) of 1.1-1.4 $Å^{-1}$) would result in a turnover number for nucleotide reduction much less than that observed for the enzyme (10 s^{-1}) (*38*). As a result, a multi-step tunneling or radical-hopping mechanism, in which hydrogen-bonded amino acid residues in R1 and R2 form radical intermediates, has been proposed. The amino acids that constitute this proposed ET pathway (Figure 1-1) are strictly conserved in all class I RNRs and are essential for the catalytic activity of the enzyme, as shown by site-directed mutagenesis studies (*39-42*).

If it assumed that the redox potentials and pKa values of the residues (Ys, W, C) in the above pathway are not perturbed, then tyrosyl radical should be unable to oxidize the cysteine (redox potentials at pH 7.0 of 0.77 and 1.33 V vs NHE (*38*), respectively). However, the redox potentials of these residues can be modulated by their protonation state (*43*). Therefore, it is likely that electron transfer between the cysteine and tyrosine residues involves coupling with proton transfer(s) (proton-coupled electron transfer (PCET)) or, alternatively, direct hydrogen atom transfers (*38-42, 44*).

To date, no direct evidence has been presented for the formation of these radical intermediates. Additionally, attempts to determine the redox potentials of the ET pathway residues have not been fruitful. A recent approach adopted by the Stubbe and Nocera groups has involved the replacement of the tyrosine residues of the pathway (Y356 in R2, Y731 and Y730 in R1) with unnatural amino acids by intein-mediated ligation technology and solid phase peptide synthesis. The goal of the approach is to perturb the pKa values and redox potentials in an attempt to examine the validity of the PCET model. Their published work showed successful substitution of Y356, which resides on the C-terminus of R2, with analogues such as 2,3-difluorotyrosine, 3-

Figure 1-1: Proposed electron transfer pathway in class I RNR from *E. coli* ((Tyr122-Asp84-His118-Asp237-Trp48-Tyr356) in R2 and (Tyr731-Tyr730-Cys439) in R1) based on the enzyme-docking model (reference 17). The last 35 amino acids of the C-terminal tail of R2, in which Y356 resides, are thermally labile and undetectable in available crystal structures. Thus, the distance between W48 on R2 and Y731 in R1 (25Å) is based solely on the docking model of a 1:1 complex of R1 and R2. The Protein Data Bank accession numbers of the crystal structures used in this model are 4R1R for R1 and 1MXR for R2. Adapted from reference 38.

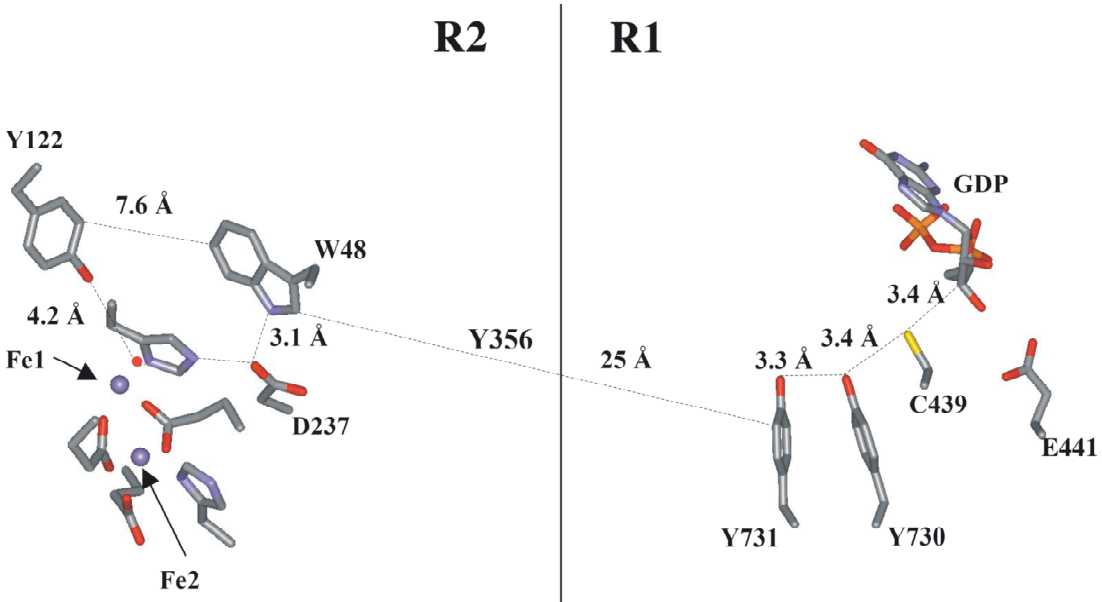
R2
R1
Y122
7.6 Å
W48
4.2 Å
3.1 Å
Fe1
D237
Fe2
Y356
25 Å
GDP
3.4 Å
3.4 Å
3.3 Å
C439
E441
Y731
Y730

nitrotyrosine, and p-aminophenylalanine (*45-48*). The results of their studies led them to propose that the pKa of Y356 is not greatly perturbed in the R1:R2 complex compared to that in solution and that the rate of radical transfer through Y356 is controlled mainly by the redox potential of this residue and not by hydrogen bonding or proton transfer. The availability of a wide range of tyrosine derivatives with altered redox potentials and p*K*as makes this approach promising with respect to testing of the PCET model.

In Chapter 4, we show that the presence of divalent-metal ions (such as Mg^{2+}) at concentrations similar to that used in RNR assays (15 mM) brings Y356 into electronic communication with the W48 cation radical ($W48^{+\bullet}$), establishing an equilibrium between W48 and Y356 radicals. Both W48 and Y356 are among the residues in the proposed R1-R2 electron transfer pathway. We suspect that the effect of Mg^{2+} is attributable to its binding to the carboxylate-rich, flexible C-terminus and inducing it to become ordered, with Y356 in close proximity to W48. Chapter 5 presents carboxylate-residues that might serve as Mg^{2+} ligands on the C-terminus and perhaps near W48 that could drive this conformational effect. It is possible that this mechanism is important in mediating electron transfer between the R1 and R2 subunits in the catalytic reaction and that the requirement of RNR for divalent metal ions reflects, at least in part, the role of the cation in redox mediation at the R1-R2 interface.

II. The Carboxylate-Bridged Diiron Protein Family

The R2 subunit of class I RNR belongs to a class of proteins that use carboxylate-bridged diiron(II) clusters to reductively activate molecular oxygen for difficult oxidation reactions (Table 1-2) (*49-51*). Other members of this class include plant fatty acyl desaturases, such as stearoyl acyl carrier protein (ACP) Δ-9 desaturase (*52-54*), and

Table 1-2: Carboxylate-bridged diiron proteins. Adapted from reference 51.

Protein	Function	Method of Characterization
Hemerythrin	Dioxygen carrier	X-ray
R2 subunit of ribonucleotide reductase	Tyrosyl radical generator	X-ray
Hydroxylase component of methane monooxygenase	Methane to methanol oxidation	X-ray
Purple acid phosphatase	Phosphate ester hydrolysis	X-ray
Ferritin	Iron storage	X-ray
Rubrerythrin	Putative peroxidase	X-ray
Δ9-desaturase	Alkane conversion to alkene	X-ray
Toluene monooxygenases	Toluene to cresol oxidation	Spectroscopy
Phenol hydroxylase	Phenol to catechol oxidation	Spectroscopy
Alkene monooxygenase	Alkene epoxidation	Spectroscopy
Butane monooxygenase	Butane oxidation to butanol	Sequence analysis
ω-alkane hydroxylase	Alkane oxidation to alcohol	Sequence analysis
DMQ monooxygenase	Quinone generation	Sequence analysis

bacterial hydrocarbon hydroxylases, such as the hydroxylase component of soluble methane monooxygenase (MMOH) (*55-58*). In the following sections, we will briefly review different structural and functional aspects of the enzymes stearoyl ACP Δ-9 desaturase and soluble methane monooxygenase (sMMO). We will then focus on the current state of knowledge of the R2 protein from *E. coli* (structure and function) and the aspects it shares with other members of the diiron-carboxylate protein family, specifically MMOH.

A. Stearoyl-ACP Δ9-Desaturase

The best-characterized stearoyl ACP desaturase is the recombinant stearoyl-ACP Δ9-desaturase from castor-oil plant *Ricinus communis* (Δ9-desaturase). This enzyme catalyzes the insertion of a cis-double bond between carbons C9 and C10 of stearoyl-ACP to generate oleoyl-ACP, a key intermediate in the biosynthesis of unsaturated cellular lipids. This reaction requires O_2, NAD(P)H, NAD(P)H ferredoxin oxidoreductase, and ferredoxin (*50, 59*). Δ9-desaturase is a homodimer of ~ 42 kDa subunits, with each subunit having one binuclear iron site. The diiron center is located at the center of a four-helix bundle and is coordinated by ligands from duplicated E-X-X-H motifs, as revealed by X-ray crystallography (*50, 59*). The diiron-cluster binding motif (E-X-X-H) of the desaturase is similar to that in other diiron proteins such as R2 and MMOH (*52, 53, 60*).

The diferric form of Δ9-desaturase has been characterized by various spectroscopic methods to reveal the presence of a μ-oxo bridge with an Fe-O-Fe unit angle corresponding to a (μ-oxo)bis(μ-carboxylato)diiron-(III) center (*53, 60*). The (μ-oxo) ligand is exchangeable with solvent and is lost upon reduction, as revealed by the

crystal structure of the diferrous form of Δ9-desaturase (*54*). The active-site structure shows two Fe(II) ions bound in a highly symmetric environment ((carboxylate)$_4$(histidine)$_2$-diiron(II)), reminiscent of the dinuclear cores in MMOH and R2 (discussed below), and a water molecule loosely coordinated to the iron centers at distances of 3.0 and 3.3 Å, from the Fe1 and Fe2 ions, respectively. The crystal structure also shows a narrow, bent, hydrophobic cavity, expected to bind the saturated fatty-acid substrate, extending from the surface down into the protein for ~ 20 Å. The catalytic mechanism of soluble desaturases remains to be fully elucidated. Reaction of the diferrous form of Δ9-desaturase, produced artificially by chemical reduction of the diferric form, with O_2 results in the accumulation of a peroxodiiron(III) intermediate similar to intermediate **P** of MMOH (discussed below). The decay of this species is too slow to be on the pathway to substrate desaturation. In fact, this intermediate is not observed in the enzymatically-reduced protein.

B. Methane Monooxygenase Hydroxylase

Methane monooxygenases are multi-component enzyme systems that catalyze the oxidation of methane to methanol. They are expressed in methanotrophic bacteria, which use methane as their only source of energy and carbon. sMMOs isolated from *Methylococcus capsulatus* (Bath) and *Methylosinus trichosporium* OB3b have been extensively investigated (*61*). These enzymes are composed of four components, a 251-kDa hydroxylase MMOH ($\alpha_2\beta_2\gamma_2$), a 15.9 kDa coupling protein MMOB, a 38.7 kDa reductase MMOR, and a 12 kDa protein MMOD, of as yet unidentified function (*62*). Substrate hydroxylation occurs at a carboxylate-bridged diiron center residing in the α subunit of MMOH. Activation of MMOH requires reduction of the active-site diiron(III)

center to the diferrous form. This is accomplished *in vivo* by MMOR, which acquires electrons from NADH and then transfers them to MMOH. MMOB is believed to regulate electron transfer from the reductase to the hydroxylase (*62*).

The diiron cluster of MMOH (each α subunit contains one diiron site) is situated at the center of a four-helix bundle, and coordinated by a single histidine per Fe, several protein-derived carboxylate ligands, and a terminal-water ligand (two EXXH segments) (Figure 1-2C). The ferrous ions in the reduced form of MMOH ($MMOH_{red}$) are five-coordinate (Figure 1-2D). Upon oxidation, the dinuclear center undergoes substantial rearrangements: E243 undergoes a carboxylate shift from a monodentate-bridging position to a terminal-monodentate position, a hydroxide bridge is formed, and a terminal hydroxide/water ligand becomes a bridging ligand. As a result of these structural changes, each iron ion in the oxidized form of MMOH ($MMOH_{ox}$) becomes effectively six-coordinate (Figure 1-2C).

Kinetic and spectroscopic studies have revealed several intermediates that form upon reaction of reduced MMOH ($MMOH_{red}$) with O_2 in the presence of two equivalents of MMOB. Two sequentially forming intermediates have been shown to accumulate, **P** (or $\mathbf{H_{peroxo}}$) and **Q**. Intermediate **P** is the first-detected intermediate in the reaction of MMOH from *M. capsulatus* and *M. trichosporium* with O_2. **P** exhibits an absorption feature at ~ 720 nm, probably associated with a peroxo-to-iron(III) charge transfer transition (Table 1-3) (*50, 63*). Extensive spectroscopic studies (Mössbauer spectroscopy, resonance Raman spectroscopy (rR), and extended-X-ray absorption fine structure spectroscopy (EXAFS)) on model compounds for **P** favor the (μ-1,2-peroxo)-diiron(III) structure assignment for this species (*51, 64, 65*). Intermediate **P** converts to

Figure 1-2: X-ray structures of the diiron clusters in (A) the reduced form of the R2 subunit from *E. coli* (Protein Data Bank (PDB) accession number 1XIK), (B) the oxidized form of the R2 subunit from *E. coli* (PDB accession number 1MXY), (C) the reduced form of MMOH from *M. capsulatus* (Bath) (PDB accession number 1MHY) and (D) the oxidized form of MMOH from *M. capsulatus* (Bath) (PDB accession number 1MTY).

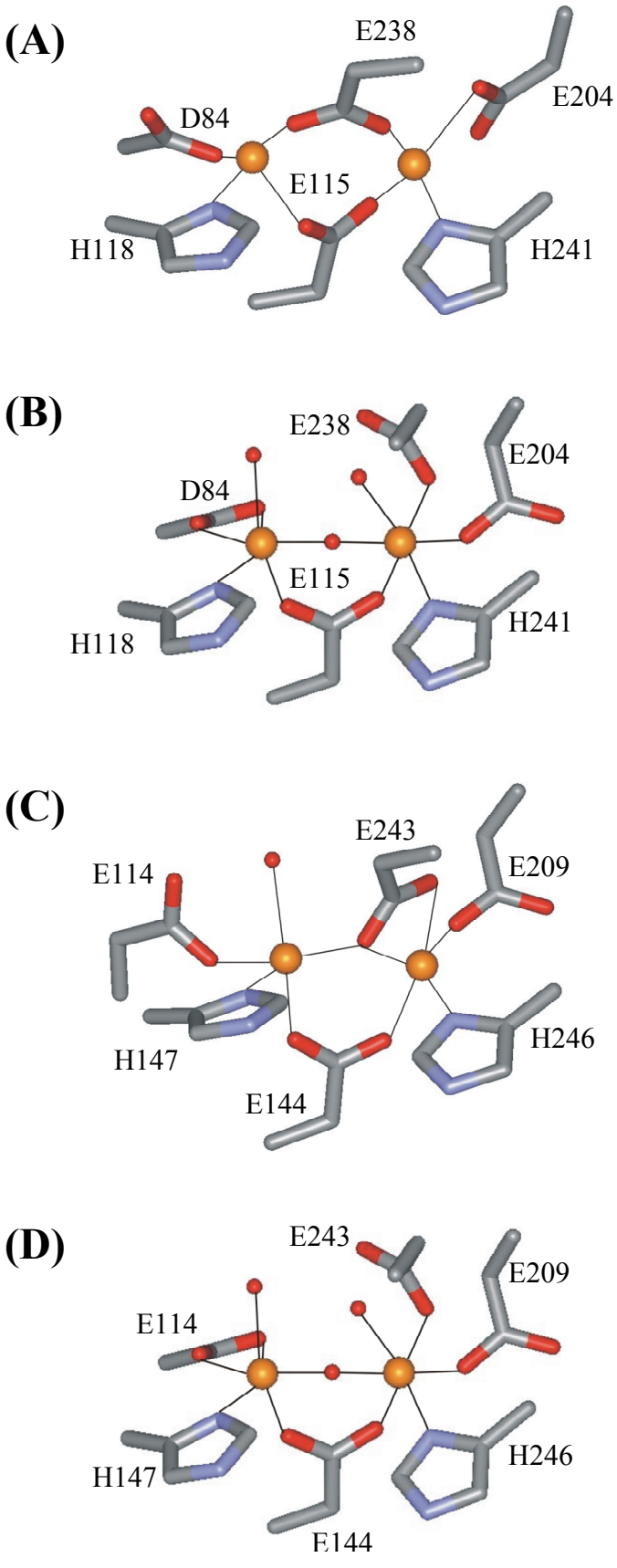
(A)
E238
E204
D84
E115
H118
H241
(B)
E238
E204
D84
E115
H118
H241
(C)
E243
E209
E114
H147
H246
E144
(D)
E243
E209
E114
H147
H246
E144

intermediate **Q**, which is believed to be responsible for methane hydroxylation (*66-69*). Based on Mössbauer spectroscopy, compound **Q** is assigned as a diiron(IV) species with a dimagnetic ground state. Rapid-freeze quench (RFQ) Mössbauer and EXAFS studies suggest a "diamond core" structure containing two single-atom bridges (bis-μ-oxo-diiron(IV)) (*69*). Interestingly, a RFQ-radiolytic reduction-Mössbauer spectroscopic study carried out on **Q** presents evidence for its reduction to a formally Fe_2(III/IV) species "**Q_x**" with Mössbauer spectroscopic features similar to those of intermediate **X**, which accumulates in the reaction of the R2 subunit of RNR from *E. coli* with O_2 (discussed below) (*70*).

C. The R2 Subunit of Ribonucleotide Reductase from E. coli

Whereas all other characterized members of the diiron-carboxylate family harness the diiron(II)-O_2 chemistry to effect two-electron oxidation outcomes (such as hydroxylation of methane by MMOH and fatty-acid desaturation by Δ9-desaturase), the R2 subunit of class I RNR is unique in its exploitation of the two oxidizing equivalents asymmetrically to effect a *one-electron oxidation* reaction that results in the formation of the catalytically essential Y122• (*71, 72*). This chemical divergence occurs in spite of the close structural similarity of the diiron clusters of these proteins and the protein folds that chelate them (*49, 50, 73*).

The structure of the R2 protein from *E. coli* has been determined in the $R2_{met}$ (R2 with a diferric cluster but no Y122•), $R2_{red}$ (R2 with a diferrous cluster and no radical), and $R2_{apo}$ (R2 with no iron cluster and no radical) forms by X-ray crystallography (*18, 37, 74, 75*). The overall tertiary structure of the R2 homodimer is best described as heart-shaped with the two binuclear clusters 25 Å apart. The structure is approximately 70%

Table 1-3: Selected Spectroscopic Properties for various forms of the diiron clusters of R2 from *E. coli* and MMOH from *M. capsulatus*. Adapted from references 58 and 107.

	$R2_{red}$	$R2_{ox}$	**X**	μ-1,2-peroxo	$MMOH_{red}$	$MMOH_{ox}$	**P**	**Q**
Optical λ, nm		325 370 412 500 600	360	700		282	700	350 420
EPR g_{max}, g_{mid}, g_{min}	~ 17	2	2.007,1.999, 1.994		16	8.0		
Raman γ_s (Fe-O-Fe), cm^{-1} γ_{as} (Fe-O-Fe), cm^{-1}		496 756		458 499			905	
Mössbauer δ ($mm\ s^{-1}$), Fe1 ΔE_Q ($mm\ s^{-1}$), Fe1 δ ($mm\ s^{-1}$), Fe2 ΔE_Q ($mm\ s^{-1}$), Fe2	1.26 3.13	0.53 1.66 0.44 2.45	0.56 -0.9 0.26 -0.6	0.63 1.58	1.3 3.1 1.3 2.4-3.0	0.51 1.16 0.5 0.87	0.66 1.51	0.21 0.68 0.14 0.55
ENDOR Fe1, A1, A2, A3 (MHz) Fe2, A1, A2, A3 (MHz) ^{17}O, A1, A2, A3 (MHz)			-74.2, -72.2, -73.2 +27.5, +36.8, +36.8 +31, +25, +25					
EXAFS Fe-Fe Å			2.5 Å			3.0[a], 3.4[b]		2.46

[a] 60% of the $MMOH_{ox}$ species is oxo-bridged.
[b] 40% of the $MMOH_{ox}$ species is hydroxo-bridged.

helical with four antiparallel helices providing ligands to the binuclear iron cluster, which is buried 10 Å from the surface. The R2 protein contains two copies of the E-X-X-H binuclear binding motif (*53*). As in MMOH, two histidines and four carboxylate residues constitute the ligands to the irons of the binuclear cluster in R2. A single nonidentity is found among the ligands of these two proteins: the counterpart of MMOH ligand E114 is D84 of R2 (Figure 1-2).

The coordination geometries at the diiron cores of $R2_{met}$ (Figure 1-2B) and $R2_{red}$ (Figure 1-2A) vary due to substantial ligand rearrangement. One such change is the "carboxylate shift" noted for E238, which converts from a bridging position between the irons in the $R2_{red}$ form to monodentate binding of Fe2 in the $R2_{met}$ form. As mentioned above, a similar "carboxylate shift" is observed for E243 in MMOH. In addition, the coordination mode of D84 changes from a monodentate to bidentate ligation of Fe1 with oxidation of the irons. A discrepancy between the coordination numbers of the iron ions in $R2_{red}$ by X-ray crystallography (two very similar four-coordinate Fe(II) sites) (*76*) and circular dichroism (CD) and magnetic circular dichroism (MCD) spectroscopies (one four-coordinate and one five-coordinate Fe(II) site) has been reported (*77*). Crystal structures of the diiron(II) forms of *E.coli* R2-wildtype (wt) and its D84E and D84E/W48F variants determined from crystals of apo protein soaked with ferrous ions reveal active site geometries different from those obtained at pH 5-6 by chemical or photoreduction of crystals of $R2_{met}$. The discrepancies between CD/MCD data and crystal structures (obtained under different experimental conditions) imply that the geometry of the reactive state of R2 has yet to be elucidated. This should be noted in consideration of possible O_2 activation mechanisms for R2.

Crystal structures of the $R2_{red}$ (*76*) and $R2_{met}$ (*18*) forms of the protein show Y122 residing in a pocket of hydrophobic residues at ~ 5 Å away from Fe1. The crystal structure for the native form, which contains the Y122•, has not been obtained, and therefore, the location and the orientation of the Y122• with respect to the diiron cluster has not been determined. Recent high-field EPR studies on Y122•-containing crystals revealed a significant rotation of the tyrosine sidechain away from Fe1 in the radical-containing form (*78*). This movement increases the distance separating the tyrosine η-oxygen and the carboxylate-oxygen of D84 from ~ 3.2 Å to > 4.0 Å, which is clearly beyond hydrogen-bonding distance. This is a very intriguing result, and it emphasizes the idea of a global function for the hydrogen-bonded network of the proposed PCET pathway, which probably includes proton handling, redox tuning, and structural stabilization of intermediate states.

The R2 cofactor (diiron(III) cluster and Y122•) exhibits an optical spectrum with maxima at 325, 370, and 411 nm. The 325 and 370 nm absorption bands are due to oxo-to-iron charge transfer transitions in the μ-oxo bridged-diiron(III) cluster. The Y122• is the source of the sharp absorption feature at 411 nm. Moreover, the Y122• exhibits a g = 2.0 EPR signal consisting of a large doublet-hyperfine coupling, which is due to one of the β-hydrogens, and a smaller triplet splitting, which arises from the ring hydrogens in positions 3 and 5 (*72, 79*). The diiron(III) cluster is EPR silent because the two irons are antiferromagnetically coupled to form a diamagnetic state (*80*). Additional spectroscopic parameters of the R2 diiron cluster in its various forms are summarized in Table 1-3.

III. Mechanism of Oxygen Activation by the R2 Subunit of *E. coli* Ribonucleotide Reductase

The cofactor in *E. coli* R2 assembles spontaneously when $R2_{apo}$ is incubated with Fe(II) ions and O_2 (*71*). In the assembly reaction the protein first binds Fe(II) ions, then the diiron(II) cluster reductively activates O_2 to effect the one-electron oxidation of the tyrosine residue to its radical form (*81-85*). In the process, the native diiron(III) form of the cluster is produced, with the μ-oxo bridge being derived from O_2 (*86*). An "extra electron," in addition to the three obtained by oxidation of two Fe(II) and the tyrosyl radical, is required to balance the four-electron reduction of O_2 to the oxidation state of $2H_2O$. Several studies have established that this electron is provided *in vitro* by oxidation of a third Fe(II) or (if present) an alternative reductant such as ascorbate (*81-85*). Studies by our group have shown that the transfer occurs rapidly in *E. coli* R2 by an electron shuttling mechanism in which a near-surface tryptophan residue (W48) is transiently oxidized to a cation radical and then reduced from solution. The formally Fe_2(III/IV) cluster that results from this electron transfer, cluster **X**, can generate the tyrosyl radical in the final and slowest step in the reaction (Scheme 1-2) (*84*).

A complete understanding of the R2 cofactor assembly reaction must include structural rationales for the divergence of its mechanism and outcome from those of the O_2-activation reactions carried out by other proteins in the important diiron-carboxylate class. Insight into how the ligand environments surrounding the metal ions contribute to the reactivity toward O_2 has been obtained by examining the intermediates that form during these reactions. The following sections will examine the intermediates that have been identified in the reaction of *E. coli* R2 and will highlight the important properties

Scheme 1-2: Electron gating by *E. coli* R2 resulting from rapid oxidation of the near-surface W48 by a kinetically masked two-electrons-oxidized diiron cluster and subsequent slow oxidation of Y122 by X. Note that no structural representation is implied for the intermediates. Adapted from reference 96.

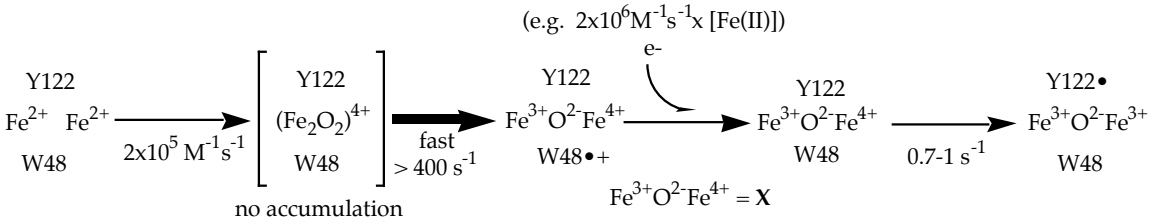

that distinguish them from those which accumulate during O_2 activation by MMOH.

A. Intermediate X

Cluster **X** is the first intermediate to be identified in the reaction of the Fe(II)-R2 protein with O_2. This intermediate is more oxidized by one electron than the diiron(III) product and is the direct oxidant of Y122 (*84*). Optical, EPR, and Mössbauer kinetic data show that **X** decays with a rate constant of 1 s^{-1} at 5 ºC, the same rate constant associated with the Y122• formation (*82*). In the site-directed variant, R2-Y122F, decay of **X** is slower ($k_{obs} \sim 0.15$ s^{-1} at 5 ºC) allowing for its stoichiometric accumulation and proving that **X** can generate Y122• (*87*). The spectroscopic and electronic properties of **X** include a broad absorption band in the 300-500 nm region with a distinct shoulder at 365 nm and an isotropic EPR singlet at $g = 2.0$, indicating an S = 1/2 ground electronic state (*82*). This cluster is assigned an Fe_2(III/IV) oxidation state based on RFQ-Mössbauer and ^{57}Fe ENDOR spectroscopic analysis (the characteristic hyperfine parameters obtained from these studies are summarized in Table 1-3). The Fe(III) site (proposed to be Fe1) of this cluster is high-spin (S = 5/2) and is antiferromagnetically coupled to the high spin Fe(IV) site (S = 2) (proposed to be Fe2) to form the S = 1/2 ground state of **X** (*88*). It has been shown that the two Fe sites of R2 bind Fe with different affinities by Mössbauer spectroscopy and use of ^{56}Fe and ^{57}Fe (*89*). Exploiting this differential affinity and the fact that the Mössbauer sub-spectra of the Fe sites are resolved, the selective enrichment procedure of one Fe site with ^{57}Fe (depending on the sequence of Fe-isotope addition) in **X** showed that the site with greater affinity becomes the Fe(IV) site (putatively Fe2) and the site with lesser affinity becomes the Fe(III) site (putatively Fe1) (*89*).

Generation of **X** is a defining step in the one-electron oxidation outcome of the R2 reaction, and, therefore, elucidating its structure is crucial to understanding the R2 pathway. **X** is believed to have a tribridge structure with at least two single-atom bridges, based on the interestingly short Fe-O-Fe distance of 2.5 Å obtained by EXAFS (*90*). ^{17}O- and ^{1,2}H-ENDOR data from the Hoffman and Stubbe groups suggested that only one of the two O-atoms from O_2 occupies a bridging position in **X** (*90-93*). A RFQ-MCD study (the first-ever on an intermediate), carried out by the Solomon group in collaboration with our group, supports, in agreement with the ENDOR results, a *mono*- rather than *bis*-μ-oxo assignment for **X** (*94*).

B. Mechanism of Rapid Electron Transfer during O_2 Activation by R2

A step that distinguishes the R2 reaction mechanism from those of the diiron hydroxylases and (presumably) desaturases is the transfer of a single electron from the surface of the protein to the intermediate formed upon or after addition of O_2 to the diiron(II) cluster during the formation of cluster **X** (Scheme 1-2) (*50, 73, 82-84, 95*). It has been shown that the electron transfer is mediated by a network of hydrogen-bonded amino acid side-chains in R2 composed of Fe1 ligand H118, the second sphere residue D237, and the near-surface residue W48. Convincing evidence has been obtained by our group for the intermediacy of a $W48^{+\bullet}$, which forms rapidly and concomitantly with **X** in a second-order reaction between the reactive Fe(II)-R2 complex and O_2 and is efficiently reduced by Fe(II)aq, 2-mercaptoethanol, and ascorbate (Scheme 1-2) (*96*). This transient species exhibits an absorption spectrum with features at 335 nm and 560 nm, which is a close match to the very distinctive spectrum of indolyl cation radicals determined by pulse radiolysis (*97, 98*) and the spectrum of $W191^{+\bullet}$ in "compound I" of the heme-

containing cytochrome *c* peroxidase from yeast, which has a H-bonded network similar to that in R2 (*99-103*). The identified $W48^{+\bullet}$ species exhibits a $g = 2.0$ EPR signal and perturbs the EPR and Mössbauer spectra of **X**.

The demonstration that the $W48^{+\bullet}$ forms concomitantly with **X** in a second-order reaction between the reactive Fe(II)-R2 complex and O_2 implies that all precursors to **X** are "kinetically masked" (i.e. they decay sufficiently rapidly that they do not accumulate). Examination of the mechanisms of O_2 activation in R2 variants in which W48 has been replaced with a less easily-oxidized residue such as phenylalanine has shown that Y122• is produced 10-fold more rapidly ($k_{obs} = 9 \pm 2\ s^{-1}$ at 5 °C) in the reaction of the variants than in the reaction of R2-wt (*104*). The radical forms as part of a "di-radical" species that also contains **X** (Scheme 1-3). The presence of both oxidized species in the same active site, which is revealed by dipolar and weak exchange coupling that affects the Mössbauer spectrum of **X** and the EPR spectra of both constituents, implies that electron injection does not occur. Presumably as a consequence of the proximity of **X** and Y122• and the inability of the protein to support reduction of either, the Y122• thus produced is not stable. The majority decays along with **X** in an uncharacterized reaction that also yields altered iron(III) products. A sub-stoichiometric quantity (~ 0.25 equiv) of Y122• does not decay, probably as a result of very inefficient electron transfer ("leaking") to **X** occurring in competition with the decay process. This Y122• is then as stable as in R2-wt, confirming that the transient behavior of Y122• is not a reflection of an inherent instability of the radical in the variant protein. The latter point is emphasized by the observation that inclusion of 2 mM dithionite in the reaction rescues Y122• from decay by forcing reduction of **X** to the normal μ-oxodiiron(III) cluster. Thus, the ten-fold faster

Scheme 1-3: Mechanism deduced for O_2 activation in R2-W48F at 5 °C. Adapted from reference 104.

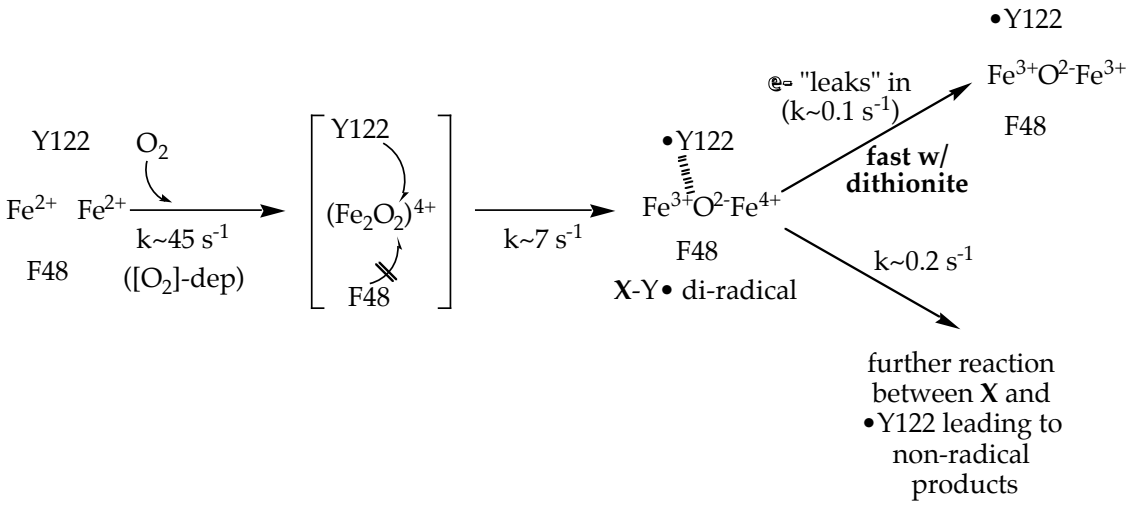

formation and transient behavior of Y122• and the formation of altered iron products in the R2-W48F variant are the specific hallmarks of *defective* electron shuttling. The existence of a lag phase in production of Y122• in the reaction of R2-W48F and the dependence of the rate constant associated with this lag on the concentration of O_2 suggest that at least one intermediate accumulates between the reactants and the **X**-Y122• species. Mössbauer evidence indicates that at least one intermediate complex, which is iso-electronic with but spectroscopically distinct from the μ-1,2-peroxo complex that accumulates in R2 variants with iron ligand D84 substituted with E (discussed in the following section) accumulates in the W48F variant. From the above results, it is inferred that at least one two-electrons-oxidized intermediate of general formula $(Fe_2O_2)^{4+}$ accumulates and that it oxidizes Y122 to yield the **X**-Y122• species (Scheme 1-3). This species is presumably the kinetically masked intermediate that would normally decay rapidly to the X-W48$^{+\bullet}$ state in the R2-wt reaction (Scheme 1-2). Assignment of the oxidation state and gross structure of this species is the focus of Chapter 3.

C. Structural Tuning of the R2 Subunit and its Mechanistic Implications

One main focus of the "Bollinger group" research has been to understand the functional significance of the subtle differences in the coordination spheres of the proteins of the diiron-carboxylate class and how they serve to dictate which of several geometrically and chemically distinct oxidized-diiron intermediates form in a given protein. As mentioned previously, the observation of a rapidly-accumulating, one electron-oxidized intermediate (**X**) in the reaction of *E. coli* R2 (Scheme 1-2), but not in the reaction of MMOH (only **P** and **Q** are detected) (Scheme 1-4A), implies that an electron is transferred into the buried cluster site of R2 shortly after O_2 adds to the

Scheme 1-4: A) Schematic mechanism for single turnover of methane monooxygenase based on spectroscopic and kinetic characterization of **P** and **Q**. B) Commonly proposed schematic mechanism for O_2 activation in R2 based on perceived analogy to methane monooxygenase.

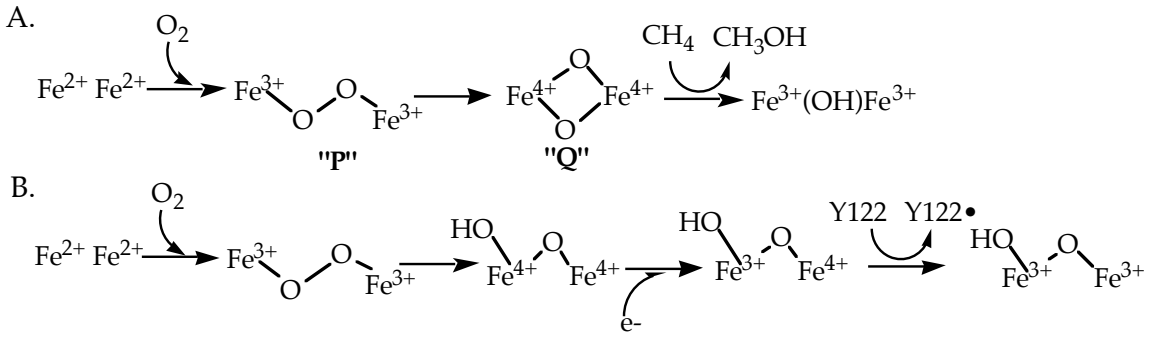

diiron(II) reactant form(*96*). This hypothesis has been advanced to include that this electron transfer step may reductively deactivate an intermediate (such as the diiron(IV) species from the MMOH catalytic cycle) (Scheme 1-4B) that would otherwise be capable of two-electron oxidation outcomes. By so doing, this step would dictate a one-electron oxidation outcome.

This hypothesis raises the question of what structural features are responsible for effecting the electron transfer step in R2 or preventing it in MMOH. Two (not mutually exclusive) scenarios arise; the first scenario includes the R2 protein possessing an efficient electron transfer pathway to conduct the electron from a surface reductant to the buried cluster site. The “Bollinger group” has provided strong evidence for this scenario by revealing the role of W48 as an “electron shuttle” to the diiron cluster in R2. This implies control of the reaction by "outer sphere" structural elements (such as W48), which would permit that the initial diiron-O_2 intermediates in R2 and MMOH might have similar or identical inherent structures and reactivities (Scheme 1-4B). The second scenario includes that the ligands of the two proteins (their inner spheres) may subtly and divergently tune the diiron clusters such that the initial diiron-O_2 intermediate in R2 is inherently reactive to one-electron reduction while the cognate species in MMOH is predisposed to react by O-O bond cleavage without change in net oxidation state of the cluster (in conversion of the peroxodiiron(III) intermediate to the diiron(IV) intermediate). Evidence presented below shows that both inner sphere and outer sphere control of the R2 reaction are operant.

Substitution of phenylalanine 208 with tyrosine in R2 to give R2-F208Y (first studied by Sjöberg and co-workers (*75*)) results in the hydroxylation of the engineered

Y208, implying that the deactivating-electron transfer step is subverted by introduction of a residue near the cluster site (Y208) that can serve as an endogenous two-electron reductant. The electron transfer step is accelerated in the O_2 reaction of R2-F208Y by inclusion of sufficiently high concentrations of a one-electron reductant, the normal one-electron oxidation of Y122 becomes predominant over Y208 hydroxylation (*105*). The effect of reductant on the reaction outcome is mediated by the aforementioned hydrogen-bond network connecting the W48 with the cluster ligand H118. When W48 is replaced with F, only Y208 hydroxylation occurs, irrespective of reductant concentration. These observations prove that an outer sphere control element (the electron transfer pathway) *can be* sufficient to dictate the outcome of O_2 activation. However, phenols (such as the sidechain of Y208) are much more easily oxidized than alkanes or unfunctionalized alkenes, and it has not been possible to characterize intermediates in this reaction to determine the extent to which the mechanism is similar to that of MMOH.

Moreover, when the electron transfer step is blocked by the W48F substitution in the R2 protein that is otherwise wildtype, intermediates similar to those from the MMOH reaction cycle are not observed, and the two-units-oxidized intermediate that does form still reacts by sequential one-electron reduction steps, albeit by a mechanism that is altered from that of the wildtype protein (Scheme 1-3) (*104*). This signifies that the R2 cluster ligand sphere is probably tuned to yield a diiron-O_2 adduct that is predisposed to one-electron reduction. In searching for a structural basis for this inner sphere tuning, a single non-identity among the amino acid iron ligands of R2 and MMOH is noted: D84 of R2 corresponds to glutamate E114 of MMOH. To assess the relevance of this non-identity, the O_2 reaction in the D84E variant of R2 has been characterized (*106*). A

peroxodiiron(III) intermediate, which has striking spectroscopic similarities with intermediate **P** in MMOH, accumulates in this reaction, and this new R2 intermediate is relatively unreactive toward one-electron reduction. Its rR spectroscopic characteristics imply that it has a symmetrically-bridging (μ-1,2) peroxide unit (Table 1-3) (*107*). Intermediates of this structural type have since been demonstrated in several other members of the diiron family, and it is presumed that the initial adduct in MMOH also has this structure.

In spite of the marked structural and mechanistic similarities of R2-D84E to MMOH, the outcome of its reaction is unaltered: one equiv of Y122 radical is produced, and the primary iron product is a μ-oxodiiron(III) cluster with Mössbauer features perturbed as a result of the ligand substitution. Kinetic characterization of the reaction with different concentrations of O_2 and at different temperatures revealed consistent temporal correlations between the formation phase of the intermediate and the lag phase of the tyrosyl radical and between the decay phase of the intermediate and the formation phase of the radical. These results imply that the peroxodiiron(III) complex is on the pathway to the tyrosyl radical (*108*). Under the assumption that this complex is sufficiently similar to MMOH **P** that it could, in principle, give rise to an intermediate that would be reactive for an oxygen transfer outcome, one interpretation of the generation of the tyrosyl radical is that the observed inner-sphere (D84) and outer-sphere (W48) control elements function somewhat redundantly. By combining the cluster re-tuning substitution (D84E) with the electron-transfer-disabling substitution (W48F), an R2 variant that forms an even more stable (by ~ 3-fold) version of the μ-1,2-peroxodiiron(III) complex was obtained. Decay of the complex at 5 °C produces an

initial brown product, which contains very little tyrosyl radical (< 0.15 equiv under optimal conditions) and which converts very slowly ($t_{1/2}$ ~ 8 h) upon incubation at 0°C to an intensely purple final product. X-ray crystallographic analysis of the purple product indicated that Phe 208 undergoes *ε*–hydroxylation and the resulting *m*-OH-phenylalanine becomes a ligand to Fe2 of the diiron cluster. rR spectra of the purple product generated with $^{16}O_2$ or $^{18}O_2$ showed appropriate isotopic shifts in bands assigned to O-phenyl and Fe-O-phenyl vibrational modes, confirming that the oxygen of the Fe(III)-phenolate species is derived from O_2.

The structural rational for the effect of the W48F substitution is clear: it essentially cuts a molecular wire that is necessary for rapid electron transfer to the buried cluster site and thereby allows a two-electrons-oxidized cluster to persist long enough to effect a two-electron oxidation outcome. The structural basis for the effect of the D84E substitution in stabilizing the MMOH-like peroxodiiron(III) complex is less obvious. The adjustments in the inner sphere associated with this substitution (*109*) might result either (1) in stabilization of the same intermediate that forms in the R2-wt or (2) in formation of a different intermediate. Resolving this issue has been one objective of the work described in this thesis.

IV. Abbreviations

RNR ribonucleotide reductase

S• thiyl radical

Y• tyrosyl radical

AdoCbl adenosylcobalamin

G• glycyl radical

SAM S-adenosyl-L-methionine

(1) 3'-nucleotide radical

(2) 3'-keto-2'-deoxynucleotide radical

(3) 3'-keto-2'-deoxynucleotide

(4) 3'-deoxynucleotide radical

ET electron transfer

PCET proton-coupled electron transfer

$W48^{+\bullet}$ W48 cation radical

Y356• Y356 radical

ACP acyl carrier protein

MMOH hydroxylase component of methane monooxygenase

sMMO soluble methane monooxygenase

Δ9-desaturase stearoyl-ACP Δ9-desaturase from *Ricinus communis*

$MMOH_{ox}$ oxidized form of MMOH

$MMOH_{red}$ reduced form of MMOH

rR resonance Raman

EXAFS extended X-ray absorption fine structure

P putatively μ-1,2-peroxodiiron(III) intermediate of MMOH

Q putatively formally diiron Fe(IV) intermediate of MMOH

$R2_{met}$ R2 protein with a diferric binuclear iron cluster but no tyrosyl radical

$R2_{red}$ R2 protein with a diferrous cluster and no radical

$R2_{apo}$ R2 protein with no iron cluster and no radical

CD circular dichroism

MCD magnetic circular dichroism

wt wildtype

k_{obs} observed first-order rate constant

RFQ rapid-freeze quench

X formally Fe_2(III/IV) intermediate in R2

V. References

1. Eklund, H., Uhlin, U., Farnegardh, M., Logan, D. T., and Nordlund, P. (2001) Structure and function of the radical enzyme ribonucleotide reductase, *Prog. Biophys. Mol. Biol. 77*, 177-268.
2. Jordan, A., and Reichard, P. (1998) Ribonucleotide reductases, *Annu. Rev. Biochem. 67*, 71-98.
3. Thelander, L., and Reichard, P. (1979) Reduction of ribonucleotides, *Annu. Rev. Biochem. 48*, 133-158.
4. Zhou, B. B., and Elledge, S. J. (2000) The DNA damage response: putting checkpoints in perspective, *Nature 408*, 433-439.
5. Stubbe, J., Ator, M., and Krenitsky, T. (1983) Mechanism of ribonucleoside diphosphate reductase from *Escherichia coli*. Evidence for 3'-C--H bond cleavage, *J. Biol. Chem. 258*, 1625-1631.
6. Reichard, P. (1997) The evolution of ribonucleotide reduction, *Trends Biochem. Sci. 22*, 81–85.
7. Stubbe, J., and van der Donk, W. A. (1998) Protein radicals in enzyme catalysis, *Chem. Rev. 98*, 705-762.
8. Hammersten, E., Reichard, P., and Saluste, E. (1950) Pyrimidine nucleosides as precursors of pyrimidines in polynucleotides, *J. Biol. Chem. 183*, 105-109.
9. Reichard, P., and Estborn, B. (1951) Utilization of desoxyribosides in the synthesis of polynucleotides, *J. Biol. Chem. 188*, 839-846.
10. Jordan, A., Pontis, E., Atta, M., Krook, M., Gibert, I., Barbe, J., and Reichard, P. (1994) A second class I ribonucleotide reductase in *Enterobacteriaceae*:

characterization of the *Salmonella typhimurium* enzyme, *Proc. Natl. Acad. Sci. U.S.A. 91*, 12892-12896.

11. Jordan, A., Gibert, I., and Barbe, J. (1994) Cloning and sequencing of the genes from *Salmonella typhimurium* encoding a new bacterial ribonucleotide reductase, *J. Bacteriol. 176*, 3420-3427.

12. Yang, F., Lu, G., and Rubin, H. (1994) Isolation of ribonucleotide reductase from *Mycobacterium tuberculosis* and cloning, expression, and purification of the large subunit, *J. Bacteriol. 176*, 6738-6743.

13. Jordan, A., Aragall, E., Gibert, I., and Barbe, J. (1996) Promoter identification and expression analysis of *Salmonella typhimurium* and *Escherichia coli* nrdEF operons encoding one of two class I ribonucleotide reductases present in both bacteria, *Mol. Microbiol. 19*, 777-790.

14. Jordan, A., Aslund, F., Pontis, E., Reichard, P., and Holmgren, A. (1997) Characterization of *Escherichia coli* NrdH. A glutaredoxin-like protein with a thioredoxin-like activity profile, *J. Biol. Chem. 272*, 18044-18050.

15. Jordan, A., Pontis, E., Aslund, F., Hellman, U., Gibert, I., and Reichard, P. (1996) The ribonucleotide reductase system of *Lactococcus lactis*. Characterization of an NrdEF enzyme and a new electron transport protein, *J. Biol. Chem. 271*, 8779-8785.

16. Högbom, M., Stenmark, P., Voevodskaya, N., McClarty, G., Gräslund, A., and Nordlund, P. (2004) The radical site in Chlamydial ribonucleotide reductase defines a new R2 subclass, *Science 305*, 245-248.

17. Uhlin, U., and Eklund, H. (1994) Structure of ribonucleotide reductase protein R1, *Nature 370*, 533-539.

18. Nordlund, P., and Eklund, H. (1993) Structure and function of the *Escherichia coli* ribonucleotide reductase, *J. Mol. Biol. 232*, 123-164.

19. Larsson, A., and Sjöberg, B.-M. (1986) Identification of the stable free radical tyrosine residue in ribonucleotide reductase, *EMBO J. 5*, 2037-2040.

20. Mao, S. S., Holler, T. P., Yu, G. X., Bollinger, J. M., Jr., Booker, S., Johnston, M. I., and Stubbe, J. (1992) A model for the role of multiple cysteine residues involved in ribonucleotide reduction: amazing and still confusing, *Biochemistry 31*, 9733-9743.

21. Stubbe, J., and Ackles, D. (1980) On the mechanism of ribonucleotide diphosphate reductase from *Escherichia coli*, *J. Biol. Chem. 255*, 8027-8030.

22. Blakley, R. L., and Barker, H. A. (1964) Cobamide stimulation of the reduction of ribotides to deoxyribotides in *Lactobacillus leichmannii*, *Biochem. Biophys. Res. Commun. 16*, 391-397.

23. Beck, W. S., and Hardy, J. (1965) Requirement of ribonucleotide reductase for cobamide coenzyme, a product of ribosomal activity, *Proc. Natl Acad. Soc. U.S.A. 54*, 286-293.

24. Gleason, F. K., and Frick, T. D. (1980) Adenosylcobalamin-dependent ribonucleotide reductase from the blue-green alga, *Anabaena sp.* Purification and partial characterization, *J. Biol. Chem. 255*, 7728-7733.

25. Panagou, D., Orr, M. D., Dunstone, J. R., and Blakley, R. L. (1972) A monomeric, allosteric enzyme with a single polypeptide chain. Ribonucleotide reductase of *Lactobacillus leichmannii*, *Biochemistry 11*, 2378-2388.

26. Eliasson, R., Pontis, E., Jordan, A., and Reichard, P. (1999) Allosteric control of three B12-dependent (class II) ribonucleotide reductases. Implications for the evolution of ribonucleotide reduction, *J. Biol. Chem. 274*, 7182-7189.

27. Booker, S., Licht, S., Broderick, J., and Stubbe, J. (1994) Coenzyme B12-dependent ribonucleotide reductase: evidence for the participation of five cysteine residues in ribonucleotide reduction, *Biochemistry 33*, 12676-12685.

28. Barlow, T. (1988) Evidence for a new ribonucleotide reductase in anaerobic *E. coli*, *Biochem. Biophys. Res. Commun. 155*, 747-753.

29. Ollagnier, S., Mulliez, E., Gaillard, J., Eliasson, R., Fontecave, M., and Reichard, P. (1996) The anaerobic *Escherichia coli* ribonucleotide reductase. Subunit structure and iron sulfur center, *J. Biol. Chem. 271*, 9410-9416.

30. Logan, D. T., Andersson, J., Sjöberg, B.-M., and Nordlund, P. (1999) A glycyl radical site in the crystal structure of a class III ribonucleotide reductase, *Science 283*, 1499-1504.

31. Stubbe, J., Ge, J., and Yee, C. S. (2001) The evolution of ribonucleotide reduction revisited, *Trends Biochem. Sci. 26*, 93-99.

32. Stubbe, J., and Riggs-Gelasco, P. (1998) Harnessing free radicals: formation and function of the tyrosyl radical in ribonucleotide reductase, *Trends Biochem. Sci. 23*, 438-443.

33. Climent, I., Sjöberg, B.-M., and Huang, C. Y. (1991) Carboxyl-terminal peptides as probes for *Escherichia coli* ribonucleotide reductase subunit interaction: kinetic analysis of inhibition studies, *Biochemistry 30*, 5164-5171.

34. Dutia, B. M., Frame, M. C., Subak-Sharpe, J. H., Clark, W. N., and Marsden, H. S. (1986) Specific inhibition of herpes virus ribonucleotide reductase by synthetic peptides, *Nature 321*, 439-441.

35. Fisher, A., Yang, F. D., Rubin, H., and Cooperman, B. S. (1993) R2 C-terminal peptide inhibition of mammalian and yeast ribonucleotide reductase, *J. Med. Chem. 36*, 3859-3862.

36. Climent, I., Sjöberg, B.-M., and Huang, C. Y. (1992) Site-directed mutagenesis and deletion of the carboxyl terminus of *Escherichia coli* ribonucleotide reductase protein R2. Effects on catalytic activity and subunit interaction, *Biochemistry 31*, 4801-4807.

37. Nordlund, P., Sjöberg, B.-M., and Eklund, H. (1990) Three-dimensional structure of the free radical protein of ribonucleotide reductase, *Nature 345*, 593-598.

38. Stubbe, J., Nocera, D. G., Yee, C. S., and Chang, M. C. Y. (2003) Radical initiation in the class I ribonucleotide reductase: long-range proton-coupled electron transfer?, *Chem. Rev. 103*, 2167-2202.

39. Ekberg, M., Pötsch, S., Sandin, E., Thunnissen, M., Nordlund, P., Sahlin, M., and Sjöberg, B.-M. (1998) Preserved catalytic activity in an engineered ribonucleotide reductase R2 protein with a non-physiological radical transfer pathway. The importance of hydrogen bond connections between the participating residues, *J. Biol. Chem. 273*, 21003-21008.

40. Ekberg, M., Sahlin, M., Eriksson, M., and Sjöberg, B.-M. (1996) Two conserved tyrosine residues in protein R1 participate in an intermolecular electron transfer in ribonucleotide reductase, *J. Biol. Chem. 271*, 20655-20659.

41. Rova, U., Adrait, A., Pötsch, S., Gräslund, A., and Thelander, L. (1999) Evidence by mutagenesis that Tyr(370) of the mouse ribonucleotide reductase R2 protein is the connecting link in the intersubunit radical transfer pathway, *J. Biol. Chem. 274*, 23746-23751.

42. Rova, U., Goodtzova, K., Ingemarson, R., Behravan, G., Gräslund, A., and Thelander, L. (1995) Evidence by site-directed mutagenesis supports long-range electron transfer in mouse ribonucleotide reductase, *Biochemistry 34*, 4267-4275.

43. Tommos, C., Skalicky, J. J., Pilloud, D. L., Wand, A. J., and Dutton, P. L. (1999) *De novo* proteins as models of radical enzymes, *Biochemistry 38*, 9495-9507.

44. Siegbahn, P. E. M., Eriksson, L., Himo, F., and Pavlov, M. (1998) Hydrogen atom transfer in ribonucleotide reductase (RNR), *J. Phys. Chem 102*, 10622-10629.

45. Chang, M. C., Yee, C. S., Nocera, D. G., and Stubbe, J. (2004) Site-specific replacement of a conserved tyrosine in ribonucleotide reductase with an aniline amino acid: a mechanistic probe for a redox-active tyrosine, *J. Am. Chem. Soc. 126*, 16702-16703.

46. Chang, M. C., Yee, C. S., Stubbe, J., and Nocera, D. G. (2004) Turning on ribonucleotide reductase by light-initiated amino acid radical generation, *Proc. Natl Acad. Soc. U.S.A. 101*, 6882-6887.

47. Yee, C. S., Seyedsayamdost, M. R., Chang, M. C., Nocera, D. G., and Stubbe, J. (2003) Generation of the R2 subunit of ribonucleotide reductase by intein

chemistry: insertion of 3-nitrotyrosine at residue 356 as a probe of the radical initiation process, *Biochemistry 42*, 14541-14552.

48. Yee, C. S., Chang, M. C., Ge, J., Nocera, D. G., and Stubbe, J. (2003) 2,3-difluorotyrosine at position 356 of ribonucleotide reductase R2: a probe of long-range proton-coupled electron transfer, *J. Am. Chem. Soc. 125*, 10506-10507.

49. Nordlund, P., and Eklund, H. (1995) Di-iron-carboxylate proteins, *Current Opinion in Structural Biology 5*, 758-766.

50. Wallar, B. J., and Lipscomb, J. D. (1996) Dioxygen activation by enzymes containing binuclear non-heme iron clusters, *Chem. Rev. 96*, 2625-2657.

51. Tshuva, E. Y., and Lippard, S. J. (2004) Synthetic models for non-heme carboxylate-bridged diiron metalloproteins: strategies and tactics, *Chem. Rev. 104*, 987-1012.

52. Fox, B. G., Shanklin, J., Somerville, C., and Münck, E. (1993) Stearoyl-acyl carrier protein Δ^9 desaturase from *Ricinus communis* is a diiron-oxo protein, *Proc. Natl Acad. Soc. U.S.A. 90*, 2486-2490.

53. Fox, B. G., Shanklin, J., Ai, J., Loehr, T. M., and Sanders-Loehr, J. (1994) Resonance Raman evidence for an Fe-O-Fe center in stearoyl-ACP desaturase. Primary sequence identity with other diiron-oxo proteins, *Biochemistry 33*, 12776-12786.

54. Lindqvist, Y., Huang, W., Schneider, G., and Shanklin, J. (1996) Crystal Structure of Δ^9 stearoyl-acyl carrier protein desaturase from castor seed and its relationship to other di-iron proteins, *EMBO Journal 15*, 4081-4092.

55. Woodland, M. P., Patil, D. S., Cammack, R., and Dalton, H. (1986) ESR studies of protein A of the soluble methane monooxygenase from *Methylococcus capsulatus* (Bath). *Biochimica et Biophysica Acta 873*, 237-242.

56. Fox, B. G., Surerus, K. K., Münck, E., and Lipscomb, J. D. (1988) Evidence for a μ-oxo-bridged binuclear iron cluster in the hydroxylase component of methane monooxygenase. Mössbauer and EPR studies, *J. Biol. Chem. 263*, 10553-10556.

57. Fox, B. G., Froland, W. A., Dege, J. E., and Lipscomb, J. D. (1989) Methane monooxygenase from *Methylosinus trichosporium* OB3b. Purification and properties of a three-component system with high specific activity from a type II methanotroph, *J. Biol. Chem. 264*, 10023-10033.

58. Rosenzweig, A. C., Nordlund, P., Takahara, P. M., Frederick, C. A., and Lippard, S. J. (1995) Geometry of the soluble methane monooxygenase catalytic diiron center in two oxidation states, *Chem. Biol. 2*, 409-18.

59. Fox, B. G., Lyle, K. S., and Rogge, C. E. (2004) Reactions of the diiron enzyme stearoyl-acyl carrier protein desaturase, *Acc. Chem. Res. 37*, 421-429.

60. Lyle, K. S., Moënne-Loccoz, P., Ai, J., Sanders-Loehr, J., Loehr, T. M., and Fox, B. G. (2000) Resonance Raman studies of the stoichiometric catalytic turnover of a substrate stearoyl-acyl carrier protein Δ-9 desaturase complex, *Biochemistry 39*, 10507-10513.

61. Baik, M.-H., Newcomb, M., Friesner, R. A., and Lippard, S. J. (2003) Mechanistic studies on the hydroxylation of methane by methane monooxygenase, *Chem. Rev. 103*, 2385-2419.

62. Merkx, M., Kopp, D. A., Sazinsky, M. H., Blazyk, J. L., Müller, J., and Lippard, S. J. (2001) Dioxygen activation and methane hydroxylation by soluble methane monooxygenase: a tale of two irons and three proteins, *Angew. Chem. Int. Ed. 40*, 2782-2807.

63. Brunold, T. C., Tamura, N., Kitajima, N., Moro-oka, Y., and Solomon, E. I. (1998) Spectroscopic study of $[Fe_2(O_2)(OBz)_2\{HB(pz')_3\}_2]$: nature of the μ-1,2 peroxide-Fe(III) bond and its possible relevance to O_2 activation by non-heme iron enzymes, *J. Am. Chem. Soc. 120*, 5674-5690.

64. Kim, K., and Lippard, S. J. (1996) Structure and Mössbauer spectrum of a (μ-1,2-peroxo)bis(μ-carboxylato)diiron(III) model for the peroxo intermediate in the methane monooxygenase hydroxylase cycle, *J. Am. Chem. Soc. 118*, 4914-4915.

65. Liu, K. E., Wang, D., Huynh, B. H., Edmondson, D. E., Salifoglou, A., and Lippard, S. J. (1994) Spectroscopic detection of intermediates in the reaction of dioxygen with the reduced methane monooxygenase/hydroxylase from *Methylococcus capsulatus* (Bath), *J. Am. Chem. Soc. 116*, 7465-7466.

66. Liu, K. E., Valentine, A. M., Wang, D., Huynh, B. H., Edmondson, D. E., Salifoglou, A., and Lippard, S. J. (1995) From the mass production of *Methylococcus capsulatus* to the efficient separation and isolation of methane monooxygenase proteins. Characterization of novel intermediates in substrate reactions of methane monooxygenase, *J. Am. Chem. Soc. 117*, 10174-10185.

67. Lee, S.-K., Fox, B. G., Froland, W. A., Lipscomb, J. D., and Münck, E. (1993) A transient intermediate of the methane monooxygenase catalytic cycle containing an FeIVFeIV cluster, *J. Am. Chem. Soc. 115*, 6450-6451.

68. Lee, S.-K., Nesheim, J. C., and Lipscomb, J. D. (1993) Transient intermediates of the methane monooxygenase catalytic cycle, *J. Biol. Chem. 268*, 21569-21577.

69. Shu, L. J., Nesheim, J. C., Kauffmann, K., Münck, E., Lipscomb, J. D., and Que, L., Jr. (1997) An Fe_2IVO_2 diamond core structure for the key intermediate Q of methane monooxygenase, *Science 275*, 515-518.

70. Valentine, A. M., Tavares, P., Pereira, A. S., Davydov, R., Krebs, C., Hoffman, B. M., Edmondson, D. E., Huynh, B. H., and Lippard, S. J. (1998) Generation of a mixed-valent Fe(III)Fe(IV) form of intermediate Q in the reaction cycle of soluble methane monooxygenase, an analog of intermediate X in ribonucleotide reductase R2 assembly, *J. Am. Chem. Soc. 120*, 2190-2191.

71. Atkin, C. L., Thelander, L., and Reichard, P. (1973) Iron and free radical in ribonucleotide reductase. Exchange of iron and Mössbauer spectroscopy of the protein B2 subunit of the *Escherichia coli* enzyme, *J. Biol. Chem. 248*, 7464-7472.

72. Sjöberg, B.-M., Reichard, P., Gräslund, A., and Ehrenberg, A. (1977) Nature of the free radical in ribonucleotide reductase from *Escherichia coli*., *J. Biol. Chem. 252*, 536-541.

73. Solomon, E. I., Brunold, T. C., Davis, M. I., Kemsley, J. N., Lee, S.-K., Lehnert, N., Neese, F., Skulan, A. J., Yang, Y.-S., and Zhou, J. (2000) Geometric and electronic structure/function correlations in non-heme iron enzymes, *Chem. Rev. 100*, 235-349.

74. Nordlund, P., Åberg, A., Uhlin, U., and Eklund, H. (1993) Crystallographic investigations of ribonucleotide reductase, *Biochem. Soc. Trans. 21*, 735-738.

75. Åberg, A., Ormö, M., Nordlund, P., and Sjöberg, B.-M. (1993) Autocatalytic generation of dopa in the engineered protein R2 F208Y from *Escherichia coli* ribonucleotide reductase and crystal structure of the dopa 208 protein, *Biochemistry 32*, 9845-9850.

76. Logan, D. T., Su, X.-D., Åberg, A., Regnström, K., Hajdu, J., Eklund, H., and Nordlund, P. (1996) Crystal structure of reduced protein R2 of ribonucleotide reductase: the structural basis for oxygen activation at a dinuclear iron site, *Structure 4*, 1053-1064.

77. Pulver, S. C., Tong, W. H., Bollinger, J. M., Jr., Stubbe, J., and Solomon, E. I. (1995) Circular dichroism and magnetic circular dichroism studies of the fully reduced binuclear non-heme iron active site in the *Escherichia coli* R2 subunit of ribonucleoside diphosphate reductase, *J. Am. Chem. Soc. 117*, 12664-12678.

78. Högbom, M., Galander, M., Andersson, M., Kolberg, M., Hofbauer, W., Lassmann, G., Nordlund, P., and Lendzian, F. (2003) Displacement of the tyrosyl radical cofactor in ribonucleotide reductase obtained by single-crystal high-field EPR and 1.4-Å X-ray data, *Proc. Natl Acad. Soc. U.S.A. 100*, 3209-3214.

79. Bender, C. J., Sahlin, M., Babcock, G. T., Barry, B. A., Chandrashekar, T. K., Salowe, S. P., Stubbe, J., Lindström, B., Petersson, L., Ehrenberg, A., and Sjöberg, B.-M. (1989) An ENDOR study of the tyrosyl free radical in ribonucleotide reductase from *Escherichia coli*, *J. Am. Chem. Soc. 111*, 8076-8083.

80. Lynch, J. B., Juarez-Garcia, C., Münck, E., and Que, L., Jr. (1989) Mössbauer and EPR studies of the binuclear iron center in ribonucleotide reductase from

Escherichia coli. A new iron-to-protein stoichiometry, *J. Biol. Chem. 264*, 8091-8096.

81. Bollinger, J. M., Jr., Edmondson, D. E., Huynh, B. H., Filley, J., Norton, J. R., and Stubbe, J. (1991) Mechanism of assembly of the tyrosyl radical-dinuclear iron cluster cofactor of ribonucleotide reductase, *Science 253*, 292-298.

82. Bollinger, J. M., Jr., Stubbe, J., Huynh, B. H., and Edmondson, D. E. (1991) Novel diferric radical intermediate responsible for tyrosyl radical formation in assembly of the cofactor of ribonucleotide reductase, *J. Am. Chem. Soc. 113*, 6289-6291.

83. Bollinger, J. M., Jr., Tong, W. H., Ravi, N., Huynh, B. H., Edmondson, D. E., and Stubbe, J. (1994) Mechanism of assembly of the tyrosyl radical-diiron(III) cofactor of *E. coli* ribonucleotide reductase. 3. Kinetics of the limiting Fe^{2+} reaction of optical, EPR, and Mössbauer spectroscopies, *J. Am. Chem. Soc. 116*, 8024-8032.

84. Bollinger, J. M., Jr., Tong, W. H., Ravi, N., Huynh, B. H., Edmondson, D. E., and Stubbe, J. (1994) Mechanism of assembly of the tyrosyl-diiron(III) cofactor of *E. coli* ribonucleotide reductase. 2. Kinetics of the excess Fe^{2+} reaction by optical, EPR, and Mössbauer spectroscopies, *J. Am. Chem. Soc. 116*, 8015-8023.

85. Ravi, N., Bollinger, J. M., Jr., Huynh, B. H., Edmondson, D. E., and Stubbe, J. (1994) Mechanism of assembly of the tyrosyl radical-diiron(III) cofactor of *E. coli* ribonucleotide reductase: 1. Mössbauer characterization of the diferric radical precursor, *J. Am. Chem. Soc. 116*, 8007-8014.

86. Ling, J., Sahlin, M., Sjöberg, B.-M., Loehr, T. M., and Sanders-Loehr, J. (1994) Dioxygen is the Source of the μ-oxo Bridge in Iron Ribonucleotide Reductase, *J. Biol. Chem. 269*, 5595-5601.

87. Tong, W., Burdi, D., Riggs-Gelasco, P., Chen, S., Edmondson, D., Huynh, B. H., Stubbe, J., Han, S., Arvai, A., and Tainer, J. (1998) Characterization of Y122F R2 of *Escherichia coli* ribonucleotide reductase by time-resolved physical biochemical methods and X-ray crystallography, *Biochemistry 37*, 3840-3848.

88. Sturgeon, B. E., Burdi, D., Chen, S., Huynh, B. H., Edmondson, D. E., Stubbe, J., and Hoffman, B. M. (1996) Reconsideration of X, the diiron intermediate formed during cofactor assembly in *E. coli* ribonucleotide reductase, *J. Am. Chem. Soc. 118*, 7551-7557.

89. Bollinger, J. M., Jr., Chen, S., Parkin, S. E., Mangravite, L. M., Ley, B. A., Edmondson, D. E., and Huynh, B. H. (1997) Differential iron(II) affinity of the sites of the diiron cluster in R2 of *Escherichia coli* ribonucleotide reductase: tracking the individual sites through the O_2 activation sequence, *J. Am. Chem. Soc. 119*, 5976-5977.

90. Riggs-Gelasco, P. J., Shu, L., Chen, S., Burdi, D., Huynh, B. H., Que, L., Jr., and Stubbe, J. (1998) EXAFS characterization of the intermediate X generated during the assembly of the *Escherichia coli* ribonucleotide reductase R2 diferric tyrosyl radical cofactor, *J. Am. Chem. Soc. 120*, 849-860.

91. Burdi, D., Sturgeon, B. E., Tong, W. H., Stubbe, J., and Hoffman, B. M. (1996) Rapid freeze-quench ENDOR of the radical X intermediate of *Escherichia coli* ribonucleotide reductase using $^{17}O_2$ and $H_2{}^{17}O$, *J. Am. Chem. Soc. 118*, 281-282.

92. Burdi, D., Willems, J.-P., Riggs-Gelasco, P., Antholine, W. E., Stubbe, J., and Hoffman, B. M. (1998) The core structure of X generated in the assembly of the diiron cluster of ribonucleotide reductase: $^{17}O_2$ and $H_2{}^{17}O$ ENDOR, *J. Am. Chem. Soc. 120*, 12910-12919.

93. Willems, J.-P., Lee, H.-I., Burdi, D., Doan, P. E., Stubbe, J., and Hoffman, B. M. (1997) Identification of the protonated oxygenic ligands of ribonucleotide reductase intermediate X by Q-Band 1,2H CW and Pulsed ENDOR, *J. Am. Chem. Soc. 119*, 9816-9824.

94. Mitic, N., Saleh, L., Schenk, G., Bollinger, J. M., Jr., and Solomon, E. I. (2003) Rapid-freeze-quench magnetic circular dichroism of intermediate X in ribonucleotide reductase: new structural insight, *J. Am. Chem. Soc. 123*, 11200-11201.

95. Tong, W. H., Chen, S., Lloyd, S. G., Edmondson, D. E., Huynh, B. H., and Stubbe, J. (1996) Mechanism of assembly of the diferric cluster-tyrosyl radical cofactor of *Escherichia coli* ribonucleotide reductase from the diferrous form of the R2 subunit, *J. Am. Chem. Soc. 118*, 2107-2108.

96. Baldwin, J., Krebs, C., Ley, B. A., Edmondson, D. E., Huynh, B. H., and Bollinger, J. M., Jr. (2000) Mechanism of rapid electron transfer during oxygen activation in the R2 subunit of *Escherichia coli* ribonucleotide reductase. 1. Evidence for a transient tryptophan radical, *J. Am. Chem. Soc. 122*, 12195-12206.

97. Solar, S., Getoff, N., Surdhar, P. S., Armstrong, D. A., and Sing, A. (1991) Oxidation of tryptophan and N-methylindole by N_3•, Br^{2-}, and $(SCN)^{2-}$ radicals in

light-and heavy-water solutions: A pulse radiolysis study, *J. Phys. Chem. 95*, 3639-3643.

98. Mishra, A. K., Chandrasekar, R., Faraggi, M., and Klapper, M. H. (1994) Long-range electron transfer in peptides. Tyrosine reduction of the indolyl radical: reaction mechanism, modulation of reaction rate, and physiological considerations, *J. Am. Chem. Soc. 116*, 1414-1422.

99. Finzel, B. C., Poulos, T. L., and Kraut, J. (1984) Crystal structure of yeast cyrochrome c peroxidase refined at 1.7 Å resolution, *J. Biol. Chem. 259*, 13027-13036.

100. Erman, J. E., Vitello, L. B., Mauro, J. M., and Kraut, J. (1989) Detection of an oxyferryl porphyrin π-cation-radical intermediate in the reaction between hydrogen peroxide and a mutant yeast cytochrome c peroxidase. Evidence for tryptophan-191 involvement in the radical site of compound I, *Biochemistry 28*, 7992-7995.

101. Houseman, A. L. P., Doan, P. E., Goodin, D. B., and Hoffman, B. M. (1993) Comprehensive explanation of the anomalous EPR spectra of wild-type and mutant cytochrome c peroxidase compound ES, *Biochemistry 32*, 4430-4443.

102. Miller, M. A., Han, G. W., and Kraut, J. (1994) A cation binding motif stabilizes the compound I radical of cytochrome c peroxidase, *Proc. Natl Acad. Soc. U.S.A. 91*, 11118-11122.

103. Elgren, T. E., Lynch, J. B., Juarez-Garcia, C., Münck, E., Sjöberg, B.-M., and Que, L., Jr. (1991) Electron transfer associated with oxygen activation in the B2

protein of ribonucleotide reductase from *Escherichia coli*, *J. Biol. Chem. 266*, 19265-19268.

104. Krebs, C., Chen, S., Baldwin, J., Ley, B. A., Patel, U., Edmondson, D. E., Huynh, B. H., and Bollinger, J. M., Jr. (2000) Mechanism of rapid electron transfer during oxygen activation in the R2 subunit of *Escherichia coli* ribonucleotide reductase. 2. Evidence for and consequences of blocked electron transfer in the W48F variant, *J. Am. Chem. Soc. 122*, 12207-12219.

105. Parkin, S. E., Chen, S., Ley, B. A., Mangravite, L., Edmondson, D. E., Huynh, B. H., and Bollinger, J. M., Jr. (1998) Electron injection through a specific pathway determines the outcome of oxygen activation at the diiron cluster in the F208Y mutant of *Escherichia coli* ribonucleotide reductase protein R2, *Biochemistry 37*, 1124-1130.

106. Bollinger, J. M., Jr., Krebs, C., Vicol, A., Chen, S., Ley, B. A., Edmondson, D. E., and Huynh, B. H. (1998) Engineering the diiron site of *Escherichia coli* ribonucleotide reductase protein R2 to accumulate an intermediate similar to Hperoxo, the putative peroxodiiron(III) complex from the methane monooxygenase catalytic cycle, *J. Am. Chem. Soc. 120*, 1094-1095.

107. Moënne-Loccoz, P., Baldwin, J., Ley, B. A., Loehr, T. M., and Bollinger, J. M., Jr. (1998) O_2 activation by non-heme diiron proteins: identification of a symmetric μ-1,2-peroxide in a mutant of ribonucleotide reductase, *Biochemistry 37*, 14659-14663.

108. Baldwin, J., Krebs, C., Saleh, L., Stelling, M., Huynh, B. H., Bollinger, J. M., Jr., and Riggs-Gelasco, P. (2003) Structural characterization of the peroxodiiron (III)

intermediate generated during oxygen activation by the W48A/D84E variant of ribonucleotide reductase protein R2 from *Escherichia coli*, *Biochemistry 42*, 13269-13279.

109. Voegtli, W. C., Khidekel, N., Baldwin, J., Ley, B. A., Bollinger, J. M., Jr., and Rosenzweig, A. C. (2000) Crystal structure of the ribonucleotide reductase R2 mutant that accumulates a μ-1,2-peroxodiiron(III) intermediate during oxygen activation, *J. Am. Chem. Soc. 122*, 3255-3261.

Chapter 2

Mediation by Indole Analogs of Electron Transfer during Oxygen Activation in Variants of *Escherichia coli* Ribonucleotide Reductase R2 Lacking the Electron-Shuttling Tryptophan 48[*]

[*]The first four authors in this published work made equal experimental contributions to it. The original manuscript was written by the first author.

FOOTNOTES

[1]Abbreviations: R2, R2 subunit of *Escherichia coli* ribonucleotide reductase; ET, electron transfer; Y122•, tyrosyl radical in *E. coli* R2; $W48^{+\bullet\bullet}$, tryptophan 48 cation radical; equiv, equivalents; wt, wildtype; k_{obs}, observed apparent first-order rate constant; 3-MI, 3-methylindole; EPR, electron paramagnetic resonance; PMSF, phenylmethylsulfonyl fluoride; Tris, *tris*-[hydroxymethyl]-aminomethane; Hepes, 4-(2-hydroxyethyl)-1-piperazineethanesulfonic acid; PCR, polymerase chain reaction; bp, base pairs; v/v, volume/volume; Buffer A, 50 mM Tris•HCl, pH 7.6, containing 10% (v/v) glycerol; Buffer B, 100 mM Na-Hepes, pH 7.6 containing 10% (v/v) glycerol.

[2]The most mechanistically detailed evidence (discussed herein) has come from investigations of *E. coli* R2 and its W48-substituted variants, but studies on mouse R2 and its variants with the counterpart to W48 (W103) substituted have also been consistent with a role for this residue in electron transfer to the diiron cluster during O_2 activation (see references 16 and 33).

ABSTRACT

Activation of dioxygen by the carboxylate-bridged diiron(II) cluster in the R2 subunit of class I ribonucleotide reductase from *Escherichia coli* results in the one-electron oxidation of tyrosine 122 (Y122) to a stable radical (Y122•). A key step in this reaction is the rapid transfer of a single electron from a near-surface residue, tryptophan 48 (W48), to an adduct between O_2 and the diiron(II) cluster to generate a readily reducible cation radical ($W48^{+\bullet}$) and the formally Fe(IV)Fe(III) intermediate known as cluster **X**. Previous work showed that this electron injection step is blocked in the R2 variant with W48 replaced by phenylalanine [Krebs, C; Chen, S; Baldwin, J; Ley, B. A., Patel, U; Edmondson, D. E.; Huynh, B. H.; and Bollinger, J. M., Jr. (2000) *J. Am. Chem. Soc. 122*, 12207-12219]. In this study, we show that substitution of W48 with alanine similarly disables the electron transfer (ET) but also permits its chemical mediation by indole compounds. In the presence of an indole mediator, O_2 activation in the R2-W48A variant produces approximately one equivalent of stable Y122• and more than one equivalent of the normal (μ-oxo)diiron(III) product. In the absence of a mediator, the variant protein generates primarily altered Fe(III) products and only one-fourth as much stable Y122•, because, as previously reported for R2-W48F, most of the Y122• that is produced decays as a consequence of the inability of the protein to mediate reductive quenching of one of the two oxidizing equivalents of the initial diiron(II)-O_2 complex. Mediation of ET is effective in W48A variants containing additional substitutions that also impact the reaction mechanism or outcome. In the reaction of R2-W48A/F208Y, the presence of mediator suppresses formation of the Y208-derived diiron(III)-catecholate product

(which is predominant in R2-F208Y in the absence of reductants) in favor of Y122•. In the reaction of R2-W48A/D84E, the presence of mediator affects the outcome of decay of the peroxodiiron(III) intermediate known to accumulate in D84E variants, increasing the yield of Y122• by as much as 2.2-fold to a final value of 0.75 equivalents and suppressing formation of a 490-nm-absorbing product that results from decay of the two-electrons-oxidized intermediate in the absence of a functional ET apparatus.

INTRODUCTION

The R2 subunit of ribonucleotide reductase from *Escherichia coli* (hereafter, simply R2[1]) uses a diiron(II) cluster to activate oxygen for the production of its catalytically essential cofactor, an oxo-bridged diiron(III) cluster and adjacent tyrosyl radical (Y122•) (*1-6*). The latter is formed via one-electron oxidation of the Y122 phenol (*1, 3*). It is proposed that the R2 cofactor functions by generating a reactive thiyl radical from C439 in the R1 subunit (*7-10*), which, in turn, is responsible for the homolytic scission of the 3' C-H bond of the nucleoside diphosphate substrate in the key step of the catalytic mechanism (*11*). In this way, the tyrosyl radical of R2 stores an oxidizing equivalent for use in catalysis by R1, and is, therefore, essential for nucleotide reduction. Computational analysis of possible docking modes for R1 and R2 from the structures of the individual subunits suggests that C439 in R1 would be located ~ 35 Å away from the Y122 residue in R2 (*10*), too far removed to accept an electron at the required rate by direct electron transfer (*12*). The oxidizing equivalent is thought to be transferred between these two residues via a pathway involving conserved amino acid residues (Tyr122-Asp84-His118-Asp237-Trp48-Tyr356 in *E. coli* R2 and Tyr731-Tyr730-Cys439 in R1) (*13-16*). Proposed mechanisms for this transfer have invoked either coupled proton and electron transfer (*12*) to create intermediate neutral radicals along the pathway or "hydrogen atom transfer along the hydrogen-bonded chain" (*17*). However, no direct demonstration of radical transfer between these residues has yet been reported, because a conformational change rate-limits the catalytic reaction and prevents accumulation of states having the oxidizing equivalent on residues other than Y122 (*12*).

The assembly of the cofactor in *E. coli* R2 is spontaneous *in vitro* (*1*). Upon incubation with Fe(II) and O_2, apo R2 first binds Fe(II) ions and then uses the diiron(II) cluster to reductively activate O_2 to effect the one-electron oxidation of Y122 to its radical form (*1, 18-22*). The four-electron reduction of molecular oxygen to water at the diiron site is balanced by oxidation of two Fe(II) ions to Fe(III), oxidation of Y122 to its radical form, and transfer of an "extra" electron from outside the protein to the reacting diiron cluster (*19, 23, 24*). The only intermediate iron complex that has been definitively identified in the reaction of R2-wt is the formally Fe(IV)Fe(III) cluster **X** (*18, 25-31*), which can oxidize Y122 in the final and rate-determining step, thereby also forming the (μ-oxo)diiron(III) cluster (*18, 19*). The oxidation state of **X** establishes that the transfer of the "extra" electron occurs during formation of the intermediate. This transfer occurs via an electron-shuttling mechanism, in which the near-surface residue, tryptophan (W) 48, is transiently oxidized to a cation radical ($W48^{+\bullet}$) by the as-yet-unidentified, one-electron-more-oxidized precursor to cluster **X** (hereafter designated as $(Fe_2O_2)^{4+}$) (*20, 32*). The $W48^{+\bullet}$ is rapidly reduced by exogenous reductants (e.g. ascorbate, $Fe(II)_{aq}$, thiols, etc.), completing the two-step electron transfer (ET) process (*32*). The oxidation of W48 in formation of the **X**-$W48^{+\bullet}$ state is sufficiently rapid to prevent accumulation of the $(Fe_2O_2)^{4+}$ precursor (*32*), explaining why the identity of this complex has not yet been definitively established.

The importance of W48 in the ET step has been demonstrated in several ways (*16, 33*).[2] In the reaction of R2-W48F, the $(Fe_2O_2)^{4+}$ intermediate oxidizes Y122 directly, due to the absence of its normal co-reactant, W48 (*34*). Y122• is produced ten-fold more rapidly ($9 \pm 2\ s^{-1}$ at 5 °C (*34*)) by this altered pathway than by cluster **X** in the reaction of

R2-wt (0.8 ± 0.2 s^{-1} at 5 °C (*19, 22, 25, 32*)). In the R2-W48F reaction, Y122• forms as part of a "di-radical" species that also contains **X** (*34*). The presence of both oxidized species in the active site, which is revealed by dipolar and weak exchange coupling that perturbs the Mössbauer spectrum of **X** and the electron paramagnetic resonance (EPR) spectra of both constituents, implies that ET has not occurred. Presumably as a result of the proximity of **X** and Y122• and the inability of the protein to support the reduction of either, the Y122• thus produced is not stable. The majority decays along with **X** in an uncharacterized reaction that also yields altered iron products. A sub-stoichiometric quantity (~ 0.25 equiv) of Y122• does not decay, probably as a result of very inefficient ET ("leaking") to **X** occurring in competition with the decay process. This Y122• is then as stable as in R2-wt, confirming that the transient behavior of Y122• is not a reflection of an inherent instability of the radical in the variant protein. The latter point is emphasized by the observation that inclusion of 2 mM dithionite in the reaction rescues Y122• from decay by forcing reduction of **X** to the normal □-(oxo)diiron(III) cluster (*34*). Thus, the ten-fold faster formation and transient behavior of Y122• and the altered iron products observed in the R2-W48F reaction are the specific hallmarks of blocked ET.

Further evidence for the electron-shuttling role of W48 has come from investigation of variants of R2 containing the F208Y substitution, which introduces an endogenous two-electron reductant (Y208) that effectively competes with the normal one-electron injection step (*35, 36*). Thus, O_2 activation in R2-F208Y results in a partition between hydroxylation (two-electron oxidation) of Y208 (*35, 36*) and the normal one-electron oxidation of Y122 (*37*). In the presence of a sufficient concentration (> 10 mM) of the facile one-electron reductant, ascorbate, the one-electron oxidation

outcome (Y122• formation) becomes predominant, presumably because the ET step necessary for this outcome is accelerated. Disabling ET by substitution of W48 with F prevents Y122• formation and makes Y208 hydroxylation the exclusive outcome, irrespective of ascorbate concentration (*37*).

In this study, we provide additional evidence for the proposed electron-shuttling role of W48 by showing that ET can be mediated by indole compounds in variants of R2 lacking W48. The experiments were formulated according to the chemical rescue approach pioneered by Kirsch and co-workers (*38*). In this approach, replacement of a functionally important residue by one with a small, non-functional side-chain (generally alanine or glycine) is intended to create an empty pocket that can be filled by a small molecule that mimics the deleted side-chain in both structure and function. Although the method has been widely used in recent years, studies by Goodin and co-workers on yeast cytochrome c peroxidase provided an example that was particularly inspirational for our study. In the catalytic cycle of yeast cytochrome c peroxidase, a tryptophan residue (W191), which resides in a hydrogen-bonded network similar to that in R2 involving W48, becomes oxidized to a cation radical in formation of the compound I (or compound ES) intermediate (*39-42*). Goodin and colleagues were able to demonstrate both binding and oxidation of cationic heterocycles bound in the pocket created by replacement of W191 with glycine (*43-46*). Analogously, we replaced W48 in R2 with alanine (A) or glycine (G) and tested indole (Figure 1) and its derivatives for the ability to impact the reaction outcome by mediating the otherwise-defective ET. Although the results are conflicting as to whether the intended mechanism (i.e., authentic chemical rescue) is actually operant, mediation of ET is definitively demonstrated by analysis of the products

Figure 2-1: Indole.

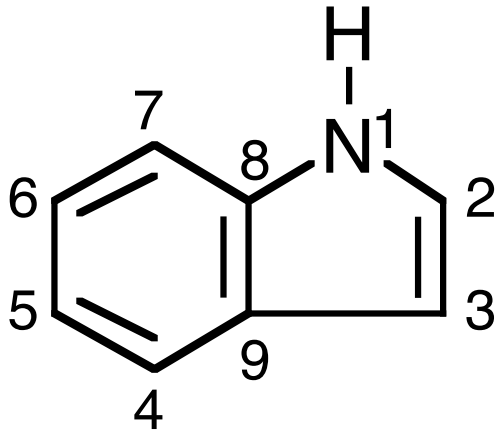
H
N
1
2
3
4
5
6
7
8
9

of the O_2 reactions, both in the absence and presence of indole compounds, of R2-W48A and two variants with additional substitutions (F208Y or D84E) that also impact the reaction mechanism and outcome (*35-37, 47, 48*). Thus, the results are not only consistent with the role of W48 in the ET step but also provide a means to trigger ET by addition of a small molecule. In the work described in the accompanying manuscript (*49*), this small-molecule trigger has permitted kinetic resolution of the spectroscopic signatures of a heretofore uncharacterized $(Fe_2O_2)^{4+}$ intermediate state that may be the precursor to cluster **X** in the reaction of wild-type R2.

MATERIALS AND METHODS

Materials. Culture media components (yeast extract and tryptone) were purchased from Marcor Development Corporation (Hackensack, NJ). Isopropy-□-D-thiogalactopyranoside (IPTG) was purchased from Biosynth International (Naperville, IL). Ampicillin was purchased from IBI (Shelton, CT). Phenylmethylsulfonyl fluoride (PMSF), streptomycin sulfate, Trizma base (Tris), and 1,10-phenanthroline were purchased from Sigma (St. Louis, MO). Glycerol, ammonium sulfate, and sodium chloride were purchased from EM Science (Gibbstown, NJ). Enzyme grade 4-(2-hydroxyethyl)-1-piperazineethanesulfonic acid (HEPES) was purchased from FisherBiotech (Pittsburgh, PA). Oligonucleotide primers were purchased from Invitrogen (Frederick, MD). Reagents for the polymerase chain reaction (PCR) and restriction enzymes were purchased from New England Biolabs (Beverly, MA). T4 DNA ligase was purchased from Roche (Indianapolis, IN). BL21(DE3) and pET vectors were purchased from Novagen (Madison, WI).

Preparation of Expression Vectors for R2-W48A, R2-W48A/F208Y, and R2-W48A/D84E. The W48G substitution was introduced into the *nrdB* gene (encoding R2), with and without the F208Y substitution, by using the polymerase chain reaction (PCR) and the previously described plasmids pR2-W48F (*34*) and pR2-W48F/F208Y (*37*) as PCR templates and vectors. Primers 1 (5'-GAA GTG GCG AGC CCG ATC TTC CCC-3') and 2 (5'-GGG AGA CGT CAA CCT CCT CCG GCC G**AC C**GA AGA AAG AGA GC-3') were used to amplify a 392 base pair (bp) fragment of these plasmids. Primer 1 anneals ~110 bp 5' of a unique *Bgl*II site, which is 105 bp 5' of the start of *nrdB* in pR2-W48F and pR2-W48F/F208Y. Primer 2 introduces a unique *Eag*I restiction site (underlined) and the desired substitution at codon W48 (TGG to GGT, complement of boldface triplet) and also spans the unique *Aat*II restriction site (double underlined) in codon V55 of *nrdB*. The PCR fragment was digested with *Bgl*II and *Aat*II and ligated with the large fragment generated by digestion of pR2-W48F or pR2-W48F/F208Y with the same enzymes. The *Eag*I restriction site introduced in the pR2-W48G/F208Y plasmid was exploited to prepare the pR2-W48A/F208Y plasmid. Primers 1 and 3 (5'-CTC CTC CGG CCG **CGC** GAA GAA AGA GAG C-3') were used to generate a 378 bp PCR fragment consisting of nucleotides 1 through 159 of coding sequence, 111 nucleotides of vector sequence upstream of the start codon (3' of the *Bgl*II restriction site), and 108 additional nucleotides 5' of the *Bgl*II site. Primer 3 also introduces the desired G48>A substitution (TGG to GCG, complement of boldface triplet). The PCR product was digested with *Bgl*II and *Eag*I and then ligated with the large fragment from digestion of pR2-W48G/F208Y with the same enzymes. The plasmid pR2-W48A was prepared by restriction digest of pR2-W48A/F208Y with *Eag*I and *Bgl*II to yield a 276 bp

fragment. This insert was ligated with the large fragment from digestion of pR2-W48G with the same enzymes. To construct pR2-W48A/D84E, the 268 bp *Bgl*II to *Aat*II restriction fragment (containing codons 1-52) from pR2-W48A/F208Y was joined with the large fragment from digestion of pR2-D84E (constructed as previously described (*50*)) with the same enzymes. The sequence of the coding region of each plasmid construct was verified to ensure that no undesired mutations had been introduced. DNA sequences were determined by the Nucleic Acid Facility of the Pennsylvania State University Biotechnology Institute.

Over-expression and Purification of W48 Variants of R2. Successful over-expression and purification of W48A-containing variants of R2 required modifications to the existing protocol (*34, 37*). Inclusion of 10% (volume/volume (v/v)) glycerol in the culture medium and buffers used in purification was found to enhance both the yield and quality (purity and quantity of Fe(II) incorporated) of W48A variants. *E. coli* strain BL21(DE3) transformed with the appropriate plasmid was grown with vigorous aeration at 37 C in enriched medium containing 35 g/L tryptone, 20 g/L yeast extract, 5 g/L NaCl, 0.15 g/L ampicillin, and 10% (v/v) glycerol. Details of the fermentation protocol have been described (*34*). The yield was approximately 20 grams of wet cell paste per liter of medium. In a typical purification, 60 grams of the frozen cell paste was thawed and resuspended at 4 C in 300 mL of buffer A (50 mM Tris, pH 7.6, 10% (v/v) glycerol) containing 0.25 mM PMSF and 1 mM 1,10-phenanthroline. Cell lysis and streptomycin sulfate precipitation steps were carried out as previously described (*37*). An additional ammonium sulfate precipitation step, in which the solution was brought to 30% of saturation and the supernatant was recovered, was performed in addition to the 60% (of

saturation) ammonium sulfate fractionation step used in earlier protocols (*19, 37, 51*). The pellet from the latter was redissolved in buffer A (1 mL/g wet cell pellet) containing 0.25 mM PMSF and 1 mM 1,10-phenanthroline, and this solution was dialyzed for 4 hours against 6 L of buffer A. An equal volume of buffer A containing 0.25 mM PMSF was added to the dialysate, and the solution was loaded onto a 5 cm x 40 cm (0.6 L) Q-sepharose Fast Flow (Pharmacia) column equilibrated in buffer A. The column was washed with 0.3 L of buffer A, followed by 1 L of buffer A containing 225 mM NaCl. The protein was eluted with buffer A containing 300 mM NaCl. Fractions containing protein (as judged by their light absorption spectra) were pooled (0.5 L), and the pool was concentrated 50-fold by ultrafiltration in an Amicon cell equipped with a YM30 membrane. The protein was dialyzed against 100 mM Na-Hepes buffer, pH 7.6 containing 10% (v/v) glycerol (buffer B), flash-frozen in liquid nitrogen, and stored at -80 °C. Denaturing polyacrylamide gel electrophoresis revealed the protein to be > 95% pure. A typical yield was 20 mg per gram cell paste.

Protein concentrations were determined spectrophotometrically by using molar absorption coefficients at 280 nm (ε_{280}) calculated according to the method of Gill and von Hippel (*52*). Values were 108 $mM^{-1}cm^{-1}$ for apo-R2-W48A and apo-R2-W48A/D84E and 111 $mM^{-1}cm^{-1}$ for apo-R2-W48A/F208Y.

Products of the Reaction of R2-W48A Variants with Fe(II) and O_2 Monitored by UV-visible Absorption Spectroscopy. Stock solutions (100-fold more concentrated than the desired final concentration in the reaction) of indole derivatives were prepared in 100% ethanol. A 3.5 L aliquot of this stock solution was added to 350 L of air-saturated apo protein (85-130 M) in buffer B. This solution was incubated on ice for 5

min. The reaction was then initiated by addition of 3.5 equiv of Fe(II) from a stock solution (typically 20-35 times the final concentration) of ferrous ammonium sulfate in 5 mN H_2SO_4. The cuvette was quickly capped and mixed by inversion. The absorption spectrum of the sample was recorded on a Hewlett-Packard HP8453 spectrophotometer. The concentration of the tyrosyl radical was calculated as previously described (*19*) from the 411-nm peak height [$A_{411} - (A_{405} + A_{417})/2$] using a molar extinction coefficient ($\Delta\varepsilon_{411 - (405 + 417)/2}$) = 2400 M^{-1} cm^{-1}. This value is significantly greater than that characteristic of the Y122• in the wild-type protein. It was determined (as previously described (*19*)) by comparison of $A_{411} - (A_{405} + A_{417})/2$ for a series of samples to the concentration of Y122• determined directly by EPR spectroscopy.

Stopped-Flow Absorption Spectrophotometry. All stopped-flow measurements were performed using a KinTek Corporation Model SF-2001 spectrofluorimeter (path length 0.5 mm, deadtime 3 ms), which was equipped with a Gilford Model 240 light source and was housed in an anoxic chamber (MBraun). Solutions of apo R2 variants were rendered free of oxygen on a vacuum/gas manifold and then mixed with Fe(II) in the anoxic chamber, as previously reported (*37*). Stock solutions (typically 100-fold more concentrated than the desired final concentration in the reaction) of indole derivatives were prepared in O_2-free 100% ethanol solution in the anoxic chamber and then added to the protein or diluted to the desired concentration with oxygen-free buffer B. Reaction conditions are given in the appropriate figure legends.

Mössbauer Spectroscopy. Mössbauer spectra were acquired at 4.2 K with a magnetic field of 50 mT applied parallel to the incident γ-beam. The spectrometer has been described previously (*26*).

RESULTS

Preparation of "Active" W48A-containing R2 Variants. Expression and purification of R2 variants with the substitutions, W48>A or W48>G, according to the established procedures (*37*) was only moderately successful. Low yield in the purification (< 8 mg/ gram cell paste), reduced Fe(II) uptake capacity (1-2 equiv), and poor yields of Y122• (even in the presence of an indole mediator) were observed. The poor "activity" of such variants could result from a conformational change that does not grossly affect the proteins' physical properties or behavior during purification. This problem was successfully overcome by over-expressing and purifying R2-W48A(G) variants in the presence of 10% (v/v) glycerol. For the case of R2-W48A, inclusion of glycerol improves the protein yield nearly 3-fold (to 20-25 mg/g wet cell paste). In addition, the protein obtained takes up nearly as much Fe(II) (~ 3.2 equiv) and produces nearly as much stable Y122• (in the presence of mediator) as the wild-type protein. Therefore, it seems that glycerol both activates these unstable variants by facilitating their otherwise inefficient folding and stabilizes them against subsequent inactivation. The "chemical chaperoning" capacity of glycerol has previously been noted in other contexts (*53, 54*).

Characterization of O_2 Activation by R2-W48A in the Absence of ET Mediators by UV-Visible Absorption Spectroscopy. Mixing of apo R2-W48A and Fe(II) in the presence of O_2 leads to the development of the 411-nm absorption characteristic of the tyrosyl radical product (Figure 2, dot-dashed trace). The 411-nm peak height [$A_{411} - (A_{405} + A_{417})/2$] at completion shows that the amount of Y122• formed in this reaction (0.28 ± 0.05 equiv) is essentially the same as that produced in R2-W48F (0.25 ± 0.03

Figure 2-2: Absorption spectra of products formed upon addition of Fe(II) to air-saturated solutions of apo R2 variants: R2-W48A (dot-dashed trace), R2-W48F (thinner dashed trace), R2-wt (dotted trace), R2-W48A in the presence of 1 mM 3-MI (solid trace), and R2-W48F in the presence of 1 mM 3-MI (thicker dashed trace). All protein concentrations were 0.10 mM, and 3.5 equiv Fe(II) were added to all samples with the exception of R2-W48F (3.0 equiv added). The inset shows the dependence of the final concentration of Y122• on the concentration of 3-MI in the R2-W48A reaction. The protein concentration was 0.12 mM in this experiment. The solid trace in the inset is a fit of the equation for a hyperbola to the data and corresponds to a $K_{0.5}$ of 9 μM and a limiting slope of 10 Y122•/3-MI.

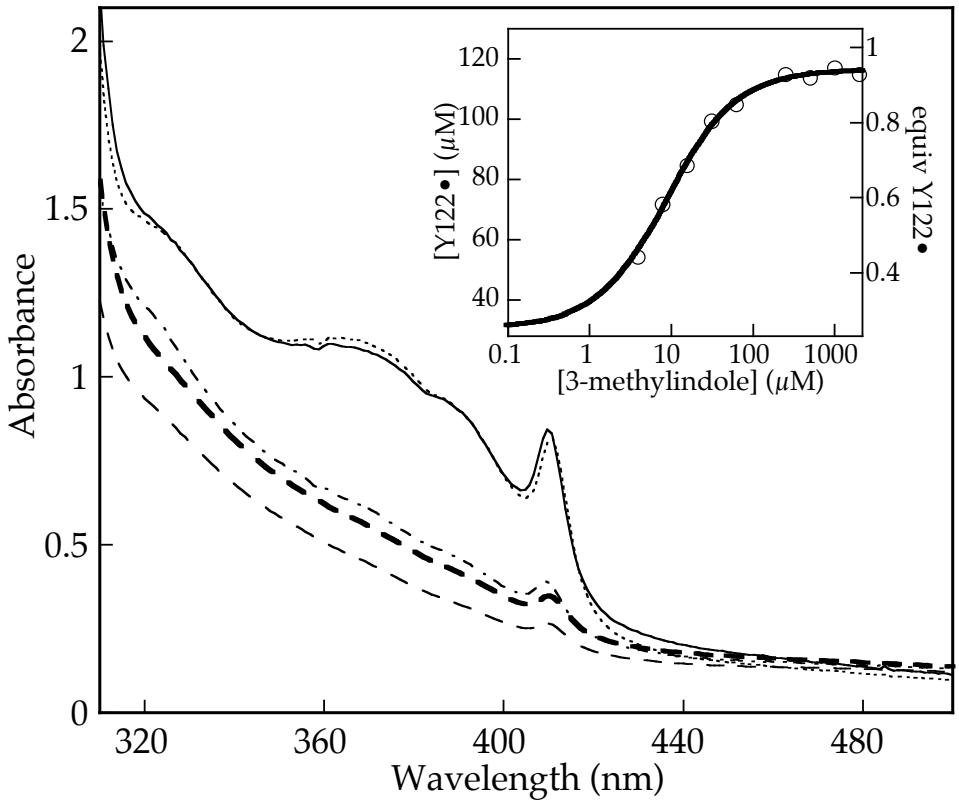
Absorbance
Wavelength (nm)
2
1.5
1
0.5
0
320
360
400
440
480
[Y122•] (μM)
equiv Y122•
[3-methylindole] (μM)
120
100
80
60
40
1
0.8
0.6
0.4
0.1
1
10
100
1000

equiv, Figure 2, thinner dashed trace). Both reactions yield much less Y122• than does the reaction of R2-wt (1.2 ± 0.1 equiv; Figure 2, dotted trace). The kinetic trace of the 411-nm peak height for the reaction of Fe(II)-R2-W48A with excess O_2 (Figure 3, triangular points) shows that, as in the reaction of R2-W48F, the poor Y122• yield is a result of the transient nature of the radical rather a failure of the radical to form at all. After an initial lag phase (k_{obs}= 40 ± 6 s^{-1}), Y122• is formed rapidly (k_{obs}= 6 ± 1 s^{-1}), reaching a maximum of 0.8 ± 0.1 equiv, and then decaying slowly (k_{obs} of 0.19 ± 0.02 s^{-1}) to its final value of 0.28 ± 0.05 equiv. Thus, the kinetics and final stoichiometry of Y122• production in the absence of mediator are strikingly similar to those previously observed in the R2-W48F reaction (*34*). The simplest interpretation is that the mechanisms of the two reactions are identical (oxidation of Y122 by the $(Fe_2O_2)^{4+}$ intermediate to form the **X**-Y122• "di-radical" species, then decay of Y122• due to its reaction with the adjacent **X**).

Mediation of ET in R2-W48A by 3-Methylindole (3-MI). The absorption spectrum of the products of the reaction of apo R2-W48A with excess Fe(II) and O_2 in the presence of 1 mM 3-MI (Figure 2, solid trace) is nearly indistinguishable from that of the products of the R2-wt reaction (dotted trace). The reaction yields ~ 3.3 times as much Y122• (1.0 ± 0.1 equiv) as in the absence of 3-MI, giving a maximal Y122•/R2 stoichiometry that is similar to that for R2-wt (1.2 ± 0.1 equiv). The presence of the same concentration of 3-MI increases the Y122• yield in the R2-W48F reaction to a much lesser extent (only 1.4-fold; Figure 2, thicker dashed trace). Moreover, 3-MI has an insignificant effect (< 1.1-fold increase) on the R2-W48F reaction at a concentration of 100 μM (not shown), which is sufficient to give > 90% of the maximal yield of Y122• in R2-W48A (Figure 2, inset).

The R2-W48Y reaction is similarly insensitive to the presence of 3-MI (not shown). The indole compound has no effect on the Y122• yield in the wild-type protein, even at a concentration of 1 mM. Conversely, ascorbate, a facile one-electron reductant that increases the overall yield and Y122•/Fe(II) stoichiometry in the reaction of R2-wt by providing the "extra" electron and thereby sparing Fe(II) from sacrificial oxidation, by itself has a minor effect on the Y122• yield in the R2-W48A reaction (< 30% increase at 0.5 mM ascorbate; Figure S1, compare red and blue traces). The markedly diminished susceptibility of the R2-W48F and R2-W48Y reactions to 3-MI and the relative insensitivity of the R2-W48A reaction to the presence of the thermodynamically better reductant (ascorbate) that functions efficiently when the electron-shuttling W48 is present suggest that the effect of the mediator is dependent on its binding specifically in the pocket created by truncation of the W48 sidechain. However, as presented below, other evidence seems to contradict this conclusion.

Y122• formation in the R2-W48A reaction in the presence of 1 mM 3-MI exhibits three kinetic phases (Figure 3, circular points): a lag phase of rate constant similar to that for the lag phase in the absence of the mediator, followed by two formation phases. The faster formation phase, which contributes ~ 60% of the total amplitude, has k_{obs} of 6 ± 1 s^{-1} and the slower phase (~ 40%) a k_{obs} of 0.8 ± 0.2 s^{-1}. The latter is identical with k_{obs} for Y122• production by **X** in the R2-wt reaction.

Verification of ET Mediation by Mössbauer Characterization of Iron Products. The formation of nearly wild-type levels of stable Y122• in R2-W48A in the presence of 3-MI suggests that the ET step, initially disabled by substitution of W48, is somehow restored by the small molecule. To corroborate this conclusion, the iron products of the

Figure 2-3: Kinetics of Y122• formation (as determined by the 411-nm peak height) in the reaction of Fe(II)-R2-W48A complex (3.5 equiv Fe) with O_2 (1.2 mM) at 5 C in the absence (triangular points) and presence (circular points) of 1 mM 3-MI. The final protein concentration was 0.12 mM. The solid line over the circular points (with 3-MI) is a fit of the equation for a single lag (k_{obs} = 38 s^{-1}) and two parallel first-order growth phases with rate constants of 6 s^{-1} and 0.8 s^{-1} and amplitudes of 0.36 and 0.62 equiv Y122•, respectively. The solid line over the triangular points (without 3-MI) is a simulation according to the published mechanism of the R2-W48F reaction (*34*) with rate constants of 45 s^{-1} for the lag in Y122• production (formation of the $(Fe_2O_2)^{4+}$ intermediate), 5.5 s^{-1} for formation of Y122• (as part of the "**X**-Y122• di-radical species"), 0.135 s^{-1} for decay of the Y122• to non-radical products, and 0.055 s^{-1} for the competing process in which an electron "leaks" in to reduce **X** and thereby prevent the Y122• from decaying (*34*).

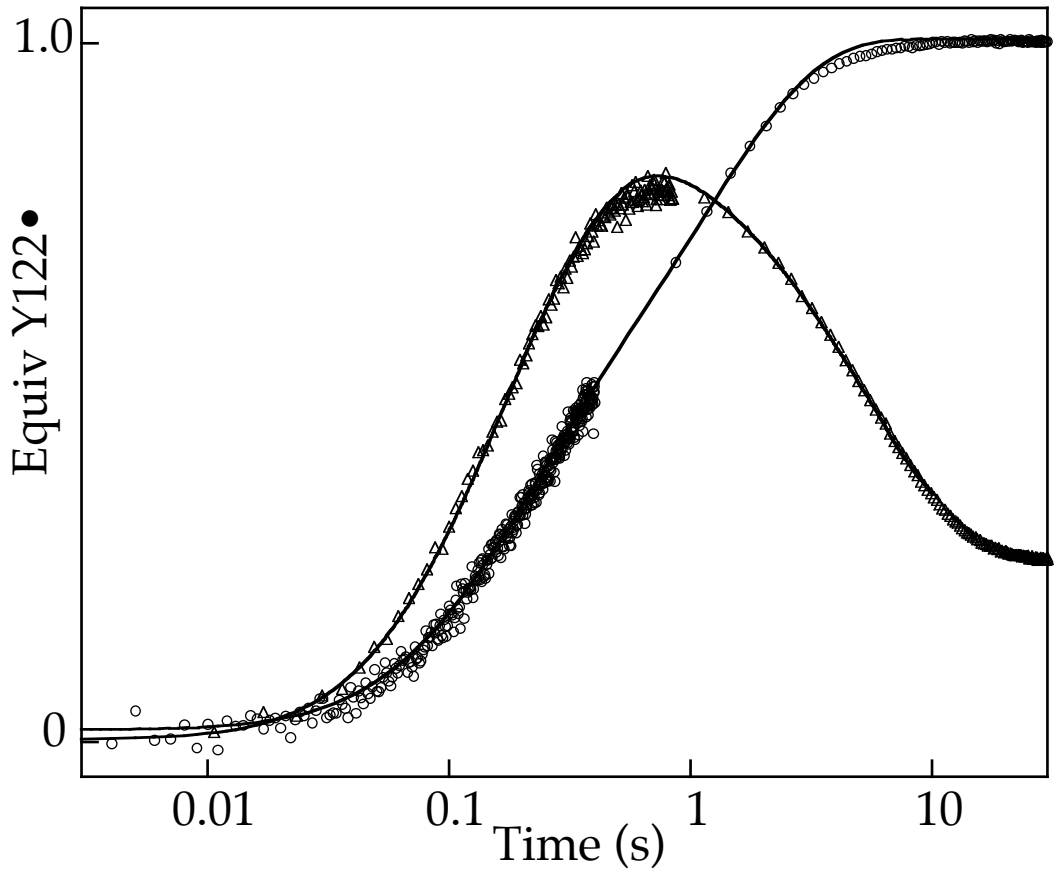
1.0
0
Equiv Y122•
0.01
0.1
1
10
Time (s)

reactions in the absence and presence of the mediator were characterized and quantified by Mössbauer spectroscopy. The spectra of product samples generated by addition at 5 °C of excess O_2 to solutions of ^{57}Fe(II)-R2-W48A (3.1 equiv Fe) reveal that three times as much of the normal (μ-oxo)diiron(III) cluster is produced in the presence of 2 mM 3-MI (Figure 4, spectrum A) than in its absence (spectrum B). The theoretical spectrum of the (μ-oxo)diiron(III) cluster (solid lines in both A and B) can account for 88% of the total absorption area (corresponding to 1.36 equiv) in A, but no more that 29% (0.45 equiv cluster) in B. The observation that altered iron products predominate in the absence of mediator underscores the similarity of the reaction of R2-W48A to the reaction of R2-W48F.

Concentration Dependencies of Mediation by Different Indole Compounds. The efficiencies of different indole compounds in mediating ET in R2-W48A (as measured by their concentration dependencies) were determined in order to assess the relative importance of steric and electronic influences. The results (Table 1) reveal that the latter are primarily, if not exclusively, important. All compounds listed in Table 1 are capable of supporting the same maximal yield of Y122• (1.0 ± 0.1 equiv), but the concentrations necessary to achieve 50% of this maximal effect ($K_{0.5}$) vary considerably. $K_{0.5}$ is approximately 12-fold less for 3-MI than for indole itself. Addition of an electron withdrawing hydroxyl group to the 3-methyl substituent (3-(hydroxymethyl)indole) increases $K_{0.5}$ by 16-fold. Conversely, separation of the hydroxyl group from the indole moiety by one additional methylene unit (3-(2-hydroxyethyl)indole) restores $K_{0.5}$ to within a factor of 3 of that for 3-MI. Compounds with exocyclic methyl substituents on atoms other than C3 (1- and 2-methylindole) are less efficient (higher $K_{0.5}$) than 3-MI.

Table 2-1: Summary of $K_{0.5}$ Values of Indole Derivatives Used in Chemical Rescue of R2-W48A and R2-W48A/F208Y.

	R2-W48A	**R2-W48A/F208Y**
Indole Derivative	**$K_{0.5}$**	**$K_{0.5}$**
1-methylindole	170 μM	not determined
2-methylindole	75 μM	not determined
3-MI	9.9 μM	1.0 mM
indole	120 μM	> 10 mM
3-(hydroxymethy)indole	450 μM	22 mM
3-(2-hydroxylethyl)indole	30 μM	6.0 mM

Figure 2-4: Mössbauer spectra of products formed after mixing at 5 ± 3 °C Fe(II)-R2-W48A (0.88 mM R2-W48A, 3.1 equiv Fe(II)) with an equal volume of O_2-saturated buffer in the presence (spectrum A) and absence (spectrum B) of 2 mM 3-MI (final concentration after mixing). The solid lines in A and B are the theoretical spectrum of the (μ-oxo)diiron(III) cluster plotted at intensities corresponding to 88% and 29%, respectively, of the experimental spectra.

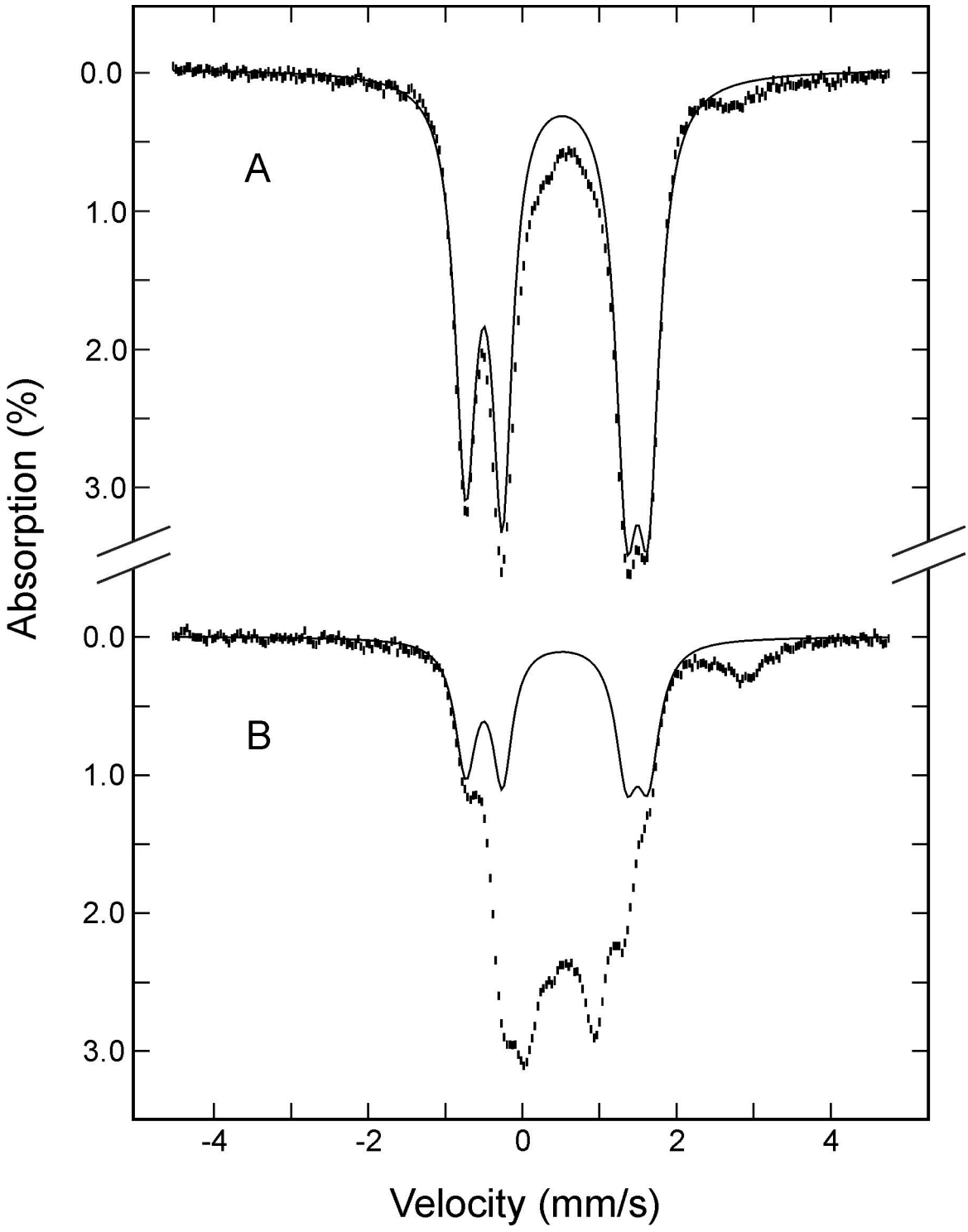
Absorption (%)
0.0
1.0
2.0
3.0
A
0.0
1.0
2.0
3.0
B
-4
-2
0
2
4
Velocity (mm/s)

These results, especially the $K_{0.5}$ values across the series 3-methylindole < 3-(2-hydroxyethyl)indole < indole and 3-(hydroxymethyl)indole, are rationalized by the fact that the spin and charge density of indolyl cation radicals is high at C3 (*55*) and, thus, that electron shuttling should be favored by the presence of an electron donating group at this position. By contrast, one would predict that, if steric considerations were important, the compounds with the bulkiest C3 substituent (3-(2-hydroxyethyl)indole) and with non-native methyl substitutions at C1 or C2 would be less efficient as mediators. This trend is not observed. In addition, the effect of the presence of a bulkier but non-aromatic sidechain at position 48 (R2-W48R, V, K, Q, or L) was examined. $K_{0.5}$ values for 3-MI with these variants were, in some cases, within a factor of 2 of that for R2-W48A. The absence of a clear steric influence on $K_{0.5}$ is potentially inconsistent with the intended mechanism of ET mediation and casts doubt on whether authentic chemical rescue is occurring.

Under the assumption that the indole compounds *do* function by authentic chemical rescue, one might be tempted to associate the $K_{0.5}$ value for a given indole compound with its dissociation constant for binding in the pocket normally filled by the W48 sidechain. This interpretation is clearly not correct. The fact can best be demonstrated by considering the concentration dependence for mediation by 3-MI. Its $K_{0.5}$ of 10 □M was determined from a series of reactions containing greater than 100 μM protein and in which a maximal increase in Y122• yield exceeding 80 μM was achieved. At a concentration of 10 μM 3-MI, the > 35 μM increase in Y122• yield (□[Y122•]) exceeds the concentration of mediator by several-fold. A limiting □[Y122•]/[3-MI] stoichiometry of 9 ± 2 can be determined from the hyperbolic fit to the data (Figure 2,

inset). In other words, 3-MI increases Y122• yield *catalytically* in the reaction of R2-W48A. Given this fact, $K_{0.5}$ clearly cannot reflect K_d for the 3-MI•R2 complex. Furthermore, if mediation of ET by 3-MI does, in fact, require prior binding of the small molecule to the protein, then the catalytic nature of the process would require that binding and dissociation both be faster than decay of the unstable Y122• in the **X**-Y122• di-radical species. The remarkable limiting □[Y122•]/[3-MI] stoichiometry of 9 establishes that 3-MI cannot be acting merely as a reductant and raises the question of what the ultimate source of the electrons is.

Identification of the Ultimate Source of the Extra Electron. One possible source of the extra electron is Fe(II). The reactions of Figure 2 were conducted by addition of excess Fe(II) (3.5 equiv) to air-saturated solutions of apo R2-W48A. Under these conditions, free Fe(II) could be present as oxygen activation takes place, depending on the kinetics of Fe(II) uptake (which have not been investigated) and the total Fe(II)/R2-W48A stoichiometry (which, from the maximal yield of μ-(oxo)diiron(III) cluster of 1.36 equiv determined in Figure 4 and the assumption that it is the exclusive protein-bound Fe product, would be estimated as ~ 2.7 equiv). $Fe(II)_{aq}$ could rapidly reduce the presumptive 3-MI cation radical, allowing Fe(II) to be the ultimate electron source for 3-MI-catalyzed ET. To test this possibility, reactions were carried out by addition of excess O_2 to solutions of the Fe(II)-R2-W48A complex formed with sufficient rather than excess Fe(II) (2.7-2.8 equiv Fe). Under these conditions, much less (or no) free Fe(II) should be present as O_2 activation takes place. In these experiments, a 3-MI concentration of 5 μM was used and a □[Y122•]/[3-MI] stoichiometry of 2.7 ± 1.0 (mean and range in three independent experiments) was measured (green trace in Figure S1). The fact that this

turnover ratio is significantly less than the value of ~ 6 seen in the experiments of Figure 2 is consistent with the notion that excess (unbound) Fe(II) served as the ultimate source of the extra electron in the latter experiments. More compellingly, under these conditions, 3-MI and ascorbate were observed to function synergistically: in the presence of both 0.5 mM ascorbate and 5 μM 3-MI (Figure S1, black trace), the increase in Y122• yield (relative to that in the absence of either, red trace) exceeded the sum of the individual effects (green and blue traces) by a factor of 1.6-1.9 (range in three experiments). After accounting for the minor enhancement in Y122• yield from ascorbate alone by subtracting it from the total Δ[Y122•], the Δ[Y122•]/[3-MI] stoichiometry was calculated to be 5.0 ± 0.5 under these conditions. The increase in the number of turnovers for the 3-MI catalyst caused by the presence of either excess Fe(II) or ascorbate indicates that, under these conditions, 3-MI serves as a mediator for ET from the reductant to the buried active site. Regardless of whether the mediator actually binds in the site vacated by the W48 sidechain, this role is directly analogous to that served by W48 in the R2-wt reaction (*19, 20, 32*).

Mediation of ET in R2-W48A/F208Y by 3-MI. As noted previously, the primary product of O_2 activation by R2-F208Y in the absence of reductants is the Y208-derived catechol (*35, 36*), but the one electron oxidation of Y122 comes to predominate in the presence of increasing concentrations of ascorbate (*37*). The effect of ascorbate is dependent on a functional electron shuttling apparatus and is eliminated by the W48F substitution (*37*). R2-W48A/F208Y, which was expected to form exclusively the hydroxylated Y208 product, was used to evaluate further the effectiveness of chemical mediation of ET by testing for the ability of indole compounds to impact the product

distribution. O_2 activation in R2-W48A/F208Y results in the development of the broad absorption band at 675 nm (Figure 5, dotted trace), which arises from □-hydroxylation of Y208 and chelation of one of the Fe(III) ions of the cluster by the resulting catechol (*35, 36*). Inclusion of 3-MI results in the production of tyrosyl radical, as reflected by the sharp absorption at 410 nm, and suppression of the 675 nm feature (Figure 5, solid trace). The yields of tyrosyl radical (triangular points and left axis in Figure 5 inset) and Fe(III)-catecholate species (circular points and right axis in Figure 5 inset) exhibit opposite hyperbolic dependencies on the concentration of 3-MI. The maximum yield of the former is approximately 0.43 equiv. This yield is less than half that formed in the reaction of R2-W48A, despite the fact that titrations of apo R2-W48A/F208Y with Fe(II) in the presence of O_2 and 3-MI indicate that 3.0 ± 0.1 equiv Fe can be incorporated. Thus, mediation of ET in this variant exhibits what may be authentic "saturation," because the maximum yield of Y122• is considerably less than it would be if the mediation were able to completely out-compete alternative pathways. The presence of the bulkier F residue at position 48 eliminates the ability of 3-MI to impact the partition between Y208 hydroxylation and Y122• radical formation. O_2 activation by R2-W48F/F208Y results in the development of the 675 nm absorption but not the sharp tyrosyl radical feature, and the presence of 3-MI has *no effect* on the reaction outcome as judged by the absorption spectrum of the products (data not shown). The trend in $K_{0.5}$ values of 3-substituted indoles parallels that determined for the R2-W48A reaction (Table 1), but the values are roughly 100-fold greater for the R2-W48A/F208Y reaction. The diminished efficiency most likely reflects the short lifetime of the $(Fe_2O_2)^{4+}$ state in R2-W48A/F208Y, which can be intercepted by the two-electron reductant, Y208, in

Figure 2-5: Effect of 3-MI on products of O_2 activation in R2-W48A/F208Y. Absorption spectra after addition of Fe(II) (3 equiv) to air-saturated apo R2-W48A/F208Y (0.11 mM) in the absence (dotted trace) and presence of 2 mM 3-MI (solid trace). The inset illustrates the [3-MI] dependencies of Y122• yield (triangular points, left axis) and suppression of the 680-nm feature of the F208-derived Fe(III)-catecholate product (circular points, right axis). A fit of the equation for a hyperbola to the former gives $K_{0.5}$ of 1.0 ± 0.1 mM and a maximum Y122• yield of 0.43 ± 0.03 equiv (solid trace in inset). In the absence of rescuing agent, no tyrosyl radical is detected (< 0.05 equiv).

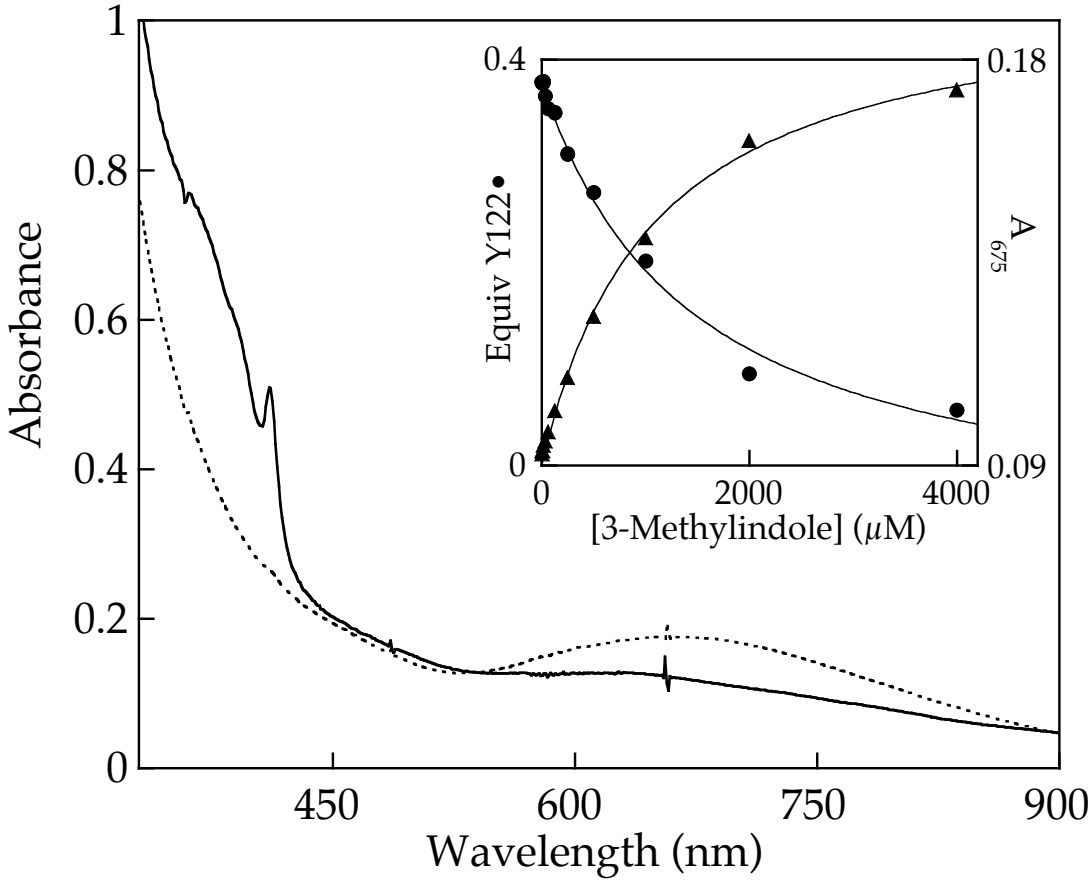
Absorbance
1
0.8
0.6
0.4
0.2
0
450
600
750
900
Wavelength (nm)
0.4
0
Equiv Y122•
0.18
0.09
A675
0
2000
4000
[3-Methylindole] (μM)

competition with ET. This observation further illustrates that the $K_{0.5}$ values are not related to thermodynamic dissociation constants.

Mediation of ET in R2-W48A/D84E by 3-MI. The replacement of iron ligand aspartate 84 of R2 with glutamate, the amino acid found in the cognate position of the structurally similar diiron-carboxylate protein, methane monooxygenase, yields a variant that accumulates a (□-1,2-peroxo)diiron (III) intermediate during O_2 activation (*47*). This intermediate does not accumulate in the reaction of R2-wt (*32*) and is probably a structural homolog of intermediate **P** ($\mathbf{H}_{peroxo}$) in the methane monooxygenase reaction (*50, 56, 57*). Y122• formation predominates in R2-D84E (*47*), but combination of the cluster re-tuning substitution (D84E) with the electron-transfer-disabling substitution (W48F) yields an R2 variant in which self-hydroxylation of F208 via the (μ-1,2-peroxo)diiron(III) intermediate predominates over the alternative one-electron oxidation of Y122 (*48*). Hydroxylation occurs concomitantly with decay of the peroxo intermediate to an initial brown product characterized by a broad absorption at 490 nm, and the latter then converts very slowly to the intensely purple final product in which the F208-derived phenolate coordinates Fe2 of the cluster (*48*). To test whether the reaction of a variant that accumulates the peroxide complex would be susceptible to 3-MI mediation of ET and, if so, to provide a tool for the study described in the accompanying manuscript (*49*), R2-W48A/D84E was prepared. As previously reported (*57*), this variant also accumulates high levels of the peroxide intermediate during its O_2 reaction. In the absence of 3-MI, Y122• is produced (Figure 6, dotted trace), but with a poor yield (0.33 ± 0.03 equiv) comparable to that in the reaction of R2-W48A. In addition, the 490 nm feature seen in the initial brown product of the R2-W48F/D84E reaction also develops.

Figure 2-6: Effect of 3-MI on products of O_2 activation in R2-W48A/D84E. Absorption spectra after addition of Fe(II) (3 equiv) to air-saturated apo R2-W48A/D84E (0.14 mM) in the absence (dotted trace) and presence of 2 mM 3-MI (solid trace). The inset illustrates the [3-MI] dependencies of Y122• yield (triangular points, left axis) and suppression of the 490-nm feature of the altered product(s) (circular points, right axis). A fit of the equation for a hyperbola to the former gives $K_{0.5}$ = 0.11 ± 0.01 mM and a maximum Y122• yield of 0.72 ± 0.05 equiv (solid trace in inset).

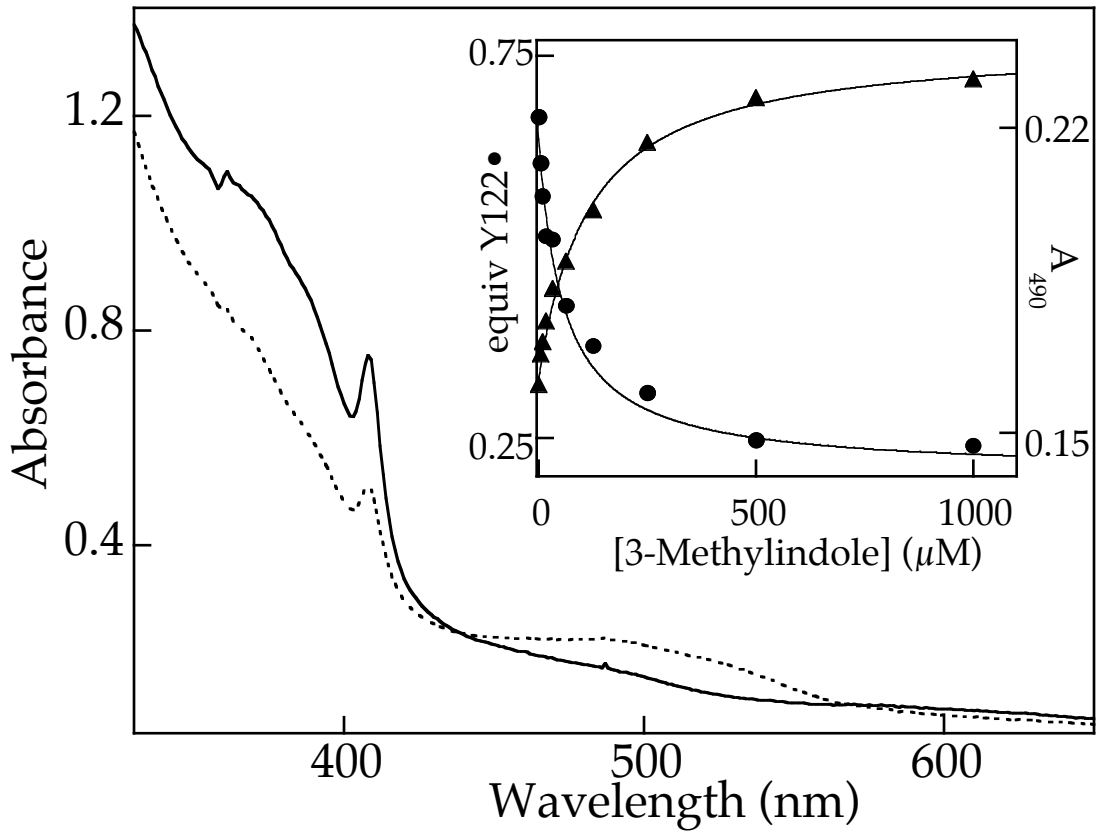
Absorbance
1.2
0.8
0.4
400
500
600
Wavelength (nm)
0.75
0.25
equiv Y122•
0.22
0.15
A490
0
500
1000
[3-Methylindole] (μM)

This observation suggests that F208 hydroxylation may also occur in the reaction of R2-W48A/D84E, but it is important to emphasize that this possibility has not been verified and that conversion of this product to the purple species obtained with R2-W48F/D84E has not yet been observed. Inclusion of 3-MI in the R2-W48A/D84E reaction increases the quantity of Y122• formed (Figure 6, solid trace) by a maximum of ~ 2.2-fold to a 0.71 ± 0.05 equiv (triangular points and left axis in Figure 6 inset) and suppresses development of the broad 490-nm feature that is characteristic of the altered products (circular points and right axis in Figure 6 inset). Thus, mediation does occur in a variant that accumulates the (μ-1,2-peroxo)diiron(III) complex.

DISCUSSION

The mediation by indole compounds of ET to the buried diiron site of R2 proteins lacking the electron shuttling W48 has been demonstrated by three different assays: (1) an increase in the yield of the otherwise transient Y122• in R2-W48A; (2) an effect on the partition between Y208 hydroxylation and Y122• formation in R2-W48A/F208Y; and (3) an effect on the partition between formation of the aberrant 490-nm-absorbing product and production of Y122• in R2-W48A/D84E. When considered with previous studies that have examined the interplay among the effects of W48 substitution, substitution of other residues, and variation of concentration of reductants (*34, 37, 48*), the results leave no doubt that the presence of 3-MI (or another indole compound) somehow reactivates ET during oxygen activation. However, as noted above, the data are conflicting regarding the mechanism of ET mediation. Evidence for the chemical specificity expected of the intended mechanism (i.e., authentic chemical rescue) is

manifold. Mediation is much less effective (by more than two orders of magnitude in concentration) when a non-functional aromatic residue (F or Y) is present at position 48. Phenol, which can undergo oxidation by one-electron at a potential similar to that required to produce indole radicals but has a structure much less similar to the W48 sidechain, is completely ineffective at mediating ET. Ascorbate, a reductant that is more potent than 3-MI by hundreds of millivolts and functions efficiently in the reaction of the wild-type protein (*19*), is much less potent than 3-MI (by ~ 2 orders of magnitude in concentration) at effecting ET in the R2-W48A reaction but functions well as ultimate reductant when 3-MI is present as mediator. In spite of these multiple observations in favor of the intended mechanism of ET mediation, the failure of indole substitutions (e.g., methylation of N1 or C2 or increasing size of the C3 alkyl substituent) to diminish efficiency and the susceptibility of variants with bulkier residues at position 48 to mediation of ET cast doubt that authentic chemical rescue is occurring. It is possible that less hydrophobic and non-aromatic sidechains simply fail to fill the W48 site due to changes in the backbone conformation. This flexibility would allow the mediator to bind except when a properly packing aromatic sidechain is present at position 48. The absence of steric influence for the indole derivatives could reflect (1) the orientation of the 3-substituent toward solution, (2) flexibility in the binding pocket, and (3) liberal orientation requirements for the indole, as would be expected for an electron transfer reaction. Resolution of the mechanism of ET mediation will require additional studies.

The second major unresolved issue is the point in the reaction sequence at which the mediator exerts its effect. Two possibilities exist (Scheme 1): it may transfer an electron to the $(Fe_2O_2)^{4+}$ precursor to **X** (Mechanism A), as does W48 in the reaction of

Scheme 2-1: Two possible mechanisms for mediation of electron transfer in R2-W48A by 3-MI.

Mechanism A (wildtype-like)

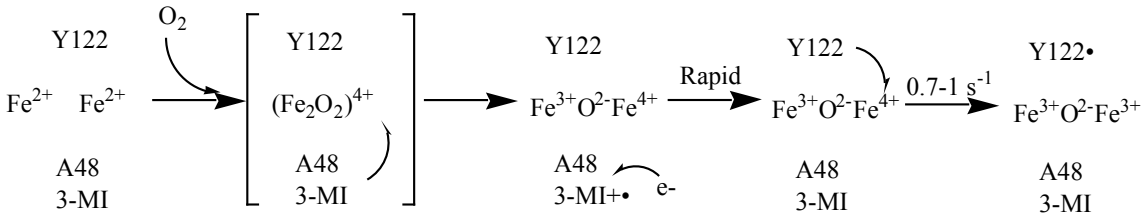

Mechanism B (W48F-like)

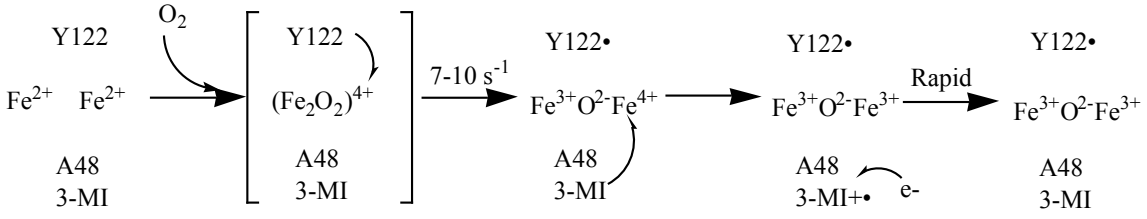

the wild-type protein (*20, 32*), or it may mediate reduction of **X** in the **X**-Y122• di-radical species (Mechanism B) (*34*). The fact that mediation by 3-MI is, under appropriate circumstances, catalytic, suggests that the latter mechanism occurs (with 3-MI vastly sub-stoichiometric with respect to protein, one would expect the di-radical species to form in the majority of events, given the short lifetime of the precursor), but it does not rule out the possibility that the first can also occur. In fact, the kinetics of Y122• formation in the R2-W48A reaction in the presence of 1 mM 3-MI (Figure 3) suggest a partition between the two mechanisms. Two formation phases are observed, with the first having the same k_{obs} as that for formation of the di-radical species (in the absence of 3-MI) and the second having the same k_{obs} as that for production of Y122• by **X** in the R2-wt reaction. The amplitudes of the two formation phases would imply that approximately 60% of the Y122• is formed by the slower, wt-like mechanism. The partitioning may reflect only partial saturation of the binding site (if binding occurs). Alternatively, the protein may be saturated, but 3-MI may be only partially effective in competition with Y122 for reduction of the $(Fe_2O_2)^{4+}$ species.

Despite these mechanistic uncertainties, the overall success of the approach suggests that the crucial ET step during O_2 activation in R2 might be triggered by addition of a small molecule. In the accompanying manuscript (*49*), addition of 3-MI is used to trigger conversion to cluster **X** of an $(Fe_2O_2)^{4+}$ intermediate state that may be identical with the precursor to cluster **X** in the reaction of the wild-type protein and to resolve kinetically the spectral features of the previously uncharacterized intermediate state.

Figure 2-S1: Absorption spectra of products of the reaction of Fe(II)-R2-W48A (2.8 equiv Fe) with excess O_2 in the absence of ascorbate and 3-MI (red trace), and in the presence of either ascorbate (blue trace), 3-MI (green trace), or both (black trace). The final concentrations of the protein, ascorbate, and 3-MI were 109.4 mM, 0.5 mM, and 0.5 mM, respectively.

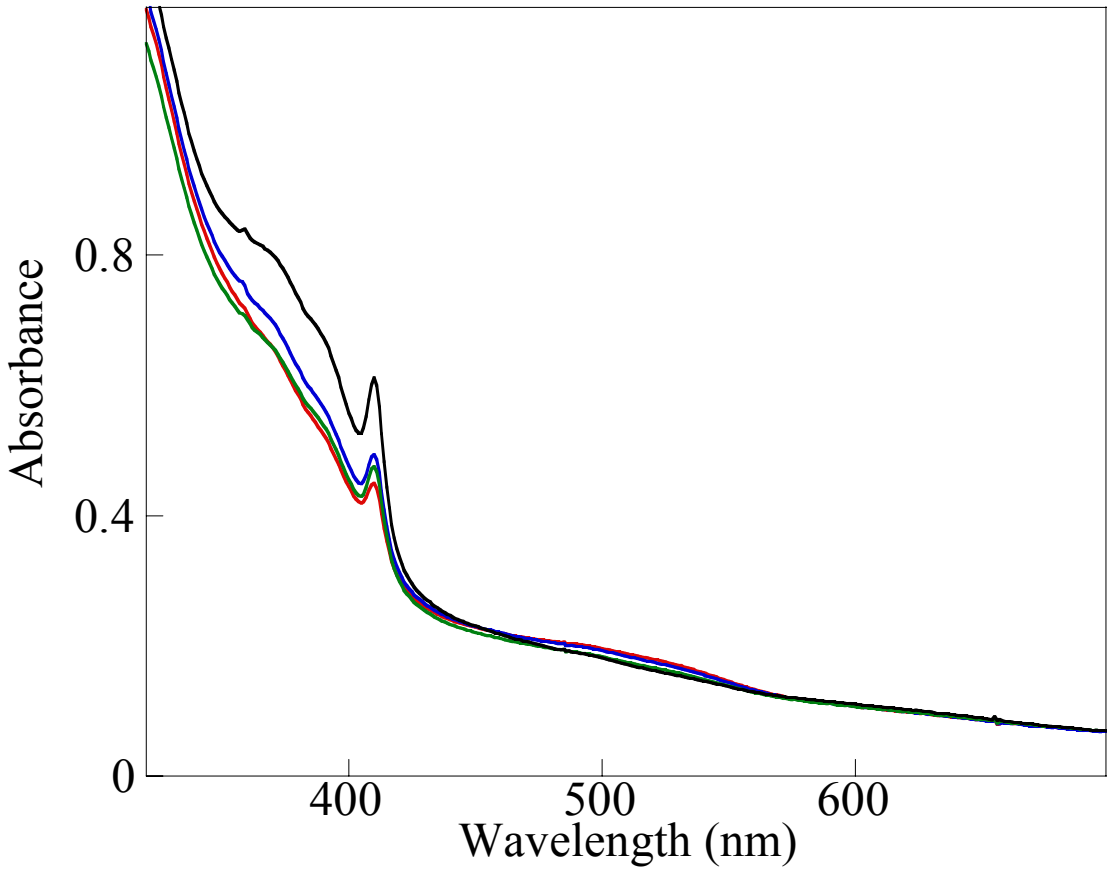
Absorbance
0.8
0.4
0
400
500
600
Wavelength (nm)

ACKNOWLEDGMENT

We thank Professor Boi Hanh Huynh and Dr. Carsten Krebs for acquisition of the Mössbauer spectra in Figure 4 and Dr. Sunail Naik for preparation of this figure.

SUPPORTING INFORMATION AVAILABLE

Absorption spectra from experiment showing source of extra electron (ascorbate) in 3-MI catalyzed ET.

REFERENCES

1. Atkin, C. L., Thelander, L., and Reichard, P. (1973) Iron and free radical in ribonucleotide reductase. Exchange of iron and Mössbauer spectroscopy of the protein B2 subunit of the *Escherichia coli* enzyme. *J. Biol. Chem. 248*, 7464-7472.
2. Sjöberg, B.-M., Reichard, P., Gräslund, A., and Ehrenberg, A. (1977) Nature of the free radical in ribonucleotide reductase from *Escherichia coli*. *J. Biol. Chem. 252*, 536-541.
3. Larsson, A., and Sjöberg, B.-M. (1986) Identification of the stable free radical tyrosine residue in ribonucleotide reductase. *EMBO J. 5*, 2037-2040.
4. Fontecave, M., Nordlund, P., Eklund, H., and Reichard, P. (1992) The redox centers of ribonucleotide reductase of *Escherichia coli*. *Adv. Enzymol. Relat. Areas Mol. Biol. 65*, 147-183.

5. Sjöberg, B.-M. (1997) Ribonucleotide reductases-A group of enzymes with different metallosites and a similar reaction mechanism. *Struct. Bond. 88*, 139-173.

6. Stubbe, J., and Riggs-Gelasco, P. (1998) Harnessing free radicals: formation and function of the tyrosyl radical in ribonucleotide reductase. *Trends Biochem. Sci. 23*, 438-443.

7. Stubbe, J. (1990) Ribonucleotide Reductases: amazing and confusing. *J. Biol. Chem. 265*, 5329-5332.

8. Mao, S. S., Yu, G. X., Chalfoun, D., and Stubbe, J. (1992) Characterization of C439SR1, a mutant of *Escherichia coli* ribonucleotide diphosphate reductase: evidence that C439 is a residue essential for nucleotide reduction and C439SR1 is a protein possessing novel thioredoxin-like activity. *Biochemistry 31*, 9752-9759.

9. Mao, S. S., Holler, T. P., Yu, G. X., Bollinger, J. M., Jr., Booker, S., Johnston, M. I., and Stubbe, J. (1992) A model for the role of multiple cysteine residues involved in ribonucleotide reduction: amazing and still confusing. *Biochemistry 31*, 9733-9743.

10. Uhlin, U., and Eklund, H. (1994) Structure of ribonucleotide reductase protein R1. *Nature 370*, 533-539.

11. Stubbe, J., and Ackles, D. (1980) On the mechanism of ribonucleotide diphosphate reductase from *Escherichia coli*. *J. Biol. Chem. 255*, 8027-8030.

12. Stubbe, J., Nocera, D. G., Yee, C. S., and Chang, M. C. Y. (2003) Radical initiation in the class I ribonucleotide reductase: long-range proton-coupled electron transfer? *Chem. Rev. 103*, 2167-2202.

13. Ekberg, M., Potsch, S., Sandin, E., Thunnissen, M., Nordlund, P., Sahlin, M., and Sjöberg, B.-M. (1998) Preserved catalytic activity in an engineered ribonucleotide reductase R2 protein with a nonphysiological radical transfer pathway. The importance of hydrogen bond connections between the participating residues. *J. Biol. Chem. 273*, 21003-21008.

14. Ekberg, M., Sahlin, M., Eriksson, M., and Sjöberg, B.-M. (1996) Two conserved tyrosine residues in protein R1 participate in an intermolecular electron transfer in ribonucleotide reductase. *J. Biol. Chem. 271*, 20655-20659.

15. Rova, U., Adrait, A., Potsch, S., Gräslund, A., and Thelander, L. (1999) Evidence by mutagenesis that Tyr(370) of the mouse ribonucleotide reductase R2 protein is the connecting link in the intersubunit radical transfer pathway. *J. Biol. Chem. 274*, 23746-23751.

16. Rova, U., Goodtzova, K., Ingemarson, R., Behravan, G., Gräslund, A., and Thelander, L. (1995) Evidence by site-directed mutagenesis supports long-range electron transfer in mouse ribonucleotide reductase. *Biochemistry 34*, 4267-4275.

17. Siegbahn, P. E. M., Eriksson, L., Himo, F., and Pavlov, M. (1998) Hydrogen atom transfer in ribonucleotide reductase (RNR). *J. Phys. Chem 102*, 10622-10629.

18. Bollinger, J. M., Jr., Edmondson, D. E., Huynh, B. H., Filley, J., Norton, J. R., and Stubbe, J. (1991) Mechanism of assembly of the tyrosyl radical-dinuclear iron cluster cofactor of ribonucleotide reductase. *Science 253*, 292-298.

19. Bollinger, J. M., Jr., Tong, W. H., Ravi, N., Huynh, B. H., Edmondson, D. E., and Stubbe, J. (1994) Mechanism of assembly of the tyrosyl-diiron(III) cofactor of *E.*

coli ribonucleotide reductase. 2. Kinetics of the excess Fe^{2+} reaction by optical, EPR, and Mössbauer spectroscopies. *J. Am. Chem. Soc. 116*, 8015-8023.

20. Bollinger, J. M., Jr., Tong, W. H., Ravi, N., Huynh, B. H., Edmondson, D. E., and Stubbe, J. (1994) Mechanism of assembly of the tyrosyl radical-diiron(III) cofactor of *E. coli* ribonucleotide reductase. 3. Kinetics of the limiting Fe^{2+} reaction by optical, EPR, and Mössbauer spectroscopies. *J. Am. Chem. Soc. 116*, 8024-8032.

21. Bollinger, J. M., Jr., Tong, W. H., Ravi, N., Huynh, B. H., Edmondson, D. E., and Stubbe, J. (1995) Use of rapid kinetics methods to study the assembly of the diferric-tyrosyl radical cofactor of *E. coli* ribonucleotide reductase. *Meth. Enzymol. 258*, 278-303.

22. Tong, W. H., Chen, S., Lloyd, S. G., Edmondson, D. E., Huynh, B. H., and Stubbe, J. (1996) Mechanism of assembly of the diferric cluster-tyrosyl radical cofactor of *Escherichia coli* ribonucleotide reductase from the diferrous form of the R2 subunit. *J. Am. Chem. Soc. 118*, 2107-2108.

23. Ochiai, E., Mann, G. J., Gräslund, A., and Thelander, L. (1990) Tyrosyl free radical formation in the small subunit of mouse ribonucleotide reductase. *J. Biol. Chem. 265*, 15758-15761.

24. Elgren, T. E., Lynch, J. B., Juarez-Garcia, C., Münck, E., Sjöberg, B.-M., and Que, L., Jr. (1991) Electron transfer associated with oxygen activation in the B2 protein of ribonucleotide reductase from *Escherichia coli*. *J. Biol. Chem. 266*, 19265-19268.

25. Bollinger, J. M., Jr., Stubbe, J., Huynh, B. H., and Edmondson, D. E. (1991) Novel diferric radical intermediate responsible for tyrosyl radical formation in assembly of the cofactor of ribonucleotide reductase. *J. Am. Chem. Soc. 113*, 6289-91.

26. Ravi, N., Bollinger, J. M., Jr., Huynh, B. H., Edmondson, D. E., and Stubbe, J. (1994) Mechanism of assembly of the tyrosyl radical-diiron(III) cofactor of *E. coli* ribonucleotide reductase: 1. Mössbauer characterization of the diferric radical precursor. *J. Am. Chem. Soc. 116*, 8007-8014.

27. Sturgeon, B. E., Burdi, D., Chen, S., Huynh, B. H., Edmondson, D. E., Stubbe, J., and Hoffman, B. M. (1996) Reconsideration of X, the diiron intermediate formed during cofactor assembly in *E. coli* ribonucleotide reductase. *J. Am. Chem. Soc. 118*, 7551-7557.

28. Burdi, D., Sturgeon, B. E., Tong, W. H., Stubbe, J., and Hoffman, B. M. (1996) Rapid freeze-quench ENDOR of the radical X intermediate of *Escherichia coli* ribonucleotide reductase using $^{17}O_2$ and $H_2{}^{17}O$. *J. Am. Chem. Soc. 118*, 281-282.

29. Willems, J.-P., Lee, H.-I., Burdi, D., Doan, P. E., Stubbe, J., and Hoffman, B. M. (1997) Identification of the protonated oxygenic ligands of ribonucleotide reductase intermediate X by Q-Band ^{1,2}H CW and pulsed ENDOR. *J. Am. Chem. Soc. 119*, 9816-9824.

30. Burdi, D., Willems, J.-P., Riggs-Gelasco, P., Antholine, W. E., Stubbe, J., and Hoffman, B. M. (1998) The core structure of X generated in the assembly of the diiron cluster of ribonucleotide reductase: $^{17}O_2$ and $H_2{}^{17}O$ ENDOR. *J. Am. Chem. Soc. 120*, 12910-12919.

31. Riggs-Gelasco, P. J., Shu, L., Chen, S., Burdi, D., Huynh, B. H., Que, L., Jr., and Stubbe, J. (1998) EXAFS characterization of the intermediate X generated during the assembly of the *Escherichia coli* ribonucleotide reductase R2 diferric tyrosyl radical cofactor. *J. Am. Chem. Soc. 120*, 849-860.

32. Baldwin, J., Krebs, C., Ley, B. A., Edmondson, D. E., Huynh, B. H., and Bollinger, J. M., Jr. (2000) Mechanism of rapid electron transfer during oxygen activation in the R2 subunit of *Escherichia coli* ribonucleotide reductase. 1. Evidence for a transient tryptophan radical. *J. Am. Chem. Soc. 122*, 12195-12206.

33. Schmidt, P. P., Rova, U., Katterle, B., Thelander, L., and Gräslund, A. (1998) Kinetic evidence that a radical transfer pathway in protein R2 of mouse ribonucleotide reductase is involved in generation of the tyrosyl free radical. *J. Biol. Chem. 273*, 21463-21472.

34. Krebs, C., Chen, S., Baldwin, J., Ley, B. A., Patel, U., Edmondson, D. E., Huynh, B. H., and Bollinger, J. M., Jr. (2000) Mechanism of rapid electron transfer during oxygen activation in the R2 subunit of *Escherichia coli* ribonucleotide reductase. 2. Evidence for and consequences of blocked electron transfer in the W48F variant. *J. Am. Chem. Soc. 122*, 12207-12219.

35. Ormö, M., deMaré, F., Regnström, K., Åberg, A., Sahlin, M., Ling, J., Loehr, T. M., Sanders-Loehr, J., and Sjöberg, B.-M. (1992) Engineering of the iron site in ribonucleotide reductase to a self-hydroxylating monoxygenase. *J. Biol. Chem. 267*, 8711-8714.

36. Åberg, A., Ormö, M., Nordlund, P., and Sjöberg, B.-M. (1993) Autocatalytic generation of dopa in the engineered protein R2 F208Y from *Escherichia coli*

ribonucleotide reductase and crystal structure of the dopa 208 protein. *Biochemistry 32*, 9845-9850.

37. Parkin, S. E., Chen, S., Ley, B. A., Mangravite, L., Edmondson, D. E., Huynh, B. H., and Bollinger, J. M., Jr. (1998) Electron injection through a specific pathway determines the outcome of oxygen activation at the diiron cluster in the F208Y mutant of *Escherichia coli* ribonucleotide reductase protein R2. *Biochemistry 37*, 1124-1130.

38. Toney, M. D., and Kirsch, J. F. (1989) Direct Brönsted analysis of the restoration of activity to a mutant enzyme by exogenous amines. *Science 243*, 1485-1488.

39. Sivaraja, M., Goodin, D. B., Smith, M., and Hoffman, B. M. (1989) Identification by ENDOR of Trp191 as the free-radical site in cytochrome c peroxidase compound ES. *Science 245*, 738-740.

40. Erman, J. E., Vitello, L. B., Mauro, J. M., and Kraut, J. (1989) Detection of an oxyferryl porphyrin π-cation-radical intermediate in the reaction between hydrogen peroxide and a mutant yeast cytochrome c peroxidase. Evidence for tryptophan-191 involvement in the radical site of compound I. *Biochemistry 28*, 7992-7995.

41. Houseman, A. L. P., Doan, P. E., Goodin, D. B., and Hoffman, D. M. (1993) Comprehensive explanation of the anomalous EPR spectra of wild-type and mutant cytochrome c peroxidase compound ES. *Biochemistry 32*, 4430-4443.

42. Huyett, J. E., Doan, P. E., Gurbiel, R., Houseman, A. L., Sivaraja, M., Goodin, D. B., and Hoffman, B. M. (1995) Compound ES of cytochrome c peroxidase contains a Trp π-Cation radical: characterization by continuous wave and pulsed

Q-Band electron nuclear double resonance spectroscopy. *J. Am. Chem. Soc. 117*, 9033-9041.

43. Fitzgerald, M. M., Churchill, M. J., McRee, D. E., and Goodin, D. B. (1994) Small molecule binding to an artificially created cavity at the active site of cytochrome c peroxidase. *Biochemistry 33*, 3807-3818.

44. Fitzgerald, M. M., Musah, R. A., McRee, D. E., and Goodin, D. B. (1996) A ligand-gated, hinged loop rearrangement opens a channel to a buried artificial protein cavity. *Nat. Struct. Biol. 3*, 626-631.

45. Fitzgerald, M. M., Trester, M. L., Jensen, G. M., McRee, D. E., and Goodin, D. B. (1995) The role of aspartate-235 in the binding of cations to an artifical cavity at the radical site of cytochrome c peroxidase. *Protein Sci. 4*, 1844-1850.

46. Musah, R. A., Jensen, G. M., Rosenfeld, R. J., McRee, D. E., and Goodin, D. B. (1997) Variation in strength of an unconventional C-H to O hydrogen bond in an engineered protein cavity. *J. Am. Chem. Soc. 119*, 9083-9084.

47. Bollinger, J. M., Jr., Krebs, C., Vicol, A., Chen, S., Ley, B. A., Edmondson, D. E., and Huynh, B. H. (1998) Engineering the diiron site of *Escherichia coli* ribonucleotide reductase protein R2 to accumulate an intermediate similar to H_{peroxo}, the putative peroxodiiron(III) complex from the methane monooxygenase catalytic cycle. *J. Am. Chem. Soc. 120*, 1094-1095.

48. Baldwin, J., Voegtli, W. C., Khidelkel, N., Moënne-Loccoz, P., Krebs, C., Pereira, A. S., Ley, B. A., Huynh, B. H., Loehr, T. M., Riggs-Gelasco, P. J., Rosenzweig, A. C., and Bollinger, J. M., Jr. (2001) Rational reprogramming of

the R2 subunit of *Escherichia coli* ribonucleotide reductase into a self-hydroxylating monooxygenase. *J. Am. Chem. Soc. 123*, 7017-7030.

49. Saleh, L., Krebs, C., Ley, B. A., Naik, S., Huynh, B. H., and Bollinger, J. M., Jr. (2004) Use of a chemical trigger for electron transfer to characterize a precursor to cluster X in assembly of the iron-radical cofactor of *Escherichia coli* ribonucleotide reductase. *Biochemistry 43*, 5953-5964.

50. Moënne-Loccoz, P., Baldwin, J., Ley, B. A., Loehr, T. M., and Bollinger, J. M., Jr. (1998) O_2 activation by non-heme diiron proteins: Identification of a symmetric μ-1,2-peroxide in a mutant of ribonucleotide reductase. *Biochemistry 37*, 14659-14663.

51. Salowe, S. P., and Stubbe, J. (1986) Cloning, overproduction, and purification of the B2 subunit of ribonucleoside diphosphate reductase. *J. Bacteriol. 165*, 363-366.

52. Gill, S. C., and von Hippel, P. H. (1989) Calculation of protein extinction coefficients from amino acid sequence data. *Anal. Biochem. 182*, 319-326.

53. Raibekas, A. A., and Massey, V. (1996) Glycerol-induced development of catalytically active conformation of *Crotalus adamanteus* L-amino acid oxidase *in vitro. Proc. Natl. Acad. Soc. U.S.A. 93*, 7546-7551.

54. Raibekas, A. A., and Massey, V. (1997) Glycerol-assisted restorative adjustment of flavoenzyme conformation perturbed by site-directed mutagenesis. *J. Biol. Chem. 272*, 22248-22252.

55. Jensen, G. M., Goodin, D. B., and Bunte, S. W. (1996) Density functional and MP2 calculations of spin densities of oxidized 3-methylindole: models for tryptophan radicals. *J. Phys. Chem. 100*, 954-959.

56. Liu, K. E., Wang, D., Huynh, B. H., Edmondson, D. E., Salifoglou, A., and Lippard, S. J. (1994) Spectroscopic detection of intermediates in the reaction of dioxygen with the reduced methane monooxygenase/hydroxylase from *Methylococcus capsulatus* (Bath). *J. Am. Chem. Soc. 116*, 7465-7466.

57. Baldwin, J., Krebs, C., Saleh, L., Stelling, M., Huynh, B. H., Bollinger, J. M., Jr., and Riggs-Gelasco, P. (2003) Structural characterization of the peroxodiiron(III) intermediate generated during oxygen activation by the W48A/D84E variant of ribonucleotide reductase protein R2 from *Escherichia coli*. *Biochemistry 42*, 13269-13279.

Chapter 3

Use of a Chemical Trigger for Electron Transfer to Characterize a Precursor to Cluster X in Assembly of the Iron-Radical Cofactor of *Escherichia coli* Ribonucleotide Reductase

FOOTNOTES

[1]Abbreviations: R2, R2 subunit of *Escherichia coli* ribonucleotide reductase; sMMO, soluble methane monooxygenase; MMOH, the hydroxylase component of sMMO; Y122•, tyrosine 122 radical; ET, electron transfer; wt, wildtype; $W48^{+\bullet}$, tryptophan 48 cation radical; v/v, volume/volume; buffer A, 100 mM Hepes buffer, 10% (v/v) glycerol, pH 7.6; RFQ-EPR, rapid freeze-quench EPR; RFQ-Möss, rapid freeze-quench Mössbauer; 3-MI, 3-methylindole.

[2] Unpublished data from our laboratories

ABSTRACT

A key step in generation of the catalytically essential tyrosyl radical (Y122•) in protein R2 of *Escherichia coli* ribonucleotide reductase is electron transfer (ET) from the near-surface residue, tryptophan 48 (W48), to an $(Fe_2O_2)^{4+}$ complex formed by addition of O_2 to the carboxylate-bridged diiron(II) cluster. Because this step is rapid, the $(Fe_2O_2)^{4+}$ complex does not accumulate and, therefore, has not been characterized. The product of the ET step is a "di-radical" intermediate state containing the well-characterized Fe(IV)Fe(III) cluster, **X**, and a W48 cation radical ($W48^{+\bullet}$). The latter may be reduced from solution to complete the two-step transfer of an electron to the buried diiron site. In this study, an $(Fe_2O_2)^{4+}$ state that is probably the precursor to the **X**-$W48^{+\bullet}$ di-radical state in the reaction of the wild-type protein (R2-wt) has been characterized by exploitation of the observation that, in R2 variants with W48 replaced with alanine (A), the otherwise disabled ET step can be mediated by indole compounds. Mixing of the Fe(II) complex of R2-W48A/Y122F with O_2 results in accumulation of an intermediate state that rapidly converts to **X** upon mixing with 3-methylindole (3-MI). The state comprises at least two species, of which each exhibits an apparent Mössbauer quadrupole doublet with parameters characteristic of high-spin Fe(III) ions. The isomer shifts of these complexes and absence of magnetic hyperfine coupling in their Mössbauer spectra suggest that both are antiferromagnetically coupled diiron(III) clusters. The fact that both rapidly convert to **X** upon treatment with a molecule (3-MI) shown in the preceding paper to mediate ET in W48A R2 variants indicates that they are more oxidized than **X** by one-electron, which suggests that they have a bound peroxide equivalent. Their failure to exhibit either the long-wavelength absorption (at 650-750 nm) or Mössbauer doublet with high isomer shift

(> 0.6 mm/s) that are characteristic of the putatively μ-1,2-peroxo-bridged diiron(III) intermediates that have been detected in the reactions of methane monooxygenase (**P** or $\mathbf{H_{peroxo}}$) and variants of R2 with the D84E ligand substitution suggests that they have geometries and electronic structures different from those of the previously characterized complexes. Supporting this deduction, the peroxodiiron(III) complex that accumulates in R2-W48A/D84E is much less reactive toward 3-MI-mediated reduction than the $(Fe_2O_2)^{4+}$ state in R2-W48A/Y122F. It is postulated that the new $(Fe_2O_2)^{4+}$ state is either an early adduct in an orthogonal pathway for oxygen activation or, more likely, the successor to a (μ-1,2-peroxo)diiron(III) complex that is extremely fleeting in R2 proteins with the wild-type ligand set but longer lived in D84E-containing variants.

INTRODUCTION

The R2 subunit of *Escherichia coli* ribonucleotide reductase (hereafter, simply R2[1]) is a member of the diiron-carboxylate family of oxidases and oxygenases (*1-3*). Proteins in this family have similar structures and carboxylate-bridged diiron(II) cofactors, which they employ to reductively activate molecular oxygen for difficult oxidation reactions. The two most extensively studied family members are R2 and soluble methane monooxygenase (sMMO). The former activates O_2 for introduction of its catalytically essential tyrosyl radical (Y122•) by one-electron oxidation of Y122 (*4-6*), whereas the latter hydroxylates methane (*7-10*). Detailed insights into the mechanisms of these two reactions have been obtained by direct detection and characterization of intermediate states. In the sMMO reaction, peroxodiiron(III) and diiron(IV) intermediates (**P** and **Q**, respectively) have been detected (*11-18*). **P** is thought to be a (μ-1,2-peroxo)diiron(III) complex (*13, 14, 16*) and **Q** a *bis*-(μ-oxo)diiron(IV) complex (*15*). Kinetic evidence indicates that they form in sequence and that **Q** hydroxylates methane (*11, 12, 14-18*). In the R2 reaction, only the Fe(IV)Fe(III) cluster, **X**, has been definitively detected (*19-27*). It forms when the near-surface residue, W48, reduces an uncharacterized adduct (hereafter denoted $(Fe_2O_2)^{4+}$) between O_2 and the diiron(II) cluster (*21, 28*). Reduction of the W48 cation radical ($W48^{+\bullet}$) constituent of the resulting **X**-$W48^{+\bullet}$ "di-radical" state by a variety of reductants (ascorbate, thiols, $Fe(II)_{aq}$) is facile (*28*), leaving cluster **X** to generate Y122• in the final and slowest step of the reaction (*20, 29*).

Electron transfer (ET) from W48 is sufficiently rapid to have prevented accumulation and detection of the $(Fe_2O_2)^{4+}$ oxidant (*28*). Consequently, it has not been

possible to establish with certainty whether the R2 and sMMO reactions proceed through one or more common intermediate or completely orthogonal pathways. Nevertheless, mounting indirect evidence has suggested that a common initial pathway is more likely. This evidence includes: (1) the observations of a **P**-like peroxodiiron(III) complex and competing self-hydroxylation and Y122-oxidation reactivities in variants of R2 (*30-36*); (2) the detection of common, very short (~ 2.5 Å) Fe-Fe distances in **Q** and **X** (*15, 27*); (3) the demonstration of □-radiolytic cryo-reduction of freeze-trapped **Q** to an Fe(IV)Fe(III) complex with marked spectroscopic similarity to cluster **X** (*37*); and (4) the assessment by computational methods that similar peroxodiiron(III) intermediates could form (*38-40*). Perhaps most compellingly, a long-wavelength (~ 700 nm) optical absorption feature and one line of what could be a Mössbauer quadrupole doublet at a position consistent with an isomer shift of 0.66 mm/s were detected shortly (milliseconds) after initiation of the R2 reaction (*22*). These features are similar to those characterizing **P** (*13, 14, 16*) and the peroxodiiron(III) complex that accumulates in R2 variants with the D84E ligand substitution (*30-32, 41*). However, the modest accumulation of the putative peroxodiiron(III) complex made it difficult to establish its competence to be the precursor to the **X**-W48$^{+\bullet}$ state, and a later kinetic study called into question whether the detected species could be on the reaction pathway (*22, 28*). Moreover, even under the presumption that a **P**-like complex is part of the R2 reaction sequence, the point of divergence from the sMMO mechanism would not be obvious. No evidence has been obtained for a **Q**-like species in the R2 reaction, leaving open the alternative possibilities that the presumptive **P**-like complex in R2 might either itself

undergo reduction by W48 to form **X** or isomerize to a distinct peroxodiiron(III) complex prior to the ET step.

Resolution of these issues by detection of the precursor to the **X**-$W48^{+\bullet}$ state in the R2 reaction has been a primary objective of our studies. Initially, O_2 activation was examined in W48-substituted R2 variants in the expectation that the "kinetically masked" intermediate would accumulate in the absence of the electron-shuttling residue (*42*). Indirect, kinetic evidence for the accumulation of a $(Fe_2O_2)^{4+}$ species was found. It oxidizes Y122 (instead of W48) to form a **X**-Y122• di-radical intermediate. The oxidation of Y122 by this species is 10-fold faster than by **X** in the R2-wt reaction (*42*), underscoring the high intrinsic reactivity of the uncharacterized $(Fe_2O_2)^{4+}$ complex toward one-electron reduction. To confer even greater stability to this species and thereby facilitate its characterization, the R2-W48F/Y122F variant was prepared. Freeze-quench Mössbauer (RFQ-Möss) experiments on the reaction of this double variant revealed the rapid development and relatively slow decay of spectral features not associated with either reactant or product(s), but, unfortunately, the multiplicity of these features (a reflection of the presence of multiple species) and their poor resolution from those associated with downstream products prevented unequivocal association of specific features with the reactive $(Fe_2O_2)^{4+}$ intermediate.[2] Moreover, even if such association had been achieved, proof of the chemical competence of this complex to be on the normal reaction pathway (i.e., to generate **X** upon its reduction) would not have been possible, because electron transfer to the presumptive $(Fe_2O_2)^{4+}$ complex is so slow in this protein that very little **X** accumulates, making it difficult to demonstrate a precursor-product relationship.[2]

The development described in Chapter 2 (*43*) of a method to reactivate ET by addition of a small molecule (3-methylindole or 3-MI) suggested an approach to surmounting each of these technical obstacles. We envisaged that exposure of the $(Fe_2O_2)^{4+}$ complex, pre-formed by mixing the Fe(II)-R2-W48A/Y122F complex with O_2, to the ET mediator might trigger conversion to **X** (Scheme 3-1). This chemical triggering would simultaneously permit kinetic resolution of the features of the intermediate complex(es) specifically reactive toward 3-MI-mediated, one-electron reduction and demonstrate its (their) chemical competence to be on the pathway to **X**. In this article, we demonstrate the realization of this strategy and document that the spectroscopic signatures of the $(Fe_2O_2)^{4+}$ state that is triggered to convert to cluster **X** are distinct from those of known peroxodiiron(III) complexes (such as **P**) and the diiron(IV) intermediate, **Q**, in the sMMO reaction. While cognizant that 3-MI may not be triggering ET according to the intended mechanism (i.e., binding in the pocket created by truncation of the indole sidechain of W48) and that the W48A and Y122F substitutions potentially could alter the O_2 activation pathway, we nevertheless propose that the detected state is identical to the kinetically masked precursor to the **X**-W48$^{+\bullet}$ state in the reaction of R2-wt. We suggest that it represents either an early adduct in a pathway for O_2 activation distinct from that beginning with the μ-1,2-peroxodiiron(III) complex or, more probably, a successor to the canonical peroxide complex.

MATERIALS AND METHODS

Materials. Materials were obtained from the sources listed in Chapter 2 (*43*).

Scheme 3-1: Mechanism of O_2 activation in R2-W48A/Y122F in the presence of 3-MI ET mediator.

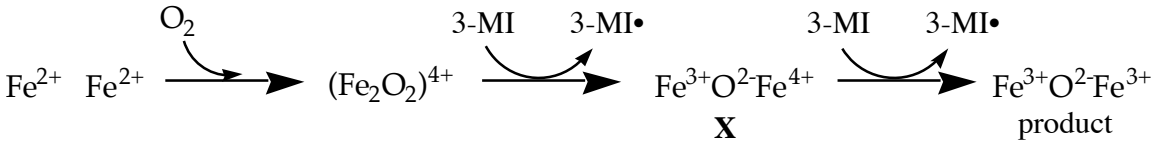

Preparation and Quantitation of Apo R2-W48A/Y122F. pR2-W48A/Y122F, the over-expression vector for R2-W48A/Y122F, was prepared from pR2-Y122F (*20, 29*), pR2-W48F (*42*), and pR2-W48A (*43*). The 358 basepair *Aat*II-*Kpn*I restriction fragment of pR2-Y122F was ligated with the large (vector) fragment from digestion of pR2-W48F with the same restriction enzymes to yield pR2-W48F/Y122F. The 251 base pairs *Bgl*II to *Aat*II restriction fragment (containing codons 1-52) from pR2-W48A was ligated with the large fragment from digestion of pR2-W48F/Y122F with the same endonucleases to give pR2-W48A/Y122F. The sequence of the coding region of each plasmid construct was verified to ensure that no undesired mutations had been introduced. DNA sequences were determined by the Nucleic Acid Facility of the Pennsylvania State University Biotechnology Institute.

The procedures used to isolate and quantify R2-W48A/Y122F were as described in Chapter 2 (*43*). The value used for the molar absorption coefficient at 280 nm (ε_{280}) for R2-W48A/Y122F was 107 $mM^{-1}cm^{-1}$, as calculated by the procedure of Gill and von Hippel (*44*).

Preparation and Quantitation of Apo R2-W48A/D84E. Preparation of the expression vector for this protein is described elsewhere (*41*). The protein was purified as described in Chapter 2 (*43*). It was quantified spectrophotometrically by assuming ε_{280} = 109 $mM^{-1}cm^{-1}$ (*44*).

Stopped-Flow Absorption Spectrophotometry. Stopped-flow absorption experiments were carried out with an Applied Photophysics SX.18MV stopped-flow apparatus equipped with a diode array detector and configured for sequential mixing (path length of 1 cm and dead-time of 1.3 ms) or a Kintek Corporation Model SF-2001

stopped-flow spectrofluorimeter equipped with a Gilford Model 240 light source and configured for sequential mixing (path length 0.5 cm, deadtime 3 ms). Both instruments were housed in an anoxic chamber (MBraun). Constant temperature was ensured with a Lauda K-4/R circulating water bath. Oxygen-free solutions of apo R2-W48A/Y122F in 100 mM Hepes buffer, 10% (v/v) glycerol, pH 7.6 (buffer A), oxygen-saturated solutions of buffer A, and oxygen-free stock solutions of 3-MI in ethanol (typically 100-fold more concentrated than the final concentration in the reaction) were prepared as described in the preceding paper (*43*). Stopped-flow measurements were carried out as previously described (*28, 45*). Specific reaction conditions are given in the appropriate figure legends.

Freeze-Quench EPR and Mössbauer Experiments. The apparatus and procedures used to prepare the rapid freeze-quench EPR (RFQ-EPR) and Mössbauer (RFQ-Möss) samples have been described (*42, 46*). Reaction conditions are given in the appropriate figure legends. The EPR and Mössbauer spectrometers have also been described (*28, 46*). The spectrometer conditions are given in the figure legends.

Kinetic Simulations. The program KinTekSim (KinTek Corp., State College, PA) was used for simulation of kinetic data.

RESULTS

Preliminary Characterization of R2-W48A/Y122F. Preliminary characterization of the protein included determination of (1) the quantity of Fe(II) that it can take up and (2) whether or not the presence of ET mediator (3-MI) affects the products of its reaction with O_2. Addition of Fe(II) to the apo protein in the presence of O_2 leads to formation of

absorbing products (Figure 3-1, dotted trace). Features of the (μ-oxo)diiron(III) cluster at ~325 and ~365 nm (*4*) can be discerned, but the shape of the spectrum indicates that the normal cluster is not the sole product. The features are more prominent following addition of Fe(II) to the apo protein in the presence of 3-MI (+3-MI, solid trace), suggesting that ET mediation is effective in this variant. Titration of the apo protein with Fe(II) in the presence of 3-MI showed that 2.0-2.7 equiv is required for completion in our best preparations (used in this work). This stoichiometry is somewhat less than for R2-wt (*20*) and several other variants (3.2 ± 0.2 equiv). In addition, the variation in this quantity from one preparation to another was greater than for R2-wt or other variants. As was found for other variants with the W48A substitution (*43*), expression of the protein in 10% (v/v) glycerol was found to be required for achieving maximum Fe(II)-uptake capacity. Subsequent purification and maintenance of the protein in 10% glycerol rendered it completely stable with respect to Fe(II)-uptake capacity.

To verify the capacity of R2-W48A/Y122F to undergo ET mediation, the iron products formed upon addition of O_2 to the Fe(II)-R2-W48A/Y122F complex in the presence (+3-MI) and absence (–3-MI) of mediator were characterized by Mössbauer spectroscopy (Figure 3-2). As suggested by the optical absorption data, significantly (44%) more (μ-oxo)diiron(III) cluster is formed in the presence of the mediator (0.84 ± 0.08 equiv, spectrum B) than in its absence (0.58 ± 0.06 equiv, spectrum A). The increase in yield of the normal product in the presence of the mediator is much less pronounced than is observed for the R2-W48A reaction (see Figure 2-4 (*43*)). The primary reason is *not* that ET mediation is less efficient in the double variant. Indeed, a product sample from the freeze-quench Mössbauer (RFQ-Möss) studies described below

Figure 3-1: Light absorption spectra of the products of the reaction of Fe(II)-R2-W48A/Y122F (3.0 equiv Fe) with excess O_2 in the absence (dotted trace) and presence (solid trace) of 1 mM 3-MI. The final protein concentration was 0.095 mM.

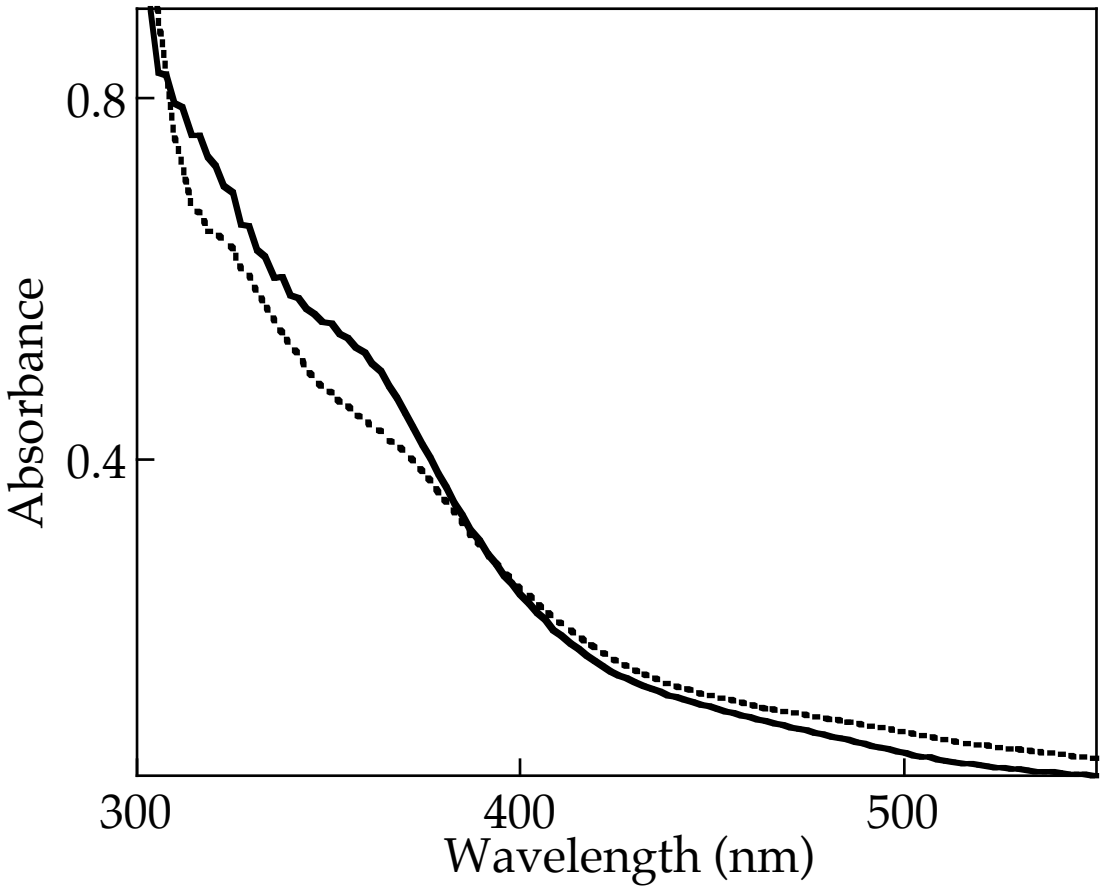
0.8
0.4
Absorbance
300
400
500
Wavelength (nm)

Figure 3-2: Mössbauer spectra of the products of the reaction of Fe(II)-R2-W48A/Y122F with excess O_2 (A) in the absence of 3-MI and (B) and (C) in the presence of 3-MI. For A and B, the Fe(II)-R2-W48A/Y122F complex (2.3 equiv) was mixed at 5 ± 3 °C with an equal volume of O_2-saturated buffer, the reaction was allowed to proceed for 5 min, and the sample was frozen in a Mössbauer cup. The final protein concentration was 0.50 mM. Spectrum C is of a recovered product sample from the sequential-mixing experiment described in the legend to Figure 5, in which the Fe(II)-R2-W48A/Y122F complex (2.2 equiv Fe) was mixed with O_2-saturated buffer, allowed to react at 11 °C for 0.20 s, mixed with an O_2-free solution of 3-MI (1mM final concentration after mixing), and then allowed to age for 5 min prior to being frozen in a Mössbauer cell. The spectra were acquired at 4.2 K with a magnetic field of 50 mT applied parallel to the □-beam. The solid lines plotted over the data in A, B, and C are the experimental spectrum of the (μ-oxo)diiron(III) product from the reaction of Fe(II)-R2-wt with O_2 plotted at intensities corresponding to 51%, 73 %, and 82%, respectively, of the experimental spectra.

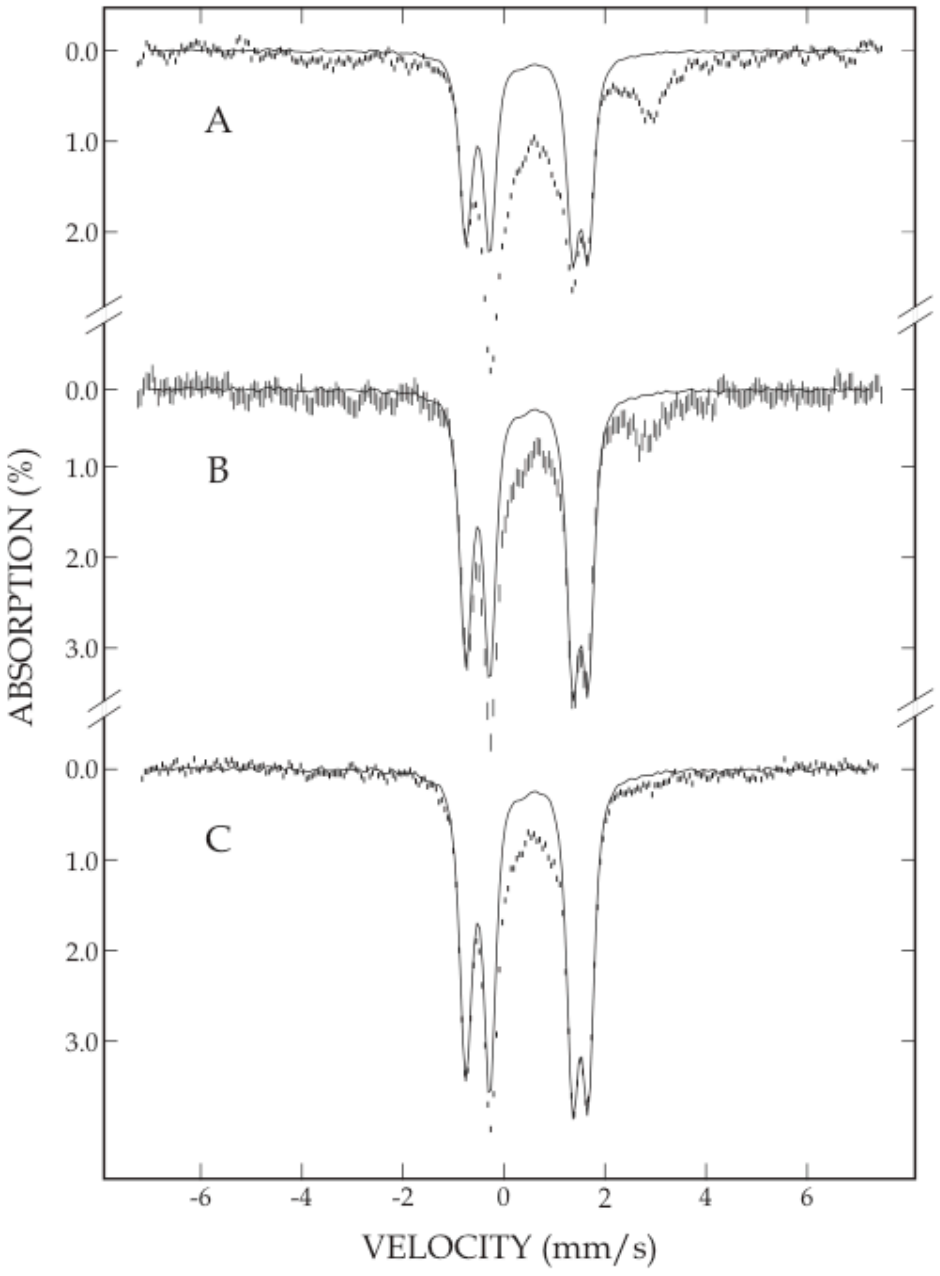
ABSORPTION (%)
A
B
C
0.0
1.0
2.0
3.0
-6
-4
-2
0
2
4
6
VELOCITY (mm/s)

was found to contain 82 ± 3% (μ-oxo)diiron(III) cluster (Figure 3-2, spectrum C), nearly equivalent to the 88 ± 3% observed in a sample of R2-W48A prepared similarly (*43*). Instead, the less drastic increase in yield of the normal product is a reflection of the fact that more is formed in the –3-MI reaction of R2-W48A/Y122F than in the –3-MI reaction of the single variant. A similar observation was made previously in comparison of the products of the R2-W48F and R2-W48F/Y122F reactions. The normal (μ-oxo)diiron(III) cluster represents only ~ 25% of the products of the former (*42*) but nearly 60% of the products of the latter.[2] It seems that the reaction pathway that proceeds through the **X**-Y122• di-radical species, which is operant in R2-W48F(A) (*42*) but can not be in R2-W48F(A)/Y122F, allows for more efficient formation of the altered Fe(III) products. In the absence of the oxidizable Y122, the normal product can form in higher yield even with the normal pathway for ET to the diiron cluster (*28*) disabled by substitution of W48 (*35, 42*). Nevertheless, the demonstration in Figure 3-2 that more of the normal product is produced in the +3-MI reaction confirms that the R2-W48A/Y122F reaction is indeed susceptible to ET mediation.

S*topped-flow Absorption and RFQ-Möss Evidence for Accumulation of an Intermediate*. In the reaction of the pre-formed Fe(II)-R2-W48A/Y122F complex with O_2 at 11 C in the absence of 3-MI, three resolved kinetic phases can be discerned in the A_{360nm}-versus-time trace (Figure 3-3). Fitting the equation for three parallel, first-order processes to these data gave rate constants of 0.6 s^{-1} and 0.1 s^{-1} for the two slower phases. The rate of the fastest phase is dependent on the O_2 concentration (Figure 3-3, compare solid and dotted traces), implying that it is in this fast phase that O_2 adds to the diiron(II) cluster. Under the assumption that the slower phases represent subsequent steps in a

Figure 3-3: Kinetics of O_2 activation at 11 C by Fe(II)-R2-W48A/Y122F monitored at 360 nm by stopped-flow absorption spectroscopy. Fe(II)-R2-W48A/Y122F (0.32 mM initial concentration, 3.0 equiv Fe) was mixed in a volume ratio of 1:2 with either 100% O_2-saturated buffer (solid trace) or 50% O_2-saturated buffer (dotted trace). The final concentrations of O_2 were 0.6 mM (dotted trace) and 1.2 mM (solid trace).

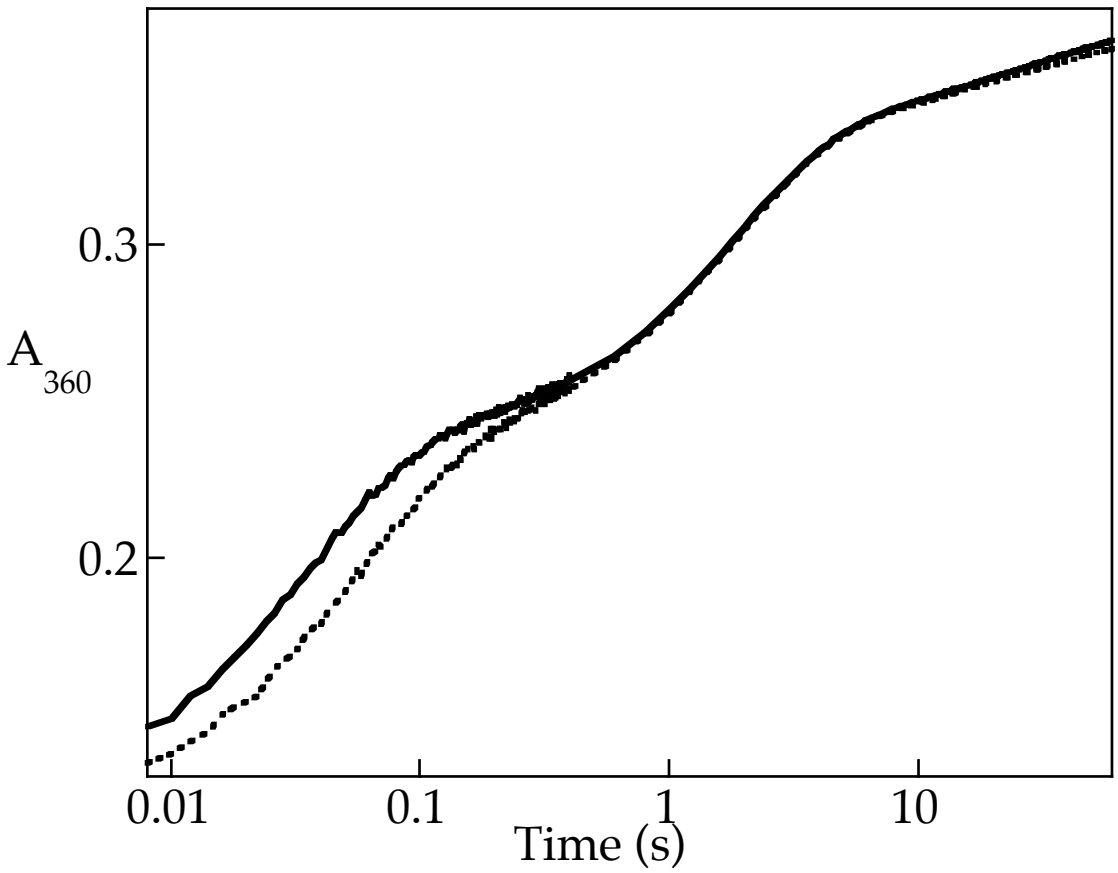
0.3
0.2
A360
0.01
0.1
1
10
Time (s)

sequence, the fact that the O_2-dependent phase is much faster implies that one or more intermediate species should accumulate to high levels. The absorption spectrum of this inferred adduct, which is obtained by subtraction of an early spectrum (~ 1.9 ms) from that corresponding to maximal accumulation of the intermediate (~ 130 ms), shows an absorption maximum at 310 nm and a shoulder at ~ 500 nm (Figure 3-4). Notably, absorption is not intense in the long-wavelength regime (600-725 nm) in which inorganic diiron(III) complexes that are known to have and protein complexes that are believed to have μ-1,2-peroxide bridges *do* absorb intensely (ε > 1000 $M^{-1}s^{-1}$) (*3, 13, 14, 16, 30-32, 41, 47-56*).

Mössbauer spectra at 4.2 K in a weak magnetic field (50 mT parallel to the γ-beam) of samples freeze-quenched during the fast, $[O_2]$-dependent phase of the reaction confirm the accumulation of an intermediate state. Features that are not attributable to the reactant diiron(II) protein, cluster **X**, or the Fe(III) products develop rapidly (Figure 3-5, spectrum A) with kinetics consistent with those of the fast phase observed by stopped-flow. Following subtraction of the spectral contributions from the known species (solid, dashed and dotted reference spectra plotted over and above the data in spectrum A), it can be seen that the rapidly developing new features are dominated by peaks at ~ 0.3 mm/s and 0.8 mm/s, with less intense peaks at ~ -0.3 mm/s and ~ 1.2 mm/s (Spectrum B). More definitive derivation of the spectrum of the intermediate state and analysis to extract Mössbauer parameters are presented below.

*Evidence for Conversion of the Intermediate to Cluster **X** Mediated by 3-MI.* The preceding paper demonstrates that ET can be mediated in W48A-containing variants by indole compounds such as 3-MI (*43*). The above product analysis indicates that ET

Figure 3-4: UV-visible absorption spectrum of intermediate species formed in the reaction of Fe(II)-R2-W48A/Y122F with O_2. Fe(II)-R2-W48A/Y122F (0.15 mM protein, 3.0 equiv Fe) was mixed at 11 °C with an equal volume of O_2-saturated buffer. The spectrum is the change observed (i.e., a difference spectrum) during accumulation of the intermediate between t = 1.9 ms and t = 130 ms.

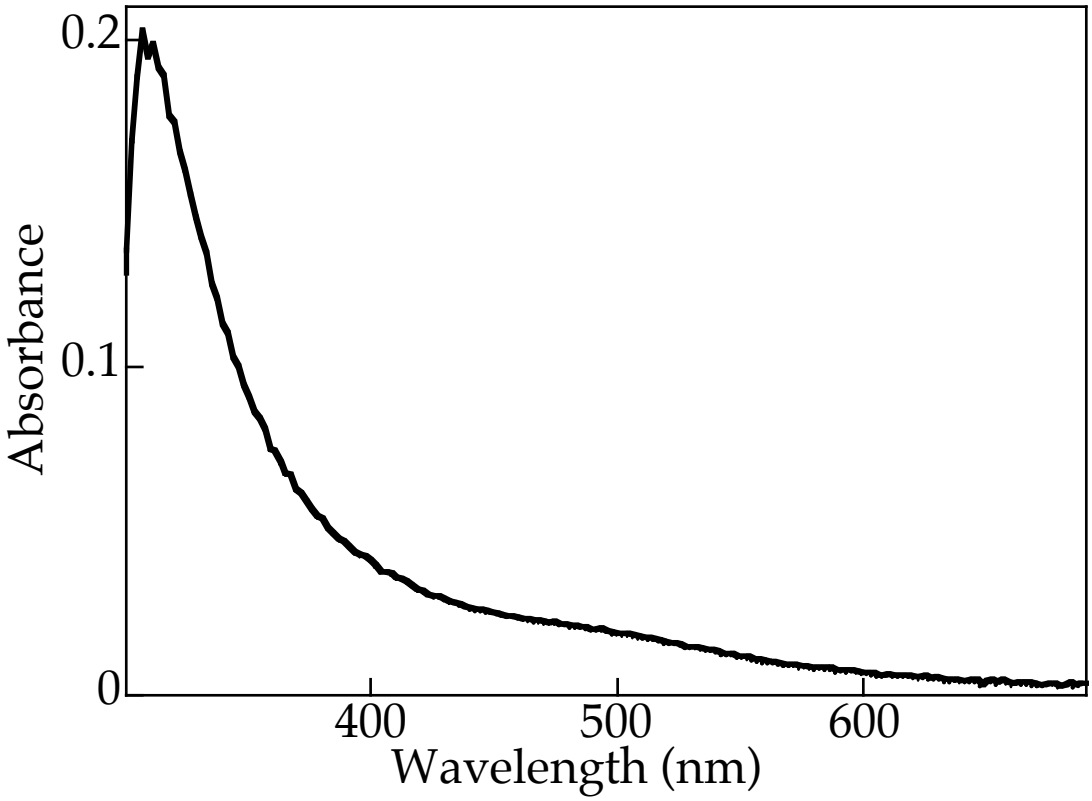
0.2
0.1
0
Absorbance
400
500
600
Wavelength (nm)

Figure 3-5: Mössbauer spectra from the reaction of Fe(II)-R2-W48A/Y122F with O_2 and the reaction of the resulting $(Fe_2O_2)^{4+}$ intermediate with 3-MI. (A) Spectrum of a sample prepared by mixing Fe(II)-R2-W48A/Y122F (1.8 mM, 2.2 equiv Fe) at 11 °C with an equal volume of O_2-saturated buffer and freeze-quenching 0.20 s after mixing. (B) Spectrum of the intermediate obtained by removing the spectral contributions from contaminating species (50% Fe(II) reactant, dashed line plotted over data; 5% cluster **X**, solid line plotted over data; and 3 % (μ-oxo)diiron(III) product, dotted line plotted above data) from spectrum A. The reference spectrum for the Fe(II) reactant was of unreacted Fe(II)-R2-W48A/Y122F complex, and the reference spectra of **X** and the (μ-oxo)diiron(III) product were derived from experimental spectra of samples from the reaction of Fe(II)-R2-wt with O_2. (C) and (D) are spectra of sequential-mix samples prepared by reaction of Fe(II)-R2-W48A/Y122F with O_2 (as in A), aging for 0.20 s, mixing of the resulting solution in a 2:1 volume ratio with either (C) O_2-free buffer or (D) O_2-free 3 mM 3-MI, and freeze-quenching 0.18 s after mixing. The spectra were acquired at 4.2 K with a magnetic field of 50 mT applied parallel to the □-beam. The leftward and rightward slanting arrows below spectrum D point to the features of cluster **X** and the (μ-oxo)diiron(III) product, respectively.

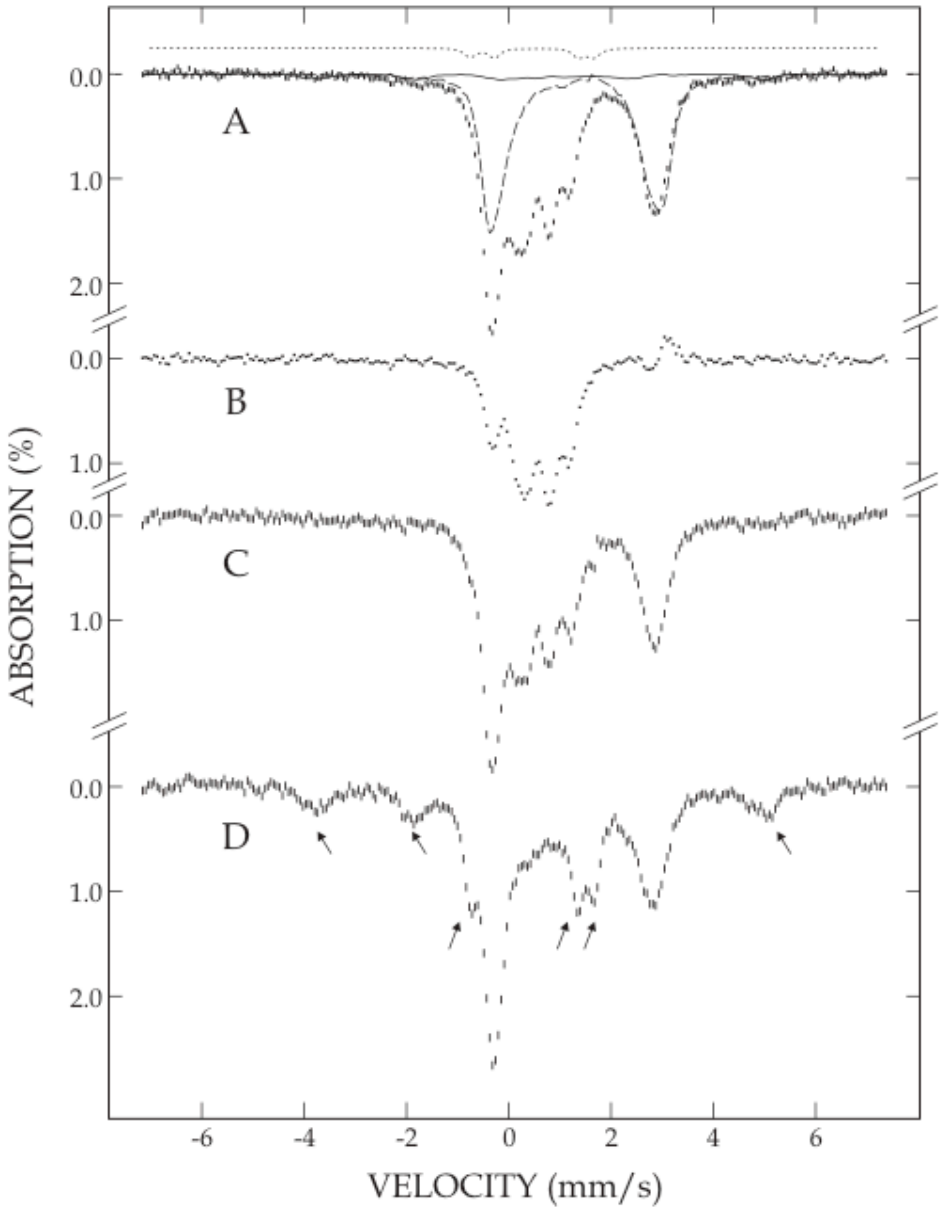
ABSORPTION (%)
0.0
1.0
2.0
A
B
C
D
-6
-4
-2
0
2
4
6
VELOCITY (mm/s)

mediation is also effective in R2-W48A/Y122F. We next sought to test whether the intermediate state suggested by the stopped-flow and RFQ-Möss results would be induced to convert to cluster **X** by exposure to 3-MI. Fe(II)-R2-W48A/Y122F was mixed with O_2, the solution was aged for sufficient time for the intermediate state to accumulate to near-maximum levels (0.12 s), and the reaction solution was then mixed with an O_2-free solution of 3-MI (final concentration of 1 mM) or with O_2-free buffer (–3-MI control). In the –3-MI control (Figure 3-6, circles), the increase in absorbance at 360 nm corresponds to the two slower kinetic phases observed in Figure 3-3, with the majority of intensity associated with the faster of the two phases (apparent first-order rate constant of 0.6 s^{-1}). In the +3-MI experiment (Figure 3-6, squares), the increase in absorbance is much faster and the amplitude greater. An apparent first-order rate constant of 3.6 s^{-1} is obtained by regression analysis, suggesting that 3-MI accelerates the reaction by more than a factor of 5. Analysis of RFQ-EPR and RFQ-Möss data implies, however, that the reaction is accelerated to an even greater extent (see below).

RFQ-EPR was used to verify the capacity of 3-MI to accelerate decay of the putative intermediate. A sequential-mixing protocol essentially identical with that in the stopped-flow experiments was employed. The X-band EPR spectrum at 20°K of the experimental sample (Figure 3-7, solid spectrum), which was quenched 0.11 s after the pre-formed intermediate was mixed with 3-MI, exhibits the sharp, isotropic, $g = 2$ singlet characteristic of cluster **X** (*19, 20, 23, 29*). A much weaker signal (< 20% of the integrated intensity) was observed for the –3-MI control sample quenched 0.11 s after a second mix with buffer (Figure 3-7, dashed spectrum). Kinetics of formation and decay of **X** after the mix with mediator (solid circles in Figure 3-8) or O_2-free buffer (triangles

Figure 3-6: Reactivity of the putative $(Fe_2O_2)^{4+}$ intermediate species toward 3-MI, as shown by stopped-flow absorption spectroscopy. Fe(II)-R2-W48A/Y122F (0.38 mM, 3.0 equiv Fe) in buffer A was mixed at 11 C with an equal volume of O_2-saturated buffer A. The solution was aged for 0.12 s before being mixed with an equal volume of either O_2-free 2 mM 3-MI solution (squares) or O_2-free buffer A (circles). The solid fit lines are the best fits of the equation describing three parallel first-order processes to the data.

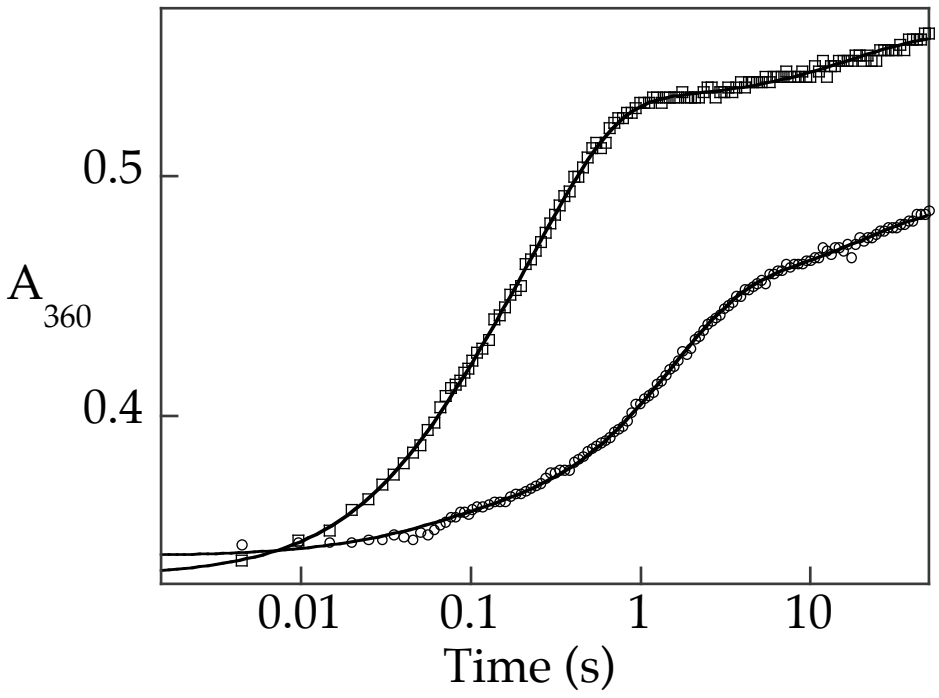
0.5
0.4
A360
0.01
0.1
1
10
Time (s)

Figure 3-7: Reactivity of the putative $(Fe_2O_2)^{4+}$ intermediate species toward 3-MI, as shown by sequential-mixing RFQ-EPR. Fe(II)-R2-W48A/Y122F (1.1 mM, 2.5 equiv Fe) in buffer A was mixed at 11 C with an equal volume of O_2-saturated buffer A. The solution was aged for 0.12 s before being mixed with an equal volume of either O_2-free 2 mM 3-MI solution (solid line) or O_2-free buffer A (dashed line). This solution was then aged for 0.11 s before being freeze-quenched. The spectra were acquired at 20 K. The spectrometer conditions were: microwave frequency, 9.47 GHz; microwave power, 6.3 μW, modulation frequency, 100 KHz; modulation amplitude, 4.0 G; scan time, 330 s; time constant, 81 ms.

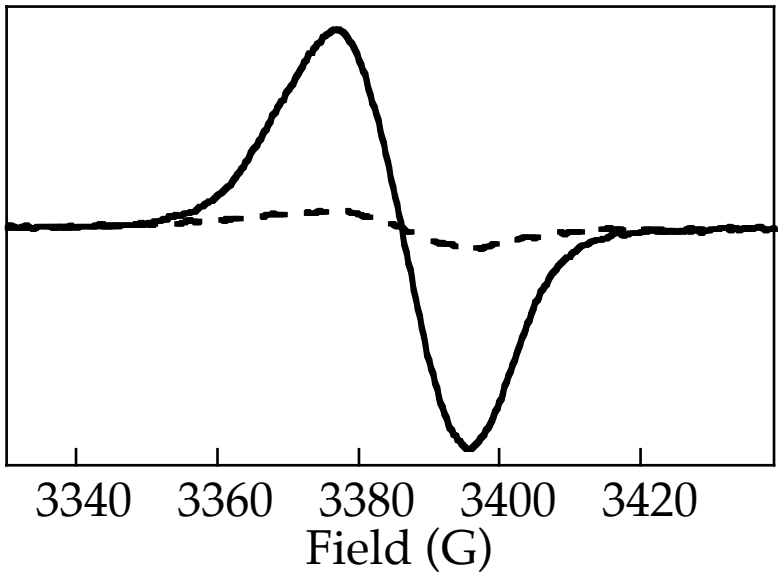
3340
3360
3380
3400
3420
Field (G)

Figure 3-8: Quantities of **X** and the (μ-oxo)diiron(III) cluster as functions of time in reaction of the putative $(Fe_2O_2)^{4+}$ intermediate species with 3-MI (circles and squares) or buffer (triangles). The data are from analysis of Mössbauer (open symbols) and EPR (closed symbols) spectra of samples prepared as in the legends to Figures 5 and 7 (with varying second aging times). The circles and triangles depict the quantities of **X** and the squares the quantities of (μ-oxo)diiron(III) cluster. The solid and dotted lines are simulations of the quantities of **X** and (μ-oxo)diiron(III) cluster, respectively, according to Scheme 1 and an initial quantity of the $(Fe_2O_2)^{4+}$ intermediate of 0.6 equiv. The dashed line plotted over the triangles is a simulation corresponding to 0.6 equiv $(Fe_2O_2)^{4+}$ and rate constants of 0.6 and 8 s^{-1} for formation and decay of **X**. Both simulations take into account the small quantities of **X** and (μ-oxo)diiron(III) cluster formed in the first aging time, as indicated by the Mössbauer and EPR spectra of single-mix samples.

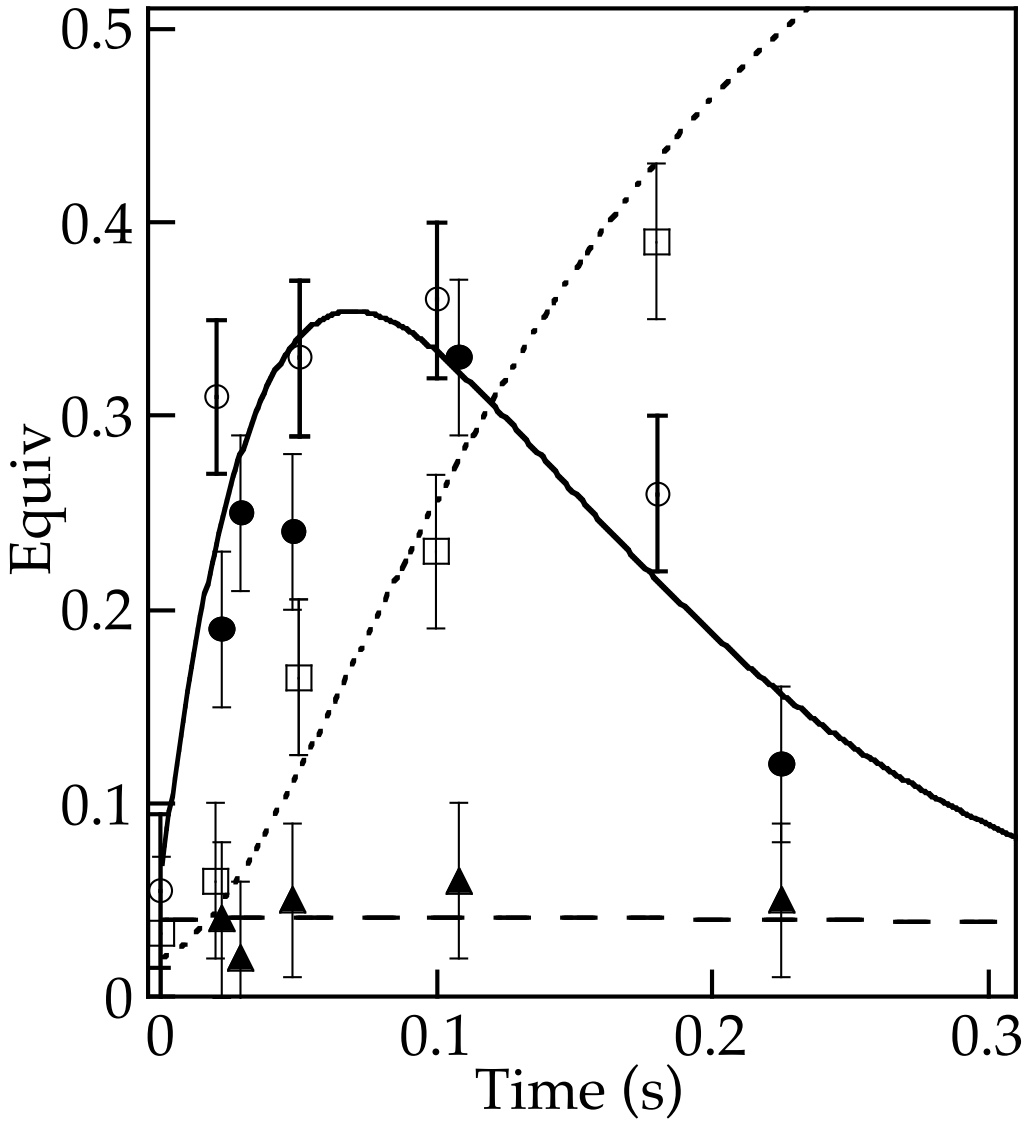
0.5
0.4
0.3
0.2
0.1
0
Equiv
0
0.1
0.2
0.3
Time (s)

in Figure 3-8) were obtained (as previously described (*20*)) by double integration of the derivative EPR spectra of samples with varying second aging time.

The 3-MI-mediated conversion of the intermediate state to cluster **X** was further verified by RFQ-Möss. As before, the intermediate was allowed to accumulate after the first mix of Fe(II)-R2-W48A/Y122F with O_2 (aging time = 0.20 s), and the reaction solution was then mixed with O_2-free 3-MI (experiment) or O_2-free buffer (–3-MI control), allowed to react for a second aging time, and then freeze-quenched. The weak-field/4.2 K Mössbauer spectra of control and experimental samples for which the second aging time was 0.18 s are shown in Figure 3-5 (spectra C and D, respectively). Comparison of the spectrum of the sample that was freeze-quenched after the initial accumulation phase of 0.20 s (A) to that of the sequential-mix –3-MI control (C) reveals that the reaction progresses to a minor extent (~ 7-10% decay in the intensity of the features attributable to the intermediate) in 0.18 s in the absence of 3-MI. This result allows a rate constant of 0.4-0.6 s^{-1} to be estimated for the decay of the intermediate state in the absence of mediator. The spectrum of the experimental sample (D) exhibits the paramagnetic signature of cluster **X** (leftward slanting arrows (*19, 23, 46*)) and the pair of quadrupole doublets characteristic of the (μ-oxo)diiron(III) product (rightward slanting arrow (*4, 20*)). As importantly, the features of the intermediate state are absent, indicating that it decays in formation of **X** and the (μ-oxo)diiron(III) product. From analysis of spectra of samples with second aging times of 0.020 s (see Figure 3-9), 0.050 s, 0.10 s, and 0.18 s, the kinetics of the 3-MI-mediated conversion of the intermediate state to cluster **X** (open circles in Figure 3-8) and the subsequent conversion of **X** to the (μ-oxo)diiron(III) product (open squares in Figure 3-8) were defined. The data (open

symbols) are plotted in Figure 3-8 along with the quantities of **X** obtained by RFQ-EPR (solid symbols). All the kinetic data can be accounted for by assumption of rate constants of 22 s^{-1} for conversion of the $(Fe_2O_2)^{4+}$ intermediate state to cluster **X** and 8 s^{-1} for conversion of **X** to the (μ-oxo)diiron(III) product (Scheme 3-1) and an initial concentration of 0.6 equiv $(Fe_2O_2)^{4+}$ relative to R2 dimer (solid and dotted traces in Figure 3-8). The magnitude of the rate constant for decay of **X** to the (μ-oxo)diiron(III) product, 8 s^{-1}, is perhaps larger than would have been expected. Decay of **X** in R2-Y122F has a rate-constant of ~ 0.3 s^{-1} at this temperature.[2] The comparison suggests that 3-MI accelerates *decay* of **X** in addition to its formation from its precursor. If this likelihood is neglected and it is assumed that decay of **X** in the absence of 3-MI also has a rate constant of 8 s^{-1}, then the kinetics of its formation and decay in the absence of mediator can be accounted for reasonably well with a formation rate constant of 0.6 s^{-1} (Figure 3-8, dashed trace), consistent with the rate-constant estimated from the stopped-flow and RFQ-Möss data. Assumption of a smaller rate constant for decay of **X** in the absence of 3-MI would require an even smaller rate constant for its formation from the $(Fe_2O_2)^{4+}$ species to account for the failure of **X** to accumulate to a greater extent. Thus, 3-MI accelerates decay of the intermediate by at least 37-fold (22 s^{-1}/0.6 s^{-1}).

As indicated in Scheme 3-1, the 3-MI-mediated reduction of the $(Fe_2O_2)^{4+}$ complex to **X** should also produce a 3-MI radical. In principle, this might be detectable either by absorption at 310 nm and 510 nm (for a neutral radical) or at 335 and 560 nm (for a cation radical) (*57*) or by a $g \sim 2$ EPR signal. Attempts to detect spectral signatures of a transient 3-MI radical were unsuccessful. This observation suggests that, if a 3-MI

radical forms in reduction of the $(Fe_2O_2)^{4+}$ complex to **X**, its decay is sufficiently rapid to prevent it from accumulating to a detectable level.

*Nature of the Precursor to **X** as Revealed by RFQ-Möss.* The single- and sequential-mixing SF-Abs, RFQ-EPR, and RFQ-Möss data establish that an intermediate state accumulates upon reaction of Fe(II)-R2-W48A/Y122F with O_2 and that this state is induced to convert rapidly to cluster **X** by the ET mediator, 3-MI. These results set the stage for the primary objective of this work, to obtain insight into the nature of the precursor to cluster **X** by resolution of its Mössbauer spectrum. The spectrum of this state was deduced by two independent "kinetic-difference" treatments. In the first, contributions of known "contaminants" (primarily diiron(II) reactant) to spectra of single-mix samples containing the intermediate were removed by subtraction of reference spectra for these species. This treatment amounts to a kinetic resolution of the features of the species that form (the intermediate state) in the first mix of Fe(II)-R2-W48A/Y122F with O_2 (the formation phase). An example was shown previously (Figure 3-5, spectrum B). In the second, subtraction of the spectrum of an experimental (+3-MI) sequential-mix RFQ-Möss sample (Figure 3-9, spectrum A, hatches) from the spectrum of the corresponding –3-MI control sample (spectrum A, solid line) generated a kinetic-difference spectrum (B) of the 3-MI-mediated reaction (the decay phase), with downward features from species that decay (the intermediate state) and upward features from species that form (**X** and the (μ-oxo)diiron(III) cluster). Removal of the upward contributions to this difference spectrum (solid line plotted over the data in spectrum B) then resolved the features of the species that decay (spectrum C). Two spectra from the formation phase (one derived from a sample with an aging time of 0.020 s, which is early in this phase,

Figure 3-9: Kinetic resolution of the Mössbauer spectrum of the $(Fe_2O_2)^{4+}$ intermediate. The two overlaid spectra in A are of –3-MI control (solid line) and +3-MI experimental (hatches) samples prepared by the same procedure used to prepare those of Figure 5, spectra C and D, but with second aging times of 0.020 s. Spectrum B is the difference spectrum obtained by subtracting the spectrum of the experimental sample from that of the control sample. The solid line plotted over B is the summed (upward pointing) contributions from **X** and the (μ-oxo)diiron(III) cluster (23 % and 4%, respectively). Spectrum C is the result of removing these contributions from B and represents the contributions of the $(Fe_2O_2)^{4+}$ state that decays upon mixing with 3-MI. The spectra were acquired at 4.2 K with a magnetic field of 50 mT applied parallel to the □-beam.

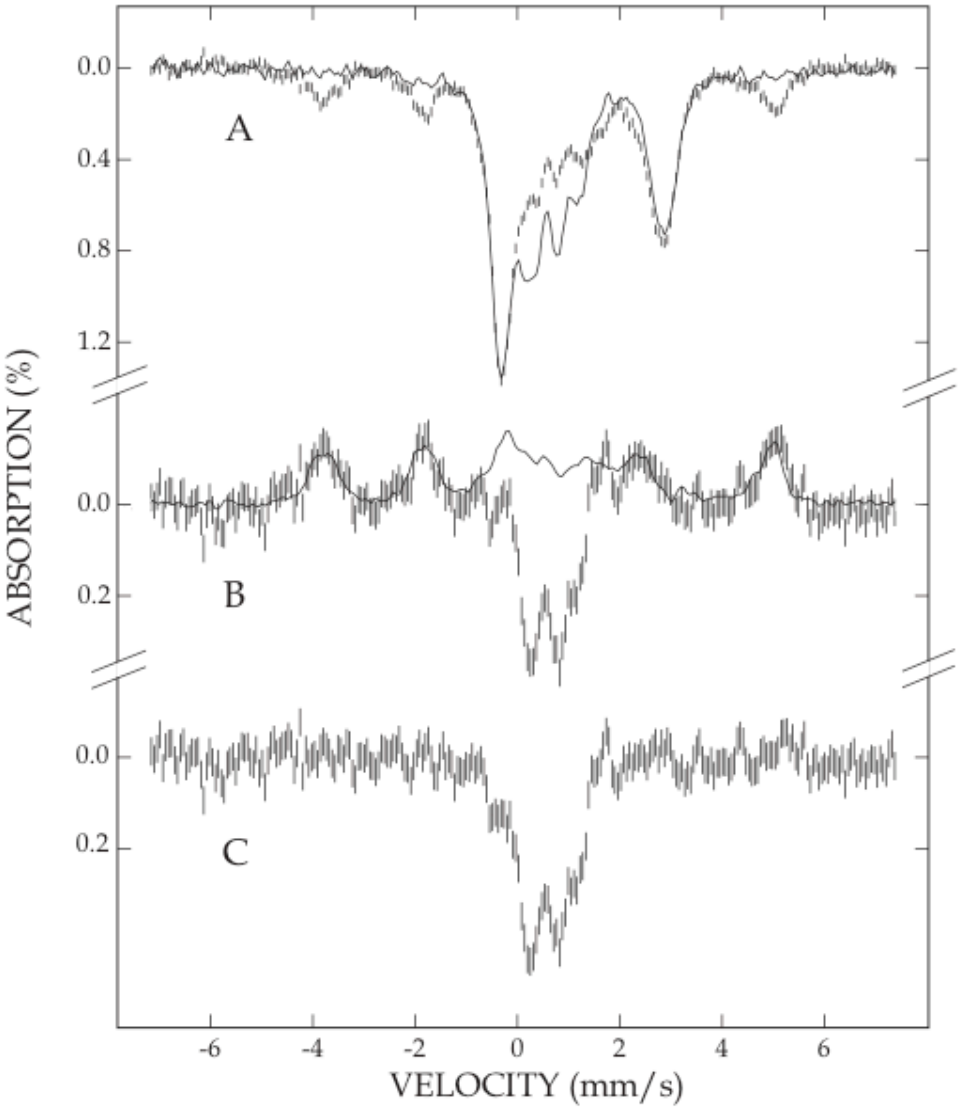
ABSORPTION (%)
0.0
0.4
0.8
1.2
A
0.0
0.2
B
0.0
0.2
C
-6
-4
-2
0
2
4
6
VELOCITY (mm/s)

and one derived from a sample with an aging time of 0.20 s, which is essentially after completion of formation) and two from the decay phase (second aging times of 0.020 s and 0.050 s) are shown in Figure 3-10. The spectra are qualitatively very similar. Each exhibits a broad central doublet with peaks at ~ 0.3 mm/s and ~ 0.8 mm/s, and a less intense but sharper outer doublet with peaks at ~ −0.3 mm/s and ~ 1.2 mm/s. Differences among the spectra can be attributed to uncertainties in the analysis and random error in the experimental spectra (of the samples and the "contaminating" species that must be accounted for). For example, the low energy line of the weaker doublet is somewhat more variable in position, extent of resolution, and intensity than the three other peaks. This variation is attributable to imperfect removal of the contribution of Fe(II)-containing reactant, a problem that also leads to a small derivative-type artifact in the spectra at the position of the higher energy line of the Fe(II) complex (~ 3 mm/s). Nevertheless, the four independent spectra obtained by two independent kinetic-resolution analyses agree quite well. This agreement is notable, because the spectra from the formation phase were generated by removing contributions almost exclusively of Fe(II) reactant, whereas the spectra from the decay phase were generated by removing contributions exclusively from **X** and the (μ-oxo)diiron(III) product. The agreement proves that the intermediate state that converts to **X** by reaction with 3-MI is also the primary state that forms during the initial reaction with O_2. Moreover, the similarity of the kinetically-resolved spectra constructed from samples quenched early or late in either the formation or the decay phase establishes that the complexes associated with the two sets of Mössbauer features form and decay together, with complete kinetic correlation.

Figure 3-10: Four independent Mössbauer spectra of the $(Fe_2O_2)^{4+}$ intermediate. The spectra were derived by subtraction analysis of experimental spectra as described in the text and the legends to Figures 3-5 and 3-9. The green and black spectra are from the intermediate's formation phase (aging times of 0.020 s and 0.20 s, respectively) and the blue and red spectra are from the decay phase (*second* aging times of 0.020 s and 0.050 s, respectively).

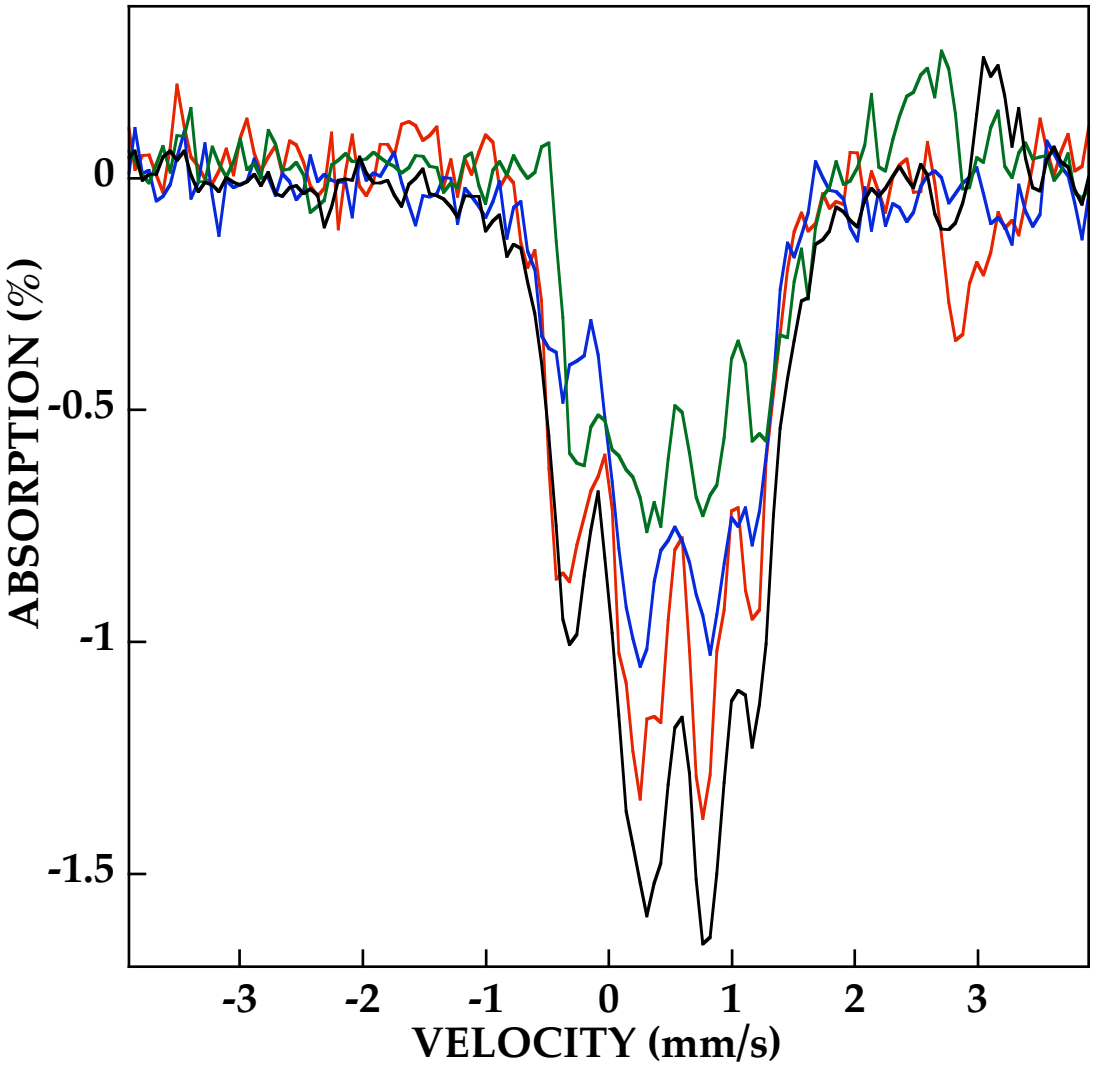
ABSORPTION (%)
0
-0.5
-1
-1.5
-3
-2
-1
0
1
2
3
VELOCITY (mm/s)

To decrease uncertainty in the spectrum of the intermediate state, the four independent, individual spectra from Figure 3-10 were averaged. In the averaging procedure, each spectrum was weighted according to the product of the relative contribution of the intermediate state to it and the baseline counts of the experimental spectrum used to generate it. The resulting spectrum was analyzed according to two alternative assumptions (Figure 3-11). Analysis of the spectrum by assumption of one inner and one outer quadrupole doublet yielded a relative intensity ratio of approximately 3:1 with Mössbauer parameters of δ = 0.52 mm/s, and ΔE_Q = 0.55 mm/s for the central doublet and δ = 0.45 mm/s, ΔE_Q = 1.53 mm/s for the outer doublet (solid line plotted over the data in Figure 3-11A). This analysis implies that the intermediate state comprises primarily two distinct diiron complexes, with each complex containing two Mössbauer-equivalent iron sites. In consideration of the fact that the intermediate complexes are most likely peroxodiiron(III) species (*vide infra*) and that asymmetric oxygen binding has been observed for oxyhemerythrin (*58*), the peroxodiiron(III) intermediate in stearoyl acyl carrier protein Δ^9-desaturase (*52*), and several inorganic peroxodiiron(III) model complexes (*59, 60*), we also examined the possibility that the presence of asymmetric peroxide coordination leads to inequivalent Fe(III) sites in the intermediate state. The spectrum was thus least-squares fitted with one outer and two inner doublets. The outer doublet and one of the inner doublets were paired to represent an asymmetric complex and were therefore constrained to have the same intensity. Regardless of whether the linewidths of each doublet were constrained to be equal or allowed to vary independently, the analysis yielded a rather constant δ of 0.6 mm/s and a narrow range of ΔE_Q, 0.43 - 0.53 mm/s, for the inner doublet that was paired with the outer doublet. The parameters

Figure 3-11: Analysis of the average derived spectrum of the $(Fe_2O_2)^{4+}$ intermediate. The spectrum was analyzed using two alternative assumptions. The solid line shown in (A) is a least-squares fit of the spectrum assuming one outer and one inner quadrupole doublet. The parameters obtained are ΔE_Q = 1.53 mm/s, δ = 0.45 mm/s, Γ (full width at half maximum) = 0.28 mm/s, and percent absorption = 23% for the outer doublet, and ΔE_Q = 0.55 mm/s, δ = 0.52 mm/s, Γ = 0.48 mm/s and percent absorption = 67% for the inner doublet. The solid line shown in (B) is a least-squares fit of the spectrum assuming one outer and two inner quadrupole doublets. The outer doublet and one of the inner doublets are constrained to have the same percent absorption and line-width to represent a diiron complex with inequivalent iron sites. The parameters obtained for the asymmetric complex are $\Delta E_Q(1)$ = 1.53 mm/s, $\delta(1)$ = 0.45 mm/s, $\Delta E_Q(2)$ = 0.53 mm/s, $\delta(2)$ = 0.60 mm/s, Γ = 0.32 mm/s, and a percent absorption of 27% for each doublet. The parameters for the unpaired inner doublet are ΔE_Q = 0.55 mm/s, δ = 0.43 mm/s, Γ = 0.42 mm/s and a percent absorption of 36%.

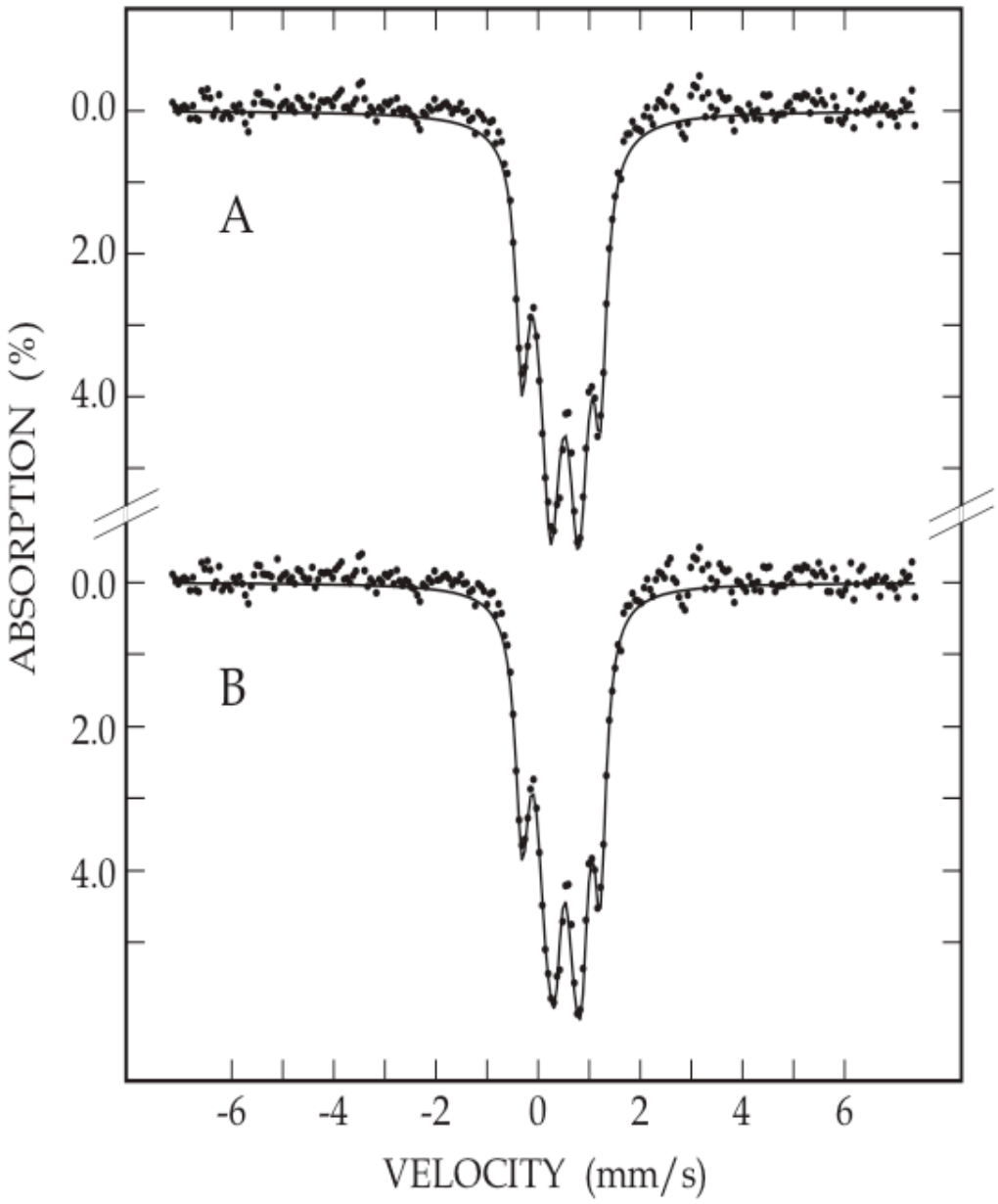
0.0
2.0
4.0
A
0.0
2.0
4.0
B
ABSORPTION (%)
-6
-4
-2
0
2
4
6
VELOCITY (mm/s)

of the outer doublet and second (unpaired) inner doublet were changed to a minor extent from those obtained in the simpler, two-doublet fit. The solid line plotted over the data in Figure 3-11B is a least-squares fit resulting from such an analysis. On the basis of the above spectral and kinetic analyses, the following conclusions can be made. The 3:1 intensity ratio of the central and outer doublets indicates that the intermediate state is heterogeneous: at least two Fe complexes are present. The invariance of the relative intensity of these doublets with time in both formation and decay phases of the reaction suggests that the two (or more) complexes exist in a rapid (with respect to formation and 3-MI-mediated decay) equilibrium. The Mössbauer parameters suggest that these complexes are composed of high-spin Fe(III) ions, and the lack of observed magnetic hyperfine interactions indicates that they are antiferromagnetically coupled diiron(III) clusters. Complexes either with nearly equivalent Fe(III) sites or with inequivalent, resolved Fe(III) sites are equally possible.

Reactivity of the (μ-1,2-peroxo)diiron(III) Complex that Accumulates in D84E R2 Variants Toward 3-MI-Mediated Reduction. Peroxodiiron(III) complexes believed to have μ-1,2 peroxide bridges have been detected in reactions of O_2 with the reduced forms of a number of diiron-carboxylate proteins (MMOH (*13, 14, 16*), variants of R2 containing the D84E substitution (*30-32, 41*), chemically reduced stearoyl acyl carrier protein Δ^9 desaturase (*51, 52*), and ferritin (*53-55*)). These complexes are distinguished by their intense long-wavelength absorption (650-725 nm, $\varepsilon > 1000$ $M^{-1}cm^{-1}$) and their unusually high (for high-spin Fe(III) species) Mössbauer isomer shifts (0.58-0.68 mm/s). As previously noted, observation of both optical and Mössbauer features potentially indicative of a similar complex in the reaction of Fe(II)-R2-wt with O_2 was reported in an

earlier study (*22*). On this basis and the expectation that the structurally similar proteins would react with O_2 through common early intermediates (*1, 61*), a (μ-1,2-peroxo)diiron(III) complex has been proposed as an early intermediate in the R2 reaction (*1, 22, 38, 39, 48, 61-63*). Direct reduction of this complex by injection of the extra electron has also been invoked (*39, 62*). To test the reactivity of a known (μ-1,2-peroxo)diiron(III) complex toward 3-MI-mediated reduction, sequential-mixing stopped-flow experiments were carried out with R2-W48A/D84E. As noted above, the D84E substitution causes the (μ-1,2-peroxo)diiron(III) complex to accumulate to stoichiometric levels (*30-32, 41*). Evidence presented in Chapter 2 establishes that this protein is also susceptible to ET mediation by 3-MI (*43*). Perhaps surprisingly, exposure of the (μ-1,2-peroxo)diiron(III) complex, formed in an initial incubation of Fe(II)-R2-W48A/D84E and O_2 (inset to Figure 3-12), to 1 mM 3-MI accelerates decay of the 700-nm absorption of the complex by less than 20% (main panel of Figure 3-12), despite the fact that the presence of the mediator results in formation of 2.2 times as much stable Y122• (*43*). This result suggests that the (μ-1,2-peroxo)diiron(III) complex itself is unreactive toward 3-MI-mediated reduction and that 3-MI-mediated ET can occur only after the relatively inert complex decays to a more reactive species. Thus, both the spectroscopic properties of the (μ-1,2-peroxo)diiron(III) complex and its reactivity contrast markedly with those of the $(Fe_2O_2)^{4+}$ intermediate state in R2-W48A/Y122F.

DISCUSSION

The complexes that accumulate in the reaction of R2-W48A/Y122F and convert to cluster **X** upon exposure to 3-MI are clearly distinct from intermediates characterized

Figure 3-12: Inertness toward 3-MI-mediated reduction of the (μ-1,2-peroxo)diiron(III) complex that accumulates in the reaction of Fe(II)-R2-W48A/D84E with O_2. Fe(II)-R2-W48A/D84E (0.35 mM, 3.5 equiv Fe) was mixed at 11 °C with an equal volume of O_2-saturated buffer. This solution was aged for 0.17 s prior to being mixed with an equal volume of either O_2-free buffer (solid line) or O_2-free 4 mM 3-MI solution (dotted line). The inset shows absorption spectra for the 3-MI control reaction shortly (3.2 ms) after the second mix (solid trace) and after completion (50 s, dotted trace) to illustrate the intense 700-nm absorption feature of the (μ-1,2-peroxo)diiron(III) complex that forms in the reactions of all R2 variants with the D84E substitution.

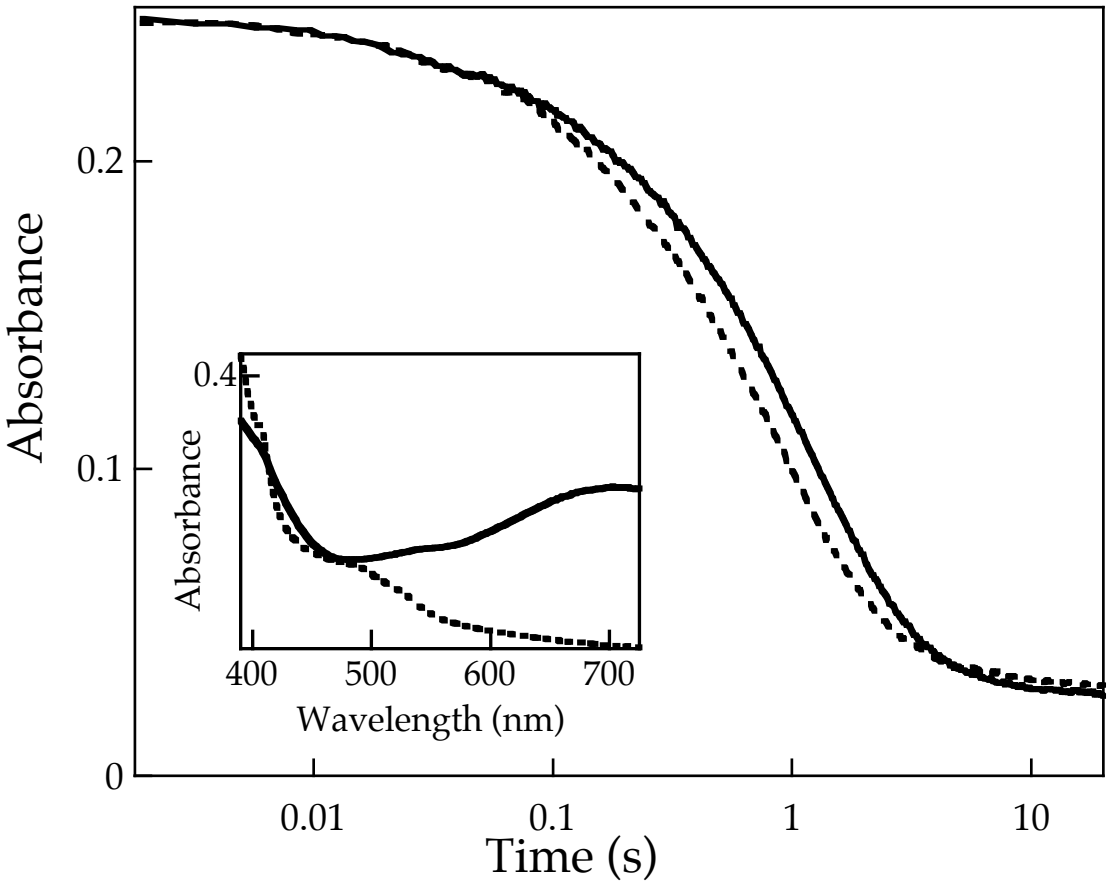
Absorbance
0.2
0.1
0
0.01
0.1
1
10
Time (s)
0.4
Absorbance
400
500
600
700
Wavelength (nm)

to date in O_2 activation by diiron-carboxylate proteins. They have isomer shifts squarely in the range of high-spin Fe(III) species, ruling out the possibility that they are Fe(IV) complexes related to sMMO **Q** (*11, 13*), and also lack the Mössbauer signature and intense low-energy optical absorption characteristic of (μ-1,2-peroxo)diiron(III) complexes such as **P** (*13, 14, 16, 30-32, 49-54, 56*). Three possibilities must be considered concerning the relationship of the $(Fe_2O_2)^{4+}$ state to the normal (wt) R2 reaction sequence. First, the state may comprise off-pathway complexes that accumulate either (1) because the ET pathway is blocked and they are more stable than the complex that would otherwise rapidly oxidize W48 or (2) because the amino acid substitutions perturb the structure or dynamics of the protein, altering the reaction pathway. The issue of whether an intermediate detected in a variant protein is on the normal (wt) pathway is a general concern, and was in this case the primary motivation for seeking a strategy to trigger the reactivity of the $(Fe_2O_2)^{4+}$ state that was previously inferred in the reactions of R2-W48F and R2-W48F/Y122F. With this strategy, the "chemical competence" of the $(Fe_2O_2)^{4+}$ state to convert to **X** has been unequivocally established. On this basis, we strongly disfavor the first possibility. Second, the state may comprise rapidly interconverting diiron(II)-O_2 complexes that form early in a pathway for O_2 activation that is orthogonal to that beginning with the (μ-1,2-peroxo)diiron(III) complex (as in sMMO and D84E R2 variants). This possibility would imply that the D84E substitution in R2 fundamentally changes the O_2 activation mechanism by causing an initial adduct with different geometry and reactivity to form. Under the assumption that the $(Fe_2O_2)^{4+}$ state formed with the wt ligands is reactive specifically toward one-electron reduction whereas the (μ-1,2-peroxo)diiron(III) complex is less reactive in this manner but more

reactive toward O-atom transfer (either directly or after conversion to, for example, a diiron(IV) complex), this scenario would rationalize the observations that hydroxylation of the nearby F208 phenyl ring occurs in R2-W48F/D84E (even though Y122 is still present), whereas F208 hydroxylation does not occur in R2-W48F/Y122F (even though both residues that are facile donors of one electron to the $(Fe_2O_2)^{4+}$ state are absent) (*32*). However, this possibility would not accommodate the previous evidence for a **P**-like complex in the reaction of R2-wt (*22*), nor would it rationalize simply the observation that the **P**-like complex decays to form Y122• in the reaction of R2-D84E (*30*). For these reasons, we favor the third possibility: that the detected intermediate state is a *successor* to the **P**-like complex (Scheme 3-2) in the R2-wt reaction pathway. This hypothesis can accommodate all the available data. With the measured rate constant for addition of O_2 in the R2-wt reaction (k_1 = 2.1 x 10^5 $M^{-1}s^{-1}$ at 5 °C) (*28*), an appropriately large rate constant (k_2 ~ 400-4000 s^{-1}) for conversion of the initial **P**-like adduct to the $(Fe_2O_2)^{4+}$ intermediate state detected herein, and a still larger rate constant (k_3) for oxidation of W48 by the $(Fe_2O_2)^{4+}$ state, the accumulation of low levels of the **P**-like complex but none of the successor $(Fe_2O_2)^{4+}$ state would be rationalized (Scheme 3-2A). In the reactions of W48 variants, the observed ~ 10-fold slowing of O_2 addition (presumably due to a secondary effect of the substitution on protein or cluster dynamics) (*42*) would cause the (μ-1,2-peroxo)diiron(III) complex to be kinetically masked, and the block in ET would allow the successor $(Fe_2O_2)^{4+}$ complex to accumulate (Scheme 3-2B). The effect of the D84E substitution would then be explained in terms of a retardation of the conversion of the **P**-like complex to the $(Fe_2O_2)^{4+}$ state, an effect on the equilibrium for this conversion, or both (Scheme 3-2C). Reversibility in this conversion could rationalize

Scheme 3-2: Proposal that the $(Fe_2O_2)^{4+}$ intermediate state is a successor to the (μ-1,2-peroxo)diiron(III) complex in the reactions of **A**) R2-wt, **B**) R2-W48A/Y122F, and **C**) R2-D84E and R2-W48F/D84E. Kinetic constants are from reference 28 (**A**) and this work (**B**).

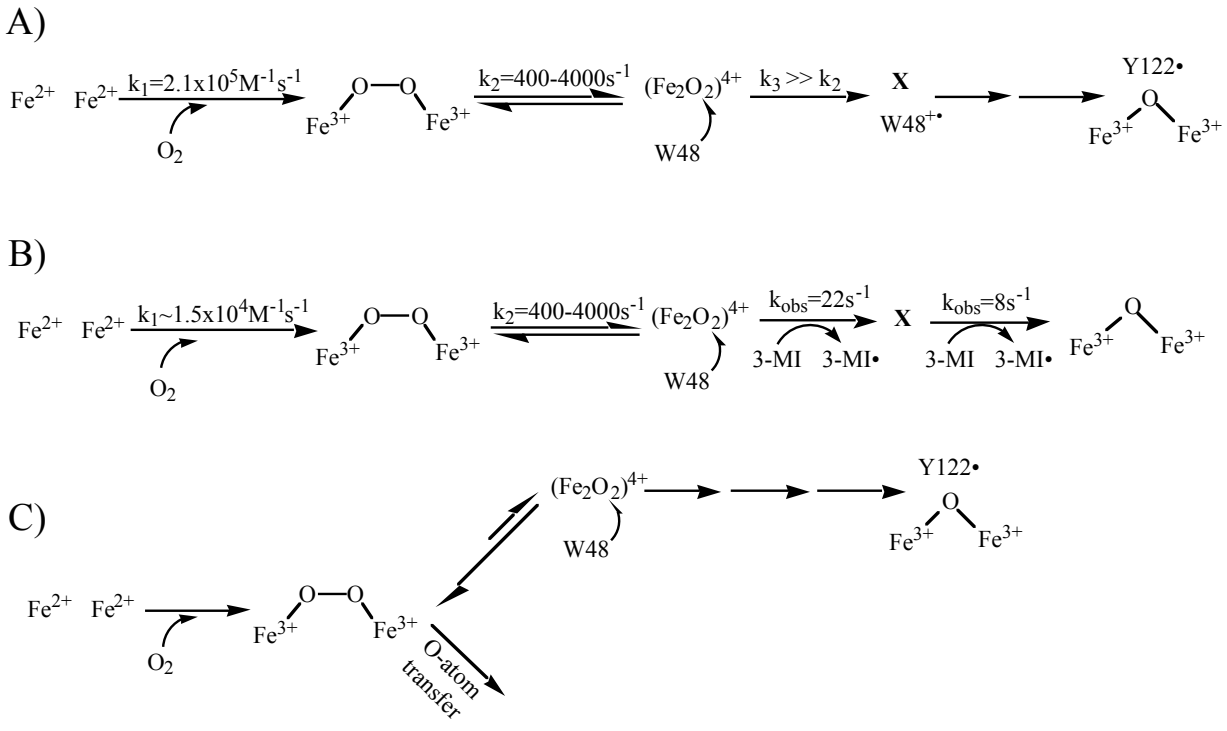

the fact that decay of the (μ-1,2-peroxo)diiron(III) complex in D84E variants can lead either to Y122• formation (with the electron-shuttling W48 present) or to F208 hydroxylation (with W48 replaced by F). If isomerization of the **P**-like complex to the $(Fe_2O_2)^{4+}$ state is still faster than the competing step that commits the reaction to O-atom transfer (F208 hydroxylation), efficient one-electron reduction of the $(Fe_2O_2)^{4+}$ state by W48 (upper pathway in Scheme 3-2C) would make the one-electron-oxidation outcome predominant. In the absence of efficient reduction, the $(Fe_2O_2)^{4+}$ state would partition back to the (μ-1,2-peroxo)diiron(III) complex, which would persist long enough to enter the O-atom transfer pathway (lower pathway in Scheme 3-2C). The very modest effect of 3-MI on the kinetics of decay of the (μ-1,2-peroxo)diiron(III) complex in the R2-W48A/D84E reaction would be explained by the fact that prior isomerization to the $(Fe_2O_2)^{4+}$ state is required and is relatively slow. Thus, our working hypothesis is that the $(Fe_2O_2)^{4+}$ state is part of the R2-wt reaction pathway and is a successor to the expected (μ-1,2-peroxo)diiron(III) complex. This hypothesis would imply that the point of divergence of the R2 and sMMO mechanisms is in the fate of the common (μ-1,2-peroxo)diiron(III) adduct: O-O bond cleavage to generate the methane-hydroxylating diiron(IV) complex, **Q**, in sMMO as opposed to isomerization to the one-electron-oxidizing $(Fe_2O_2)^{4+}$ state in R2. The presence of aspartate at position 84 in R2 (as opposed to glutamate at the corresponding position of MMOH) would be seen as an adaptation to favor the conversion of the initial intermediate to the complex that is more reactive for one-electron reduction.

At present, it is impossible to say what the structures of the complexes in the $(Fe_2O_2)^{4+}$ intermediate state might be. The deduced Mössbauer parameters do not match

those of any structurally characterized complex of which we are aware. Complicating the situation further, it is impossible to choose between the two alternative analyses corresponding to (1) two diiron complexes with relative abundance ~ 1:3 (outer doublet:inner doublet) and unresolved Fe sites or (2) two complexes, one with inequivalent and resolved Fe sites (the outer doublet and paired inner doublet) and one with unresolved Fe sites (the second inner doublet), at relative abundances of 1.5:1. There is ample precedent for the site inequivalency required by the latter analysis (*52, 58-60*), but the absence of either spectral or kinetic resolution of the presumed two doublets constituting the broad inner features precludes an unambiguous choice of the correct analysis. In principle, application of additional spectroscopic methods (e.g., resonance Raman or EXAFS) could yield more detailed structural insight, but its lack of a strong visible chromophore and the heterogeneity of the state will mitigate against these approaches. Synthetic inorganic chemistry and density functional theory (DFT) calculations are perhaps more likely to yield greater structural insight. These studies should seek to identify a pair of peroxodiiron(III) complexes that are distinct from the **P**-like (presumably (μ-1,2-peroxo)diiron(III)) structure and that have similar free energies and a low barrier for interconversion. Arguably, the complexes should be favored thermodynamically over the **P**-like complex for the case of addition of O_2 to the diiron(II) cluster with the wt ligand sphere, but disfavored relative to the **P**-like complex in R2 variants with the D84E substitution. Correlation of experimental Mössbauer parameters with those determined for model complexes or calculated for the computationally-derived structures might then be used to validate candidate structures. We are pursuing these and other strategies to clarify the nature of the $(Fe_2O_2)^{4+}$ state.

REFERENCES

1. Nordlund, P., and Eklund, H. (1995) Di-iron-carboxylate proteins. *Curr. Opin. Struct. Biol. 5*, 758-766.
2. Wallar, B. J., and Lipscomb, J. D. (1996) Dioxygen activation by enzymes containing binuclear non-heme iron clusters. *Chem. Rev. 96*, 2625-2657.
3. Solomon, E. I., Brunold, T. C., Davis, M. I., Kemsley, J. N., Lee, S.-K., Lehnert, N., Neese, F., Skulan, A. J., Yang, Y.-S., and Zhou, J. (2000) Geometric and electronic structure/function correlations in non-heme iron enzymes. *Chem. Rev. 100*, 235-349.
4. Atkin, C. L., Thelander, L., and Reichard, P. (1973) Iron and free radical in ribonucleotide reductase. Exchange of iron and Mössbauer spectroscopy of the protein B2 subunit of the *Escherichia coli* enzyme. *J. Biol. Chem. 248*, 7464-7472.
5. Sjöberg, B.-M., Reichard, P., Gräslund, A., and Ehrenberg, A. (1977) Nature of the free radical in ribonucleotide reductase from *Escherichia coli*. *J. Biol. Chem. 252*, 536-541.
6. Larsson, A., and Sjöberg, B.-M. (1986) Identification of the stable free radical tyrosine residue in ribonucleotide reductase. *EMBO J. 5*, 2037-2040.
7. Dalton, H. (1980) Oxidation of hydrocarbons by methane monooxygenases from a variety of microbes. *Adv. Appl. Microbiol. 26*, 71-87.
8. Woodland, M. P., Patil, D. S., Cammack, R., and Dalton, H. (1986) ESR studies of protein A of the soluble methane monooxygenase from *Methylococcus capsulatus* (Bath). *Biochim. Biophys. Acta 873*, 237-242.

9. Fox, B. G., Surerus, K. K., Münck, E., and Lipscomb, J. D. (1988) Evidence for a μ-oxo-bridged binuclear iron cluster in the hydroxylase component of methane monooxygenase. Mössbauer and EPR studies. *J. Biol. Chem. 263*, 10553-10556.

10. Merkx, M., Kopp, D. A., Sazinsky, M. H., Blazyk, J. L., Müller, J., and Lippard, S. J. (2001) Dioxygen activation and methane hydroxylation by soluble methane monooxygenase: a tale of two irons and three proteins. *Angew. Chem. Int. Ed. 40*, 2782-2807.

11. Lee, S.-K., Fox, B. G., Froland, W. A., Lipscomb, J. D., and Münck, E. (1993) A transient intermediate of the methane monooxygenase catalytic cycle containing an $Fe^{IV}Fe^{IV}$ cluster. *J. Am. Chem. Soc. 115*, 6450-6451.

12. Lee, S.-K., Nesheim, J. C., and Lipscomb, J. D. (1993) Transient intermediates of the methane monooxygenase catalytic cycle. *J. Biol. Chem. 268*, 21569-21577.

13. Liu, K. E., Wang, D., Huynh, B. H., Edmondson, D. E., Salifoglou, A., and Lippard, S. J. (1994) Spectroscopic detection of intermediates in the reaction of dioxygen with the reduced methane monooxygenase/hydroxylase from *Methylococcus capsulatus* (Bath). *J. Am. Chem. Soc. 116*, 7465-7466.

14. Liu, K. E., Valentine, A. M., Wang, D., Huynh, B. H., Edmondson, D. E., Salifoglou, A., and Lippard, S. J. (1995) From the mass production of *Methylococcus capsulatus* to the efficient separation and isolation of methane monooxygenase proteins. Characterization of novel intermediates in substrate reactions of methane monooxygenase. *J. Am. Chem. Soc. 117*, 10174-10185.

15. Shu, L. J., Nesheim, J. C., Kauffmann, K., Münck, E., Lipscomb, J. D., and Que, L., Jr. (1997) An $Fe_2^{IV}O_2$ diamond core structure for the key intermediate Q of methane monooxygenase. *Science 275*, 515-518.

16. Valentine, A. M., Stahl, S. S., and Lippard, S. J. (1999) Mechanistic studies of the reaction of reduced methane monooxygenase hydroxylase with dioxygen and substrates. *J. Am. Chem. Soc. 121*, 3876-3887.

17. Lee, S.-K., and Lipscomb, J. D. (1999) Oxygen activation catalyzed by methane monooxygenase hydroxylase component: proton delivery during the O-O bond cleavage steps. *Biochemistry 38*, 4423-4432.

18. Brazeau, B. J., and Lipscomb, J. D. (2000) Kinetics and activation thermodynamics of methane monooxygenase compound Q formation and reaction with substrates. *Biochemistry 39*, 13503-13515.

19. Bollinger, J. M., Jr., Stubbe, J., Huynh, B. H., and Edmondson, D. E. (1991) Novel diferric radical intermediate responsible for tyrosyl radical formation in assembly of the cofactor of ribonucleotide reductase. *J. Am. Chem. Soc. 113*, 6289-6291.

20. Bollinger, J. M., Jr., Tong, W. H., Ravi, N., Huynh, B. H., Edmondson, D. E., and Stubbe, J. (1994) Mechanism of assembly of the tyrosyl-diiron(III) cofactor of *E. coli* ribonucleotide reductase. 2. Kinetics of the excess Fe^{2+} reaction by optical, EPR, and Mössbauer spectroscopies. *J. Am. Chem. Soc. 116*, 8015-8023.

21. Bollinger, J. M., Jr., Tong, W. H., Ravi, N., Huynh, B. H., Edmondson, D. E., and Stubbe, J. (1994) Mechanism of assembly of the tyrosyl radical-diiron(III) cofactor of *E. coli* ribonucleotide reductase. 3. Kinetics of the limiting Fe^{2+} reaction by optical, EPR, and Mössbauer spectroscopies. *J. Am. Chem. Soc. 116*, 8024-8032.

22. Tong, W. H., Chen, S., Lloyd, S. G., Edmondson, D. E., Huynh, B. H., and Stubbe, J. (1996) Mechanism of assembly of the diferric cluster-tyrosyl radical cofactor of *Escherichia coli* ribonucleotide reductase from the diferrous form of the R2 subunit. *J. Am. Chem. Soc. 118*, 2107-2108.

23. Sturgeon, B. E., Burdi, D., Chen, S., Huynh, B. H., Edmondson, D. E., Stubbe, J., and Hoffman, B. M. (1996) Reconsideration of X, the diiron intermediate formed during cofactor assembly in *E. coli* ribonucleotide reductase. *J. Am. Chem. Soc. 118*, 7551-7557.

24. Burdi, D., Sturgeon, B. E., Tong, W. H., Stubbe, J., and Hoffman, B. M. (1996) Rapid freeze-quench ENDOR of the radical X intermediate of *Escherichia coli* ribonucleotide reductase using $^{17}O_2$ and $H_2{}^{17}O$. *J. Am. Chem. Soc. 118*, 281-282.

25. Willems, J.-P., Lee, H.-I., Burdi, D., Doan, P. E., Stubbe, J., and Hoffman, B. M. (1997) Identification of the protonated oxygenic ligands of ribonucleotide reductase intermediate X by Q-Band ^{1,2}H CW and pulsed ENDOR. *J. Am. Chem. Soc. 119*, 9816-9824.

26. Burdi, D., Willems, J.-P., Riggs-Gelasco, P., Antholine, W. E., Stubbe, J., and Hoffman, B. M. (1998) The core structure of X generated in the assembly of the diiron cluster of ribonucleotide reductase: $^{17}O_2$ and $H_2{}^{17}O$ ENDOR. *J. Am. Chem. Soc. 120*, 12910-12919.

27. Riggs-Gelasco, P. J., Shu, L., Chen, S., Burdi, D., Huynh, B. H., Que, L., Jr., and Stubbe, J. (1998) EXAFS characterization of the intermediate X generated during the assembly of the *Escherichia coli* ribonucleotide reductase R2 diferric tyrosyl radical cofactor. *J. Am. Chem. Soc. 120*, 849-860.

28. Baldwin, J., Krebs, C., Ley, B. A., Edmondson, D. E., Huynh, B. H., and Bollinger, J. M., Jr. (2000) Mechanism of rapid electron transfer during oxygen activation in the R2 subunit of *Escherichia coli* ribonucleotide reductase. 1. Evidence for a transient tryptophan radical. *J. Am. Chem. Soc. 122*, 12195-12206.

29. Bollinger, J. M., Jr., Edmondson, D. E., Huynh, B. H., Filley, J., Norton, J. R., and Stubbe, J. (1991) Mechanism of assembly of the tyrosyl radical-dinuclear iron cluster cofactor of ribonucleotide reductase. *Science 253*, 292-298.

30. Bollinger, J. M., Jr., Krebs, C., Vicol, A., Chen, S., Ley, B. A., Edmondson, D. E., and Huynh, B. H. (1998) Engineering the diiron site of *Escherichia coli* ribonucleotide reductase protein R2 to accumulate an intermediate similar to H_{peroxo}, the putative peroxodiiron(III) complex from the methane monooxygenase catalytic cycle. *J. Am. Chem. Soc. 120*, 1094-1095.

31. Moënne-Loccoz, P., Baldwin, J., Ley, B. A., Loehr, T. M., and Bollinger, J. M., Jr. (1998) O_2 activation by non-heme diiron proteins: Identification of a symmetric μ-1,2-peroxide in a mutant of ribonucleotide reductase. *Biochemistry 37*, 14659-14663.

32. Baldwin, J., Voegtli, W. C., Khidelkel, N., Moënne-Loccoz, P., Krebs, C., Pereira, A. S., Ley, B. A., Huynh, B. H., Loehr, T. M., Riggs-Gelasco, P. J., Rosenzweig, A. C., and Bollinger, J. M., Jr. (2001) Rational reprogramming of the R2 subunit of *Escherichia coli* ribonucleotide reductase into a self-hydroxylating monooxygenase. *J. Am. Chem. Soc. 123*, 7017-7030.

33. Ormö, M., deMaré, F., Regnström, K., Åberg, A., Sahlin, M., Ling, J., Loehr, T. M., Sanders-Loehr, J., and Sjöberg, B.-M. (1992) Engineering of the iron site in

ribonucleotide reductase to a self-hydroxylating monoxygenase. *J. Biol. Chem. 267*, 8711-8714.

34. Åberg, A., Ormö, M., Nordlund, P., and Sjöberg, B.-M. (1993) Autocatalytic generation of dopa in the engineered protein R2 F208Y from *Escherichia coli* ribonucleotide reductase and crystal structure of the dopa 208 protein. *Biochemistry 32*, 9845-9850.
35. Parkin, S. E., Chen, S., Ley, B. A., Mangravite, L., Edmondson, D. E., Huynh, B. H., and Bollinger, J. M., Jr. (1998) Electron injection through a specific pathway determines the outcome of oxygen activation at the diiron cluster in the F208Y mutant of *Escherichia coli* ribonucleotide reductase protein R2. *Biochemistry 37*, 1124-1130.
36. Logan, D. T., deMaré, F., Persson, B. O., Slaby, A., Sjöberg, B.-M., and Nordlund, P. (1998) Crystal structures of two self-hydroxylating ribonucleotide reductase protein R2 mutants: structural basis for the oxygen-insertion step of hydroxylation reactions catalyzed by diiron proteins. *Biochemistry 57*, 10798-10807.
37. Valentine, A. M., Tavares, P., Pereira, A. S., Davydov, R., Krebs, C., Hoffman, B. M., Edmondson, D. E., Huynh, B. H., and Lippard, S. J. (1998) Characterization of a mixed-valent Fe(III)Fe(IV) form of intermediate Q in the reaction cycle of soluble methane monooxygenase, an analog of intermediate X in ribonucleotide reductase R2 assembly. *J. Am. Chem. Soc. 120*, 2190-2191.
38. Yang, Y.-S., Baldwin, J., Ley, B. A., Bollinger, J. M., Jr., and Solomon, E. I. (2000) Spectroscopic and electronic structure description of the reduced binuclear non-heme iron active site in ribonucleotide reductase from *E. coli*: Comparison to reduced ^{9}

desaturase and electronic structure contributions to differences in O_2 reactivity. *J. Am. Chem. Soc. 122*, 8495-8510.

39. Siegbahn, P. E. M. (2002) A comparison of dioxygen bond cleavage in RNR and methane monooxygenase. *Chem. Phys. Lett. 351*, 311-318.
40. Torrent, M., Djamaladdin, G. M., Basch, H., and Morokuma, K. (2002) Computational studies of reaction mechanisms of methane monooxygenase and ribonucleotide reductase. *J. Computat. Chem. 23*, 59-76.
41. Baldwin, J., Krebs, C., Saleh, L., Stelling, M., Huynh, B. H., Bollinger, J. M., Jr., and Riggs-Gelasco, P. (2003) Structural characterization of the peroxodiiron(III) intermediate generated during oxygen activation by the W48A/D84E variant of ribonucleotide reductase protein R2 from *Escherichia coli*. *Biochemistry 42*, 13269-13279.
42. Krebs, C., Chen, S., Baldwin, J., Ley, B. A., Patel, U., Edmondson, D. E., Huynh, B. H., and Bollinger, J. M., Jr. (2000) Mechanism of rapid electron transfer during oxygen activation in the R2 subunit of *Escherichia coli* ribonucleotide reductase. 2. Evidence for and consequences of blocked electron transfer in the W48F variant. *J. Am. Chem. Soc. 122*, 12207-12219.
43. Saleh, L., Kelch, B. A., Pathickal, B. A., Baldwin, J., Ley, B. A., and Bollinger, J. M., Jr. (2004) Mediation by indole analogs of electron transfer during oxygen activation in variants of *Escherichia coli* ribonucleotide reductase R2 lacking the electron-shuttling tryptophan 48. *Biochemistry 43*, 5943-5952.
44. Gill, S. C., and von Hippel, P. H. (1989) Calculation of protein extinction coefficients from amino acid sequence data. *Anal. Biochem. 182*, 319-326.

45. Yun, D., Krebs, C., Gupta, G. P., Iwig, D. F., Huynh, B. H., and Bollinger, J. M., Jr. (2002) Facile electron transfer during formation of cluster X and kinetic competence of X for tyrosyl radical production in protein R2 of ribonucleotide reductase from mouse. *Biochemistry 41*, 981-990.

46. Ravi, N., Bollinger, J. M., Jr., Huynh, B. H., Edmondson, D. E., and Stubbe, J. (1994) Mechanism of assembly of the tyrosyl radical-diiron(III) cofactor of *E. coli* ribonucleotide reductase: 1. Mössbauer characterization of the diferric radical precursor. *J. Am. Chem. Soc. 116*, 8007-8014.

47. Dong, Y., Yan, S., Young, V. G., Jr., and Que, L., Jr. (1996) Crystal structure analysis of a synthetic non-heme diiron-O_2 adduct: insight into the mechanism of oxygen activation. *Angew. Chem. Int. Ed. Engl 35*, 618-620.

48. Dong, Y., Zang, Y., Shu, L., Wilkinson, L., and Que, L., Jr. (1997) Models for non-heme diiron enzymes. Assembly of a high-valent $Fe_2(\mu\text{-}O)_2$ diamond core from its peroxo precursor. *J. Am. Chem. Soc. 119*, 12683-12684.

49. Kim, K., and Lippard, S. J. (1996) Structure and Mössbauer spectrum of a (μ-1,2-peroxo)bis(μ-carboxylato)diiron(III) model for the peroxo intermediate in the methane monooxygenase hydroxylase cycle. *J. Am. Chem. Soc. 118*, 4914-4915.

50. Ookubo, T., Sugimoto, H., Nagayama, T., Masuda, H., Sato, T., Tanaka, K., Maeda, Y., Okawa, H., Hayashi, Y., Uehara, A., and Suzuki, M. (1996) *Cis*-μ-1,2-peroxo diiron complex: Structure and reversible oxygenation. *J. Am. Chem. Soc. 118*, 701-702.

51. Broadwater, J. A., Ai, J., Loehr, T. M., Sanders-Loehr, J., and Fox, B. G. (1998) Peroxodiferric intermediate of stearoyl-acyl carrier protein Δ9 desaturase: oxidase

reactivity during single turnover and implications for the mechanism of desaturation. *Biochemistry 37*, 14664-14671.

52. Broadwater, J. A., Achim, C., Münck, E., and Fox, B. G. (1999) Mössbauer studies of the formation and reactivity of a quasi-stable peroxo intermediate of stearoyl-acyl carrier protein ∂9-desaturase. *Biochemistry 38*, 12197-12204.
53. Pereira, A. S., Small, W., Krebs, C., Tavares, P., Edmondson, D. E., Theil, E. C., and Huynh, B. H. (1998) Direct spectroscopic and kinetic evidence for the involvement of a peroxodiferric intermediate during the ferroxidase reaction in fast ferritin mineralization. *Biochemistry 37*, 9871-9876.
54. Moënne-Loccoz, P., Krebs, C., Herlihy, K., Edmondson, D. E., Theil, E. C., Huynh, B. H., and Loehr, T. M. (1999) The ferroxidase reaction of ferritin reveals a diferric μ-1,2 bridging peroxide intermediate in common with other O_2-activating non-heme diiron proteins. *Biochemistry 38*, 5290-5295.
55. Huang, J., Krebs, C., Huynh, B. H., Edmondson, D. E., Theil, E. C., and Penner-Hahn, J. E. (2000) A short Fe-Fe distance in peroxodiferric ferritin: control of Fe substrate versus cofactor decay? *Science 287*, 122-125.
56. Brunold, T. C., Tamura, N., Kitajima, N., Moro-oka, Y., and Solomon, E. I. (1998) Spectroscopic study of $[Fe_2(O_2)(OBz)_2\{HB(pz')_3\}_2]$: Nature of the □-1,2 peroxide-Fe(III) bond and its possible relevance to O_2 activation by non-heme iron enzymes. *J. Am. Chem. Soc. 120*, 5674-5690.
57. Solar, S., Getoff, N., Surdhar, P. S., Armstrong, D. A., and Sing, A. (1991) Oxidation of tryptophan and N-methylindole by N_3•, Br_2-, and $(SCN)^{2-}$ radicals in light-and heavy-water solutions: A pulse radiolysis study. *J. Phys. Chem. 95*, 3639-3643.

58. Que, L., Jr., and True, A. E. (1990) Dinuclear iron- and manganese-oxo sites in biology in *Progress in Inorganic Chemistry* (Lippard, S. J., Ed.) pp. 97-200, John Wiley & Sons, New York.

59. Mizoguchi, T. J., Kuzelka, J., Spingler, B., DuBois, J. L., Davydov, R. M., Hedman, B., Hodgson, K. O., and Lippard, S. J. (2001) Synthesis and spectroscopic studies of non-heme diiron(III) species with a terminal hydroperoxide ligand: Models for hemerythrin. *Inorg. Chem. 40*, 4662-4673.

60. He, C., Barrios, A. M., Lee, D., Kuzelka, J., Davydov, R. M., and Lippard, S. J. (2000) Diiron complexes of 1,8-naphthyridine-based dinucleating ligands as models for hemerythrin. *J. Am. Chem. Soc. 122*, 12683-12690.

61. Edmondson, D. E., and Huynh, B. H. (1996) Diiron-cluster intermediates in biological oxygen activation reactions. *Inorg. Chim. Acta 252*, 399-404.

62. Stubbe, J., and Riggs-Gelasco, P. (1998) Harnessing free radicals: formation and function of the tyrosyl radical in ribonucleotide reductase. *Trends Biochem. Sci. 23*, 438-443.

63. Andersson, M. E., Högbom, M., Rinaldo-Matthis, A., Andersson, K. K., Sjöberg, B.-M., and Nordlund, P. (1999) The crystal structure of an azide complex of the diferrous R2 subunit of ribonucleotide reductase displays a novel carboxylate shift with important mechanistic implications for diiron-catalyzed oxygen activation. *J. Am. Chem. Soc. 121*, 2346-2352.

Chapter 4

Cation Mediation of Radical Transfer between Trp48 and Tyr356 during O_2 Activation by Protein R2 of *Escherichia coli* Ribonucleotide Reductase: Relevance to R1-R2 Radical Transfer in Nucleotide Reduction?

Footnotes

[1]Abbreviations: RNR, ribonucleotide reductase; R2, R2 subunit of *Escherichia coli* ribonucleotide reductase; Y122•, tyrosyl radical in *E. coli* R2; $W48^{+\bullet}$, tryptophan 48 cation radical; wt, wild-type; IPTG, isopropy-β-D-thiogalactopyranoside; PMSF, phenylmethylsulfonyl fluoride; Tris, *tris*-[hydroxymethyl]-aminomethane; EPPS, (N-[2-hydroxyethyl]piperazine-N'-[3-propane-sulfonic acid]; HEPES, 4-(2-hydroxyethyl)-1-piperazineethanesulfonic acid; PCR, polymerase chain reaction; bp, base pairs; buffer A, 25 mM EPPS, pH 8.2; $(A_{411} - (A_{405} + A_{417})/2)$, peak height proportional to the concentration of tyrosyl radical; ε_{280}, molar absorption coefficients at 280 nm; k_{obs}, observed apparent first-order rate constant;

[2]In fact, radical transfer has never actually been directly demonstrated. Indirect evidence that it occurs is, nevertheless, overwhelming and consists of the demonstrations that (1) R2 proteins lacking the tyrosyl radical (the "met," apo, and reduced forms of wild-type R2s and the Y→F variants) are inactive (*1, 2*), (2) variants of R2 and R1 with residues in the putative radical-transfer pathway replaced have no or drastically diminished activity (*3-9*), (3) one of these variants (the Y370W variant of mouse R2) causes loss of the tyrosyl radical (Y177•) in a process that is dependent on substrate and R1 (*9*), (4) the C225S and E441Q variants of *E. coli* R1 mediate loss of the Y122• and the latter formation of new substrate and R1 radicals (in sequence) (*3, 10-14*), and (5) substrates with radical-trapping functional groups (e.g., 2'-deoxy-2'-azido-nucleoside diphosphates and 2'-deoxy-2'-fluoromethylene-nucleoside diphosphates) cause decay of the tyrosyl radical and formation of new substrate- or R1-derived radicals (*15-19*).

[3]These conditions consist of an absence of reductants and an Fe(II)/R2 ratio, 2.7-3.0 equiv, that balances the opposing requirements for a filled diiron site (to give rapid O_2 activation) and only low levels of unbound Fe(II) (to prevent the rapid reduction of the W48+• that occurs if $[Fe(II)_{aq}]$ approaches the concentration of the O_2-reactive Fe(II)-R2 complex) (*20*).

[4]The cited study was conducted at 5 °C. The presence of the Y122F substitution introduces kinetic complexity in the O_2 addition step below 10 °C. Consequently, this study has been carried out at 11 °C to obviate this additional complexity. The rate constants for reduction of $W48^{+\bullet}$ by the exogenous reductants refer to 5 °C, but all other rate constants refer to 11 °C.

ABSTRACT

A cation radical of the near-surface tryptophan residue, W48, forms concomitantly with the Fe_2(III/IV) cluster, **X**, during O_2 activation for tyrosyl radical (Y122•) production in the R2 subunit of class I ribonucleotide reductase (RNR) from *Escherichia coli*. A W48 cation radical ($W48^{+\bullet}$) is also likely to be an intermediate in the long-range radical transfer between R2 and R1 in the RNR holoenzyme, the step that reversibly generates the R1 cysteine radical (from C439) that initiates nucleotide reduction by abstraction of the 3'-hydrogen atom. In this R2↔R1 radical transfer step, Y356, a residue in the flexible C-terminus that is not observed in crystal structures of the R2 protein, is believed to form the link between R1 and the hypothetical $W48^{+\bullet}$ intermediate in R2. A kinetic analysis of pathways for decay of the $W48^{+\bullet}$ during O_2 activation in the absence of an obvious reductant, both in wild-type (wt) R2 and in variants with either Y122, Y356, or both replaced by phenylalanine (F), has revealed that the presence of divalent cations at concentrations similar to the [Mg^{2+}] employed in the standard RNR assay (15 mM) mediates a rapid radical-transfer equilibrium between W48 and Y356. Cation-mediated propagation of the radical from W48 to Y356 gives rise to a fast phase of Y• production that is essentially coincident with $W48^{+\bullet}$ formation and creates an efficient pathway for decay of the $W48^{+\bullet}$. It is suggested that the presence of divalent cations may induce greater order in the C-terminus and greater proximity of Y356 to W48 by coordinating specific C-terminal residues, including, perhaps, Y356 itself. The possibility that this phenomenon also occurs in radical transfer during RNR catalysis is considered.

Ribonucleotide reductases (RNRs[1]) catalyze conversion of ribonucleoside di- or triphosphates to the corresponding 2'-deoxyribonucleotides (*21-24*). The reaction proceeds via a free-radical mechanism that is initiated by abstraction of the 3'-hydrogen of the substrate (*25-27*) by a protein radical (*3, 4, 28*). The multiplicity of strategies for generation of the 3'-H-abstracting protein radical, which for all known RNRs is believed to be a cysteine thiyl radical, is the primary basis for the definition of three classes (I-III) of RNRs (*24, 29-31*). The 5'-deoxyadenosyl radical, produced either by homolysis of the Co-C bond of 5'-deoxyadenosylcob(II)alamin (*32*) or by reductive cleavage of the C5'-S bond of S-adenosyl-*L*-methionine (*33, 34*), is the ultimate source of the oxidizing equivalent for protein radical production in the class II and class III RNRs, respectively. In class I RNRs, such as those found in aerobically-growing *Escherichia coli* and in eukaryotes from *Saccharomyces cerevisiae* to *Homo sapiens*, activation of dioxygen at the carboxylate-bridged diiron(II) cluster harbored in the enzyme's R2 subunit introduces a stable tyrosyl free-radical in R2 by univalent oxidation of a buried tyrosine (Y122 in *E. coli* R2, which is the subject of this study) (*1, 2, 35, 36*). This stoichiometric, auto-activation process yields the active R2 subunit, which functions catalytically in nucleotide reduction. Transient transfer of the oxidizing equivalent from the Y122 radical (Y122•) to a cysteine residue in the R1 subunit (C439 (*3, 4, 28*)) prepares R1 for the crucial 3'-H abstraction (*37*). Chemical steps involving additional cysteine residues in R1 (C225 and C462) then convert the 3'-centered substrate radical to the corresponding 3' product radical, with formation of a C225-C462 disulfide (*3, 10, 11*). The 3'-H is then returned to complete the transformation to product, and subsequent reverse radical transfer regenerates the Y122• in R2 and reduced (non-radical) C439 in R1 (*3, 37*).

The mechanistic pathway for Y122• formation has been mapped in some detail, beginning with the seminal studies in the early 1990s led by Stubbe (*38-44*). Addition of O_2 to the reactive form of the diiron(II) cluster, which is formed after acquisition of two Fe(II) ions and a conformational change by the R2 protein, leads to accumulation of a state containing the Fe_2(III/IV) cluster, **X** (*38-40, 45*), and a cation radical harbored on the near-surface residue, W48 (*20, 42*). In the presence of a one-electron reductant (e.g., ascorbate, thiols, $Fe(II)_{aq}$), the $W48^{+\bullet}$ is rapidly reduced (*20, 39, 42*). Under these conditions, the Y122• and (μ-oxo)diiron(III) cluster of the native protein are generated in the last and slowest step of the reaction when cluster **X** oxidizes Y122 (*39, 41*). The identities of precursors to the **X**-$W48^{+\bullet}$ state having both oxidizing equivalents of the initial diiron(II)-O_2 complex still localized on the diiron cluster have not been definitively established, but Stubbe and co-workers presented evidence that a μ-(1,2-peroxo)diiron(III) complex is among them (*44*). Indeed, our recent studies support this proposal (*46*) and further suggest (1) that the μ-1,2-peroxide isomerizes rapidly to a state with two structurally distinct peroxodiiron(III) complexes in rapid equilibrium, and (2) that this state is the immediate precursor to the **X**-$W48^{+\bullet}$ state (*47*).

The mechanism of the radical-transfer step that initiates nucleotide reduction is less well understood.[2] The structure of the holoenzyme (R1•R2) complex has been not been reported, but *in silico* docking of structures of the individual subunits of the *E. coli* enzyme at their most likely interface would position C439 in R1 > 35 Å from the buried Y122• in R2 (*24, 28, 48*), much too great a distance for the reaction to occur at the required rate ($\geq 10^0$-10^1 s^{-1}, the rate constant reported both for steady-state and single turnover) via a single-step, electron-tunneling mechanism (*37*). A network of hydrogen-

bonded, mostly aromatic amino acid residues that extends from the Y122• in R2 toward the putative interface and from the interface toward C439 in the active site of R1 (Y122•-W48-Y356--Y731-Y730-C439, where the double hyphen marks the R2--R1 interface) is thought to mediate radical transfer by a multi-step-tunneling ("radical-hopping") mechanism that may also involve coupled proton transfer (*37*). In the simplest version of such a mechanism, the first and second steps would be oxidation of W48 by the Y122• and reduction of the resulting $W48^{+\bullet}$ by Y356 (and the last and penultimate steps of the reverse radical transfer would be the reverse of these two steps, respectively). Thus, according to this scenario, the $W48^{+\bullet}$ is likely to be an intermediate in inter-subunit radical transfer, as it is in O_2 activation and Y122• formation.

The accumulation of $W48^{+\bullet}$ to more than 0.6 equiv during O_2 activation by the reduced *E. coli* R2 protein under appropriate reaction conditions[3] (*20*) creates the opportunity to study mechanisms of electron transfer to this likely intermediate in R1-R2 radical transfer. Earlier work showed that, in addition to its reduction by $Fe(II)_{aq}$ or other reductants, the $W48^{+\bullet}$ can also be reduced by Y122 (*20, 42*). This step, which would be analogous to the last step in the reverse (R1→R2) radical transfer occurring in each turnover, is ~ 10-fold faster than oxidation of Y122 by **X** and thus gives rise to a fast phase of Y122• production specifically when the reaction is carried out in the absence of an exogenous $W48^{+\bullet}$ reductant. In this study, we have characterized the kinetics of decay of the $W48^{+\bullet}$ in the absence of reductants in the reactions of the wild-type R2 protein and its Y122F, Y356F, and Y122F/Y356 variants, thereby dissecting the decay process into constituent pathways in order to more thoroughly understand electron/radical flow in R2 and as a first step toward testing for possible transfer into R1 of oxidizing equivalents

generated during O_2 activation in R2. The latter notion, originally suggested by the work of Cooperman and co-workers showing that the mouse R2-Y177F (Y177 is the cognate residue of Y122 in *E. coli*) variant retains a low level of RNR activity in the presence of R1 (*49*), has become particularly relevant with the recent report that R2 subunits in certain hyperthermophilic archaea and pathogenic eubacteria lack the radical tyrosine (*50, 51*) and the hypothesis that these RNRs may function by using an intermediate in O_2 activation to generate the R1 radical (*51*). Here we show that the presence of Mg^{2+} at concentrations similar to that used in RNR activity assays brings Y356 into a rapid radical-transfer equilibrium with the $W48^{+\bullet}$, leading to a very rapid phase of Y• formation (Y356•) and an efficient pathway for decay of the $W48^{+\bullet}$.

MATERIALS AND METHODS

Materials. Culture media components (yeast extract and tryptone) were purchased from Marcor Development Corporation (Hackensack, NJ). Isopropy-β-D-thiogalactopyranoside (IPTG) was purchased from Biosynth International (Naperville, IL). Ampicillin was purchased from IBI (Shelton, CT). Phenylmethylsulfonyl fluoride (PMSF), streptomycin sulfate, *tris*-[hydroxymethyl]-aminomethane (Tris), 1,10-phenanthroline, and (N-[2-hydroxyethyl]piperazine-N'-[3-propane-sulfonic acid]) (EPPS) were purchased from Sigma (St. Louis, MO). Glycerol, ammonium sulfate, sodium chloride, sodium sulfate, and potassium chloride were purchased from EM Science (Gibbstown, NJ). Calcium chloride was purchased from Fisher Scientific (Fair Lawn, NJ). Magnesium sulfate and magnesium chloride were purchased from J. T. Baker Chemical Co. (Phillipsburg, N.J.). Enzyme grade 4-(2-hydroxyethyl)-1-

piperazineethanesulfonic acid (HEPES) was purchased from FisherBiotech (Pittsburgh, PA). Oligonucleotide primers were purchased from Invitrogen (Frederick, MD). Reagents for the polymerase chain reaction (PCR) and restriction enzymes were purchased from New England Biolabs (Beverly, MA). T4 DNA ligase was purchased from Roche (Indianapolis, IN). BL21(DE3) and pET vectors were purchased from Novagen (Madison, WI).

Preparation of Expression Vectors for R2-Y122F, R2-Y356F, and R2-Y122F/Y356F. Over-expression of R2-Y122F was directed by the plasmid pR2-Y122F(*Hind*III). This plasmid was prepared from two previously described plasmids: the smaller fragment (containing codons 52-210) from digestion of pR2-W48F/Y122F (*47*) with *Aat*II and *Hind*III was ligated with the larger fragment from digestion of pR2wt-*Hind*III (*52*) with the same enzymes. The codon change giving the Y356F substitution was introduced into the *nrdB* gene (encoding R2) by using PCR. The 3'-most third of the gene was amplified in two fragments by using four primers and pR2wt-*Hind*III (*52*), as template. Primers 1 (5'-CGT TTC TAC GT**A AGC TT**T GCT TGT TCC-3') and 2 (5'-GAC CAG **AAA** AGA GCT CAC TTC CAC TTC C-3') were used to amplify a 456 base-pair (bp) fragment of the pR2wt-*Hind*III. Primer 1 anneals ~ 620 bp 3' of the start of *nrdB* and contains the unique *HindIII* restriction site (in boldface type) previously introduced at codon V210 of *nrdB* (*52*). Primer 2 introduces a translationally silent unique *SacI* restiction site (underlined) at codon 354 of *nrdB* for internal ligation of the two fragments, and the desired substitution at codon Y356 (TAT to TTT, complement of boldface triplet). A 1429 bp fragment of the pR2wt-*Hind*III was amplified by using primers 3 (5'-GTG GAA GTG AGC TCT **TTT** CTG GTC-3') and 4 (5'-CGC AAC GTT

GTT GCC ATT G**CT GCA G**GC-3'). Primer 3 introduces the aforementioned *SacI* restriction site (underlined) and the desired substitution at codon Y356 (boldface triplet) and primer 4 contains the unique *PstI* site (in boldface type) 3' of the *nrdB* gene for ligation with pR2wt-*Hind*III. The 5' PCR fragment was digested with *HindIII* and *SacI*, the 3' PCR fragment was digested with *SacI* and *PstI*, and the vector pR2wt-*Hind*III was digested with *HindIII* and *PstI*. The fragments were joined in a three-piece ligation reaction to give the expression vector pR2-Y356F.

The over-expression vector for R2-Y122F/Y356F was prepared from pR2-Y122F and pR2-Y356F. The 532 bp *HindIII-XhoI* restriction fragment of pR2-Y356F was ligated with the large (vector) fragment from restriction of pR2-Y122F with the same enzymes to yield pR2-Y122F/Y356F.

The sequence of the coding region of each plasmid construct was verified to ensure that no undesired mutations had been introduced. DNA sequences were determined by the Nucleic Acid Facility of the Pennsylvania State University Biotechnology Institute.

Over-expression and Purification of R2-wt, R2-Y122F, R2-Y356F, and R2-Y122F/Y356F. Procedures used to over-express and purify the proteins in the apo form have been described elsewhere (*53*). Protein concentrations were determined spectrophotometrically by using molar absorption coefficients at 280 nm (ε_{280}) calculated according to the method of Gill and von Hippel (*54*). The ε_{280} values are 118 mM^{-1} cm^{-1} for apo R2-Y122F and apo R2-Y356F and 115 mM^{-1} cm^{-1} for apo R2-Y122F/Y356F.

Stopped-Flow Absorption Spectrophotometry. Stopped-flow absorption experiments were carried out with an Applied Photophysics SX.18MV stopped-flow

apparatus (path length of 1 cm and dead-time of 1.3 ms) equipped with a diode array detector and housed in an anoxic chamber (MBraun). Solutions of apo-R2 proteins in 25 mM EPPS, pH 8.2 (buffer A), were rendered free of oxygen on a vacuum/gas manifold and then mixed with Fe(II) in the anoxic chamber, as previously described (*53*). Oxygen-free Fe(II)-R2 samples were mixed with oxygen-saturated salt solutions prepared in buffer A. The temperature was maintained at 11 ˚C with a Lauda K-4/R circulating water bath. Kinetic traces shown represent averages of at least three trials. Specifics of reaction conditions are given in the figure legends.

RESULTS

The results presented below demonstrate that decay of the $W48^{+\bullet}$ is complex and consists of at least four constituent pathways (Scheme 4-1). Fast reduction of the $W48^{+\bullet}$ by thiols, ascorbate, or $Fe(II)_{aq}$ when one of these is present (pathway **A**), and somewhat slower reduction by Y122 when reductants are absent (pathway **B**), have previously been demonstrated (*20, 42*).[4] A third pathway (**C**) explains the eventual decay of the $W48^{+\bullet}$ even when reductants and both relevant tyrosines (Y122 and Y356) are absent (i.e., in R2-Y122F/Y356F). Associated with this pathway, a transient Y• is produced from one of the 14 remaining (irrelevant) tyrosines. Thus, transient Y radicals are observed in the reactions of both R2-Y122F and R2-Y122F/Y356F, but only in the former are the kinetics of the transient Y• sensitive to variation in $[Mg^{2+}]$ (as described in detail below). Because the quantity of transient Y• in the reaction of the double variant appears to be insufficient to account for all the $W48^{+\bullet}$ that decays (based on the known molar absorptivity of the $W48^{+\bullet}$ (*20, 42*) and reasonable estimates for that of the Y•), this

Scheme 4-1: Pathways for decay of W48 cation radical ($W48^{+\bullet}$) during oxygen activation by *E.coli* R2.

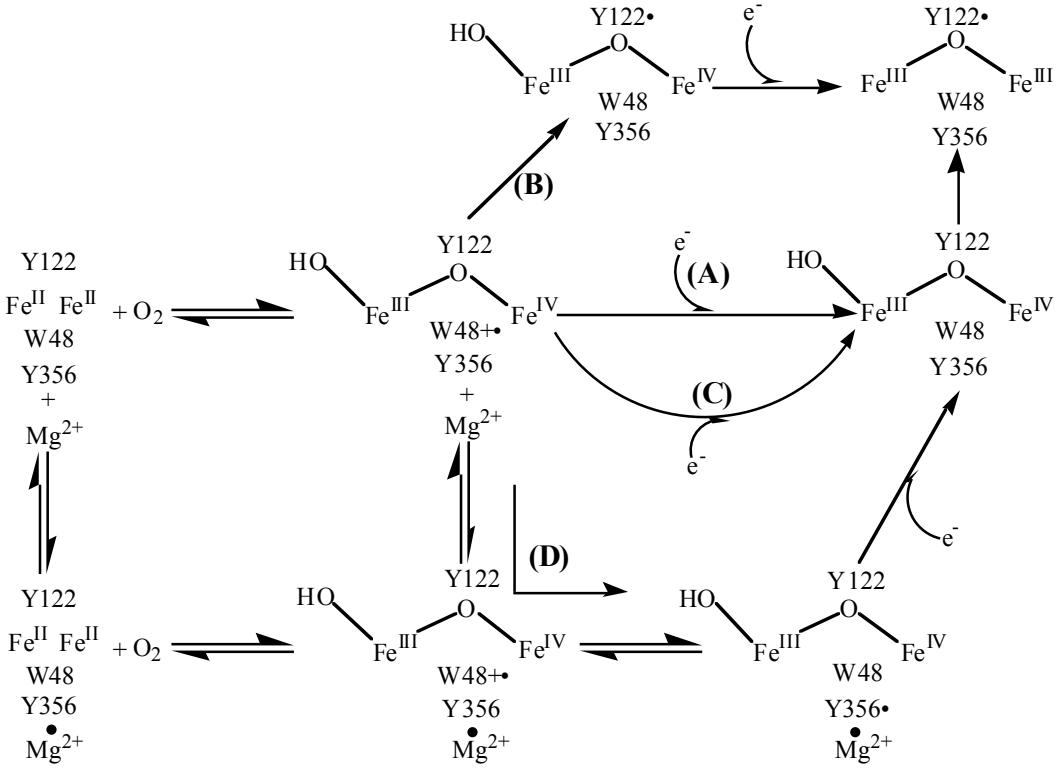

pathway is probably decomposable into additional components, of which one (or more) generates a Y• and one (or more) does not. Because all of its constituent processes are relatively slow, this pathway competes ineffectively with other pathways in all reactions but that of the double variant and is not considered in detail. Pathways **A**-**C** are all independent of both Mg^{2+} and Y356. The fourth and, for the purposes of this study, most interesting pathway (**D**) results from a Mg^{2+}-dependent interaction of the $W48^{+\bullet}$ with Y356. Kinetic manifestations of it and evidence that it results from a Mg^{2+}-dependent radical-transfer equilibrium between W48 and Y356 are summarized below.

Mixing of the Fe(II)-R2-wt complex at 11 °C with O_2-saturated buffer containing varying [Mg^{2+}] results in the rapid development of the broad 560-nm absorption band of the $W48^{+\bullet}$. The kinetics of its development depend to a minor extent on [Mg^{2+}], appearing to be faster at higher [Mg^{2+}] (~ 2-fold effect over the range interrogated). We did not attempt to assess the impact of Mg^{2+} on O_2 solubility, and, therefore, the apparent effect on the rate-constant for O_2 addition and formation of the **X**-$W48^{+\bullet}$ state could be attributable, at least in part, to variation in [O_2]. The kinetics of decay of the $W48^{+\bullet}$ and timing of this decay relative to other events depend markedly on Mg^{2+} concentration (Figure 4-1). With increasing [Mg^{2+}], decay of the 560-nm feature becomes increasingly rapid (Figure 4-1A). The observed first-order rate constant for decay increases hyperbolically with [Mg^{2+}] (Figure 4-2, filled circles and solid line), "saturating" at a value of 108 ± 3 s^{-1}, nine times the k_{obs} in the absence of Mg^{2+}. The [Mg^{2+}] at half-maximal acceleration ($K_{0.5}$) of 26 ± 3 mM *could* represent the K_D for an R2•Mg^{2+} complex, assuming that binding and dissociation are fast (in equilibrium) with respect to decay of the $W48^{+\bullet}$, but it is not clear that this situation obtains. The effect of Mg^{2+} on

Figure 4-1: Effect of increasing [$MgCl_2$] on the formation and decay rates of (A) the transient $W48^{+\bullet}$ monitored at 560 nm and (B) the 411-nm peak height (A_{411} - (A_{405} + A_{417})/2) in the reaction of Fe(II)-R2-wt with O_2 as monitored by stopped-flow absorption spectrophotometry. A solution of O_2-free Fe(II)-R2-wt in buffer A was mixed at 11 ˚C with an equal volume of O_2-saturated buffer A containing different concentrations of $MgCl_2$. The final concentrations of $MgCl_2$ after mixing were 0 mM (red trace), 21 mM (blue trace), and 210 mM (black trace). The solid lines in (A) are fits of the equation for three parallel first-order processes to the data. The final concentration of the protein after mixing was 0.1 mM (Fe(II)/R2 = 2.7).

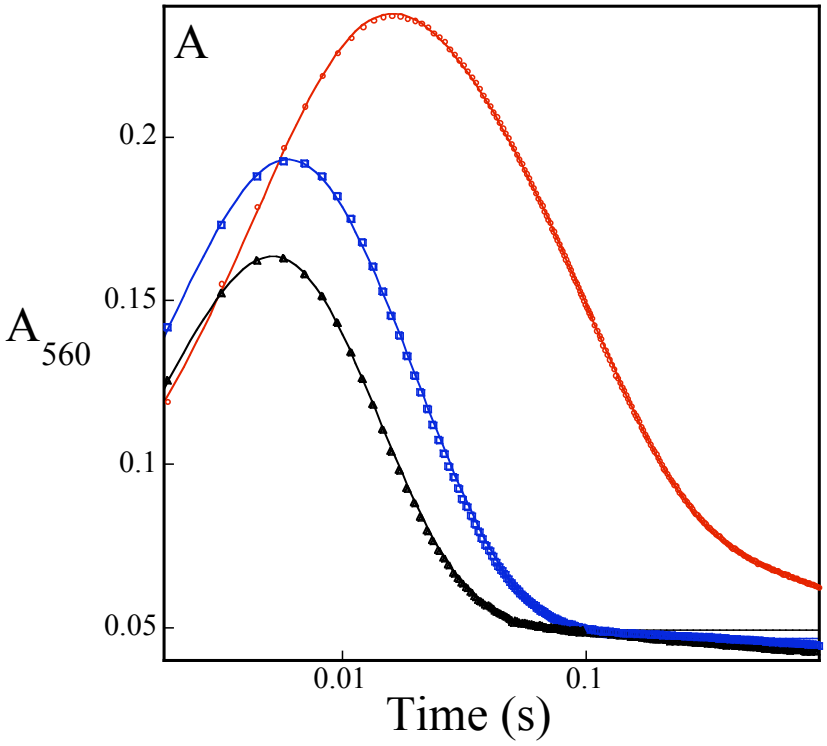
A
0.2
0.15
0.1
0.05
A560
0.01
0.1
Time (s)

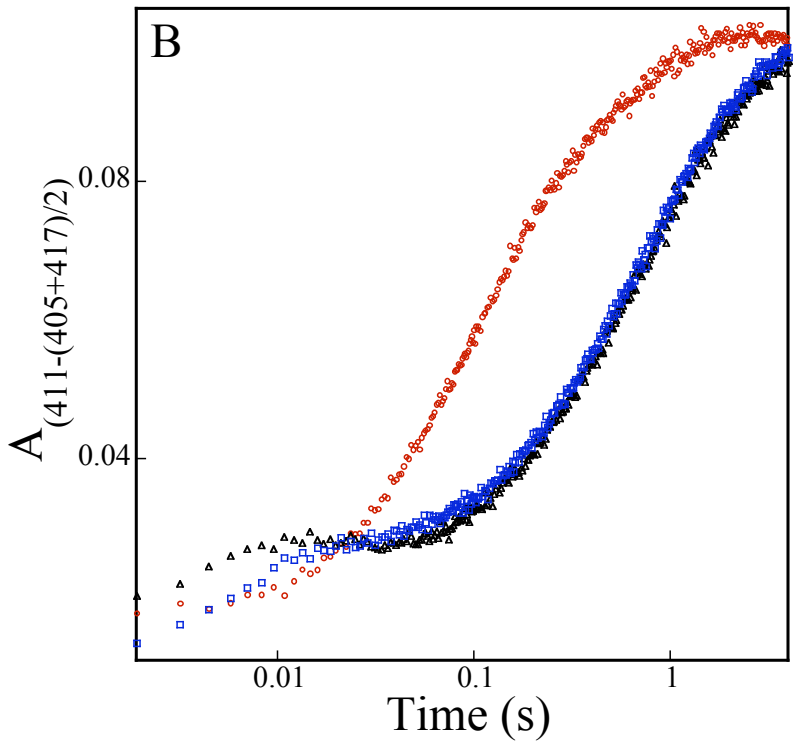
B
0.08
0.04
A(411-(405+417)/2)
0.01
0.1
1
Time (s)

Figure 4-2: Dependence of the observed rate constants of the decay phases of $W48^{+\bullet}$ on [$MgCl_2$] in the reactions of R2-wt (filled circles and solid line), R2-Y122F (filled squares and dashed line), R2-Y356F (open circles and dotted line) and R-Y122F/Y356F (open squares and dotted-dashed line). The solid lines are fits of the equation for a hyperbola to the data and correspond to $K_{0.5}$ values of 26 ± 3 mM, 8 ± 1 mM, 9 ± 3 mM and 2 ± 2 mM for R2-wt, R2-Y122F, R2-Y356F and R2-Y122F/Y356F respectively. The experimental conditions are described in legends to Figure 4-1 (R2-wt), Figure 4-6 (R2-Y122F), Figure 4-4 (R2-Y356F) and Figure 4-7 (R2-Y122F/Y356F).

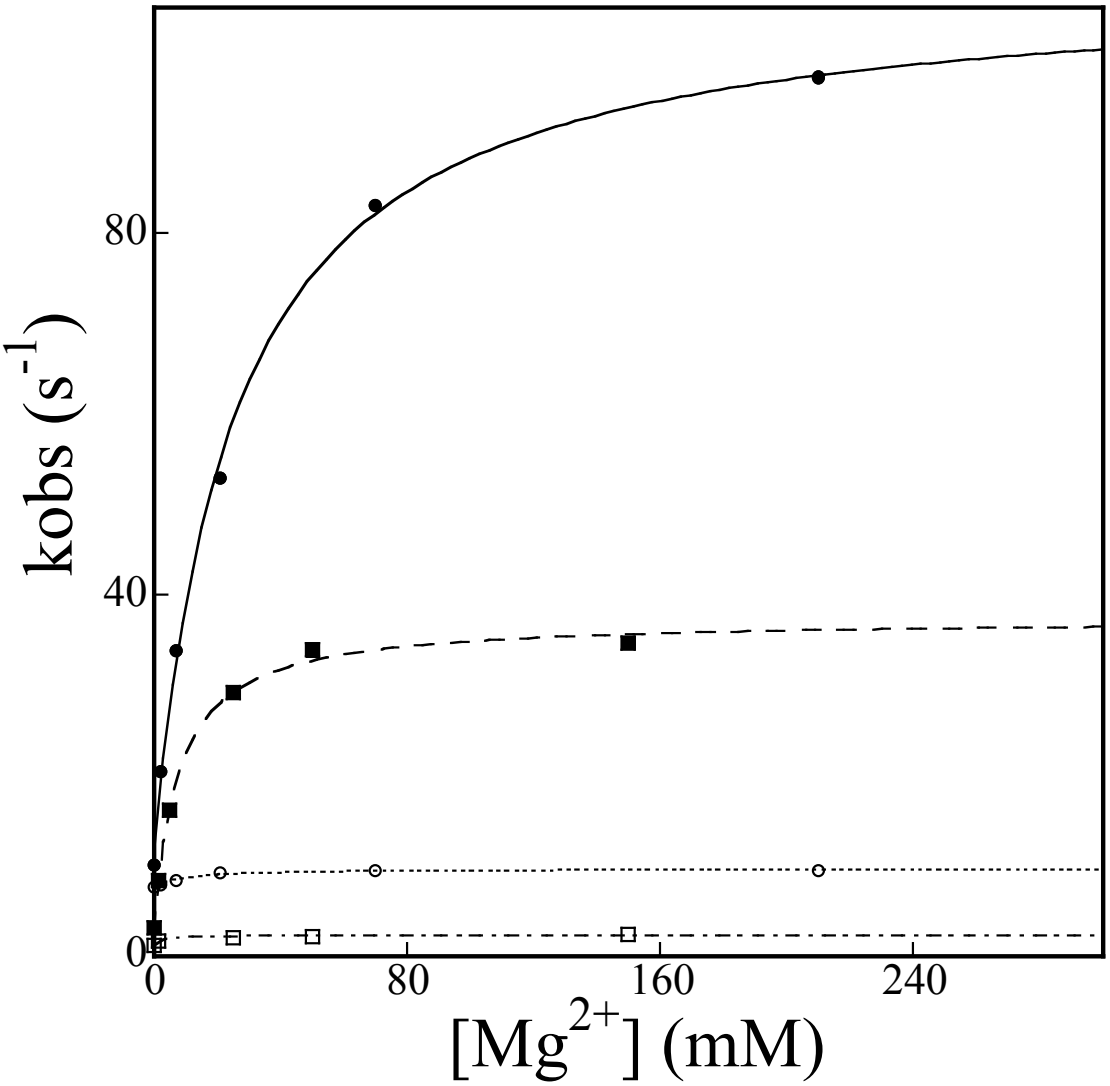
kobs (s^{-1})
80
40
0
0
80
160
240
[Mg^{2+}] (mM)

the kinetics of Y• formation (as assessed by the intensity of the diagnostic sharp ~ 411 nm peak characteristic of Y radicals) is complex (Figure 4-1B). At high [Mg^{2+}], a minor phase of very rapid Y• formation is observed and is nearly coincident with development of the 560-nm feature of the $W48^{+\bullet}$ (Figure 4-3). This rapid phase is followed by overall *slower* stable Y• (presumably Y122•) formation. Comparison of these pronounced effects of Mg^{2+} on the R2-wt reaction to its effects on the kinetics of $W48^{+\bullet}$ formation and decay and Y• formation in the reaction of R2-Y356F (Figure 4-4) shows that the surface tyrosine mediates both effects. Increasing [Mg^{2+}] does not accelerate decay of the 560-nm absorption feature in this variant (or does so to a much lesser extent) (Figure 4-4A and Figure 4-2, open circles and dotted line). In addition, Mg^{2+} barely affects the kinetics of Y122• formation (Figure 4-4B). Notably, the very fast phase of Y• formation is absent in the variant, implying that the fast phase in the reaction of R2-wt arises from Y356• formation. Evidence suggesting oxidation of this residue in O_2 activation by R2-Y122F was previously presented (*38, 55*), but the linkage of this process to the presence of cations was not explored. The fact that Y356• formation is, at high [Mg^{2+}], roughly coincident with $W48^{+\bullet}$ formation suggests that the two radicals are in equilibrium, and the fact that the fast phase has a much smaller amplitude than that of subsequent Y122• formation implies that the Y356• is disfavored in its equilibrium with the $W48^{+\bullet}$. The overall slowing of Y122• formation by increasing [Mg^{2+}] is attributable to engagement of a pathway for reduction of the $W48^{+\bullet}$ (via quenching of the Y356•) that is faster than reduction of the $W48^{+\bullet}$ by Y122, which is the primary pathway for decay in the absence of the more efficient, Mg^{2+}- and Y356-dependent pathway. This effect is equivalent to that seen (and previously reported) for inclusion of a reductant to quench the $W48^{+\bullet}$. It

Figure 4-3: Kinetics of formation and decay of $W48^{+\bullet}$ (as reported by A_{560}) and Y• (as reported by (A_{411} - (A_{405} + A_{417})/2)) in the reaction of R2-wt reveal temporal correlation between the rapid phase of Y• and the 560-nm feature of the $W48^{+\bullet}$ at high [$MgCl_2$]. The experimental details are described in the legend to Figure 4-1. The red traces are plots of *A*560-*versus*-time (closed circles) and (A_{411} - (A_{405} + A_{417})/2)-*versus*-time (opened circles) in the absence of $MgCl_2$. The black traces plots of *A*560-*versus*-time (closed squares) and (A_{411} - (A_{405} + A_{417})/2)-*versus*-time (opened squares) in the presence of 210 mM $MgCl_2$.

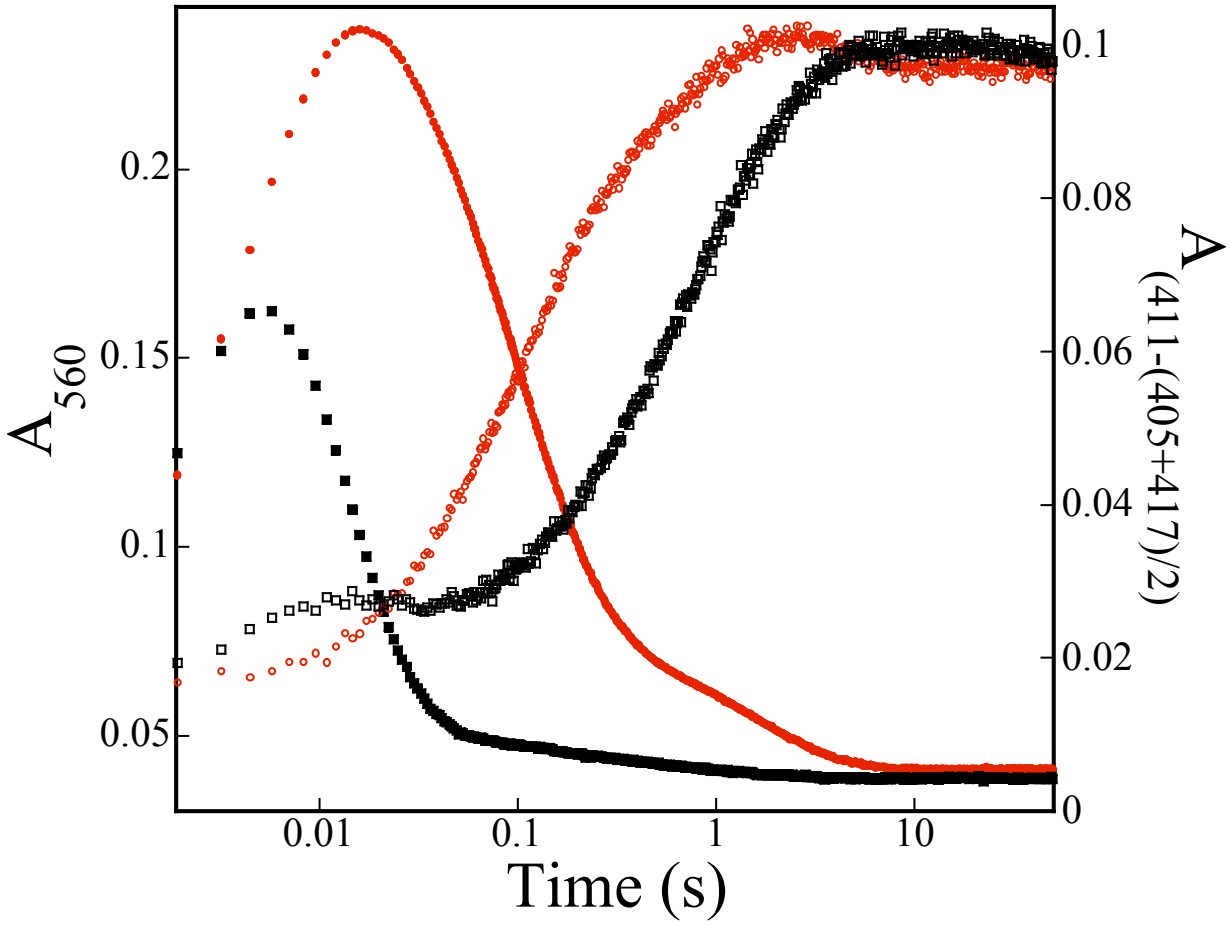
0.2
0.15
0.1
0.05
A560
0.1
0.08
0.06
0.04
0.02
0
A(411-(405+417)/2)
0.01
0.1
1
10
Time (s)

Figure 4-4: Effect of increasing [$MgCl_2$] on the formation and decay rates of (A) the transient $W48^{+\bullet}$ monitored at 560 nm and (B) the 411-nm peak height (A_{411} - (A_{405} + A_{417})/2) in the reaction of Fe(II)-R2-Y356F with O_2 as monitored by stopped-flow absorption spectrophotometry. A solution of O_2-free Fe(II)-R2-Y356F in buffer A was mixed at 11 ˚C with an equal volume of O_2-saturated buffer A containing different concentrations of $MgCl_2$. The final concentrations of $MgCl_2$ after mixing were 0 mM (red trace), 21 mM (blue trace), and 210 mM (black trace). The solid lines in (A) are fits of the equation for three parallel first-order processes to the data. The final concentration of the protein after mixing was 0.1 mM (Fe(II)/R2 = 2.7).

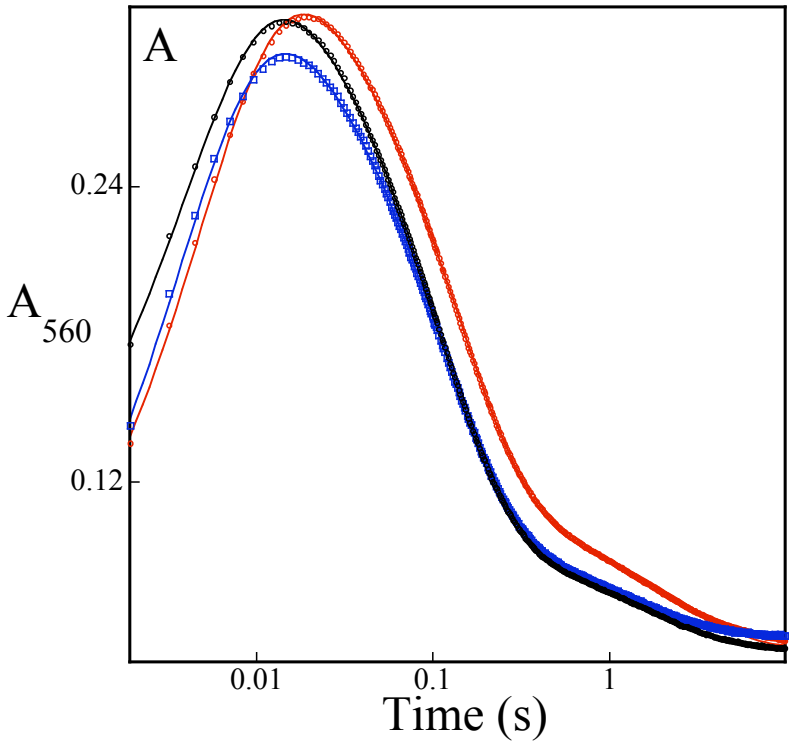
A
0.24
A560
0.12
0.01
0.1
1
Time (s)

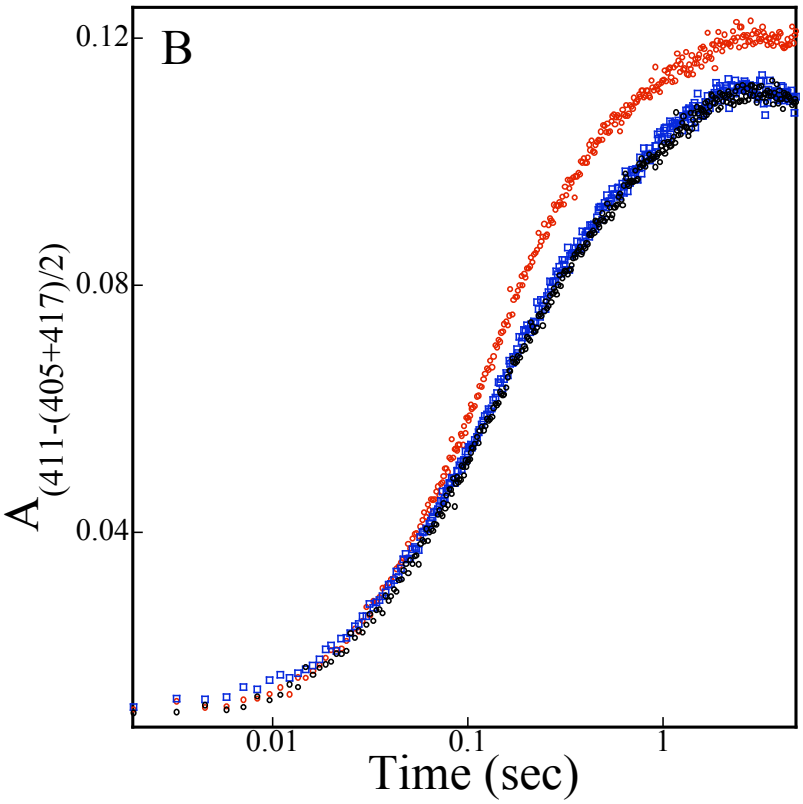
B
0.12
0.08
A(411-(405+417)/2)
0.04
0.01
0.1
1
Time (sec)

should be noted that the source of the reducing equivalent for pathway **D** (to quench the Y356•) is not clear.

The effects of Mg^{2+} on the kinetics of the reactions of R2-Y122F and R2-Y122F/Y356F are consistent with the above interpretation. $W48^{+\bullet}$ decay is slower overall in these variants, as a result of the absence of the pathway for its reduction by Y122. In addition, and as expected, no stable Y• is produced. In the single variant, increasing [Mg^{2+}] is, as in the reaction of R2-wt, associated with increasingly rapid decay of the $W48^{+\bullet}$ (Figure 4-5A). The dependence on [Mg^{2+}] is again hyperbolic (Figure 4-2, filled squares and dashed line), but in this case the limiting value of k_{obs} for decay is 37 ± 2 s^{-1}. This increase represents a 12-fold acceleration relative to decay in the absence of Mg^{2+}. The $K_{0.5}$ is 8 ± 1 mM, ~ 3-fold less than that for R2-wt. Associated with faster decay of the $W48^{+\bullet}$, formation and decay of a transient Y• become much faster at high [Mg^{2+}] (Figure 4-5B). The peak of [Y•] shifts to earlier time by ~ 17-fold, and the formation phase becomes, as for the fast phase of Y• in the R2-wt reaction at high [Mg^{2+}], roughly coincident with formation of the $W48^{+\bullet}$ (Figure 4-6). None of these effects occurs in R2-Y122F/Y356F: W48+• is accelerated to a minor extent (Figure 4-7A and Figure 4-2, open squares and dot-dashed line) and the kinetics of transient Y• are hardly affected (Figure 4-7B) by increasing [Mg^{2+}]. The fact that a transient Y• is observed at all in the double variant implies that one or more of the 14 tyrosines other than Y122 and Y356 can be oxidized during decay of the $W48^{+\bullet}$. The important point is that this process is relatively slow and unaffected by Mg^{2+}, whereas the Mg^{2+}-dependent transient Y• requiring the presence of Y356 forms rapidly, on the same timescale as O_2 addition. Efficient decay of the $W48^{+\bullet}$ depends on the formation of this Y356•, whereas

Figure 4-5: Effect of increasing [$MgCl_2$] on the formation and decay rates of (A) the transient $W48^{+\bullet}$ monitored at 560 nm and (B) the 411-nm peak height (A_{411} - (A_{405} + A_{417})/2) in the reaction of Fe(II)-R2-Y122F with O_2 as monitored by stopped-flow absorption spectrophotometry. A solution of O_2-free Fe(II)-R2-Y122F in buffer A was mixed at 11 ˚C with an equal volume of O_2-saturated buffer A containing different concentrations of $MgCl_2$. The final concentrations of $MgCl_2$ after mixing were 0 mM (red trace), 5 mM (blue trace), and 50 mM (black trace). The solid lines in (A) are fits of the equation for three parallel first-order processes to the data. The final concentration of the protein after mixing was 0.06 mM (Fe(II)/R2 = 2.7).

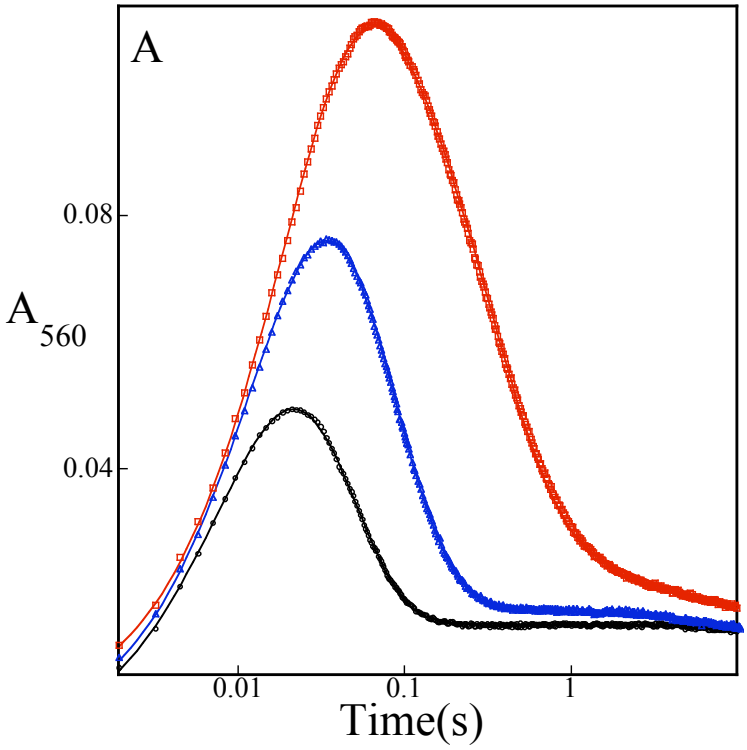
A
0.08
0.04
A560
0.01
0.1
1
Time(s)

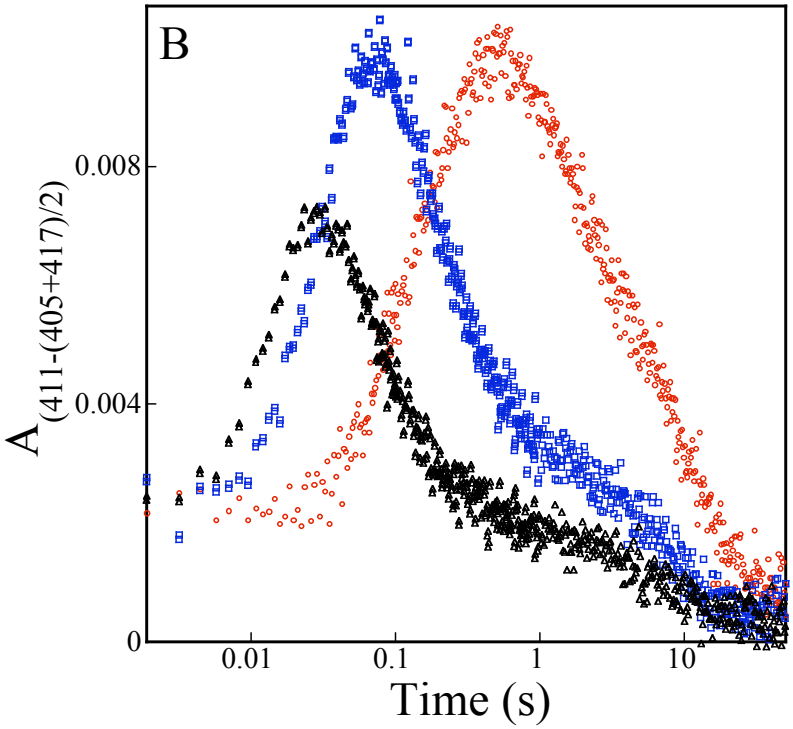
B
0.008
0.004
0
A(411-(405+417)/2)
0.01
0.1
1
10
Time (s)

Figure 4-6: Kinetics of formation and decay of $W48^{+\bullet}$ (as reported by A_{560}) and Y356• (as reported by (A_{411} - (A_{405} + A_{417})/2)) in the reaction of R2-Y122F reveal temporal correlation between the rise and decay phases of the 560-nm feature and the 411-nm peak height at high [$MgCl_2$]. The experimental details are described in the legend to Figure 4-5. The red traces are plots of *A*560-*versus*-time (closed circles) and (A_{411} - (A_{405} + A_{417})/2)-*versus*-time (opened circles) in the absence of $MgCl_2$. The black traces plots of *A*560-*versus*-time (closed squares) and (A_{411} - (A_{405} + A_{417})/2)-*versus*-time (opened squares) in the presence of 50 mM $MgCl_2$.

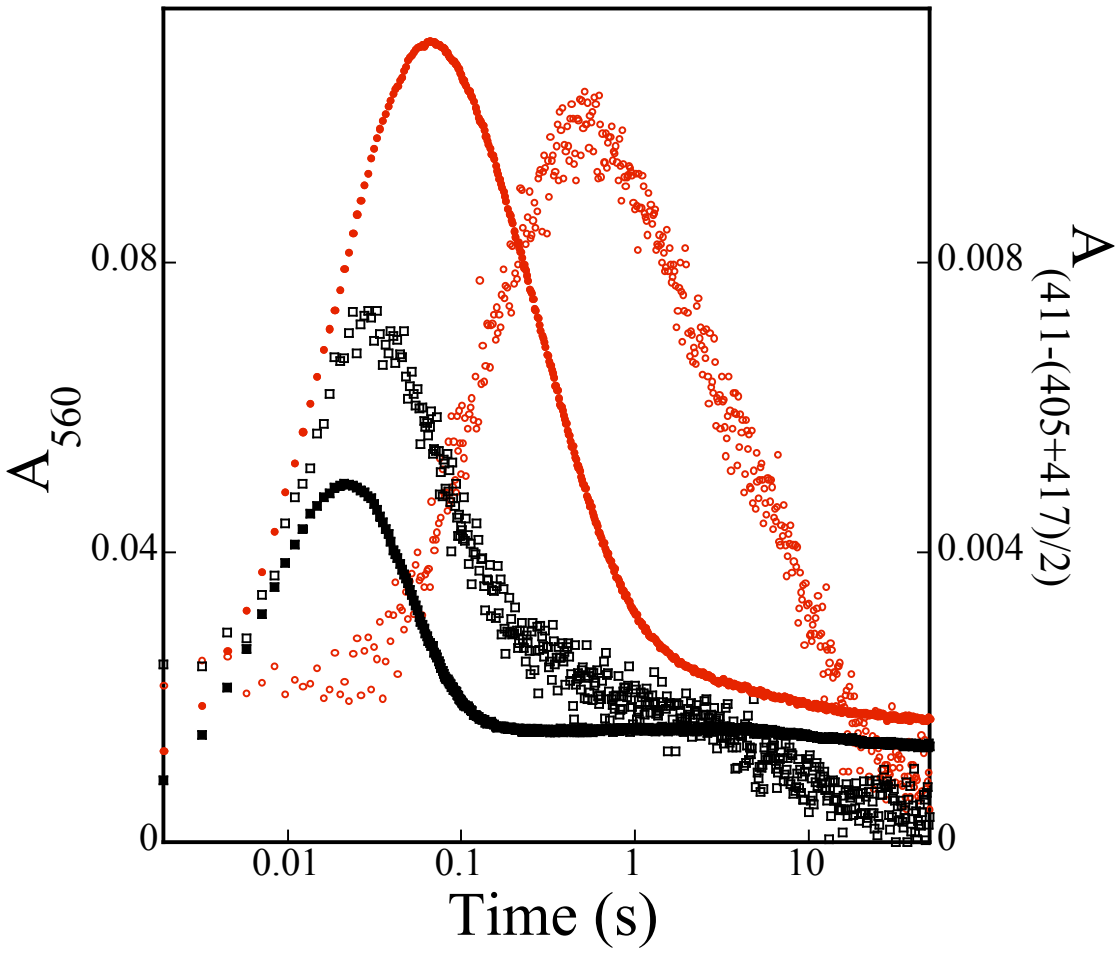
0.08
0.04
0
0.008
0.004
0
0.01
0.1
1
10
Time (s)
A560
A(411-(405+417)/2)

Figure 4-7: Effect of increasing [$MgCl_2$] on the formation and decay rates of (A) the transient $W48^{+\bullet}$ monitored at 560 nm and (B) the 411-nm peak height (A_{411} - (A_{405} + A_{417})/2) in the reaction of Fe(II)-R2-Y122F/Y356F with O_2 as monitored by SF-Abs spectroscopy. A solution of O_2-free Fe(II)-R2- Y122F/Y356F in buffer A was mixed at 11 ˚C with an equal volume of O_2-saturated buffer A containing different concentrations of $MgCl_2$. The final concentrations of $MgCl_2$ after mixing were 0 mM (red trace), 21 mM (blue trace), and 210 mM (black trace). The solid lines in (A) are fits of the equation for three parallel first-order processes to the data. The final concentration of the protein after mixing was 0.09 mM (Fe(II)/R2 = 2.7).

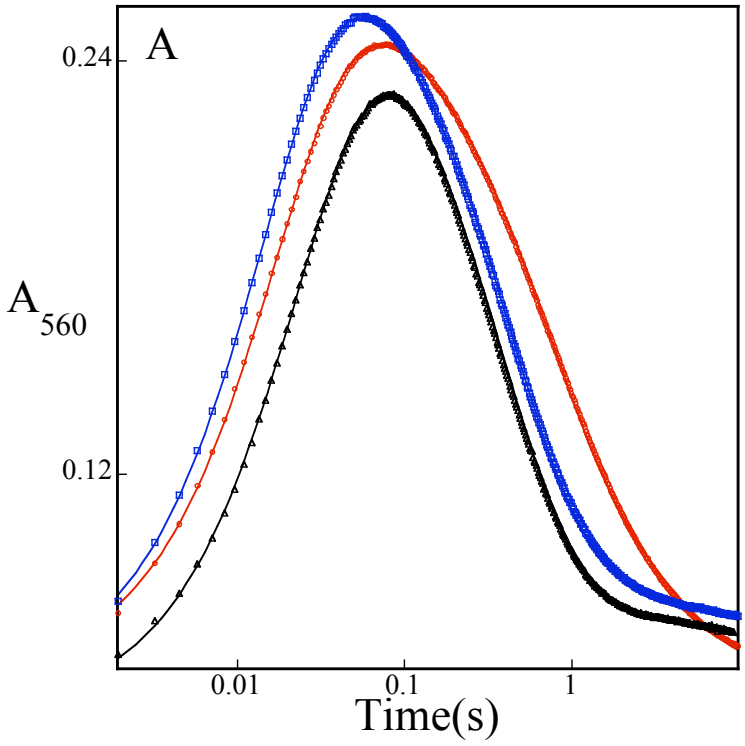
A
0.24
0.12
A560
0.01
0.1
1
Time(s)

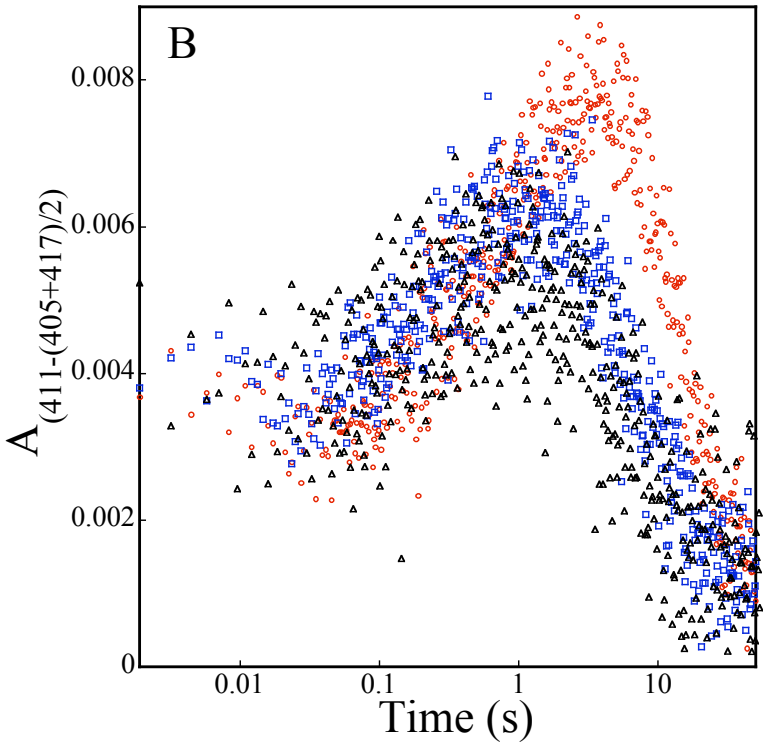
B
0.008
0.006
0.004
0.002
0
A(411-(405+417)/2)
0.01
0.1
1
10
Time (s)

the other Y residues either reduce the $W48^{+\bullet}$ very inefficiently or reduce **X** after the $W48^{+\bullet}$ decays.

Variation of the anion and cation in the reaction of R2-Y122F was undertaken to verify that the latter is the relevant mediator of the W48-Y356 radical-transfer equilibrium (Figure 4-8). Chloride and sulfate salts of Mg^{2+} and Ca^{2+} have equivalent effects and concentration dependencies (filled symbols). The identity of the anion is unimportant. Salts of monovalent cations also mediate the effect, but much higher concentrations (hundreds of millimolar) are required (open symbols). Again, the identity of the anion is unimportant. These data establish that the cation is the mediator and that divalent cations are ~ 33-fold better at this mediation (comparing the limiting slopes of plots of k_{obs} versus $[M^{n+}]$). Notably, this difference is greater than the three-fold difference between monovalent and divalent cations that would be expected if the effect were due merely to increasing ionic strength.

DISCUSSION

The kinetic data for the reactions of the four R2 proteins demonstrate a cation-dependent radical-transfer equilibrium between W48 and Y356. The mechanism by which this phenomenon arises and its functional significance remain open questions. The simplest possibility is that Mg^{2+} binds in the vicinity of Y356, inducing order in this region of the protein that is otherwise disordered. The C-terminus is rich in carboxylate residues that could serve as Mg^{2+} ligands (see Figure 5-1). In addition, Y356 could itself serve as a Mg^{2+} ligand. Simultaneous coordination of one or more sidechain both in the C-terminus and in the main domain of the protein in the vicinity of W48 could "tether"

Figure 4-8: Titration effect of different salts on the observed rate constant of decay of $W48^{+\bullet}$ in the reaction of R2-Y122F. A solution of O_2-free Fe(II)-R2-Y122F complex (0.1-0.2 mM; Fe(II)/R2 = 2.7) was mixed at 11 ˚C with an equal volume of O_2-saturated buffer containing different concentrations of Na_2SO_4 (open squares), NaCl (open circles), KCl (open triangles), $MgCl_2$ (closed squares), $CaCl_2$ (closed circles), or $MgSO_4$ (closed triangles) in a stopped-flow apparatus. The rate constants of decay of $W48^{+\bullet}$ were obtained from the fits of the kinetic traces of $W48^{+\bullet}$ under the conditions described (as previously described in Figure 4-6). The solid and dashed lines are fits of the equation for a hyperbola to the data of the divalent metal ion and monovalent metal ion titrations respectively and the values at half-maximal enhancement of $W48^{+\bullet}$ decay ($K_{0.5}$) are calculated to be 8.6 ± 0.5 mM for divalent metal ions and 210 ± 27 mM for monovalent metal ions. As a control, a solution of O_2-free Fe(II)-R2-Y122F/Y356F complex (0.13 mM; Fe(II)/R2 = 2.7) was mixed at 11 ˚C with an equal volume of O_2-saturated buffer containing different concentrations of $MgSO_4$ (open diamonds). The dotted line is a fit of the equation for a hyperbola to the obtained data and the resulting $K0.5$ value is 2.0 ± 1 mM.

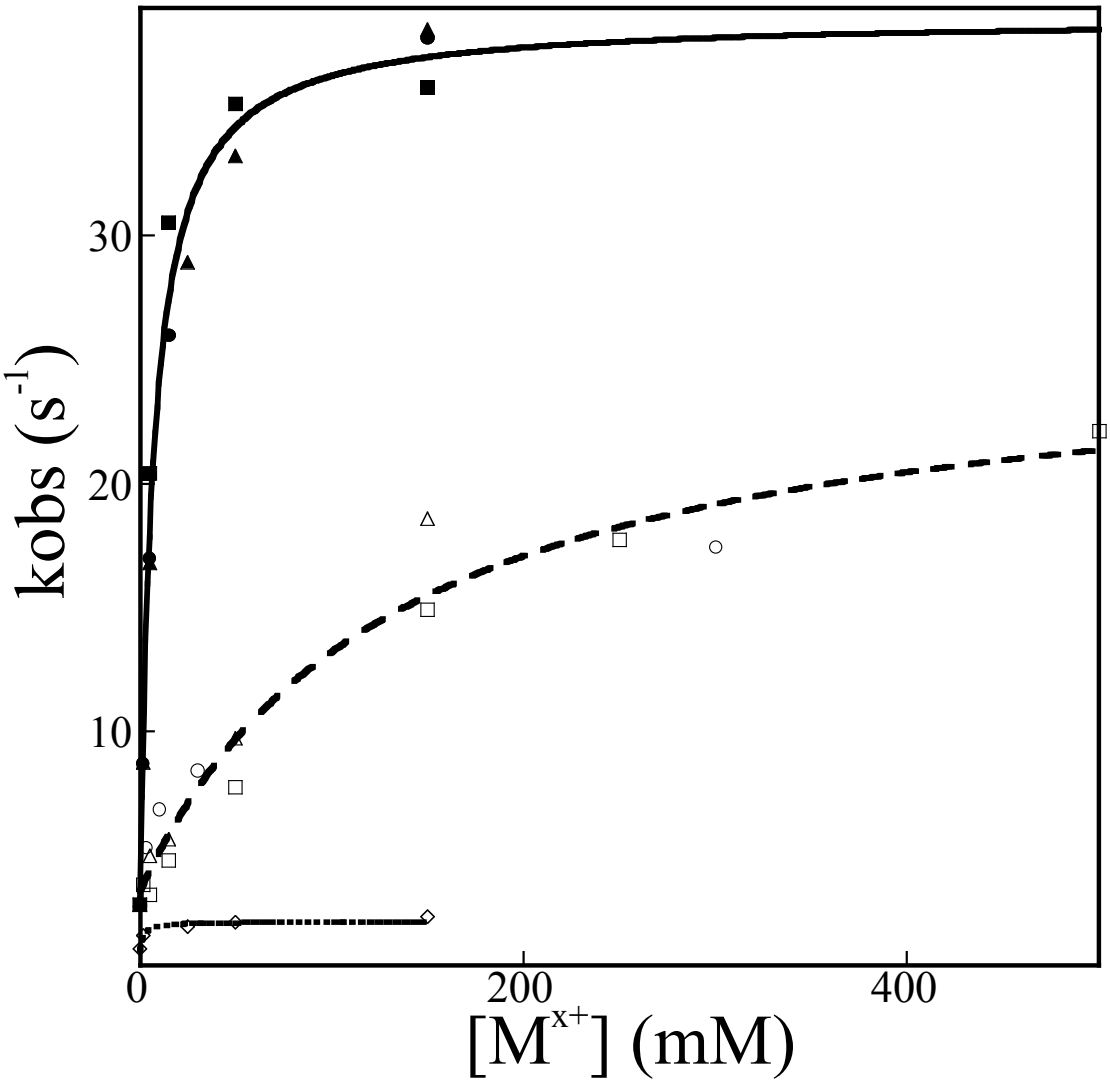
kobs (s^{-1})
30
20
10
0
200
400
[M^{x+}] (mM)

the flexible C-terminus to the protein to mediate the radical-transfer equilibrium between W48 and Y356. Interestingly, two carboxylate residues are present within 8 Å of W48 (*36, 56, 57*). E51 and E52 would be excellent candidates for C-terminus-tethering Mg^{2+} ligands. In fact, E52 is conserved among R2 sequences. Even more intriguingly, C-terminal carboxylate residue E350 is also conserved (one of a few residues in the C-terminus) and has been subjected to site-directed mutagenesis (*5*). The E350A variant was found to be *inactive in nucleotide reduction*, even though its affinity for R1 is normal (*5*). The inactivity of this variant, which, to our knowledge, has not been explained, raises the possibility that E350 may function as a Mg^{2+} ligand to mediate communication between W48 and Y356 as part of the radical-transfer steps that initiate and culminate nucleotide reduction. Indeed, the standard RNR assay includes 15 mM Mg^{2+}, similar to the $K_{0.5}$ value determined for R2-wt in our experiments and greater than that for R2-Y122F. Moreover, binding of Mg^{2+} and R1 by R2 could be synergistic, reducing the concentration of Mg^{2+} needed to mediate communication between Y356 and W48 in the R1•R2 complex. We are not aware of any report in which the dependence of turnover on $[Mg^{2+}]$ was documented, and so our suggestion that one role of Mg^{2+} (in addition to binding of nucleotides and its reported requirement for maintenance of the functional R1 homodimer (*58*)) could be to mediate inter-subunit radical transfer must be considered as speculative. Mutagenesis experiments and activity measurements to test the intriguing possibility are in progress.

REFERENCES

1. Atkin, C. L., Thelander, L., and Reichard, P. (1973) Iron and free radical in ribonucleotide reductase. Exchange of iron and Mössbauer spectroscopy of the protein B2 subunit of the *Escherichia coli* enzyme, *J. Biol. Chem. 248*, 7464-7472.

2. Larsson, A., Karlsson, M., Sahlin, M., and Sjöberg, B.-M. (1988) Radical formation in the dimeric small subunit of ribonucleotide reductase requires only one tyrosine 122, *J. Biol. Chem. 263*, 17780-4.

3. Mao, S. S., Holler, T. P., Yu, G. X., Bollinger, J. M., Jr., Booker, S., Johnston, M. I., and Stubbe, J. (1992) A model for the role of multiple cysteine residues involved in ribonucleotide reduction: amazing and still confusing, *Biochemistry 31*, 9733-9743.

4. Mao, S. S., Yu, G. X., Chalfoun, D., and Stubbe, J. (1992) Characterization of C439SR1, a mutant of *Escherichia coli* ribonucleotide diphosphate reductase: evidence that C439 is a residue essential for nucleotide reduction and C439SR1 is a protein possessing novel thioredoxin-like activity, *Biochemistry 31*, 9752-9759.

5. Climent, I., Sjöberg, B.-M., and Huang, C. Y. (1992) Site-directed mutagenesis and deletion of the carboxyl terminus of *Escherichia coli* ribonucleotide reductase protein R2. Effects on catalytic activity and subunit interaction, *Biochemistry 31*, 4801-4807.

6. Rova, U., Goodtzova, K., Ingemarson, R., Behravan, G., Gräslund, A., and Thelander, L. (1995) Evidence by site-directed mutagenesis supports long-range electron transfer in mouse ribonucleotide reductase, *Biochemistry 34*, 4267-4275.

7. Ekberg, M., Sahlin, M., Eriksson, M., and Sjöberg, B.-M. (1996) Two conserved tyrosine residues in protein R1 participate in an intermolecular electron transfer in ribonucleotide reductase, *J. Biol. Chem. 271*, 20655-20659.

8. Ekberg, M., Pötsch, S., Sandin, E., Thunnissen, M., Nordlund, P., Sahlin, M., and Sjöberg, B.-M. (1998) Preserved catalytic activity in an engineered ribonucleotide reductase R2 protein with a non-physiological radical transfer pathway. The importance of hydrogen bond connections between the participating residues, *J. Biol. Chem. 273*, 21003-21008.

9. Rova, U., Adrait, A., Pötsch, S., Gräslund, A., and Thelander, L. (1999) Evidence by mutagenesis that Tyr(370) of the mouse ribonucleotide reductase R2 protein is the connecting link in the intersubunit radical transfer pathway, *J. Biol. Chem. 274*, 23746-23751.

10. Mao, S. S., Johnston, M. I., Bollinger, J. M., and Stubbe, J. (1989) Mechanism-based inhibition of a mutant *Escherichia coli* ribonucleotide reductase (cysteine-225----serine) by its substrate CDP, *Proc. Natl. Acad. Sci. U S A 86*, 1485-1489.

11. Mao, S. S., Holler, T. P., Bollinger, J. M., Jr., Yu, G.-X., Johnston, M. I., and Stubbe, J. (1992) Interaction of C225SR1 mutant subunit of ribonucleotide reductase with R2 and nucleoside diphosphates: tales of a suicidal enzyme, *Biochemistry 31*, 9744-9751.

12. Persson, A. L., Eriksson, M., Katterle, B., Pötsch, S., Sahlin, M., and Sjöberg, B.-M. (1997) A New Mechanism-Based Radical Intermediate in a Mutant R1 Protein Affecting the Catalytically Essential Glu441 in Escherichia coli Ribonucleotide Reductase, *J. Biol. Chem. 272*, 31533-31541.

13. Persson, A. L., Sahlin, M., and Sjöberg, B.-M. (1998) Cysteinyl and substrate radical formation in active site mutant E441Q of Escherichia coli class I ribonucleotide reductase, *J. Biol. Chem. 273*, 31016-31020.

14. Lawrence, C. C., Bennati, M., Obias, H. V., Bar, G., Griffin, R. G., and Stubbe, J. (1999) High-field EPR Detection of a Disulfide Radical Anion in the Reduction of Cytidine 5'-Diphosphate by the E441Q R1 Mutant of Escherichia coli Ribonucleotide Reductase, *Proc. Natl. Acad. Sci. U. S. A. 96*, 8979-8984.

15. Ator, M., Salowe, S. P., Stubbe, J., Emptage, M. H., and Robins, M. J. (1984) 2'-Azido-2'-Deoxynucleotide Interaction with E. coli Ribonucleotide Reductase: Generation of a New Radical Species, *J. Am. Chem. Soc. 106*, 1886-7.

16. Salowe, S. P., Ator, M. A., and Stubbe, J. (1987) Products of the inactivation of ribonucleoside diphosphate reductase from *Escherichia coli* with 2'-azido-2'-deoxyuridine 5'-diphosphate, *Biochemistry 26*, 3408-3416.

17. Stubbe, J., Booker, S., Broderick, J., Mao, S. S., Ator, M., Harris, G., Ashley, G., Linn, A. E., and Yu, G. X. (1993) Ribonucleotide reductases: Radical enzymes with suicidal tendencies, *Nucleic Acids Symp. Ser. 29*, 107.

18. van der Donk, W. A., Yu, G., Silva, D. J., Stubbe, J., McCarthy, J. R., Jarvi, E. T., Matthews, D. P., Resvick, R. J., and Wagner, E. (1996) Inactivation of Ribonucleotide Reductase by (E)-2'-Fluoromethylene-2'-deoxycytidine 5'-Diphosphate: A Paradigm for Nucleotide Mechanism-Based Inhibitors, *Biochemistry 35*, 8381-8391.

19. Gerfen, G. J., van der Donk, W. A., Yu, G., McCarthy, J. R., Jarvi, E. T., Matthews, D. P., Farrar, C., Griffin, R. G., and Stubbe, J. (1998) Characterization

of a Substrate-Derived Radical Detected during the Inactivation of Ribonucleotide Reductase from Escherichia coli by 2'-Fluoromethylene-2'-deoxycytidine 5'-Diphosphate, *J. Am. Chem. Soc. 120*, 3823-3835.

20. Baldwin, J., Krebs, C., Ley, B. A., Edmondson, D. E., Huynh, B. H., and Bollinger, J. M., Jr. (2000) Mechanism of rapid electron transfer during oxygen activation in the R2 subunit of *Escherichia coli* ribonucleotide reductase. 1. Evidence for a transient tryptophan radical, *J. Am. Chem. Soc. 122*, 12195-12206.

21. Thelander, L., and Reichard, P. (1979) Reduction of ribonucleotides, *Annu. Rev. Biochem. 48*, 133-158.

22. Stubbe, J. (1990) Ribonucleotide reductases., *Adv. Enzymol. Relat. Areas Mol. Biol. 63*, 349-419.

23. Jordan, A., and Reichard, P. (1998) Ribonucleotide reductases, *Annu. Rev. Biochem. 67*, 71-98.

24. Eklund, H., Uhlin, U., Farnegardh, M., Logan, D. T., and Nordlund, P. (2001) Structure and function of the radical enzyme ribonucleotide reductase, *Prog. Biophys. Mol. Biol. 77*, 177-268.

25. Stubbe, J., and Ackles, D. (1980) On the mechanism of ribonucleotide diphosphate reductase from *Escherichia coli*, *J. Biol. Chem. 255*, 8027-8030.

26. Stubbe, J., Ackles, D., Segal, R., and Blakley, R. L. (1981) On the mechanism of ribonucleoside triphosphate reductase from *Lactobacillus leichmannii*. Evidence for 3' carbon-hydrogen bond cleavage, *J. Biol. Chem. 256*, 4843-4846.

27. Stubbe, J., Ator, M., and Krenitsky, T. (1983) Mechanism of ribonucleoside diphosphate reductase from *Escherichia coli*. Evidence for 3'-C--H bond cleavage, *J. Biol. Chem. 258*, 1625-1631.

28. Uhlin, U., and Eklund, H. (1994) Structure of ribonucleotide reductase protein R1, *Nature 370*, 533-539.

29. Reichard, P. (1993) From RNA to DNA, why so many ribonucleotide reductases?, *Science 260*, 1773-1776.

30. Reichard, P. (1997) The evolution of ribonucleotide reduction, *Trends Biochem. Sci. 22*, 81–85.

31. Stubbe, J., and van der Donk, W. A. (1998) Protein radicals in enzyme catalysis, *Chem. Rev. 98*, 705-762.

32. Booker, S., Licht, S., Broderick, J., and Stubbe, J. (1994) Coenzyme B12-dependent ribonucleotide reductase: evidence for the participation of five cysteine residues in ribonucleotide reduction, *Biochemistry 33*, 12676-12685.

33. Ollagnier, S., Mulliez, E., Gaillard, J., Eliasson, R., Fontecave, M., and Reichard, P. (1996) The anaerobic *Escherichia coli* ribonucleotide reductase. Subunit structure and iron sulfur center, *J. Biol. Chem. 271*, 9410-9416.

34. Ollagnier, S., Mulliez, E., Schmidt, P. P., Eliasson, R., Gaillard, J., Deronzier, C., Bergman, T., Gräslund, A., Reichard, P., and Fontecave, M. (1997) Activation of the anaerobic ribonucleotide reductase from *Escherichia coli*. The essential role of the iron-sulfur center for S-adenosylmethionine reduction, *J. Biol. Chem. 272*, 24216-24223.

35. Larsson, A., and Sjöberg, B. M. (1986) Identification of the stable free radical tyrosine residue in ribonucleotide reductase, *EMBO J. 5*, 2037-2040.

36. Nordlund, P., and Eklund, H. (1993) Structure and function of the *Escherichia coli* ribonucleotide reductase, *J. Mol. Biol. 232*, 123-164.

37. Stubbe, J., Nocera, D. G., Yee, C. S., and Chang, M. C. Y. (2003) Radical initiation in the class I ribonucleotide reductase: long-range proton-coupled electron transfer?, *Chem. Rev. 103*, 2167-2202.

38. Bollinger, J. M., Jr., Stubbe, J., Huynh, B. H., and Edmondson, D. E. (1991) Novel diferric radical intermediate responsible for tyrosyl radical formation in assembly of the cofactor of ribonucleotide reductase, *J. Am. Chem. Soc. 113*, 6289-6291.

39. Bollinger, J. M., Jr., Edmondson, D. E., Huynh, B. H., Filley, J., Norton, J. R., and Stubbe, J. (1991) Mechanism of assembly of the tyrosyl radical-dinuclear iron cluster cofactor of ribonucleotide reductase, *Science 253*, 292-298.

40. Ravi, N., Bollinger, J. M., Jr., Huynh, B. H., Edmondson, D. E., and Stubbe, J. (1994) Mechanism of assembly of the tyrosyl radical-diiron(III) cofactor of *E. coli* ribonucleotide reductase: 1. Mössbauer characterization of the diferric radical precursor., *J. Am. Chem. Soc. 116*, 8007-8014.

41. Bollinger, J. M., Jr., Tong, W. H., Ravi, N., Huynh, B. H., Edmondson, D. E., and Stubbe, J. (1994) Mechanism of assembly of the tyrosyl-diiron(III) cofactor of E. coli ribonucleotide reductase. 2. Kinetics of the excess Fe^{2+} reaction by optical, EPR, and Mössbauer spectroscopies, *J. Am. Chem. Soc. 116*, 8015-8023.

42. Bollinger, J. M., Jr., Tong, W. H., Ravi, N., Huynh, B. H., Edmondson, D. E., and Stubbe, J. (1994) Mechanism of assembly of the tyrosyl radical-diiron(III) cofactor of *E. coli* ribonucleotide reductase. 3. Kinetics of the limiting Fe^{2+} reaction of optical, EPR, and Mössbauer spectroscopies, *J. Am. Chem. Soc. 116*, 8024-8032.

43. Bollinger, J. M., Jr., Tong, W. H., Ravi, N., Huynh, B. H., Edmondson, D. E., and Stubbe, J. (1995) Use of rapid kinetics methods to study the assembly of the diferric-tyrosyl radical cofactor of *E. coli* ribonucleotide reductase., *Methods in Enzymology 258*, 278-303.

44. Tong, W. H., Chen, S., Lloyd, S. G., Edmondson, D. E., Huynh, B. H., and Stubbe, J. (1996) Mechanism of assembly of the diferric cluster-tyrosyl radical cofactor of *Escherichia coli* ribonucleotide reductase from the diferrous form of the R2 subunit., *J. Am. Chem. Soc. 118*, 2107-2108.

45. Sturgeon, B. E., Burdi, D., Chen, S., Huynh, B. H., Edmondson, D. E., Stubbe, J., and Hoffman, B. M. (1996) Reconsideration of **X**, the diiron intermediate formed during cofactor assembly in *E. coli* ribonucleotide reductase, *J. Am. Chem. Soc. 118*, 7551-7557.

46. Bollinger, J. M., Jr., Krebs, C., Vicol, A., Chen, S., Ley, B. A., Edmondson, D. E., and Huynh, B. H. (1998) Engineering the diiron site of *Escherichia coli* ribonucleotide reductase protein R2 to accumulate an intermediate similar to Hperoxo, the putative peroxodiiron(III) complex from the methane monooxygenase catalytic cycle, *J. Am. Chem. Soc. 120*, 1094-1095.

47. Saleh, L., Krebs, C., Ley, B. A., Naik, S., Huynh, B. H., and Bollinger, J. M., Jr. (2004) Use of a chemical trigger for electron transfer to characterize a precursor to cluster X in assembly of the iron-radical cofactor of *Escherichia coli* ribonucleotide reductase, *Biochemistry 43*, 5953-5964.

48. Sahlin, M., and Sjöberg, B.-M. (2000) Ribonucleotide reductase. A virtual playground for electron transfer reactions, *Subcell. Biochem. 35*, 405-443.

49. Henriksen, M. A., Cooperman, B. S., Salem, J. S., Li, L.-S., and Rubin, H. (1994) The stable tyrosyl radical in mouse ribonucleotide reductase is not essential for enzymic activity, *J. Am. Chem. Soc. 116*, 9773-9774.

50. Roshick, C., Iliffe-Lee, E. R., and McClarty, G. (2000) Cloning and characterization of ribonucleotide reductase from *Chlamydia trachomatis*, *J. Biol. Chem. 275*, 38111-38119.

51. Högbom, M., Stenmark, P., Voevodskaya, N., McClarty, G., Gräslund, A., and Nordlund, P. (2004) The radical site in Chlamydial ribonucleotide reductase defines a new R2 subclass, *Science 305*, 245-248.

52. Moënne-Loccoz, P., Baldwin, J., Ley, B. A., Loehr, T. M., and Bollinger, J. M., Jr. (1998) O_2 activation by non-heme diiron proteins: identification of a symmetric μ-1,2-peroxide in a mutant of ribonucleotide reductase, *Biochemistry 37*, 14659-14663.

53. Parkin, S. E., Chen, S., Ley, B. A., Mangravite, L., Edmondson, D. E., Huynh, B. H., and Bollinger, J. M., Jr. (1998) Electron injection through a specific pathway determines the outcome of oxygen activation at the diiron cluster in the F208Y

mutant of *Escherichia coli* ribonucleotide reductase protein R2, *Biochemistry 37*, 1124-1130.

54. Gill, S. C., and von Hippel, P. H. (1989) Calculation of protein extinction coefficients from amino acid sequence data, *Anal. Biochem. 182*, 319-326.

55. Sahlin, M., Lassmann, G., Pötsch, S., Sjöberg, B.-M., and Gräslund, A. (1995) Transient free radicals in iron/oxygen reconstitution of mutant protein R2 Y122F. Possible participants in electron transfer chains in ribonucleotide reductase, *J. Biol. Chem. 270*, 12361-12372.

56. Nordlund, P., Sjöberg, B.-M., and Eklund, H. (1990) Three-dimensional structure of the free radical protein of ribonucleotide reductase, *Nature 345*, 593-598.

57. Högbom, M., Galander, M., Andersson, M., Kolberg, M., Hofbauer, W., Lassmann, G., Nordlund, P., and Lendzian, F. (2003) Displacement of the tyrosyl radical cofactor in ribonucleotide reductase obtained by single-crystal high-field EPR and 1.4-Å X-ray data, *Proc. Natl Acad. Soc. U.S.A. 100*, 3209-3214.

58. Thelander, L. (1973) Physicochemical Characterization of Ribonucleoside Diphosphate Reductase from *Escherichia coli*, *Journal of Biological Chemistry 248*, 4591-4601.

Chapter 5

Investigating the Role of Conserved Carboxylate Ligands Located on the C-terminus and Surface of *E. coli* R2 in Binding to Mg^{2+} and Mediating W48-Y356 Radical Transfer

Footnotes

[1]Abbreviations: RNR, ribonucleotide reductase; Y122•, tyrosyl radical in *E. coli* R2; $W48^{+\bullet}$, tryptophan 48 cation radical; wt, wild-type; $K_{0.5}$, concentration needed for 50% of maximal enhancement of $W48^{+\bullet}$ decay; k, observed first-order rate constant; IPTG, isopropy-β-D-thiogalactopyranoside; PMSF, phenylmethylsulfonyl fluoride; Tris, *tris*-[hydroxymethyl]-aminomethane; EPPS, N-[2-hydroxyethyl]piperazine-N'-[3-propane-sulfonic acid]; PCR, polymerase chain reaction; bp, base pairs; 5' R.E., a restriction enzyme which cleaves a specific DNA sequence upstream the *nrdB* gene; 3' R.E., a restriction enzyme which cleaves a specific DNA sequence downstream the *nrdB* gene; ε_{280}, molar absorption coefficients at 280 nm; $(A_{411} - (A_{405} + A_{417})/2)$, peak height proportional to the concentration of tyrosyl radical; SDSL, site-directed spin labeling; EPR, electron paramagnetic resonance.

ABSTRACT

Activation of oxygen at the carboxylate-bridged diiron(II) cluster in the R2 subunit of class I ribonucleotide reductase (RNR) from *Escherichia coli* leads to the formation of the catalytically essential tyrosyl radical (Y122•) by one-electron oxidation of tyrosine 122. The transfer of an "extra" electron from solution to the buried diiron site is required for the formation of the formally Fe_2(III/IV) intermediate species, cluster **X**, on the reaction pathway that generates the Y122• along with the adjacent μ-oxo-diiron(III) cluster. The mechanism of rapid transfer of this "extra" electron during the conversion to **X**, of its precursor, **L**, involves transient oxidation of the near-surface residue tryptophan 48 to a cation radical ($W48^{+\bullet}$). The $W48^{+\bullet}$ is readily reduced in the presence of reductants (e.g $Fe(II)_{aq}$, ascorbate, β-mercaptoethanol). In the absence of these reductants, this radical decays by the oxidation of neighboring amino acids such as Y122 and Y356. In Chapter 4, we showed that one pathway for $W48^{+\bullet}$ decay involves reduction by Y356, the catalytically essential tyrosine in the flexible C-terminus. Mediation of $W48^{+\bullet}$ reduction by Y356 was shown to be very inefficient except in the presence of divalent cations such as Mg^{2+}. We theorized that Mg^{2+} binds to the C-terminus of the protein, fixing Y356 in proximity to W48, allowing for facile electron transfer between it and W48. We also proposed that this "metal-ion" switch that connects the electron transfer pathway is likely also to be important in electron transfer between R1 and R2. In this chapter, we have tested the hypothesis that conserved carboxylic acid residues in the flexible C-terminus (E350 and D362) and near W48 (E51, E52, and D54) are ligands in Mg^{2+} binding. Examination of the kinetics of formation and decay of the transient $W48^{+\bullet}$ and Y• in the reactions of the carboxylate-substituted

variants of R2 with O_2 by stopped-flow absorption spectrophotometry did not provide any conclusive evidence for a Mg^{2+}-coordinating role for any of these residues. Further investigation is required.

The four-electron reduction of dioxygen to water at the carboxylate–bridged diiron(II) site of the R2 subunit of ribonucleotide reductase (RNR^{1}) from *Escherichia coli* is balanced by oxidation of two Fe(II) ions to Fe(III), oxidation of tyrosine 122 (Y122) by one-electron to the catalytically essential Y122•, and transfer of an "extra" electron from an exogenous source. In the transfer of the extra electron, a near-surface tryptophan residue (W48) is transiently oxidized ($k > 400\ s^{-1}$ at 5 °C) by a kinetically masked two-electron-oxidized adduct (**L**) between the diiron cluster and oxygen, generating a "di-radical" intermediate state that contains a W48 cation radical (hereafter, $W48^{+\bullet}$) and the Fe_2(III/IV) cluster **X** (*1-3*). The $W48^{+\bullet}$ may then be reduced by a facile one-electron reductant (e.g. ascorbate, Fe(II)aq, thiols, etc). Under these conditions, the last step in the reaction is the slow oxidation of Y122 by **X** to produce Y122• and the product μ-oxodiiron(III) cluster ($k \sim 0.7\ s^{-1}$ at 5 °C).

In the previous chapter, the pathways for decay of $W48^{+\bullet}$ in the absence of a facile reductant were dissected. It was observed that the presence of Mg^{2+} at concentrations similar to that used in RNR assays (15 mM) brings Y356, which is located at the surface of R2 on the flexible C-terminus, into electronic communication with the $W48^{+\bullet}$, establishing an equilibrium (that may be rapid with respect to O_2 addition and formation of the **X**-$W48^{+\bullet}$ state) between W48 and Y356 radicals. Propagation of the radical from the near-surface W48 to the (presumptively) surface Y356 (which is not observed in the crystal structures of R2 proteins, because this C-terminal fragment is disordered in crystals) (*4*) makes available a more efficient pathway for decay of the $W48^{+\bullet}$, although the source of the reducing equivalent in this pathway is still not clear. Thus, manifestations of the Mg^{2+}-dependent W48-Y356 radical equilibrium are: (1) the

presence of a fast phase of Y• (Y356•) formation, which is nearly coincident with formation of $W48^{+\bullet}$, in the wild-type (wt) protein but not the Y356F variant and in the presence of Mg^{2+} but not in its absence; (2) an acceleration by Mg^{2+} of decay of the $W48^{+\bullet}$ (followed by its 560-nm absorption) in the wild-type protein but not (or much less so) in the Y356F variant, in a manner that "saturates" at high Mg^{2+}; (3) a slowing of subsequent stable Y122• formation by Mg^{2+} in the wild-type protein but not the Y356 variant as a direct consequence of the faster decay of the $W48^{+\bullet}$, which, if allowed to persist, can itself oxidize Y122 with a rate constant (7 s^{-1} at 11 °C) greater than that for the generation of Y122• by **X** that occurs when decay of the $W48^{+\bullet}$ is accelerated by Mg^{2+}.

On the basis of these observations and the facts that (1) Mg^{2+} has always been included in assays of RNR and (2) the determinants for binding of R1 by R2 are present exclusively in the C-terminus of R2, we posited that Mg^{2+} acts as part of the “switch” that gates electron transfer into R2 by binding to the carboxylate-rich C-terminus of R2, bringing Y356 into proximity with W48, and inducing in this region of R2, which is known to provide essentially all of the driving force for binding to R1, the proper conformation for subunit binding and subsequent intersubunit electron transfer. We further speculated that the rather high Mg^{2+} concentration needed for 50% of maximal enhancement of $W48^{+\bullet}$ decay ($K_{0.5}$ ~ 25 mM), which *could* represent the K_D for a R2•Mg^{2+} complex, in the reaction of R2-wt, will be reduced by synergy between Mg^{2+} and R1 binding to R2. We envisaged that Mg^{2+} might bind to residues on the C-terminus and perhaps near W48 to exert the proposed conformational effect. In this chapter, we have tested for the binding of Mg^{2+} to potential ligands by examining the behavior of

variant proteins substituted at these carboxylate residues in terms of the kinetics of $W48^{+\bullet}$ formation and decay and Y122• formation in their O_2 activation reactions. We anticipated that the variant protein(s) with the ligand(s) substituted with residue(s) deficient in binding Mg^{2+} would show either a decreased efficiency in the Y356-mediated pathway for $W48^{+\bullet}$ decay or an increase in the metal ion concentration needed to activate this pathway. No drastic changes in the values of $K_{0.5}$ or the maximum observed first-order rate constant ($k_{obs\ max}$) for decay of $W48^{+\bullet}$ at saturating Mg^{2+} concentrations were detected in any of these variants. Interpretation of these results is presented below.

MATERIALS AND METHODS

Materials. Culture media components (yeast extract and tryptone) were purchased from Marcor Development Corporation (Hackensack, NJ). Isopropy-β-D-thiogalactopyranoside (IPTG) was purchased from Biosynth International (Naperville, IL). Ampicillin was purchased from IBI (Shelton, CT). Phenylmethylsulfonyl fluoride (PMSF), streptomycin sulfate, *tris*-[hydroxymethyl]-aminomethane (Tris), 1,10-phenanthroline, and (N-[2-hydroxyethyl]piperazine-N'-[3-propane-sulfonic acid] (EPPS) were purchased from Sigma (St. Louis, MO). Glycerol, ammonium sulfate, and sodium chloride were purchased from EM Science (Gibbstown, NJ). Magnesium chloride was purchased from J. T. Baker Chemical Co. (Phillipsburg, N.J.). Oligonucleotide primers were purchased from Invitrogen (Frederick, MD). Reagents for the polymerase chain reaction (PCR) and restriction enzymes were purchased from New England Biolabs (Beverly, MA). T4 DNA ligase was purchased from Roche (Indianapolis, IN). BL21(DE3) and pET vectors were purchased from Novagen (Madison, WI).

Preparation of Expression Vectors for the R2-Carboxylate Variants. All the substitutions discussed below were introduced into the *nrdB* gene (encoding R2) by using PCR. For each of the D54N, D54A, E350Q, E350A, D362N and D362Q substitutions, the gene was amplified into two fragments by using four primers and the previously described vector pR2-wt-*Hind*III (*5*) as template. Table 5-1 summarizes the primers used in the above PCR reactions, the restriction enzyme sites introduced by these primers and the amplified base pairs (bp) of the pR2-wt-*Hind*III. In addition to introduction of the desired substitutions at the appropriate codons, these primers introduce silent unique restriction sites (Table 5-1) for internal ligation of the two amplified fragments (the 5' PCR fragment and 3' PCR fragment). Each 5' PCR fragment was digested with two restriction enzymes: the first restriction enzyme cleaves a specific DNA sequence upstream the *nrdB* gene (5' R. E.) while the second restriction enzyme cleaves at the unique restriction site introduced by the primers (Table 5-1). The 3' PCR fragment was also digested with two restriction enzymes: the first restriction enzyme cleaves a specific DNA sequence downstream the *nrdB* gene (3' R.E.) and the second enzyme cleaves the unique restriction site (Table 5-1). The vector pR2wt-*Hind*III was digested with 5' R. E. and 3' R. E. The fragments (the digested-PCR fragments and the large fragment from digestion of pR2wt-*Hind*III) were then joined in a three-piece ligation reaction to give the desired expression vectors. The sequence of the coding region of each plasmid construct was verified to ensure that no undesired mutations had been introduced. DNA sequences were determined by ACGT, Inc. (Wheeling, IL.)

Also each of the E51Q, E51A and E52Q substitutions were introduced into the *nrdB* gene by using PCR and the previously described vector pR2-wt-*Hind*III as PCR

Table 5-1: Summary of primers, amplified fragments and restriction enzyme sites in the site-directed mutagenesis experiments described in the text.

pET-R2	Primers	Codons Amplified	Length (bp)	Restriction Sites
E51A	ggccacgatgcgtccgacgtagaggatcg gtcgcgggagacgtcaacttctgccggacgc	0-58	316	*Bgl*II *Aat*II
E51Q	ggccacgatgcgtccgacgtagaggatcg gtcgcgggagacgtcaacttcttgcggacgc	0-58	316	*Bgl*II *Aat*II
E52Q	ggccacgatgcgtccgacgtagaggatcg tatacggtcgcgggagacgtcaacttgttccggacgc	0-60	323	*Bgl*II *Aat*II
D54A	ggccacgatgcgtccgacgtagaggatcg atacggtcccgggagacggcaacttcttccg	0-59.2	321	*Bgl*II *Sma*I
	gaagaagttgccgtctcccgggaccgtatagattacc ggaacaagcaaagcttacgtagaaacgaatcgc	50.2-215	497	*Sma*I *Hind*III
D54N	ggccacgatgcgtccgacgtagaggatcg atacggtcccgggagacgttaacttcttccg	0-59.2	321	*Bgl*II *Sma*I
	gaagaagttaacgtctcccgggaccgtatagattacc ggaacaagcaaagcttacgtagaaacgaatcgc	50.2-215	497	*Sma*I *Hind*III
E350A	cgtttctacgtaagctttgcttgttcc gaccagataagagctcacttccactgcctgcggagc	207-358	460	*Hind*III *Sac*I
	ccgcaggcagtggaagtgagctcttatctggtcg gttgccattgctgcaggcatcgtggtgtcacgc	348-375	1429	*Sac*I PstI
E350Q	cgtttctacgtaagctttgcttgttcc ccgaccagataagagctcacttccacctgctggg	207-358.2	460	*Hind*III *Sac*I
	ccgcagcaggtggaagtgagctcttatctggtcgg gttgccattgctgcaggcatcgtggtgtcacgc	348-375	1429	*Sac*I PstI
D362A	cgtttctacgtaagctttgcttgttcc gtcggtgtcgacttccgaggcaatctgccc	207-368	488	*Hind*III *Sal*I
	cagattgcctcggaagtcgacaccgacgatttgagt gttgccattgctgcaggcatcgtggtgtcacgc	360-375	1393	*Sal*I PstI
D362N	cgtttctacgtaagctttgcttgttcc gtcggtgtcgacttccgaattaatctgccc	207-368	488	*Hind*III *Sal*I
	cagattaattcggaagtcgacaccgacgatttgagt gttgccattgctgcaggcatcgtggtgtcacgc	360-375	1393	*Sal*I PstI

template. For each of these variants, two primers were used to amplify a ~ 320 bp fragment (316 bp for E51Q and E51A; 323 bp for E52Q) of these plasmids (Table 5-1). The sense primer anneals ~ 110 bp 5' of a unique *Bgl*II site, which is 105 bp 5' of the start of *nrdB* in pR2-E51Q, pR2-E51A and pR2-E52Q. The anti-sense primer introduces the desired substitutions at each corresponding codon and also spans the unique *Aat*II restriction site in codon V55 of *nrdB*. The PCR fragments were digested with *Bgl*II and *Aat*II and ligated with the large fragment generated by digestion of pR2-wt-*Hind*III with the same enzymes. The sequence of the coding region of each plasmid construct was verified to ensure that no undesired mutations had been introduced. DNA sequences were determined by the Nucleic Acid Facility of the Pennsylvania State University Biotechnology Institute.

Over-expression vectors for R2-E51A/E350A and R2-E51A/D362N were prepared from pR2-E51A and pR2-E350A, in the case of pR2-E51A/E350A, and pR2-E51A and pR2-D362NA, in the case of pR2-E51A/D362N. The 747 *Bgl*II-*Hind*III restriction fragment of pR2-E51A was ligated with the large (vector) fragment from digestion of pR2-E350A or pR2-D362N with the same restriction enzymes to yield pR2-E51A/E350A or pR2-E51A/D362N, respectively. The sequence of the coding region of each plasmid construct was verified to ensure that no undesired mutations had been introduced. DNA sequences were determined by ACGT, Inc. (Wheeling, IL.).

Over-expression and Purification of the R2-Carboxylate Variants. Procedures used to over-express and purify the proteins in the apo forms have been described elsewhere (*6*). Protein concentrations were determined spectrophotometrically by using

molar absorption coefficients at 280 nm (ε_{280}) calculated according to the method of Gill and von Hippel (*7*). The ε_{280} value is 120 mM^{-1} cm^{-1} for all the R2-carboxylate variants.

Stopped-Flow Absorption Spectrophotometry. Stopped-flow measurements were carried out as previously described in Chapter 4. All stopped-flow experiments were carried out with an Applied Photophysics SX.18MV stopped-flow apparatus (path length of 1 cm and dead-time of 1.3 ms) equipped with a diode array detector and housed in an anoxic chamber (MBraun). The reactive Fe(II)-R2 protein complexes were prepared as reported in Chapter 4. Specific reaction conditions are given in the appropriate figure legends.

RESULTS

Alignment of the sequence of *E. coli* R2 with those of eleven other class I RNRs (Figure 5-1) and the crystal structure of *E. coli* R2 (Figure 5-2) suggest the conserved residues discussed below as good candidates for ligands to Mg^{2+}: E51, E52, and D54 are positioned at the surface of R2 and are in close proximity to W48 (distance of 4.5-10 Å) (Figure 5-2), E350 and D362 are positioned on the C-terminus of R2, which is not visible in the crystal structure of *E. coli* R2. E52, D54, and E350 are all strictly conserved among the class I R2s (Figure 5-1). We thus prepared variant proteins in which these carboxylate residues are substituted, either singly or in combination, with their neutral carboxamide counterpart or Ala. DNA plasmid constructs encoding a total of 11 variants were prepared (Table 5-2), and over-expression and purification of these variants were attempted. All variants were expressed in high yield and were stable to the purification

FIGURE 5-1: Sequence alignment of selected residues of *E. coli* R2 with R2s from 10 other class I ribonucleotide reductases. E51, E52, D54, E350, and Y356 are conserved among these sequences.

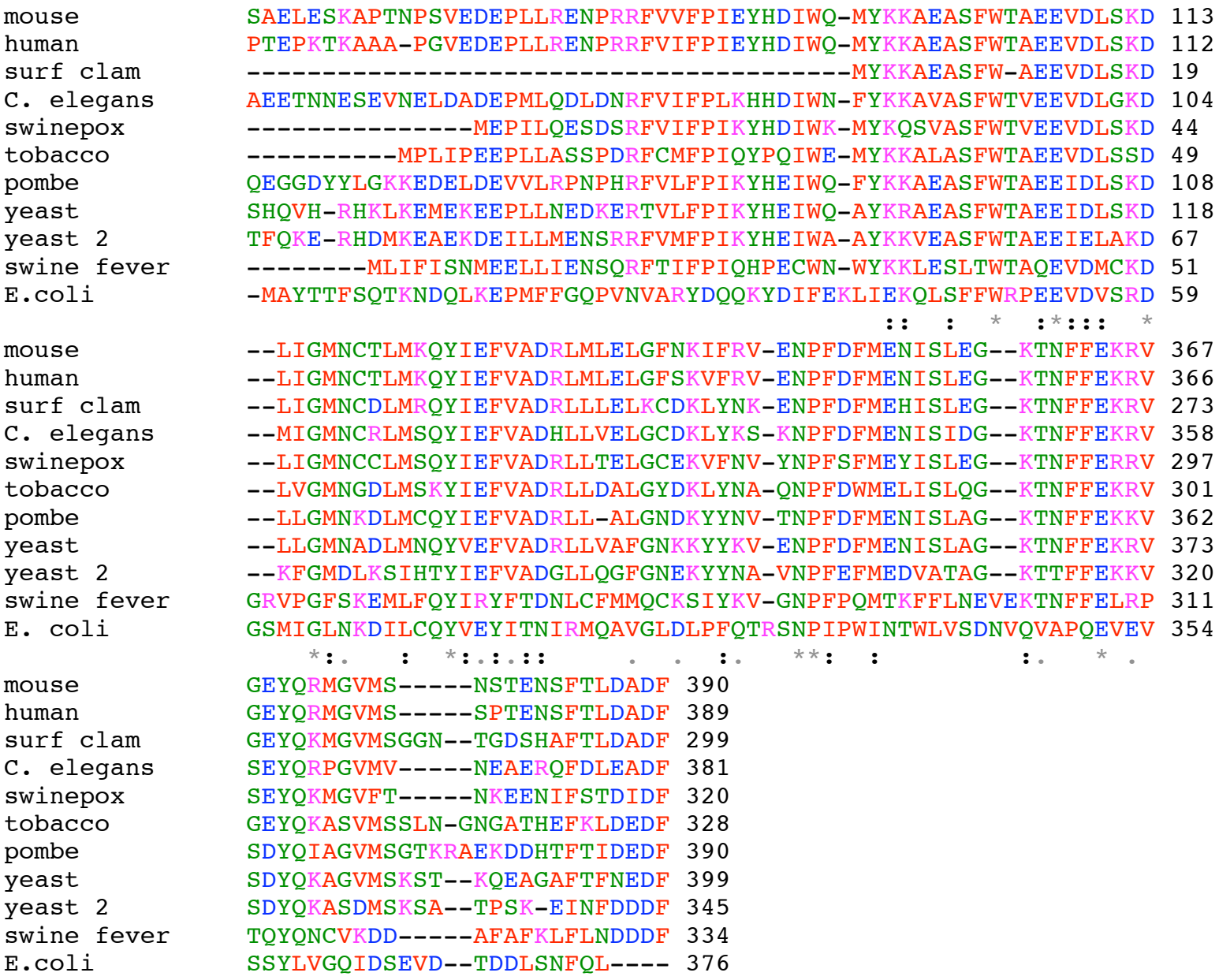
mouse SAELESKAPTNPSVEDEPLLRENPRRFVVFPIEYHDIWQ-MYKKAEASFWTAEEVDLSKD 113
human PTEPKTKAAA-PGVEDEPLLRENPRRFVIFPIEYHDIWQ-MYKKAEASFWTAEEVDLSKD 112
surf clam ----------MYKKAEASFW-AEEVDLSKD 19
C. elegans AEETNNESEVNELDADEPMLQDLDNRFVIFPLKHHDIWN-FYKKAVASFWTVEEVDLGKD 104
swinepox ----------MEPILQESDSRFVIFPIKYHDIWK-MYKQSVASFWTVEEVDLSKD 44
tobacco ----------MPLIPEEPLLASSPDRFCMFPIQYPQIWE-MYKKALASFWTAEEVDLSSD 49
pombe QEGGDYYLGKKEDELDEVVLRPNPHRFVLFPIKYHEIWQ-FYKKAEASFWTAEEIDLSKD 108
yeast SHQVH-RHKLKEMEKEEPLLNEDKERTVLFPIKYHEIWQ-AYKRAEASFWTAEEIDLSKD 118
yeast 2 TFQKE-RHDMKEAEKDEILLMENSRRFVMFPIKYHEIWA-AYKKVEASFWTAEEIELAKD 67
swine fever --------MLIFISNMEELLIENSQRFTIFPIQHPECWN-WYKKLESLTWTAQEVDMCKD 51
E.coli -MAYTTFSQTKNDQLKEPMFFGQPVNVARYDQQKYDIFEKLIEKQLSFFWRPEEVDVSRD 59
mouse --LIGMNCTLMKQYIEFVADRLMLELGFNKIFRV-ENPFDFMENISLEG--KTNFFEKRV 367
human --LIGMNCTLMKQYIEFVADRLMLELGFSKVFRV-ENPFDFMENISLEG--KTNFFEKRV 366
surf clam --LIGMNCDLMRQYIEFVADRLLLELKCDKLYNK-ENPFDFMEHISLEG--KTNFFEKRV 273
C. elegans --MIGMNCRLMSQYIEFVADHLLVELGCDKLYKS-KNPFDFMENISIDG--KTNFFEKRV 358
swinepox --LIGMNCCLMSQYIEFVADRLLTELGCEKVFNV-YNPFSFMEYISLEG--KTNFFERRV 297
tobacco --LVGMNGDLMSKYIEFVADRLLDALGYDKLYNA-QNPFDWMELISLQG--KTNFFEKRV 301
pombe --LLGMNKDLMCQYIEFVADRLL-ALGNDKYYNV-TNPFDFMENISLAG--KTNFFEKKV 362
yeast --LLGMNADLMNQYVEFVADRLLVAFGNKKYYKV-ENPFDFMENISLAG--KTNFFEKRV 373
yeast 2 --KFGMDLKSIHTYIEFVADGLLQGFGNEKYYNA-VNPFEFMEDVATAG--KTTFFEKKV 320
swine fever GRVPGFSKEMLFQYIRYFTDNLCFMMQCKSIYKV-GNPFPQMTKFFLNEVEKTNFFELRP 311
E. coli GSMIGLNKDILCQYVEYITNIRMQAVGLDLPFQTRSNPIPWINTWLVSDNVQVAPQEVEV 354
mouse GEYQRMGVMS-----NSTENSFTLDADF 390
human GEYQRMGVMS-----SPTENSFTLDADF 389
surf clam GEYQKMGVMSGGN--TGDSHAFTLDADF 299
C. elegans SEYQRPGVMV-----NEAERQFDLEADF 381
swinepox SEYQKMGVFT-----NKEENIFSTDIDF 320
tobacco GEYQKASVMSSLN-GNGATHEFKLDEDF 328
pombe SDYQIAGVMSGTKRAEKDDHTFTIDEDF 390
yeast SDYQKAGVMSKST--KQEAGAFTFNEDF 399
yeast 2 SDYQKASDMSKSA--TPSK-EINFDDDF 345
swine fever TQYQNCVKDD-----AFAFKLFLNDDDF 334
E.coli SSYLVGQIDSEVD--TDDLSNFQL---- 376

Figure 5-2: Crystal structure of *E. coli* R2 shows that E51, E52 and D54 are located on the surface of R2 within a distance of 5-9 Å from W48. V340 is the last visible residue of the C-terminus. Distances that separate the carboxylate residues from W48 are shown in solid lines. Protein Data Bank accession number is 1XIK.

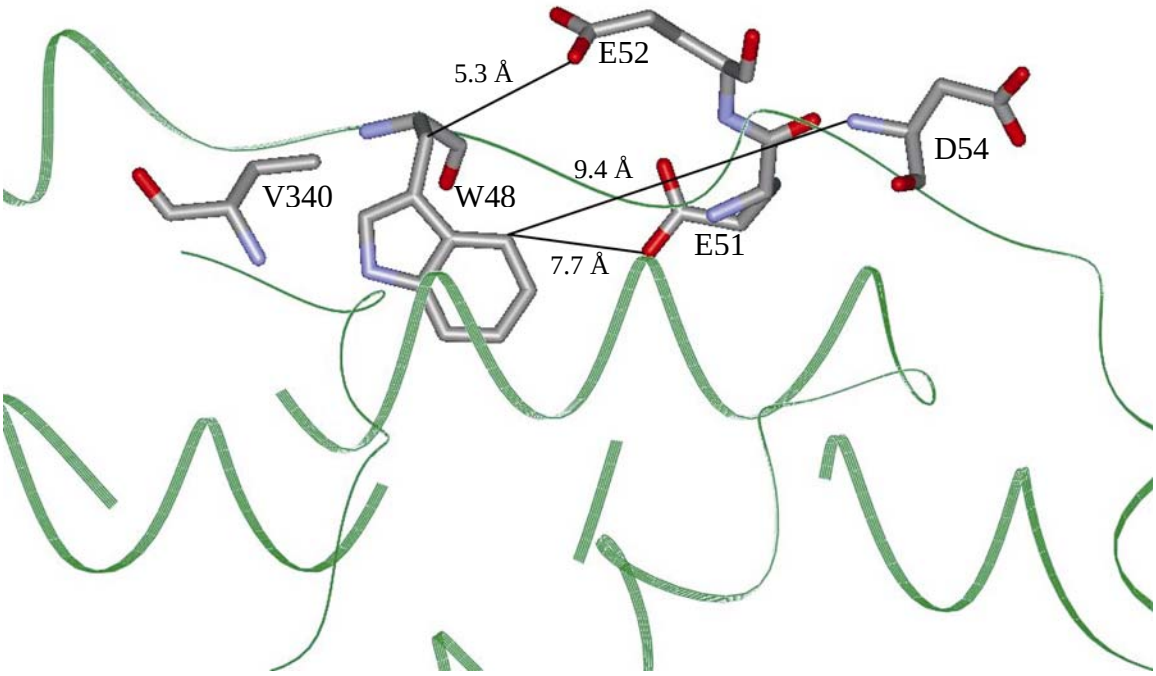
E52
5.3 Å
D54
9.4 Å
V340
W48
E51
7.7 Å

procedure. SDS-PAGE analysis of the purified proteins showed that all were > 90% pure.

Stopped-flow absorption analysis of the reactions at 11 °C of Fe(II)-R2-E51A(Q), Fe(II)-R2-E52Q, Fe(II)-R2-D54A(N), Fe(II)-R2-E350A(Q), Fe(II)-R2-D362A(N), Fe(II)-R2-E51A/E350A and Fe(II)-R2-E51A/D362N with O_2 in the presence of varying [Mg^{2+}] was carried out. All variant proteins rapidly activate O_2, generating the broad 560-nm feature characteristic of the $W48^{+\bullet}$ and the sharp 41l-nm peak of the Y122•. Analysis of the kinetic traces at 560 nm indicates that decay of the $W48^{+\bullet}$ is in all cases accelerated in a saturable fashion by Mg^{2+}, similar to what has been previously reported in Chapter 5 for the reactions of Fe(II)-R2-wt and Fe(II)-R2-Y122F with O_2 (Figures 4-1A and 4-5A). Also, the kinetic behavior of the 411-nm peak height ($A_{411} - (A_{405} + A_{417})/2$) in all the R2-carboxylate variants is nearly identical to that in R2-wt (Figure 4-1B). In the absence of Mg^{2+}, a lag phase that corresponds to the formation of $W48^{+\bullet}$-**X** is followed by two formation phases. In the presence of Mg^{2+}, the lag phase is replaced by a very rapid formation phase that is essentially coincident with $W48^{+\bullet}$ formation and for which the rate constant is dependent on [Mg^{2+}]. This rapid formation phase is followed by a slow formation phase.

Table 5-2 and Figure 5-3 summarize the [Mg^{2+}]-dependencies of the reactions of the variant proteins. As previously noted, $K_{0.5}$ *could* reflect K_D for the Mg^{2+}-R2 complex. The initial slope of plots of k_{obs}-versus-[Mg^{2+}] ($(k_{max}-k_{min})/K_{0.5}$) is used as a qualitative measure of the "efficiency" of the Mg^{2+}-dependent pathway, in the manner that k_{cat}/K_M is used as a measure of catalytic efficiency. We anticipated that variants with Mg^{2+} ligands substituted might display $K_{0.5}$ values higher than that observed for the R2-wt protein,

Table 5-2: Summary of the $K_{0.5}$ (concentration needed for 50% of maximal enhancement of $W48^{+\bullet}$ decay) and $k_{obs\ max}/K_{0.5}$ (the initial-slope) values from the plots of k_{obs}-*versus*-$[Mg^{2+}]$ obtained from the analysis of kinetic traces of $W48^{+\bullet}$ and Y•. The protein concentration varied between 90-150 μM with Fe(II)/R2 = 2.7. Experimental details are as described in Materials and Methods.

Protein	$K_{0.5}$ **(mM)**	$k_{obs\ max}/K_{0.5}$ **(s^{-1} mM^{-1})**
R2-wt	26 ± 3	3.7 ± 0.6
R2-Y122F	8 ± 1	4.3 ± 0.7
R2-E51A	15 ± 2	6 ± 1
R2-E51Q	9 ± 1	9 ± 1
R2-E52Q	7 ± 2	19 ± 6
R2-D54A	12 ± 2	9 ± 2
R2-D54N	10 ± 2	9 ± 2
R2-E350A	10 ± 2	11 ± 2
R2-E350Q	10 ± 3	6 ± 2
R2-D362A	28 ± 5	4.2 ± 0.9
R2-D362N	25 ± 9	3 ± 1
R2-E51A/E350A	6 ± 3	18 ± 6
R2-E51A/D362N	6 ± 3	13 ± 2

Figure 5-3: Representative traces of the titration effect of [Mg^{2+}] on the observed rate constants (k_{obs}) of decay of $W48^{+\bullet}$ in the reactions of R2-carboxylate variants: R2-D54A (blue filled squares), R2-E350A (black filled diamonds), R2-D362N (purple filled triangles), R2-E51A (deep pink open triangles), R2-E52Q (cyan open circles) and R2-E51A/D362N (green open squares). Also shown are the traces of the titration effect of [Mg^{2+}] on the k_{obs} of decay of $W48^{+\bullet}$ in the reactions of R2-wt (red filled circles) and R2-Y122F (orange open diamonds). A solution of O_2-free Fe(II) complex of R2 (0.09-0.15 mM; Fe(II)/R2 = 2.7) was mixed at 11 ˚C with an equal volume of O_2-saturated buffer containing different concentrations of $MgCl_2$ in a stopped-flow apparatus. The rate constants of decay of $W48^{+\bullet}$ were obtained from the fits of the kinetic traces of $W48^{+\bullet}$ (as described in Figure 5-4). The solid lines are fits of the equation for a hyperbola to the titration data obtained from the described reactions. The values at half-maximal enhancement of $W48^{+\bullet}$ decay ($K_{0.5}$) are summarized in Table 5-3.

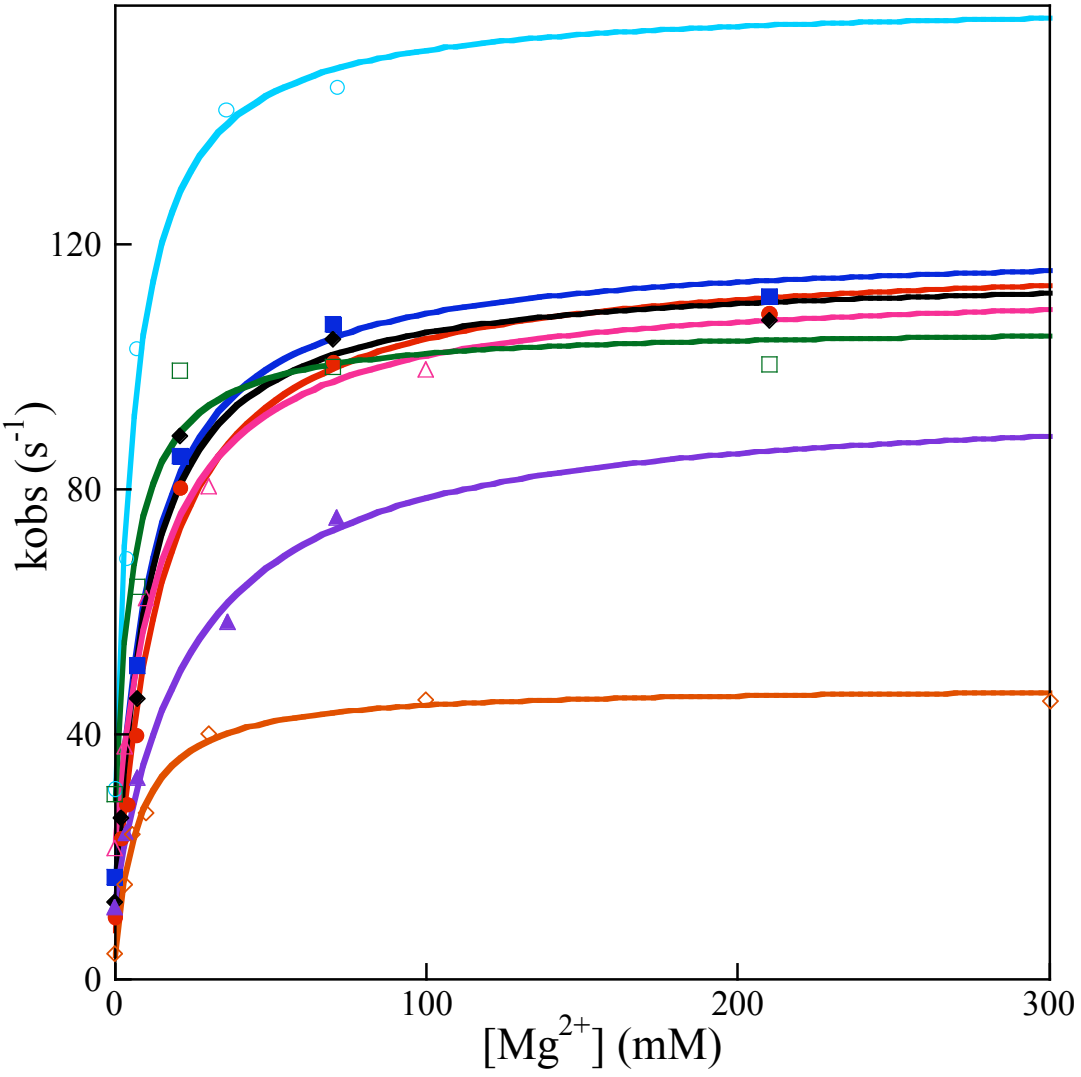
kobs (s-1)
120
80
40
0
0
100
200
300
[Mg2+] (mM)

indicative of weakened interactions between the protein and Mg^{2+}. By contrast, all the $K_{0.5}$ values obtained were either similar to of less than the value for R2-wt. Furthermore, higher values of $(k_{max}-k_{min})/K_{0.5}$ were observed for most of the variants. Thus, the data do not support identification of the Mg^{2+} ligands, if indeed a specific binding event is involved in mediating the observed communication between W48 and Y356.

In addition to the anticipated primary effects on Mg^{2+} affinity and efficiency of the Mg^{2+}-dependent pathway for $W48^{+\bullet}$ decay, we considered that the carboxylate substitutions might alter the reduction potential of the $W48^{+\bullet}$, the Y356•, or both, thus perturbing the equilibrium between the two radicals. In fact, the elevated values of $(k_{max}-k_{min})/K_{0.5}$ for some of the variants might suggest that this equilibrium is indeed biased to favor Y356• to a greater extent. Of particular interest are the behaviors of the single variant R2-E52Q and the double variants R2-E51A/E350A and R2-E51A/D362N (Figure 5-4), which exhibit depressed $K_{0.5}$ values and elevated $(k_{max}-k_{min})/K_{0.5}$ values as compared to R2-wt (Table 5-2). The effect on $K_{0.5}$ values and $(k_{max}-k_{min})/K_{0.5}$ values observed upon substitution of D/E with A does not seem to be that different from that associated with substitution of D/E with N/Q as shown in Table 5-2.

DISCUSSION

We posited that the coordination of Mg^{2+} to ligands positioned on the C-terminus and the surface of R2 would result in the ordering of Y356, bringing it into closer proximity to the W48 residue and thereby allowing for facile electron transfer between the two redox-active residues. Analysis of the time-courses of formation and decay of $W48^{+\bullet}$ and Y•, monitored at 560 nm and 411 nm respectively, in the reactions of the R2-

Figure 5-4: Effect of increasing [$MgCl_2$] on the formation and decay rates of the transient $W48^{+\bullet}$ monitored at 560 nm (filled symbols) and the 411-nm peak height (A_{411} - (A_{405} + A_{417})/2) (open symbols) in the reactions of Fe(II)-R2-E52Q and Fe(II)-R2-E51A/D362N with O_2 as monitored by stopped-flow absorption spectrophotometry. A solution of O_2-free Fe(II)-R2-E52Q(E51A/D362N) in 25mM EPPS, pH 8.2 buffer (buffer A) was mixed at 11 ˚C with an equal volume of O_2-saturated buffer A containing different concentrations of $MgCl_2$. The final concentrations of $MgCl_2$ after mixing were 0 mM (R2-E52Q, red traces; R2-E51A/D362N, green traces), 70 mM (R2-E51A/D362N, blue traces trace) and 71 mM (R2-E52Q, black traces). The final concentration of the proteins after mixing were 0.14 mM and 0.1 mM for Fe(II)-R2-E52Q and Fe(II)-R2-E51A/D362N, respectively. The ratio of Fe(II) to R2 is 2.7 in both protein samples.

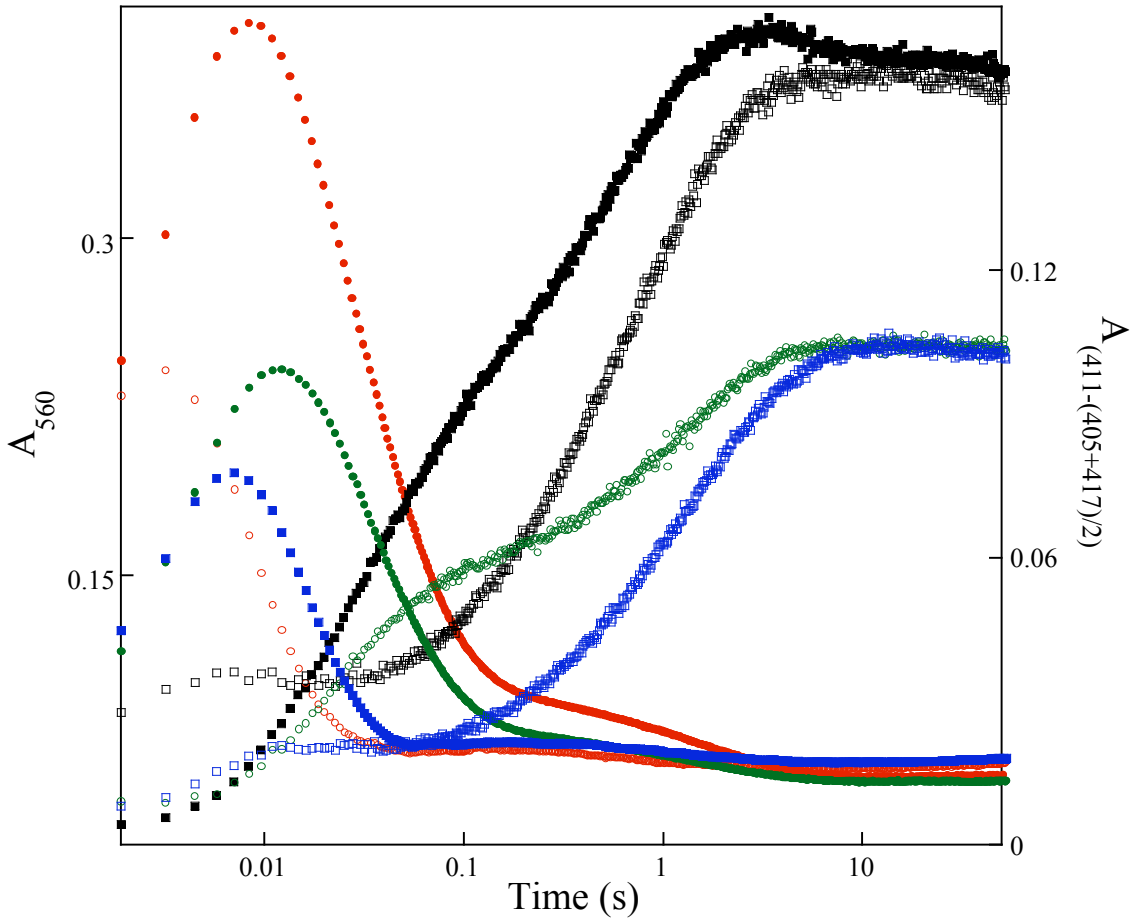
0.3
0.15
A_{560}
0.12
0.06
0
$A_{(411-(405+417)/2)}$
0.01
0.1
1
10
Time (s)

carboxylate variants with O_2 did not yield results indicative of weakened binding of Mg^{2+} to the protein (elevated $K_{0.5}$) or interrupted communication between $W48^{+\bullet}$ and Y356• (depressed $(k_{max}-k_{min})/K_{0.5}$). Preliminary kinetic simulations of the reactions of Fe(II)-R2-wt and Fe(II)-R2-Y122F with O_2 in the presence of different concentrations of Mg^{2+} suggest that the decay pathways for $W48^{+\bullet}$ are somewhat more complex than those presented in Chapter 4 (Scheme 4-1) and reveal that Mg^{2+} binding may not be rapid. The relatively slow Mg^{2+} binding would imply that the $K_{0.5}$ values from the $[Mg^{2+}]$ dependencies (26 mM for R2-wt and 8 mM for R2-Y122F) do not reflect the K_D for the R2-Mg^{2+} complex. Actually, K_D could be much less than $K_{0.5}$. Furthermore, Y356 itself may coordinate Mg^{2+}, altering the pK_a and oxidation potential of this tyrosine. Therefore, the results presented above do not rule out the proposed mechanism for Mg^{2+} mediation of W48-Y356 communication nor the postulated role for one or more of the conserved carboxylate residues in coordination of Mg^{2+}. In fact, (1) the compelling evidence for formation of a Y356• and the potentially physiologically-relevant conditions ($[Mg^{2+} \sim$ 10-25 mM) under which it can exist in a radical-transfer equilibrium with the $W48^{+\bullet}$, (2) the unknown function(s) of the strictly evolutionary conserved-carboxylate residues, (3) the dependence of the catalytic activity of RNR on Mg^{2+} (thought to keep R1 in its proper homodimeric state) and (4) the fact that R2-E350A exhibits tight binding to R1 but very low catalytic activity (*8*) compel us to pursue other approaches to test for the hypothesized conformational effect of Mg^2 on the C-terminus of R2 and the putative role of this metal ion in redox mediation at the R1-R2 interface. Collaborative efforts with the Rosenzweig group at Northwestern University are in progress to obtain a crystal structure of R2 with Mg^{2+} bound to it. Further examination of the effect of Mg^{2+} on the dynamics

of the C-terminus is currently being pursued by site-directed spin labeling (SDSL) of the C-terminus (cysteine substitutions of residues close to Y356) and the surface of R2 (cysteine substitutions of residues close to W48), a technique that uses electron paramagnetic resonance (EPR) to measure the spin-label rotational mobility and accessibility, which are direct reflections of the local structure and dynamics of the protein. Last but not least, the catalytic activities of these variants and the concentrations of Mg^{2+} needed to stimulate these activities are to be investigated.

REFERENCES

1. Bollinger, J. M., Jr., Tong, W. H., Ravi, N., Huynh, B. H., Edmondson, D. E., and Stubbe, J. (1994) Mechanism of assembly of the tyrosyl radical-diiron(III) cofactor of *E. coli* ribonucleotide reductase. 3. Kinetics of the limiting Fe^{2+} reaction of optical, EPR, and Mössbauer spectroscopies, *J. Am. Chem. Soc. 116*, 8024-8032.
2. Baldwin, J., Krebs, C., Ley, B. A., Edmondson, D. E., Huynh, B. H., and Bollinger, J. M., Jr. (2000) Mechanism of rapid electron transfer during oxygen activation in the R2 subunit of *Escherichia coli* ribonucleotide reductase. 1. Evidence for a transient tryptophan radical, *J. Am. Chem. Soc. 122*, 12195-12206.
3. Krebs, C., Chen, S., Baldwin, J., Ley, B. A., Patel, U., Edmondson, D. E., Huynh, B. H., and Bollinger, J. M., Jr. (2000) Mechanism of rapid electron transfer during oxygen activation in the R2 subunit of *Escherichia coli* ribonucleotide reductase. 2. Evidence for and consequences of blocked electron transfer in the W48F variant, *J. Am. Chem. Soc. 122*, 12207-12219.

4. Nordlund, P., and Eklund, H. (1993) Structure and function of the *Escherichia coli* ribonucleotide reductase, *J. Mol. Biol. 232*, 123-164.

5. Moënne-Loccoz, P., Baldwin, J., Ley, B. A., Loehr, T. M., and Bollinger, J. M., Jr. (1998) O_2 activation by non-heme diiron proteins: identification of a symmetric μ-1,2-peroxide in a mutant of ribonucleotide reductase, *Biochemistry 37*, 14659-14663.

6. Parkin, S. E., Chen, S., Ley, B. A., Mangravite, L., Edmondson, D. E., Huynh, B. H., and Bollinger, J. M., Jr. (1998) Electron injection through a specific pathway determines the outcome of oxygen activation at the diiron cluster in the F208Y mutant of *Escherichia coli* ribonucleotide reductase protein R2, *Biochemistry 37*, 1124-1130.

7. Gill, S. C., and von Hippel, P. H. (1989) Calculation of protein extinction coefficients from amino acid sequence data, *Anal. Biochem. 182*, 319-326.

8. Climent, I., Sjöberg, B.-M., and Huang, C. Y. (1992) Site-directed mutagenesis and deletion of the carboxyl terminus of *Escherichia coli* ribonucleotide reductase protein R2. Effects on catalytic activity and subunit interaction, *Biochemistry 31*, 4801-4807.

Chapter 6

Preliminary Evidence for a Remodeled Pathway for Electron Transfer to the Diiron Center During Oxygen Activation in the Newly Recognized Class Ic Ribonucleotide Reductase Protein R2 from *Chlamydia trachomatis*

"Reproduced with permission from Saleh, L., Jiang, W., Yun, D., Krebs, C. and Bollinger, J. M, Jr. Preliminary Evidence for a Remodeled Pathway for Electron Transfer to the Diiron Center During Oxygen Activation in the Newly Recognized Class Ic Ribonucleotide Reductase Protein R2 from *Chlamydia trachomatis*, manuscript in preparation"

Footnotes

[1]Abbreviations: RNR, ribonucleotide reductase; Y122•, tyrosyl radical in *E. coli* R2; MMOH, the hydroxylase subunit of methane monooxygenase; $R2_{Ct}$, *C. trachomatis* R2; $\mathbf{X}_{\mathbf{Ct}}$, **X**-like complex in *C. trachomatis* R2; IPTG, Isopropyl-β-D-thiogalactopyranoside; PMSF, phenylmethylsulfonyl fluoride; Tris, *tris*-(hydroxymethyl)-aminomethane; ferrozine, 3-(2-pyridyl)-5,6-*bis*-(4-phenyl-sulfonic acid)-1,2,4-triazine; HEPES, 4-(2-hydroxyethyl)-1-piperazineethanesulfonic acid; PCR, polymerase chain reaction; bp, basepair; wt, wildtype; $(His)_6$-$R2_{Ct}$, $(His)_6$-tagged-$R2_{Ct}$; buffer A, 50 mM TRIS-HCl (pH 7.6) and 10% (v/v) glycerol; SDS-PAGE, sodium dodecyl sulfate polyacrylamide gel electrophoresis; buffer B, 100 mM HEPES (pH 7.6); ε_{280}, molar absorptivity at 280 nm; k_{obs}, observed apparent first-order rate constant; EPR, electron paramagnetic resonance; $[A_{411} - (A_{405} + A_{417})/2]$, 411-nm peak height; $W48^{+\bullet}$, tryptophan 48 cation radical; $A_{max} - A_{completion}$, difference between maximum and minimum absorbances in stopped-flow experiments.

ABSTRACT

Protein R2 of ribonucleotide reducatse (RNR) from *Escherichia coli*, the prototype of class I RNRs, contains a dinuclear iron cluster, which reductively activates O_2 to produce the enzyme's functionally essential tyrosyl radical (Y122•) by one-electron oxidation of residue Y122. A key step of this reaction is the transient one-electron oxidation of tryptophan 48 to a cation radical ($W48^{+\bullet}$) during formation of the Y122•-generating intermediate, cluster **X**, from the diiron(II) cluster and O_2. Reduction of the $W48^{+\bullet}$ by an exogenous reductant completes the shuttling of an electron to the diiron center, permitting an odd-electron oxidation reaction (Y122• formation) from even-electron reactants (2 Fe(II) and O_2). Our studies presented in Chapter 4 demonstrated the cation-mediated propagation of this radical onto the C-terminal tyrosine, Y356, that is thought to be a key element of the R2->R1 radical-transfer pathway. In this study, we present evidence for the evolution of an *alternative* electron injection pathway in the R2 subunit of the newly discovered **class Ic** RNR from the human pathogen *Chlamydia trachomatis* ($R2_{Ct}$). $R2_{Ct}$ and other class Ic R2 proteins have phenylalanine (F) residues in place of the otherwise-conserved radical tyrosine (e.g., Y122) of the standard (class Ia and b) R2 proteins and thus do not form stable Y radicals. It has been shown that O_2 activation by $R2_{Ct}$ proceeds through an intermediate similar to cluster **X** in the reactions of *E. coli* and mouse R2, and it has been proposed that this diiron intermediate ($\mathbf{X}_{Ct}$) directly generates the R1 cysteine radical that initiates nucleotide reduction by abstraction of the 3' hydrogen atom. Here we show that formation of $\mathbf{X_{Ct}}$ is accompanied by production of a transient tyrosyl radical. The formation of the $\mathbf{X_{Ct}}$–Y• di-radical intermediate is supported by optical absorption, EPR, and Mössbauer spectroscopic evidence.

Substitution of Y338 residue, the cognate of Y356 in *E. coli* R2, with F results in an increase in the absorption of the Y• and a decrease in the rate of its decay. Excess Fe(II) efficiently reduces the Y• in $R2_{Ct}$-wt, with one extra equivalent almost completely suppressing its accumulation. This reduction is less efficient in the reaction of $R2_{Ct}$-Y338F, suggesting that Y338 mediates reduction of the Y• by Fe(II). No spectral evidence for the formation of $W51^{+\bullet}$, cognate of $W48^{+\bullet}$ in the *E. coli* R2 reaction, was detected. Our observations suggest that a tyrosine residue, and *not* W51, acts as electron shuttle to the diiron cluster of $R2_{Ct}$, forming a transient Y•, which communicates with Y338.

Ribonucleotide reductases (RNRs[1]) provide 2'-deoxynucleotides for DNA replication, and thus are essential to all organisms (although certain parasitic microbes rely on their hosts' RNRs) (*1-4*). This remarkable stereo- and regio-specific, reductive C-O cleavage is initiated by abstraction of the 3'-H of the substrate by a protein radical (*5-8*). Despite the central metabolic importance of the reaction and conserved catalytic strategy (protein-radical-mediated 3'-H abstraction), RNRs exhibit remarkable structural and functional diversity. Known RNRs have been divided into three classes (I-III), primarily on the basis of their distinct strategies for generating the 3'-H-abstracting protein radical, which is thought to be a cysteine thiyl radical for every RNR, irrespective of its class (*5, 9-12*). For class II and class III RNRs, which will not be discussed further, the 5'-deoxyadenosyl radical, generated either from 5'-deoxyadenosylcob(II)alamin (class II) or from S-adenosyl-L-methionine (class III), is the ultimate source of the oxidizing equivalent needed to produce the cysteine radical. Eukaryotes from *Saccharomyces cerevisiae* to *Homo sapiens* and many aerobic prokaryotes, including *Escherichia coli* and *Salmonella typhimurium*, employ class I RNRs. A class I RNR has two subunits, R1 and R2, which are both required for catalytic activity (*12*). R1 is the enzyme subunit, containing the binding sites for substrates and allosteric effectors, the 3'-H-abstracting cysteine, and additional cysteine residues that deliver reducing equivalents to the substrate. R2 is the cofactor subunit, functioning only to generate the cysteine radical in R1. The class I RNRs from *E. coli*, *S. cerevisiae*, *M. musculus*, and *H. sapiens* (which have been called class Ia) use a carboxylate-bridged diiron(II) cluster in R2 to activate O_2 for the univalent oxidation of an internal tyrosine residue (Y122 in the best-studied R2 from *E. coli*). The tyrosyl radical produced in this reaction (hereafter denoted Y122•) is

remarkably stable (half-life of many hours at room temperature), even in the presence of compounds that are thermodynamically competent to reduce it (e.g., thiols, ascorbate). It is protected from reduction in the isolated R2 subunit, in part by its containment in a hydrophobic pocket but, in the R1•R2 (holoenzyme) complex, accepts an electron originating from the R1 catalytic cysteine (C439) to generate the thiyl radical. It is thought that, in the R1•R2 complex, a pathway is opened, allowing the "hole" on the tyrosine to be propagated to the cysteine in R1 and initiating the catalytic reaction (*12-14*). This radical transfer may require that substrate and allosteric activator be bound to R1. Indirect evidence suggests that transfer of the radical to the cysteine in R1 (which is expected to be a remarkable 35 Å from the Y122• in *E. coli* RNR (*9*)) is mediated by a network of hydrogen-bonded residues between the two sites (Figure 6-1) (*9, 14, 15*), but direct observation of the radical-transfer step and interrogation of its mechanism have been thwarted by unfavorable kinetics in the RNR reactions that have been studied to date (*13*).

Recent analyses of genome sequences of several pathogenic eubacteria, including species in the genera *Chlamydia* and *Mycobacteria*, have revealed the existence of class I RNRs with unique characteristics. These RNRs have been designated by Nordlund and co-workers as **class Ic** (*16, 17*). Class Ic R2 proteins lack the conserved tyrosine that forms the radical in class Ia and Ib RNRs. Whereas some of the genomes in which class Ic RNRs are encoded also contain genes for other RNR proteins (in the case of *M. tuberculosis*, two standard R2 subunits, a class II RNR, and a class III RNR), precluding the presumption that the unique R2 proteins are functional, a subset of them (e.g., the *Chlamydia* species) have no other recognizable RNR. Indeed, RNR activity of the class

Figure 6-1: Proposed electron transfer pathway in class I RNR from *E. coli* ((Tyr122-Asp84-His118-Asp237-Trp48-Tyr356) in R2 and (Tyr731-Tyr730-Cys439) in R1) based on the enzyme-docking model (reference 15). The last 35 amino acids of the C-terminal tail of R2, in which Y356 resides, are thermally labile and undetectable in available crystal structures. Thus, the distance between W48 on R2 and Y731 in R1 (25Å) is based solely on the docking model of a 1:1 complex of R1 and R2. The Protein Data Bank accession numbers of the crystal structures used in this model are 4R1R for R1 and 1MXR for R2. Adapted from reference 13.

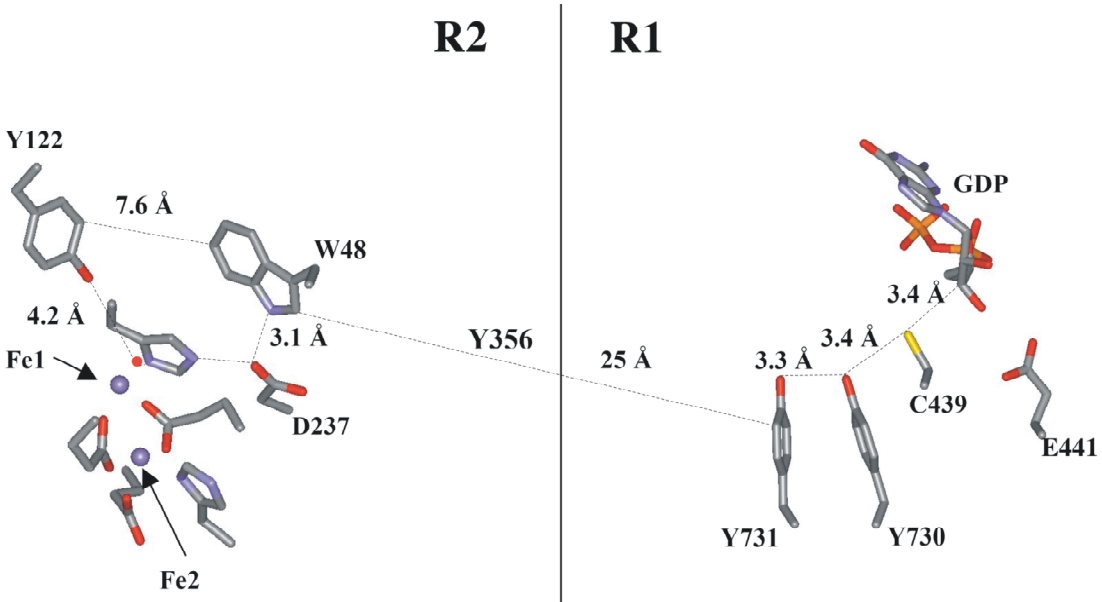
R2
R1
Y122
7.6 Å
W48
4.2 Å
3.1 Å
Fe1
D237
Fe2
Y356
25 Å
GDP
3.4 Å
3.4 Å
3.3 Å
C439
E441
Y731
Y730

Ic R2 subunit from *Chlamydia trachomatis* ($R2_{Ct}$) (in the presence of R1) has recently been demonstrated (*17*). In addition, evidence suggests that *C. trachomatis* is unable to take up deoxynucleotides from its host (*18, 19*), implying that the class Ic RNR is essential. The structure of the class Ic R2 protein, solved by the Nordlund group and reported last year in *Science* (*16*), reveals the presence of a phenylalanine (F) residue at the location of the Y• in class Ia and Ib R2 proteins. Most of the other residues known to be important for R2 function, including the iron ligands and those thought to participate in the long-range radical transfer pathway, are conserved. One notable difference is that the most N-terminal iron ligand, which is usually an aspartate (D84 in *E. coli*), is conservatively substituted with a glutamic acid (E89), the residue found at the cognate position of the structurally similar hydroxylase component of methane monooxygenase (MMOH) (Figure 6-2). The substitution of D84 in *E. coli* R2 with E has been shown to have profound effects on the kinetics of the reaction, as noted in previous chapters. O_2 activation at the diiron(II) cluster in $R2_{Ct}$ results in accumulation of an oxidized iron species with EPR spectral characteristics nearly identical with those of the Fe_2(III/IV) cluster **X** that generates the Y• in the R2 proteins from *E. coli* and mouse. Based only on these observations, the Nordlund group put forth the provocative hypothesis that the cluster **X**-like complex in $R2_{Ct}$ ($\mathbf{X_{Ct}}$) generates the cysteine radical in R1, by-passing the intermediate Y• radical that serves this function in class Ia and Ib RNRs. In other words, they proposed that, *in class Ic RNRs, O_2 activation at the diiron(II) center in R2 is coupled directly to production of the catalytically essential radical in R1* (*16*).

The use of diiron(II)-O_2 chemistry directly to generate the R1 radical would represent a *significant* departure from the standard *modus operandi* of class I RNRs. The

Figure 6-2: Crystallographically-derived models of the diiron(III) clusters in (A) the R2 subunit from *Chlamydia trachomatis* (Protein Data Bank (PDB) accession number 1SYY), (B) the R2 subunit from *E. coli* (PDB accession number 1MXY), and (C) MMOH (PDB accession number 1MTY). The first-sphere residues (ligands to the diiron cluster) and second-sphere residues in $R2_{Ct}$ and MMOH display symmetry with respect to an axis perpendicular to the plane of the iron ions. This symmetry is not observed in *E. coli* R2 (D84 is E89 in $R2_{Ct}$ and E114 in MMOH; S114 is E119 in $R2_{Ct}$ and D143; no cognate residue to R115 in $R2_{Ct}$ and R146 in MMOH). Proposed hydrogen-bond networks to the iron centers in these proteins are shown in dotted lines. The electron-injection step into the diiron cluster of (A) $R2_{Ct}$ is proposed to be mediated by a hydrogen-bond network which includes Y112, a water molecule, E119, and H230 (ligand to Fe2), as opposed to a network, similar to that shown to occur in *E. coli*, constituted of residues W51, D226, and His 123, (ligand to Fe1); (B) *E. coli* R2 occurs via a network of hydrogen-bond residues which include W48, D237, and H118 (ligand to the Fe1).

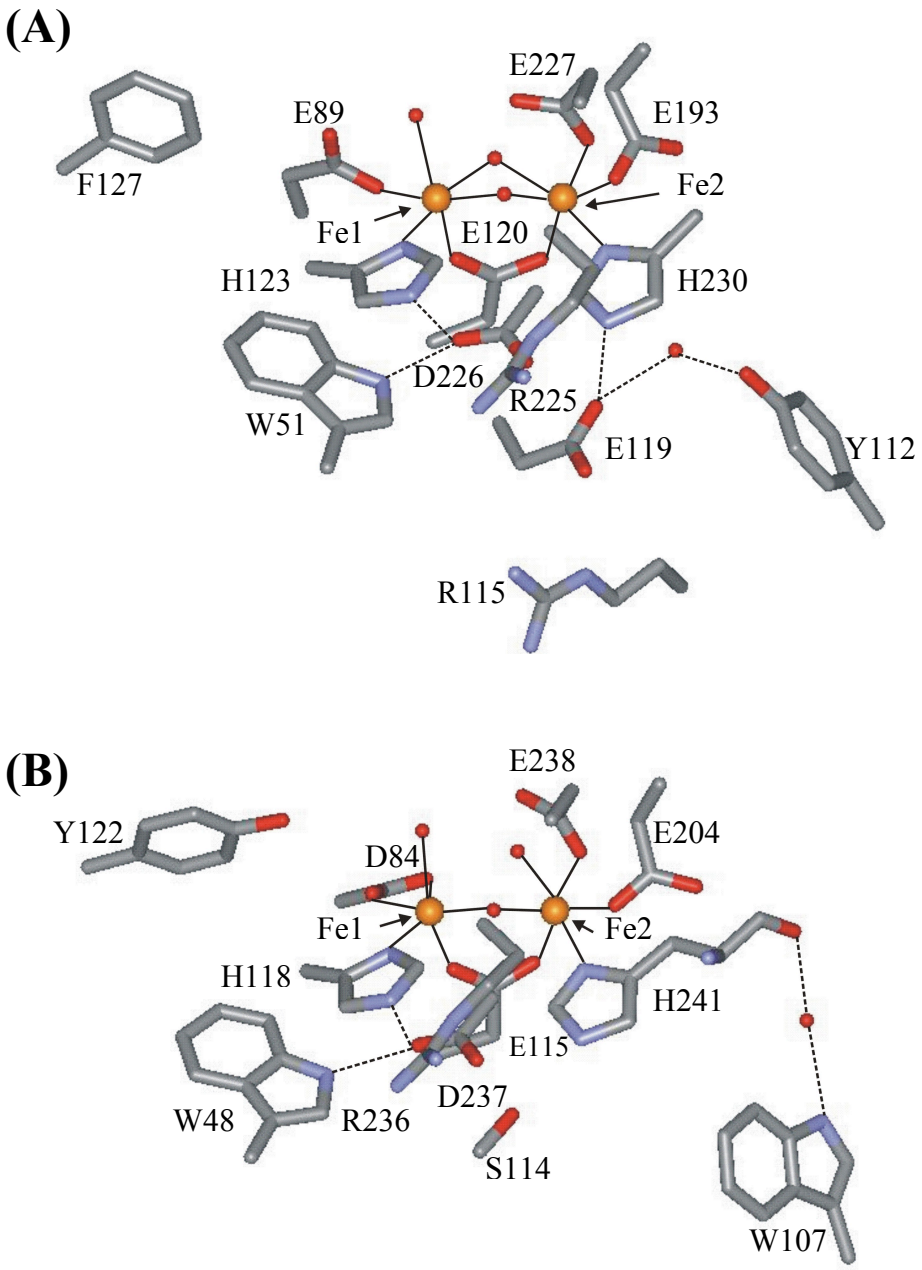
(A)
E227
E89
E193
F127
Fe2
Fe1
E120
H123
H230
D226
R225
W51
E119
Y112
R115
(B)
E238
Y122
E204
D84
Fe1
Fe2
H118
H241
E115
D237
W48
R236
S114
W107
(C)
E114
E243
E209
E144
H147
H246
R245
D242
R146
D143

hypothesis, although not yet validated by direct experimental evidence, is, nevertheless, the simplest explanation for the activity of the Y•-less *C. trachomatis* RNR. Moreover, this altered mechanism of radical generation was foreshadowed by work on the class Ia mouse RNR system (*20*). Cooperman and co-workers reported that the Y177F variant of mouse R2 retains a low but significant level of activity in the presence of R1 and a chemical reductant (dithiothreitol). Speculation on the origin of this activity had focused on the potential for some intermediate in O_2 activation at the diiron center to serve, albeit inefficiently, as R1-radical generator. Nordlund's hypothesis that this is the normal *modus operandi* of class Ic RNRs raises several compelling questions. First, what is the mechanism of O_2 activation and generation of the *bis*-(μ-hydroxo)diiron(III) cluster in isolated $R2_{CT}$, and which intermediate state in this pathway is intercepted by R1 for radical generation? Nordlund proposed $\mathbf{X_{Ct}}$ as the R1 radical generator, but our work on Y122• formation in *E. coli* R2 has demonstrated the accumulation of W48 and (under appropriate reaction conditions) Y356 radicals in provision of the "extra" electron needed to form **X**. Radicals on these putatively interfacial sidechains have been proposed as intermediates in the R1>R2 electron transfer, and their cognates, if generated during formation of $\mathbf{X_{Ct}}$, would obviously be excellent candidates for the R1 radical generator. Second, might the R1 oxidant in R2 function, in direct analogy to the Y• in class Ia and Ib RNRs, *catalytically*, thereby allowing a single O_2 activation event to yield multiple deoxynucleotides? Or are all radicals in R2 (including $\mathbf{X_{Ct}}$) quenched at the end of each turnover, requiring reduction of the diiron center to Fe_2(II/II) and subsequent O_2 activation for each turnover? Catalytic O_2 activation would triple the expenditure of reducing equivalents (which could otherwise yield energy) for nucleotide reduction (6 e-

/dCDP rather than 2 e-/dCDP), seemingly disadvantaging the microbes that employ this system. Might this disadvantage be offset by some selective advantage in coping with the host immune response? Nordlund and colleagues proposed essentially this, arguing that the altered radical-generation mechanism might render the enzyme less vulnerable to radicals such as $O_2^{-\bullet}$ and $NO^{\bullet}$ produced as part of the immune response (*16*). Third, what is the mechanism of propagation of the oxidizing equivalent on R2 (whether it be $\mathbf{X_{Ct}}$ or a sidechain radical generated during formation of $\mathbf{X_{Ct}}$) to the active site of R1 (presumably to C672, the cognate of C439 in *E. coli* R1)? Are radicals produced by oxidation of putative pathway residues W51, Y338 (in R2), Y990, or Y991 (in R1), the cognates of W48, Y356, Y730, and Y731, respectively, in *E. coli* class I RNR, intermediates in this propagation? If so, what are the kinetics and thermodynamics governing the individual radical-hopping events, and to what extent (if any) is each redox step coupled to proton transfer?

Answering the questions posed above will require achievement of the following objectives: (1) dissecting the mechanism of O_2 activation in *C. trachomatis* R2, (2) determining the stoichiometry and kinetics of this step relative to nucleotide reduction and testing for inter-subunit radical transfer, and (3) elucidating the mechanism of radical transfer and the roles of residues in the putative transfer pathway. Herein, the first objective is addressed and the mechanism of O_2 activation in the $R2_{Ct}$-wildtype (wt) protein is dissected by kinetic (stopped-flow and freeze-quench) and spectroscopic (optical absorption, electron paramagnetic resonance, and Mössbauer) methods. Using these techniques, we demonstrate that an additional intermediate, a transient Y•, forms concomitantly with the $\mathbf{X_{Ct}}$ cluster. We further demonstrate that the Y• does not reside

on Y338, although the data suggest that this tyrosine communicates with and mediates reduction of the Y•. In summary, we provide evidence for a *remodeled* electron injection pathway in the R2 subunit of *C. trachomatis* RNR.

MATERIALS AND METHODS

Materials. Culture media components (yeast extract and tryptone) were purchased from Marcor Development Corporation (Hackensack, NJ). Isopropyl-β-D-thiogalactopyranoside (IPTG) was purchased from Biosynth International (Naperville, IL). Kanamycin, phenylmethylsulfonyl fluoride (PMSF), *tris*-(hydroxymethyl)-aminomethane (Tris), imidazole, methyl viologen, sodium dithionite, and 3-(2-pyridyl)-5,6-bis(4-phenyl-sulfonic acid)-1,2,4-triazine (ferrozine) were purchased from Sigma (St. Louis, MO). Glycerol, ammonium sulfate, and sodium chloride were purchased from EM Science (Gibbstown, NJ). L-ascorbic acid was purchased from Fischer Scientific Company (First Lawn, N.J.). Enzyme grade 4-(2-hydroxyethyl)-1-piperazineethanesulfonic acid (HEPES) was purchased from FisherBiotech (Pittsburgh, PA). Oligonucleotide primers were purchased from Invitrogen (Frederick, MD). Reagents for the polymerase chain reaction (PCR) and restriction enzymes were purchased from New England Biolabs (Beverly, MA). T4 DNA ligase was purchased from Roche (Indianapolis, IN). BL21(DE3) cells and pET vectors were purchased from Novagen (Madison, WI). Genomic DNA of *Chlamydia trachomatis* was a kind gift from Dr. R. Stephens at the School of Public Health, University of California Berkeley (Berkeley, CA).

Preparation of Vectors and Strains for Over-Expression of $R2_{CT}$-wt and $R2_{CT}$-Y338F. Plasmid pET28a-$R2_{Ct}$-wt, which contains the *Chlamydia trachomatis* R2 gene inserted into the pET28a expression vector, was constructed as follows. The open reading frame of $R2_{Ct}$ was amplified from the genomic DNA of *C. trachomatis* by using the primers 1 (5'-TTA ACG GTT **CAT ATG** CAA GCA GAT ATT TTA GAT GG-3', *NdeI* site shown in bold) and 2 (5'-ATG **CTC GAG** GCT TTC TCC TAT TTT GAT ATC AGG-3', *XhoI* site shown in bold). The 1040 basepair (bp) PCR fragment was purified by gel electrophoresis, extracted from the gel using the Qiagen (Valencia, CA) Qiaquick system as instructed by the manufacturer, restricted with *NdeI* and *XhoI*, re-purified as before, and ligated with pET28a, which had been digested with the same enzymes and gel purified. The sequence of the coding region of the vector was verified by ACGT, Inc. (Wheeling, IL.). pET28a-$R2_{Ct}$-wt was used to transform BL21(DE3) cells to generate the overproducing strain for $(His)_6$-tagged-$R2_{Ct}$-wt ($(His)_6$-$R2_{Ct}$-wt).

The Y338F substitution (TAT to TTT, complement of underlined triplet) was introduced by PCR using primer 1 and primer 3 (5'-GGT GGT G**CT CGA G**CT ACC AAG TTA AGC TTG CTG CAT GTT G<u>AA A</u>TT CTA TAA CCC-3', *XhoI* site shown in bold), and pET28a-$R2_{Ct}$-wt as template. The 1086 bp fragment was gel purified, restricted with *NdeI* and *XhoI*, re-purified, and ligated with *NdeI*/*XhoI*-restricted pET28a-$R2_{Ct}$-wt. The sequence of the coding region of the vector was verified by ACGT, Inc. pET28a-$R2_{Ct}$-Y338F was used to transform BL21(DE3) cells to generate the overproducer for $(His)_6$-$R2_{Ct}$-Y338F.

Expression and Purification of the Diiron(III) Forms of $(His)_6$-$R2_{Ct}$-wt and $(His)_6$-$R2_{Ct}$-Y338F. The overproducing strains were grown at 37 °C in rich LB broth,

containing 35 g/L tryptone, 20 g/L yeast extract, 5 g/L NaCl, and 0.05 g/L kanamycin, to an OD_{600} of 0.7-1.0, cooled rapidly to 18 °C by incubation on ice for 15 min, induced by addition of 0.2 mM IPTG, and grown for 16-18 h at 18 °C. The cells were then harvested by centrifugation and the cell pellet was washed with cold 25 mM Tris HCl (pH 7.4) containing 70 mM NaCl and 4 mM KCl prior to being frozen in liquid N_2 and stored at -80 ° C. A typical yield was ~ 16 g of wet cell paste/L of culture.

The frozen cells (~ 100 g wet cell paste) were thawed in buffer A [50 mM Tris-HCl (pH 7.6) and 10% (v/v) glycerol] containing 0.25 mM PMSF and 10 mM imidazole and lysed in a french pressure cell at 16,000 psi. Cell debris was removed by centrifugation at 14,000 *g* for 10 min and the resulting supernatant was stirred gently with Ni-NTA resin (Qiagen GmbH) (~ 1 mL of resin was used per 20 ml of lysate). The slurry was then loaded into a column and the column was washed with buffer A containing 20 mM imidazole (twice the volume of the column), followed by buffer A containing 250 mM imidazole to elute the protein. Fractions containing $(His)_6$-$R2_{Ct}$, as identified by SDS-PAGE, were pooled (typically six equivalent volumes of the column) and concentrated to approximately 60 mg/mL in an Amicon (Beverly, MA) ultrafiltration cell with a YM30 membrane. The protein was dialyzed against 2 L of either buffer B [100 mM HEPES (pH 7.6)] or buffer B with 10% (v/v) glycerol for 4 h to remove the imidazole and exchange the buffer. A typical yield from this chromatography step was 14 mg of protein per g of wet cell paste. The protein was ~ 95% pure as estimated by SDS-PAGE with coomassie staining.

Preparation of the Apo Forms of $(His)_6$-$R2_{Ct}$-wt and $(His)_6$-$R2_{Ct}$-Y338F. The diiron(III) cluster was reduced by a ~ 1 h incubation with sodium dithionite (6 mM) and

methyl viologen (20 μM) under anaerobic conditions at room temperature. The blue color of the reduced form of methyl viologen served as a redox indicator. The resulting diiron(II) form of $(His)_6$-$R2_{Ct}$ was mixed with excess ferroin chelator, ferrozine, and the resulting dark purple solution was passed through a Sephadex-G-25 superfine column (Amersham Biosciences) in buffer B (or buffer B with 10 % (v/v) glycerol). Fractions containing $(His)_6$-$R2_{Ct}$, as judged by SDS-PAGE, were pooled, concentrated to ~ 60 mg/mL, frozen in liquid N_2, and stored at – 80 °C. The yield in the iron-removal step was ~ 50%. The Fe content of the protein before and after chelation was determined by a previously described colorimetric procedure which employs ferrozine (*21, 22*). The His-tagged-$R2_{Ct}$ prepared in this manner contained ≤ 0.4 Fe/R2 per dimer.

Determination of Protein Concentrations. The proteins were quantified spectrophotometrically by assuming molar absorptivities (ε_{280}) of 115,500 M^{-1} cm^{-1} for the $(His)_6$-$R2_{Ct}$-wt dimer and 112,940 $M^{-1}cm^{-1}$ for $(His)_6$-$R2_{Ct}$-Y338F dimer, as calculated by the method of Gill and von Hippel (*23*).

Preparation of the Fe(II)-$(His)_6$-$R2_{CT}$ Complex. Solutions of apo-$(His)_6$-$R2_{Ct}$ were rendered free of oxygen on a vacuum/gas manifold and then mixed with Fe(II) in an anoxic chamber (MBraun), as previously described (*24*). The ^{57}Fe(II) stock solution used to prepare Mössbauer samples was prepared by dissolution of the metal in 1 M H_2SO_4, as previously described (*25*).

Stopped-Flow Absorption Spectrophotometry. Stopped-flow absorption experiments were carried out with an Applied Photophysics SX.18MV stopped-flow apparatus equipped with a diode array detector and housed in the anoxic chamber. Constant temperature was ensured with a Lauda K-4/R circulating water bath. Specific

reaction conditions are given in the appropriate figure legends.

Freeze-Quench Electron Paramagnetic Resonance (EPR) and Mössbauer Experiments. The apparatus and procedures used to prepare the rapid freeze-quench EPR (RFQ-EPR) and Mössbauer (RFQ-Möss) samples have been described (*26, 27*). Reaction conditions are given in the appropriate figure legends. EPR spectra were acquired on a Bruker ESP 300 spectrometer equipped with an Oxford Instruments Model ESP 900 continuous flow cryostat. Mössbauer spectra were recorded on a spectrometer from WEB research (Edina, MN) operating in the constant acceleration mode in a transmission geometry. During the measurement the sample was kept inside a SVT-400 dewar from Janis (Wilmington, MA) at a temperature of 4.2 K in a magnetic field of 40 mT applied parallel or perpendicular to the γ-beam. The isomer shifts quoted are relative to the centroid of the spectrum of a metallic foil of α-Fe at room temperature. Data analysis was performed using the program WMOSS from WEB research.

RESULTS

Preparation of the Apo Forms of $(His)_6$-$R2_{Ct}$-wt and $(His)_6$-$R2_{Ct}$-Y338F. SDS-PAGE analysis of total extracts of BL21(DE3)-pET28a-$R2_{Ct}$-wt and BL21(DE3)-pET28a-$R2_{Ct}$-Y338F harvested from rich media after an ~ 18 h induction at 18 °C with 0.2 mM IPTG revealed a band at the correct molecular weight (~ 42 kDa) for $(His)_6$-$R2_{Ct}$. Purification of $(His)_6$-$R2_{Ct}$-wt and $(His)_6$-$R2_{Ct}$-Y338F from these extracts by affinity chromatography on a Ni-NTA resin yielded hundreds of milligrams of protein that was estimated to be > 95% pure by examination of coomassie stained SDS-PAGE gels.

Our published procedure for isolation of the apo forms of the R2 proteins from *E. coli* and mouse (*24, 28*), which employs chelation of the available Fe(II) by addition of

the cell-permeative 1,10-phenanthroline shortly before induction of protein expression and again during early steps of purification, was not applied in the preparation of the apo forms of $(His)_6$-$R2_{Ct}$-wt and $(His)_6$-$R2_{Ct}$-Y338F. It was anticipated that the Ni-NTA affinity chromatography would be incompatible with the presence of phenanthroline. Thus, the purified proteins contained unacceptably high levels of bound iron, presumably in the form of the diiron(III) product form of the cluster. Iron was reductively chelated from the proteins by treatment in the absence of O_2 with the reductant, sodium dithionite, and the redox mediator, methylviologen, followed by the high-affinity ferroin chelator, ferrozine. Separation of the resulting purple Fe(II)-$(ferrozine)_3$ complex from the protein was performed by gel filtration chromatography. Fe removal by this procedure was almost complete. The $(His)_6$-$R2_{Ct}$ proteins contained ~ 0.2-0.4 Fe/R2 per dimer as determined by the published denaturing ferrozine-colorimetric assay (*21, 22*). The $(His)_6$-tagged forms of both proteins were used in all the experiments described in this chapter and, for simplicity, are referred to hereafter as $R2_{Ct}$-wt and $R2_{Ct}$-Y338F.

Stopped-flow Absorption and RFQ-EPR Evidence for an $\boldsymbol{X_{Cr}}$*-Y• Di-Radical Intermediate during* O_2 *Activation by Fe(II)-*$R2_{Ct}$*-wt.* Mixing of the pre-formed Fe(II)-$R2_{Ct}$-wt complex (Fe(II)/R2 = 3.0) with O_2 at 5 °C results in rapid development of absorption in the 300-500 nm range, with a detectable shoulder at ~ 360 nm (Figure 6-3, solid and dashed traces) that is similar to that characteristic of cluster **X** in the reactions of *E. coli* and mouse R2 (*28, 29*). Monitoring the timecourse at 360 nm reveals three kinetic phases that can be fit by the equation for three parallel first-order processes: two formation phases with apparent first-order rate constants (k_{obs}) of 0.29 s^{-1} and 29 s^{-1} and a slow decay phase with k_{obs} of 0.2 s^{-1} (Figure 6-4, circles). To test if the absorbing species

Figure 6-3: O_2 activation by $R2_{Ct}$-wt monitored by stopped-flow absorption spectroscopy. Development of the absorption spectrum was monitored after equal-volume mixing at 5°C of an O_2-free solution of Fe(II)-$R2_{Ct}$-wt (0.22 mM initial concentration, Fe(II)/R2 = 3 equiv) in buffer B with an O_2-saturated solution of buffer B. The spectra shown were acquired 0.0019 s (dotted line), 0.049 s (solid line), and 1 s (dashed line) after mixing. The initial Fe content of the protein was negligible as determined by the ferrozine colormetric assay.

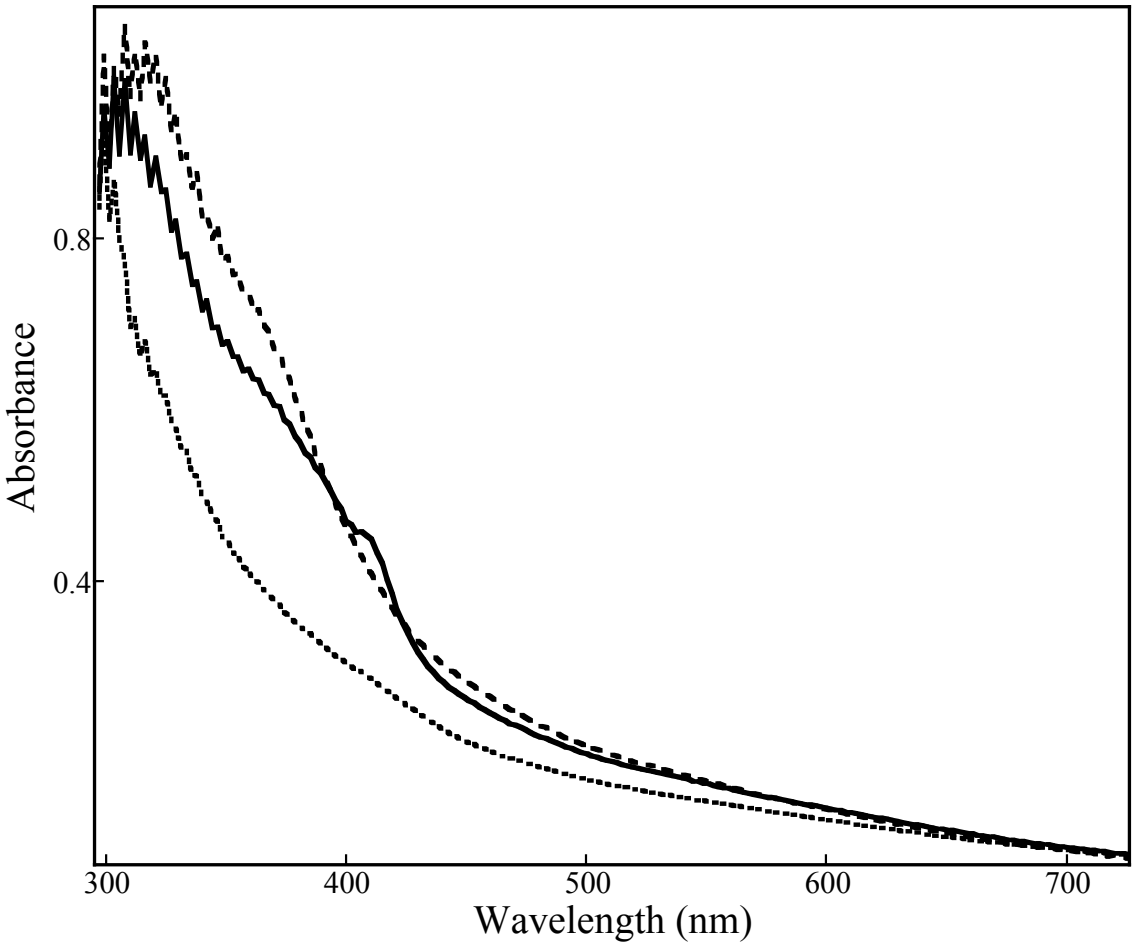
Absorbance
0.8
0.4
300
400
500
600
700
Wavelength (nm)

Figure 6-4: Timecourse of O_2 activation at 5°C by Fe(II)-$R2_{Ct}$-wt (Fe(II)/R2 = 3 equiv) monitored at A_{411} - (A_{405} + A_{417})/2 (squares) and 360 nm (circles) by stopped-flow absorption spectroscopy. The solid line on top of the circles is the best fit of the equation describing three parallel first-order processes to the data. The solid line on top of the squares is the best fit of the equation describing the formation of an intermediate B in the reaction A→B→C. Experimental details are given in the legend to Figure 6-3.

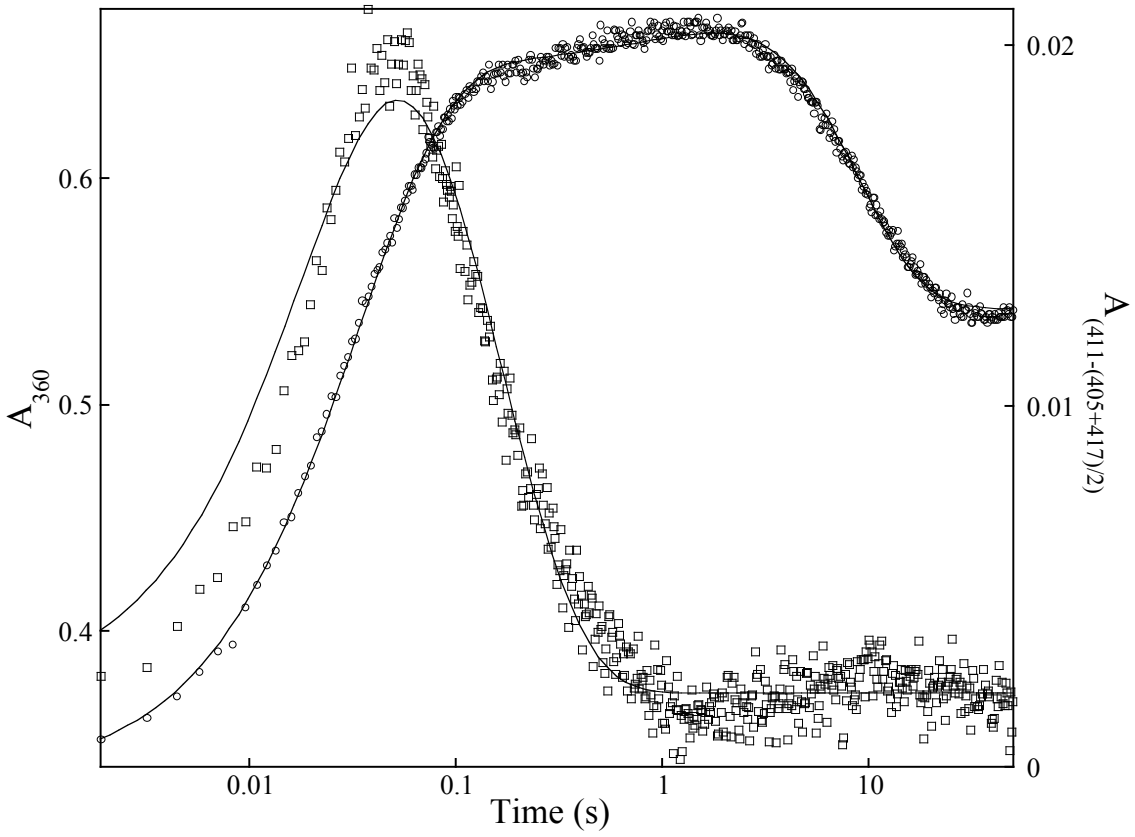
0.6
0.5
0.4
A_{360}
0.02
0.01
0
$A_{(411-(405+417)/2)}$
0.01
0.1
1
10
Time (s)

detected in stopped-flow spectroscopy is **X**, samples for EPR characterization were prepared by mixing the Fe(II)-$R2_{Ct}$-wt complex (Fe(II)/R2 = 2.8) with O_2 and freeze-quenching at early reaction times and at reaction times similar to those at which the absorbance at 360 nm reaches its maximum value. Observation of the characteristic sharp, g = 2.0 EPR singlet at these reaction times (Figure 6-5, spectra A-C) but not at completion (Figure 6-5, spectrum D) establishes that $\mathbf{X_{Ct}}$ is indeed forming and then decaying.

Along with the 360-nm absorption band, a sharp feature at 411 nm, diagnostic of a Y•, develops (Figure 6-3, solid line) with similar kinetics ($k_{obs} \sim 40\ s^{-1}$) but decays at a much faster rate (~ 70 fold greater) than the 360-nm feature (5 ºC; Fe(II)/$R2_{Ct}$ = 3 equiv) (Figure 6-4, squares). Kinetic simulation of the timecourse of A_{411} - (A_{405} + A_{417})/2 is required to attain more accurate values for k_{obs}. The RFQ-EPR spectrum of the limiting Fe(II) reaction quenched at 0.05 s (Figure 6-6, spectrum A, solid line), the time of maximal concentration of Y• as determined by stopped-flow spectroscopy, has additional breadth and a different line-shape in comparison with the spectrum of the sample quenched at 1 s (Figure 6-6, spectrum A, dashed line), a time point at which the transient Y• has already decayed (Figure 6-4, squares). The broader features are, therefore, associated with the transient Y• detected by stopped-flow spectroscopy. A preliminary difference spectrum (Figure 6-6, spectrum B) shows that these features have an overall doublet structure, which is characteristic of many tyrosyl radicals and arises from strong hyperfine coupling with one of the β-hydrogens (the magnitude of the coupling is extremely dependent on the angle between the C_β-H bond and the phenol ring, and, in most orientations, one of the protons couples strongly and the other weakly) (*30, 31*).

Figure 6-5: EPR spectra from the reaction of Fe(II)-$R2_{Ct}$-wt with O_2 at 5°C. The samples were prepared by mixing O_2-free Fe(II)-$R2_{Ct}$-wt (0.73 mM initial concentration, Fe(II)/R2 = 2.8 equiv) in buffer B with an O_2-saturated solution of buffer B in a 1:2 ratio and freeze-quenching at (**A**) 0.02 s, (**B**) 0.05 s, (**C**) 1 s, and (**D**) ~ 10 min. The initial Fe content of the protein was negligible as determined by the ferrozine colormetric assay. All spectra were recorded at 20 K with a microwave power of 0.01 mW and a modulation amplitude of 4 G. A scan time of 167 s and a time constant of 0.167 s were used. Integrated spectral intensities were related to concentration by use of a copper perchlorate standard, as previously described (reference 25).

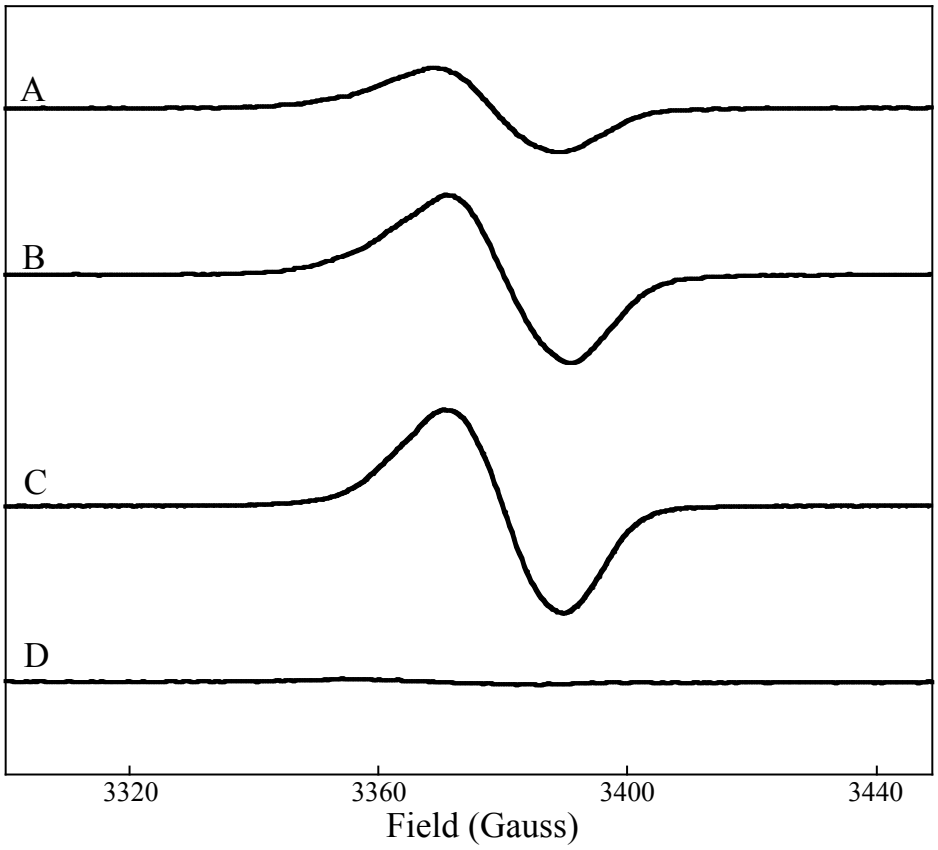
A
B
C
D
3320
3360
3400
3440
Field (Gauss)

Figure 6-6: Component analysis of EPR spectra obtained from the reaction of Fe(II)-$R2_{Ct}$-wt with O_2. In spectrum A, the solid spectrum and dashed spectrum are identical to spectra B and C in Figure 6-5, respectively. The circle-point spectrum A is of the 0.05 s sample obtained by a 1:2 mix at 5°C of an O_2-free solution of Fe(II)-$R2_{Ct}$-wt (Fe(II)/R2 = 6.0 equiv) in buffer B with an O_2-saturated solution of buffer B. Spectrum B is the difference spectrum of the solid and dashed spectra in A. The protein concentration as well as the details of spectral acquisition and analysis are given in the legend to Figure 6-5.

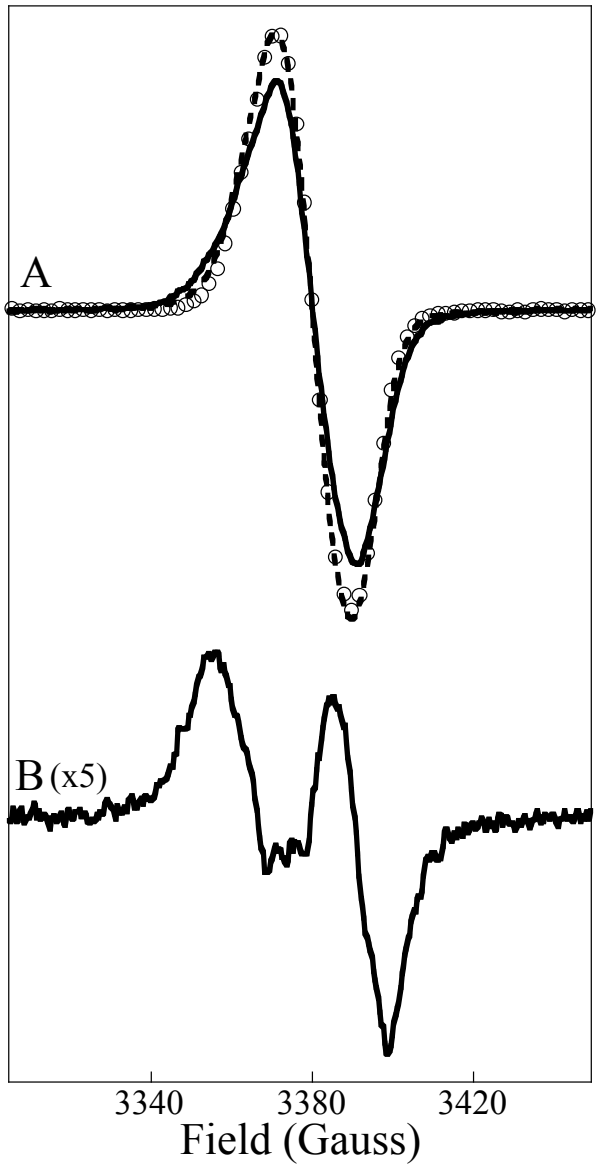
A
B (x5)
3340
3380
3420
Field (Gauss)

The subtraction analysis would imply that 23% of the total integrated intensity is contributed by the broad features, which would correspond to a species distribution of ~ 0.16 equiv of Y• and ~ 0.54 equiv of $\mathbf{X_{Ct}}$.

Reactivity of the Transient Di-Radical Intermediate toward Reductants. The peak height [A_{411} - (A_{405} + A_{417})/2] of the transient Y• is very sensitive to the ratio of Fe(II)/R2 (Figure 6-7A, inset). It reaches a maximum with an Fe(II)/R2 ratio near 3.0 (Figure 6-7A, black trace) and is much less intense when only a slight excess of Fe(II) is used (4 equiv) (Figure 6-7A, blue trace). Also, the peak does not develop at all when ascorbate is included (Figure 6-7A, purple trace). This correlation implies (in analogy to results on the tryptophan cation radical ($W48^{+\bullet}$) in the reaction of *E. coli* R2) (*32*) that the Y• can be rapidly reduced by exogenous reductants (e.g. $Fe(II)_{aq}$, ascorbate). Consistent with this conclusion is a prolonged lag phase that is apparent in the (A_{411} - (A_{405} + A_{417})/2)-versus-time trace from the reaction of $R2_{Ct}$-wt with O_2 in the presence of 4 equiv of Fe(II) and which corresponds to the kinetically preferred reduction of the Y• with the free Fe(II) (Figure 6-7A, blue trace). Furthermore, the EPR spectrum from the excess Fe(II) reaction (6 equiv) at 0.05 s (Figure 6-6, spectrum A, circles) is indistinguishable from that of the limiting Fe(II) reaction at 1 s (at which time the Y• has decayed; Figure 6-6, spectrum A, dashed line) confirming that the Y• is reduced by the $Fe(II)_{aq}$, leaving behind intermediate $\mathbf{X_{Ct}}$.

Apparently, the presence of excess Fe(II) imposes the same reductive effect on the 360 nm absorption feature (compare black and blue traces in Figure 6-7B), which presumably reflects the reduction of $\mathbf{X_{Ct}}$. On the other hand, the absorption at 360 nm increases when ascorbate is present, suggesting that more $\mathbf{X_{Ct}}$ is accumulating (Figure 6-

Figure 6-7: The dependence of the amplitudes of the transient absorbances at (A) A_{411} - (A_{405} + A_{417})/2 and (B) 360 nm on the ratio Fe(II)/R2 in the reaction of $R2_{Ct}$-wt. Apo $R2_{Ct}$-wt was mixed in the absence of O_2 with Fe(II) in a molar ratio of 1.0 (green trace), 2.0 (red trace), 3.0 (black trace), or 4.0 (blue trace). This solution was mixed in the stopped-flow apparatus at 5 °C in a 1:1 volume ratio with buffer B, which had been saturated at 5 °C with O_2. The final concentration of $R2_{Ct}$-wt after mixing in the stopped-flow was 0.11 mM. The initial Fe content was negligible as determined by the ferrozine colormetric assay. The inset in Figure (A) shows a plot of the maximum value of A_{411} - (A_{405} + A_{417})/2 minus the final value for each trace. The purple traces reflect the reactivity of the (A) (A_{411} - (A_{405} + A_{417})/2)-peak height and (B) 360-nm absorbing species with ascorbate. Apo $R2_{Ct}$-wt was mixed in the absence of O_2 with 3.0 equiv of Fe(II) and 2.5 mM L-ascorbic acid prior to loading into the stopped-flow. This solution was mixed in the stopped-flow apparatus at 5 °C with an equal volume of O_2-saturated buffer B. The final concentration of $R2_{Ct}$-wt after mixing in the stopped-flow was 0.12 mM. The absorbances of both purple traces were corrected for the slightly greater protein concentration for comparison to the traces from the Fe(II)-dependence experiment.

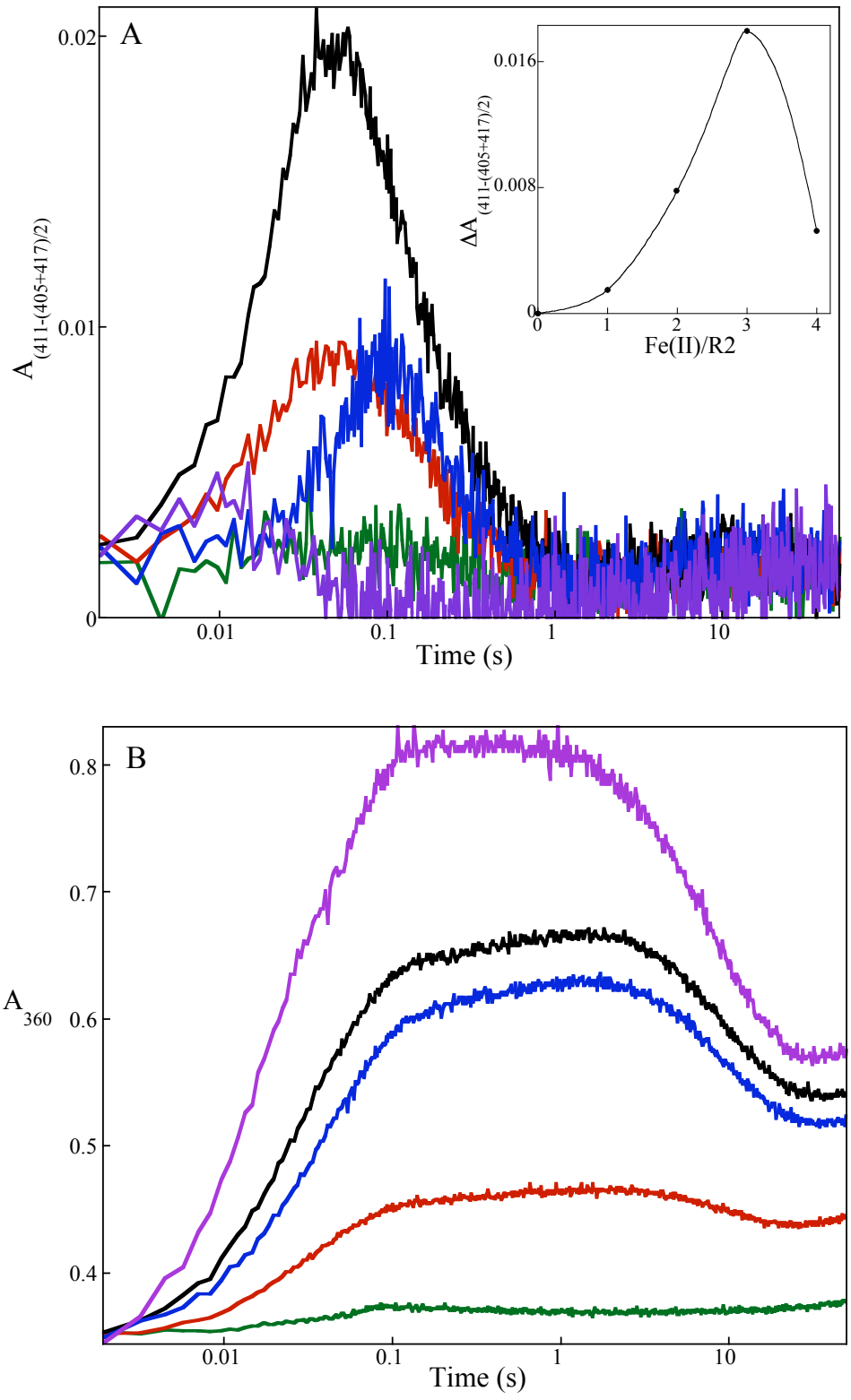
A
0.02
0.01
0
A(411-(405+417)/2)
0.01
0.1
1
10
Time (s)
0.016
0.008
0
ΔA(411-(405+417)/2)
0
1
2
3
4
Fe(II)/R2
B
0.8
0.7
0.6
0.5
0.4
A360
0.01
0.1
1
10
Time (s)

7B, purple trace). Comparison of the integrated intensities of the EPR spectra of the 1-s samples from the limiting Fe(II) reaction and the excess Fe(II) reaction (of which both contain *only* $\mathbf{X_{Ct}}$) reveals that less $\mathbf{X_{Ct}}$ is present in the former than in the latter (Figure 6-8). This result is contradictory to that obtained by stopped-flow spectroscopy. Precipitation of the protein in the presence of excess Fe(II) at 5°C was observed, and reduction in the concentration of reactive complex may be responsible for the diminution of the A_{360} nm amplitude in the excess Fe(II) reaction. The precipitate was observed to re-dissolve upon warming of the protein + excess Fe(II) solutions. Therefore, repetition of the above experiments at higher temperatures should be carried out before these results can be unambiguously interpreted.

In the reaction of the *E. coli* R2 protein, the dependence of the amplitude of the 560-nm absorbance transient arising from the $W48^{+\bullet}$ on the Fe(II)/R2 ratio is complex and reflects features of both Fe(II) binding and $W48^{+\bullet}$ reactivity (*32*). The concave-up increase between Fe(II)/R2 = 0 and 3 reflects the fact that one of the two sites of the diiron cluster has at least 6-fold greater affinity for Fe(II) than the other site, favoring binding of Fe(II) in a mononuclear configuration at very low Fe(II)/R2. As the ratio increases, an increasingly large fraction of the bound Fe(II) ions are in fully constituted and reactive diiron(II) clusters, leading to greater accumulation of the $W48^{+\bullet}$ intermediate. Further increase in the Fe(II)/R2 ratio results in a greater fraction of unbound Fe(II), which rapidly reduces the $W48^{+\bullet}$ and diminishes its accumulation. The dependence of the transient Y• radical on Fe(II)/R2 ratio in the reaction of $R2_{Ct}$-wt (inset to Figure 6-7A) mirrors that of the $W48^{+\bullet}$ in the *E. coli* R2 reaction, suggesting that the two sites of the diiron cluster in this class Ic R2 also have different affinities. This can be

Figure 6-8: Determination of the effect of Fe(II) on $\mathbf{X_{Ct}}$ by RFQ-EPR spectroscopy. The dashed spectrum is of the 1-s sample obtained by a 1:2 mix at 5°C of an O_2-free solution of Fe(II)-$R2_{Ct}$-wt (Fe(II)/R2 = 2.8 equiv) in buffer B with an O_2-saturated solution of buffer B. The dotted spectrum is of the 1 s sample obtained by a 1:2 mixing at 5°C of an O_2-free solution of Fe(II)-$R2_{Ct}$-wt (Fe(II)/R2 = 6.0 equiv) in buffer B with an O_2-saturated solution of buffer B. The protein concentration as well as the details of spectral acquisition and analysis are given in the legend to Figure 6-5.

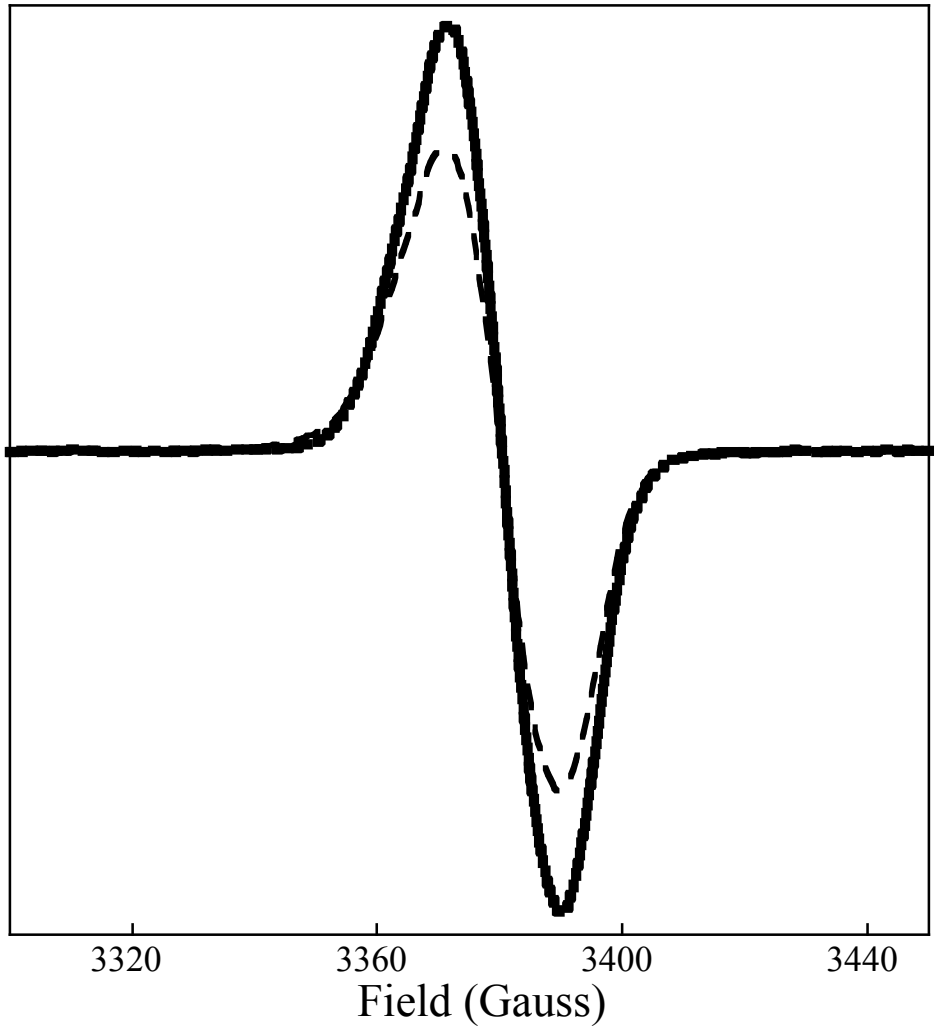
3320
3360
3400
3440
Field (Gauss)

tested by the use the two iron isotopes, ^{56}Fe and ^{57}Fe, and Mössbauer spectroscopy. Any Fe(II) bound in mononuclear fashion after anaerobic complexation with a limiting quantity of one isotope might be "trapped" by reaction with O_2 in a heteroisotopic cluster following addition of an O_2-saturated solution of the second isotope (*33*). Any differential affinity would then be evident in the Mössbauer spectrum of $\mathbf{X_{Ct}}$, in which only ^{57}Fe is detected and the two sites of the cluster are well resolved (see below).

Dependencies of the Kinetics of Y• and $\boldsymbol{X_{Ct}}$ Formation on O_2 Concentration. The dependencies of the rates of Y• and $\mathbf{X_{Ct}}$ formation on O_2 concentration were examined in a series of stopped-flow experiments in which the 411-nm peak height and the absorbance at 360 nm were monitored. The concentration of O_2 was varied at a fixed concentration of Fe(II)-$R2_{CT}$-wt complex (with O_2 maintained in excess). An increase in O_2 concentration results in a linear increase in the observed first-order rate constants of the rise phases of the transient 411-nm peak height and the transient 360-nm feature, but has no significant effect on the rate constants for decay of either feature (Figure 6-9). The observation of second-order kinetics ($(5 \pm 1) \times 10^4$ M^{-1} s^{-1} (inset to Figures 6-9 A) and ($4 \pm 1) \times 10^4$ M^{-1} s^{-1} (inset to Figures 6-9 B)) implies a collisional reaction between the Fe(II)-$R2_{CT}$-wt complex and O_2 which results in the formation of the $\mathbf{X_{CT}}$-Y• di-radical, as opposed to mechanisms involving significant accumulation of a precursor to the $\mathbf{X_{CT}}$-Y• or a protein unimolecular isomerization prior to O_2 activation.

Characterization of the Fe(II)-$R2_{Ct}$-wt Reaction with O_2 by RFQ- Mössbauer Spectroscopy. A series of freeze-quenched Mössbauer samples were prepared to obtain more definitive evidence for the accumulation of cluster $\mathbf{X_{Ct}}$ in the reaction of Fe(II)-$R2_{Ct}$-wt with O_2 and to analyze the nature of the iron sites in both the reactant and

Figure 6-9: Dependence of the (A) (A_{411} - (A_{405} + A_{417})/2)-peak height and (B) 360-nm feature on the concentrations of O_2 at 5 °C in the reaction of $R2_{Ct}$-wt. The O_2-free Fe(II)-$R2_{Ct}$ complex (0.24 mM initial concentration, Fe(II)/R2 = 3.0) was mixed with an equal volume of buffer B at various O_2 concentrations: [O_2] ~ 0.396 mM (red traces), [O_2] ~ 0.95 mM (blue traces), and [O_2] ~ 1.89 mM (black traces). In both A and B, the insets show plots of observed first-order rate constants for formation (obtained by non-linear regression fitting) versus concentrations of O_2 in buffer B.

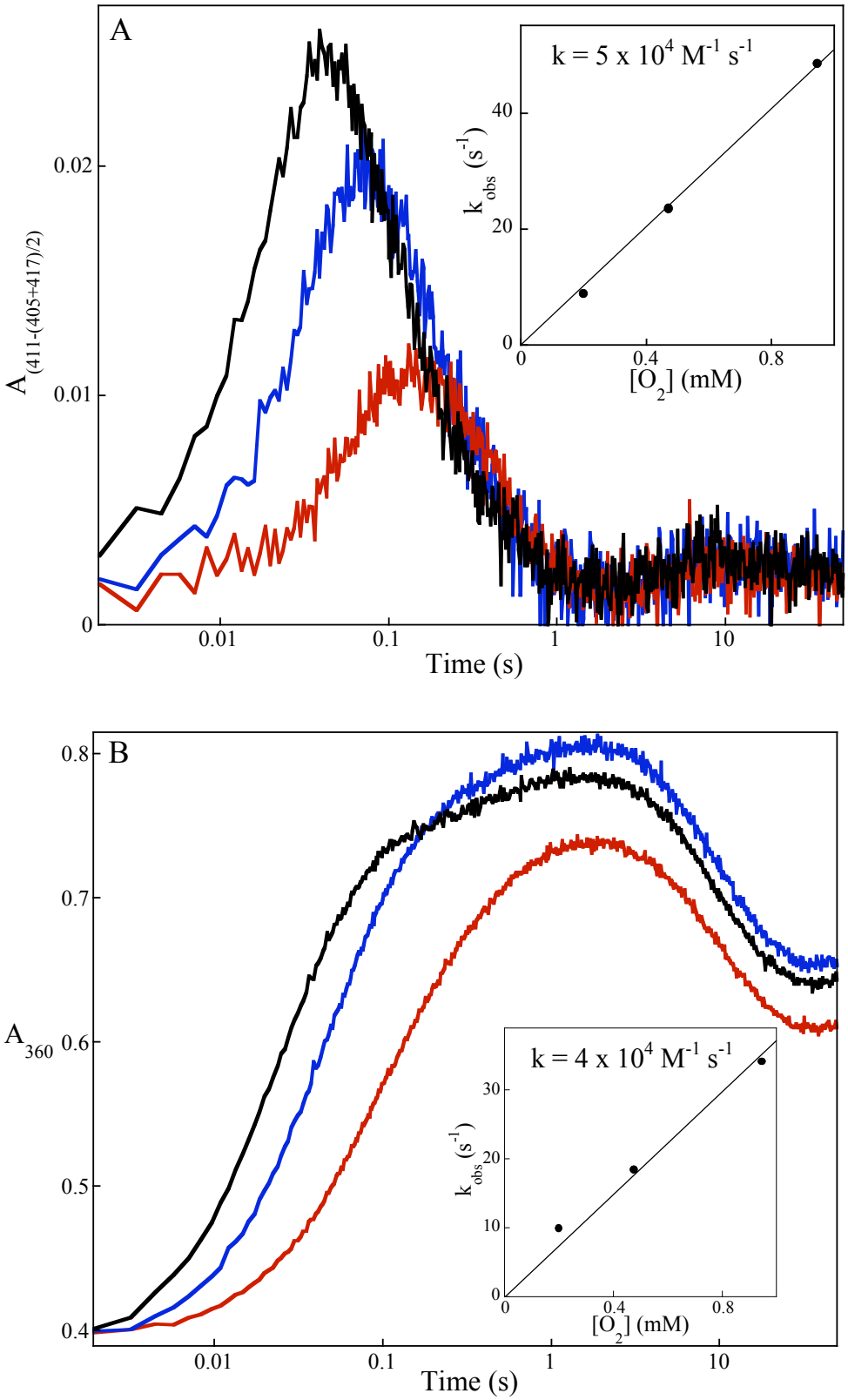
A
$A_{(411-(405+417)/2)}$
0.02
0.01
0
0.01
0.1
1
10
Time (s)
k = 5 x 10^4 M^{-1} s^{-1}
k_{obs} (s^{-1})
40
20
0
0
0.4
0.8
[O_2] (mM)
B
A_{360}
0.8
0.7
0.6
0.5
0.4
0.01
0.1
1
10
Time (s)
k = 4 x 10^4 M^{-1} s^{-1}
k_{obs} (s^{-1})
30
20
10
0
0
0.4
0.8
[O_2] (mM)

product. Paramagnetic features very similar to those characterizing **X** in the reactions of *E. coli* and mouse R2 (*26, 28, 34, 35*) are most prominent in the spectrum of a sample that was freeze-quenched at a reaction time of 1 s (Figure 6-10, spectra C and D), which is similar to the time at which the concentration of the intermediate is predicted by the stopped-flow kinetic trace to reach its maximum value (Figure 6-4, dashed trace). The spectrum of a sample quenched at a shorter reaction time (0.05 s) (Figure 6-10, spectrum B) has less intensity attributable to $\mathbf{X_{Ct}}$. The features of $\mathbf{X_{Ct}}$ are undetectable in the spectrum of a sample frozen after completion of the reaction (Figure 6-10, spectrum F).

The solid lines overlaid with the experimental data in spectra **C** (parallel field) and **D** (perpendicular field) are theoretical simulations of $\mathbf{X_{Ct}}$ according to the parameters listed in Table 6-1. The theoretical spectra are scaled to 56 % of the integrated intensities of the experimental spectra. This corresponds to 0.84 equiv of $\mathbf{X_{Ct}}$ accumulating in the reaction of Fe(II)-$R2_{Ct}$-wt with O_2, which is in satisfactory agreement with the quantity of this species estimated from the analysis of the EPR spectra. Subtraction of spectrum **D** from **C** (to give spectrum **E**) effectively cancels the contributions from any integer-spin species (such as the diferrous center, shown by arrows) that may be present in the sample and shows the field-direction dependence of the spectra of half-integer spin species that are present ($\mathbf{X_{Ct}}$). This difference spectrum is in good agreement with the theoretical spectrum of $\mathbf{X_{Ct}}$ (solid line in **E**) and is closely related to the corresponding difference spectrum of **X** from *E. coli* R2 (*35*).

Serendipitously, the Mössbauer spectrum of the sample freeze-quenched at 0.05 s (Figure 6-10, spectrum B) suggest the presence of another intermediate (upward-solid arrow) in addition to $\mathbf{X_{Ct}}$ in the reaction of Fe(II)-$R2_{Ct}$-wt with O_2. Following subtraction

Figure 6-10: Mössbauer spectra from the reaction of Fe(II)-$R2_{Ct}$-wt (1.56 mM, 3.0 equiv of $^{57}Fe(II)$) with O_2. Spectrum **A** is of the reactant Fe(II)-$R2_{Ct}$-wt used in preparation of the freeze-quenched samples. Spectra **B-F** are of samples prepared by mixing O_2-free Fe(II)-$R2_{Ct}$-wt at 5 ºC with O_2-saturated buffer B with 10 % (v/v) glycerol in a ratio of 1:2 and freeze-quenching at either 0.05 s (**B**) or 1 s (**C**-**E**). **F** is the spectrum of the product (reaction time ~ 5 min) recovered from the aging hose in the freeze-quench experiments. Spectra **C** and **D** are of the 1 s sample and differ only in the direction of the 40-mT magnetic field relative to that of the g-beam (parallel in **C** and perpendicular in **D**. **E** is the difference spectrum obtained by subtracting **D** from **C**. Each experimental spectrum was recorded at 4.2 K in a 40-mT magnetic field (parallel to the γ-beam in all but **D**). The solid lines plotted over the data are simulated spectra of (**B**) the peroxodiiron(III) intermediate normalized to 6 % of the total absorption intensity; (**C**-**E**) $\mathbf{X_{Ct}}$ normalized to 56 % of the total absorption intensity in each spectrum; (**F**) the *bis*-(μ-hydroxo)diiron(III) cluster intermediate normalized to 70 % of the total absorption intensity. The parameters used in the above simulations are summarized in Table 6-1. The solid arrow below spectrum **B** points to the features of the peroxodiiron(III) species. The dashed arrows above spectra C and D point to the features of the diferrous reactant.

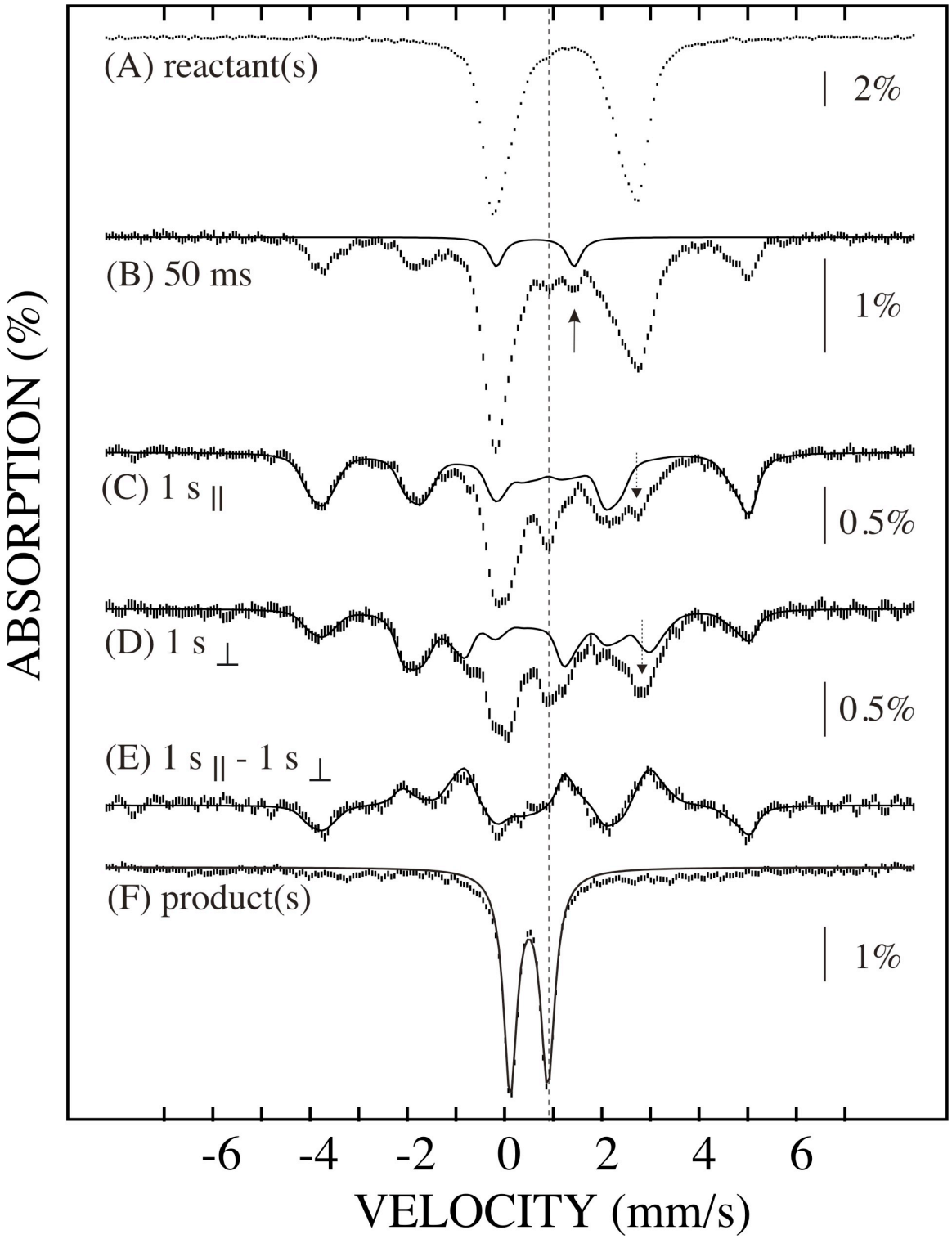
(A) reactant(s)
2%
(B) 50 ms
1%
(C) 1 s ||
0.5%
(D) 1 s ⊥
0.5%
(E) 1 s || - 1 s ⊥
(F) product(s)
1%
ABSORPTION (%)
-6
-4
-2
0
2
4
6
VELOCITY (mm/s)

Table 6-1: Mössbauer parameters for the detected diiron species in the reaction of $R2_{Ct}$-wt.

Diiron Species	Fe site	δ (mm/s)	ΔE_Q (mm/s)	A_x, A_y, A_z (MHz)	line-width (mm/s)	η
P		0.63	1.60		$\gamma_L = 0.35$ $\gamma_R = 0.35$	
X	Fe(III) Fe(IV)	0.56 0.20	-0.90 -0.60	-541, -527, -535 200, 260, 260	0.35 0.35	0.50 0.50
diferric		0.50	0.77		$\gamma_L = 0.34$ $\gamma_R = 0.35$	

of the spectral contributions from the identified species (Fe(II) species, $\mathbf{X}_{Ct}$, and product(s)), it can be seen that additional features comprising a quadrupole doublet (spectrum B, solid line) best fit by the parameters $\delta = 0.63$ mm/s and $\Delta E_Q = 1.60$ mm/s are present at this early reaction time. This doublet contributes 6.0% of the total iron absorption in spectrum A, which corresponds to 0.17 equiv of Fe or 0.09 equiv of a diiron complex. The δ and ΔE_Q deduced are strikingly similar to those associated with the μ-1,2-peroxodiiron(III) intermediate in the *E. coli* R2-D84E variant (*36*) and H_{peroxo} in MMOH (*37*). The indication of a peroxodiiron(III) species in the reaction of Fe(II)-$R2_{Ct}$-wt by Mössbauer spectroscopy but not by stopped-flow absorption spectroscopy (Figure 6-3) is attributed to variations in the experimental conditions, such as protein concentration, oxygen concentration, and presence/absence of glycerol (legends to Figures 6-3 and 6-10). The presence of glycerol has been demonstrated to promote the accumulation of a μ-1,2-peroxodiiron(III) intermediate in the reaction of R2-wt from mouse (*38*). The enhancement in the level of accumulation of this species is ascribed to a decrease in the anticooperativity in Fe(II) binding between the protomers of the mouse R2 homodimer, a phenomenon that has been demonstrated for *E. coli* R2 by Hendrich and co-workers (*39*). These authors showed that glycerol can relieve the anticooperativity in Fe(II) binding that otherwise disfavors binding of metal ions by both protomers. Replication of experimental conditions described in the legend to Figure 6-10 in stopped-flow experiments to test for development of the the 700-nm absorption of the μ-1,2-peroxodiiron(III) is in progress.

The spectrum of the reactant (Figure 6-10, spectrum A) exhibits a very large line-width (~ 0.6 mm/s at 4.2 K), which probably suggests either that the diferrous species has

inequivalent and partially resolved (by Mösssbauer) iron sites or that the reactant solution is heterogeneous. For example, both free and bound Fe(II) may be present, and these species may have different Mössbauer signatures.

The spectrum of the diferric product is best fit by one quadrupole doublet (δ = 0.50 mm/s and ΔE_Q = 0.77 mm/s) (Table 6-1) corresponding to 70 ± 5 % of the total Fe absorption (solid line above the data in Figure 6-10, spectrum **F**). These parameters are consistent with the presence of high-spin ferric ions and are similar to those reported for other diiron proteins such as MMOH. The estimated ΔE_Q value is significantly smaller than those reported for the oxo-bridged diiron(III) clusters of the *E. coli* and mouse R2 proteins. The Mössbauer parameters, combined with the observation that the product of the O_2 activation reaction by $R2_{Ct}$ does not exhibit the 325 and 365 nm features characteristic of μ-oxodiiron(III) clusters, are consistent with the absence of an oxo-bridge deduced by crystallography (Figure 6-2) (*40*).

Effect of the Y338F Substitution on the Mechanism of O_2 Activation by $R2_{Ct}$ as Monitored by Stopped-Flow Absorption Spectroscopy. Mixing at 5 °C of pre-formed Fe(II)-$R2_{Ct}$-Y338F with O_2 results in the rapid development of the same transient features observed in the $R2_{Ct}$-wt reaction, the 411-nm peak and the 360 nm shoulder. Interestingly, the amplitude (A_{max} - $A_{completion}$) of the 411-nm transient is ~ 2.5-fold greater in the reaction of the variant, and the feature decays approximately 4-fold less rapidly than that in the reaction of Fe(II)-$R2_{Ct}$-wt in the presence of limiting Fe(II) (compare black traces in Figures 6-7A and 6-11A). Additionally, the introduction of excess Fe(II) to this reaction does not reduce the maximum amplitude of the transient Y• with the same efficiency as it does in the reaction of $R2_{Ct}$-wt with O_2, although it imposes a similar

Figure 6-11: The dependence of the amplitude of the transient absorbances at (A) A_{411} - (A_{405} + A_{417})/2 and (B) 360 nm on the ratio Fe(II)/R2 in the reaction of $R2_{Ct}$-Y338F. Apo $R2_{Ct}$-Y338F was mixed in the absence of O_2 with Fe(II) in a molar ratio of 2.0 (red trace), 3.0 (black trace), or 4.0 (blue trace). This solution was mixed in the stopped-flow apparatus at 5 °C in a 1:1 volume ratio with buffer B (with 10 % (v/v) glycerol), which had been saturated at 5 °C with O_2. The final concentration of $R2_{Ct}$-Y338F after mixing in the stopped-flow was 0.1 mM. The initial Fe content was 0.4/dimer as determined by the ferrozine colormetric assay.

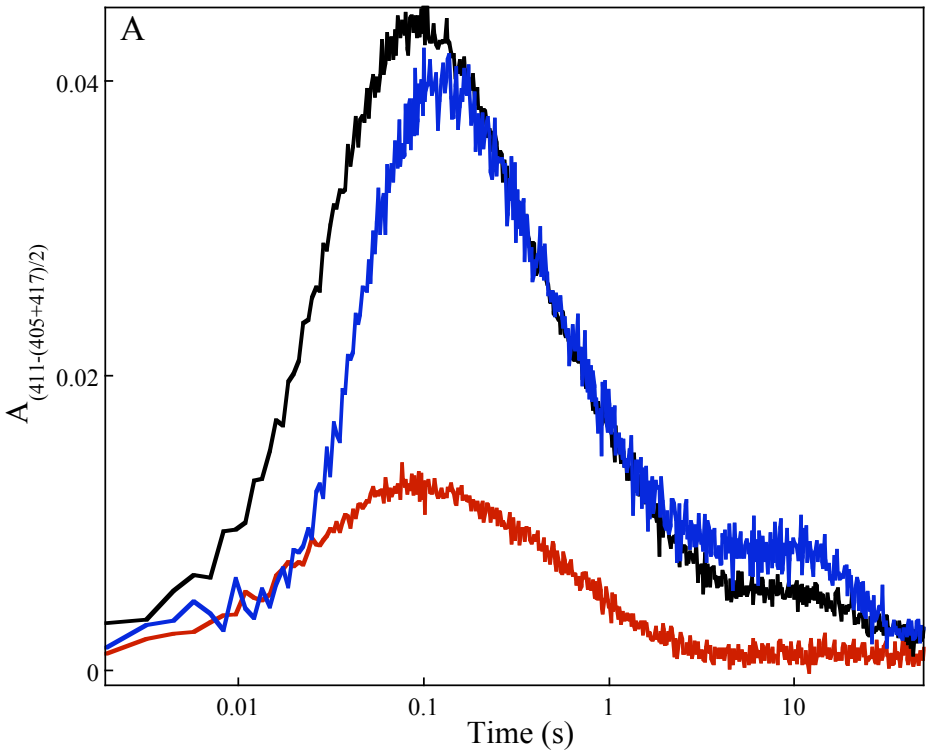
A
0.04
0.02
0
A(411-(405+417)/2)
0.01
0.1
1
10
Time (s)

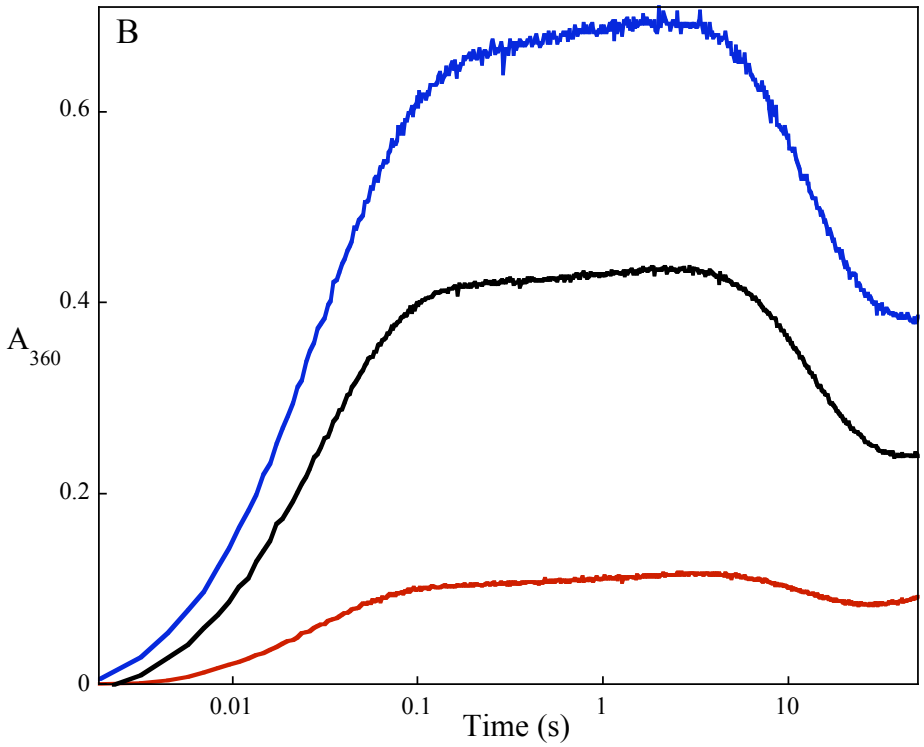
B
0.6
0.4
0.2
0
A360
0.01
0.1
1
10
Time (s)

kinetic effect on the Y• (appearance of a lag phase indicative of the reaction of a fraction of the Y• with the free Fe(II)) (compare blue traces in Figures 6-7A and 6-11A).

Interestingly, excess Fe(II) does not diminish the amplitude of the 360-nm feature, as previously observed in the reaction of $R2_{Ct}$-wt (compare blue traces in Figures 6-7B and 6-11B); on the contrary, the amplitude is greater with excess Fe(II) (compare blue and black traces in Figure 6-11B). The increase in the 360 nm amplitude is reminiscent of that previously observed in the reaction of $R2_{Ct}$-wt with O_2 in the presence of ascorbate (Figure 6-6B, purple trace). As mentioned previously, these experiments will be repeated at higher temperatures at which the Fe(II)-$R2_{Ct}$-Y338F protein is entirely soluble to confirm the results obtained.

The $[A_{411} - (A_{405} + A_{417})/2]$-versus-time traces at different Fe(II) concentrations reveal the slow formation of another transient Y• species which maximizes at ~ 11 s and forms to a larger extent at higher Fe(II) concentrations (Figure 6-11A). The formation of this species, which is not as apparent in the reaction of $R2_{Ct}$-wt with O_2 at any Fe(II) concentration, seems to be kinetically associated with the decay of cluster $\mathbf{X_{Ct}}$, which might suggest that its formation results from the reduction of $\mathbf{X_{Ct}}$ by a tyrosine residue. Whether this species is or is not on the pathway to product formation in the reaction of $R2_{Ct}$-wt is not clear and requires further examination.

DISCUSSION

In the *E. coli* R2 reaction, the oxidation state of **X** and the fact that its formation precedes that of Y122• imply that an "extra" electron, which is required to balance the four electron reduction of O_2 with the 3 electrons obtained by conversion of the

diiron(II)-Y122 reactant to the diiron(III)-Y122• product, is transferred to the cluster during formation of **X**. Detailed work from our laboratory showed that this electron is shuttled by the near-surface residue, W48, which is connected to the buried diiron cluster by a hydrogen-bond chain involving the second-sphere residue D237 and the Fe1 ligand H118, to the $(Fe_2O_2)^{4+}$ adduct "**L**," which forms when O_2 adds to the diiron(II) cluster. Reduction of **L** by W48 produces the di-radical intermediate, **X**-$W48^{+\bullet}$. Thus, W48 functions to split the two oxidizing equivalents of "**L**" by shuttling one equivalent to the surface of the protein ($W48^{+\bullet}$), where it can be efficiently quenched by an exogenous reductant. The second equivalent is retained on the buried diiron cluster (**X**) for conversion of Y122 to the radical (*27, 32*).

In this study, examination of O_2 activation at the diiron(II) cluster of the wild-type *C. trachomatis* R2 by stopped flow absorption spectroscopy and rapid freeze-quench EPR and Mössbauer spectroscopies has confirmed the formation of $\mathbf{X_{Ct}}$ prior to formation of the *bis*-(μ-hydroxo)diiron(III) product. Formation of a one-electron oxidized intermediate requires, as in the case of *E. coli* R2, the reduction of the diiron(II)-O_2 adduct by one electron. The concomitant formation of a Y• species during O_2 activation, as shown by stopped-flow and EPR spectroscopies, and the clear temporal correlation between the formation of these two radical species suggest a situation analogous to that of the formation of the **X**-$W48^{+\bullet}$ di-radical intermediate in the reaction of *E. coli* R2, only in this case the di-radical intermediate is $\mathbf{X_{Ct}}$-Y•. Formation of both $\mathbf{X_{Ct}}$ (as monitored at 360 nm) and the Y• (as monitored by the sharp 411 nm peak) is kinetically first-order in O_2, implying that precursors to the $\mathbf{X_{Ct}}$-Y• state do not accumulate significantly under these conditions. Thus, it seems that a $W51^{+\bullet}$ is not observed prior to or in equilibrium

with the transient Y•, as might have been anticipated from our work on *E. coli* R2. This does not necessarily imply that a $W51^{+\bullet}$ does not form; it may simply not accumulate due to unfavorable kinetics or an unfavorable equilibrium with the Y•. The sub-stoichiometry of the Y•, as calculated from subtraction analysis of the EPR spectra, may be due to the facts that (1) any unbound Fe(II) present in the reactant solution would have efficiently reduced a fraction of the Y• initially generated and (2) even in the absence of reductant, the Y• decays on a timescale (5 s^{-1}) that is significant relative to its formation (~ 40 s^{-1} at this [O_2]), whereas decay of $\mathbf{X_{Ct}}$ is slow enough (0.2 s^{-1}) not to compete well with its formation. Thus, a reducible (and, therefore, probably solvent-accessible) Y• is generated to provide the extra electron needed for formation of $\mathbf{X_{Ct}}$, in analogy to oxidation of W48 for this purpose in the *E. coli* R2 reaction.

We have shown in Chapter 4 of this thesis the cation-mediated propagation of the radical from W48 to the C-terminal residue, Y356, in the *E. coli* R2 reaction, resulting in a Y356• species in equilibrium with $W48^{+\bullet}$. Based on this observation, we suspected that the transient radical in $R2_{Ct}$-wt might be Y338•, the cognate of Y356•. This tentative assignment would imply that Mg^{2+} is not required to mediate communication between Y338 and W51, or that Y338 is, in contrast to what happens in the *E. coli* R2 reaction, oxidized in preference to the tryptophan. If the assignment were correct, substitution of Y338 with F would be expected to prevent or delay transient Y• formation and allow for the accumulation of an alternative oxidized species, the most obvious possibilities being a $W51^{+\bullet}$ and an $(Fe_2O_2)^{4+}$-precursor to $\mathbf{X_{Ct}}$. Instead, the transient Y• still forms with similar kinetics, implying that a tyrosine residue other than Y338 is oxidized to effect electron injection in the $R2_{Ct}$-wt reaction. The greater accumulation of this radical

species in the $R2_{Ct}$-Y338F reaction in the presence of limiting Fe(II) and its inefficient reduction in the presence of excess Fe(II), as judged by the optical absorption spectroscopy, suggest that the radical residing on this unidentified tyrosine residue and Y338 communicate and that Y338 plays a role in the mediation of electron transfer from free Fe(II) to the Y•.

Alignment of the sequences of $R2_{Ct}$ with those of R2 proteins from other organisms reveals six tyrosines that are strictly conserved in the R2 proteins of organisms that contain only class Ic RNR. Examination of the crystal structure of the R2 subunit from *C. trachomatis* shows that, of these tyrosines, Y112 is closest to the diiron center (7.2 Å from the closest iron ion, Fe2; Figure 6-2). The cognate position is a phenylalanine in human and mouse R2s and a tryptophan in *E. coli* R2. Several observations implicate Y112 as the best candidate for the Y•-forming tyrosine residue. First, evidence (albeit not definitive) has been presented for inefficient oxidation of the corresponding residue, W107, in the reaction of the Y122F variant of *E. coli* R2 (*41*). Better evidence for oxidation of Y107 in the W107Y/Y122F double variant has also been presented (*42*). Thus, although electron injection in the reaction of *E. coli* R2 appears to occur efficiently only to Fe1 via the network of hydrogen-bonded residues that includes the near-surface residue W48, the second-sphere D237, and the H118 ligand to Fe1, inefficient Fe2-side electron transfer appears to be possible. Second, interesting additional structural differences between the *E. coli* and *C. trachomatis* R2 proteins suggest that the latter may be remodeled specifically to promote Fe2-side electron transfer. Fe2 ligand H230 of $R2_{Ct}$, the cognate of H241 of the *E. coli* protein, hydrogen bonds to Glu residue 119, the cognate of the *neutral* S114 of *E. coli* R2, which hydrogen

bonds to H241. Glu119 hydrogen-bonds with a water molecule, which hydrogen-bonds with Y112. Thus, the second- and third-sphere residues projecting out from Fe2 in $R2_{Ct}$ are reminiscent of the ET-mediating, Fe1-side H118-D237-W48 chain in the *E. coli* protein and differ from those on the Fe2 side of the *E. coli* protein in a manner that is consistent with a remodeled electron transfer pathway. Third, Fe1 ligand D84 of *E. coli* R2 is conservatively replaced by *E* in the class Ic R2 proteins. This change could deactivate the Fe1-side pathway, which otherwise would appear to be conserved in $R2_{Ct}$ (H123-D226-W51). On the basis of this analysis, we tentatively propose that *C. trachomatis* R2 and the other class Ic R2 proteins have been remodeled by evolution to employ an Fe2-side specific electron transfer pathway. This would represent a remarkable diversion for the class Ic R2s from the mechanism of oxygen activation and electron transfer employed by the class Ia R2 proteins.

This study is the first step toward a detailed understanding of O_2 activation by $R2_{Ct}$. Further experiments are required to address the outstanding compelling questions, such as the role of W51 and the importance of the presence in class Ic R2 of E at the position corresponding to Fe1 ligand D84 in *E. coli* R2. Nevertheless, the formation of the $\mathbf{X_{Ct}}$-Y• di-radical intermediate on the pathway to the *bis*-(μ-hydroxo)diiron(III) product in O_2 activation by the R2 subunit from *C. trachomatis* indicates that variations from the *modus operandi* of the better-studied class Ia R2 proteins may be profound. These variations are virtually certain to be important in control of R1 radical formation during nucleotide reduction, which has been proposed to be coupled directly to O_2 activation in the class Ic RNRs.

REFERENCES

1. Stubbe, J. (1991) *Current Opinion in Structural Biology 1*, 788-795.
2. Fontecave, M., Nordlund, P., Eklund, H., and Reichard, P. (1992) The redox centers of ribonucleotide reductase of *Escherichia coli*., *Advances in Enzymology and Related Areas of Molecular Biology 65*, 147-183.
3. Reichard, P. (1993) From RNA to DNA, why so many ribonucleotide reductases?, *Science 260*, 1773-1776.
4. Sjöberg, B.-M. (1994) The ribonucleotide reductase jigsaw puzzle: a large piece fits into place, *Structure 2*, 793-796.
5. Jordan, A., and Reichard, P. (1998) Ribonucleotide reductases, *Annu. Rev. Biochem. 67*, 71-98.
6. Stubbe, J. (1990) Ribonucleotide reductases., *Adv. Enzymol. Relat. Areas Mol. Biol. 63*, 349-419.
7. Stubbe, J., and Ackles, D. (1980) On the mechanism of ribonucleotide diphosphate reductase from *Escherichia coli*, *J. Biol. Chem. 255*, 8027-8030.
8. Stubbe, J., Ackles, D., Segal, R., and Blakley, R. L. (1981) On the mechanism of ribonucleoside triphosphate reductase from *Lactobacillus leichmannii*. Evidence for 3' carbon-hydrogen bond cleavage, *J. Biol. Chem. 256*, 4843-4846.
9. Eklund, H., Uhlin, U., Farnegardh, M., Logan, D. T., and Nordlund, P. (2001) Structure and function of the radical enzyme ribonucleotide reductase, *Prog. Biophys. Mol. Biol. 77*, 177-268.
10. Thelander, L., and Reichard, P. (1979) Reduction of ribonucleotides, *Annu. Rev. Biochem. 48*, 133-158.

11. Zhou, B. B., and Elledge, S. J. (2000) The DNA damage response: putting checkpoints in perspective, *Nature 408*, 433-439.

12. Stubbe, J., and Riggs-Gelasco, P. (1998) Harnessing free radicals: formation and function of the tyrosyl radical in ribonucleotide reductase, *Trends Biochem. Sci. 23*, 438-443.

13. Stubbe, J., Nocera, D. G., Yee, C. S., and Chang, M. C. Y. (2003) Radical initiation in the class I ribonucleotide reductase: long-range proton-coupled electron transfer?, *Chem. Rev. 103*, 2167-2202.

14. Sahlin, M., and Sjöberg, B.-M. (2000) Ribonucleotide reductase. A virtual playground for electron transfer reactions, *Subcell. Biochem. 35*, 405-443.

15. Uhlin, U., and Eklund, H. (1994) Structure of ribonucleotide reductase protein R1, *Nature 370*, 533-539.

16. Högbom, M., Stenmark, P., Voevodskaya, N., McClarty, G., Gräslund, A., and Nordlund, P. (2004) The radical site in Chlamydial ribonucleotide reductase defines a new R2 subclass, *Science 305*, 245-248.

17. Roshick, C., Iliffe-Lee, E. R., and McClarty, G. (2000) Cloning and characterization of ribonucleotide reductase from *Chlamydia trachomatis*, *J. Biol. Chem. 275*, 38111-38119.

18. McClarty, G., and Tipples, G. (1991) *In situ* studies on incorporation of nucleic acid precursors into *Chlamydia trachomatis* DNA, *J. Bacteriol. 173*, 4922-4931.

19. Tipples, G., and McClarty, G. (1993) The obligate intracellular bacterium *Chlamydia trachomatis* is auxotrophic for three of the four ribonucleoside triphosphates, *Molec. Microbiol. 8*, 1105-1114.

20. Henriksen, M. A., Cooperman, B. S., Salem, J. S., Li, L.-S., and Rubin, H. (1994) The stable tyrosyl radical in mouse ribonucleotide reductase is not essential for enzymic activity, *J. Am. Chem. Soc. 116*, 9773-9774.

21. Massey, V. (1957) Studies on succinic dehydrogenase. VII. Valency state of the iron in beef heart succinic dehydrogenase., *J. Biol. Chem. 229*, 763-770.

22. Salowe, S. P., Ator, M. A., and Stubbe, J. (1987) Products of the inactivation of ribonucleoside diphosphate reductase from *Escherichia coli* with 2'-azido-2'-deoxyuridine 5'-diphosphate, *Biochemistry 26*, 3408-3416.

23. Gill, S. C., and von Hippel, P. H. (1989) Calculation of protein extinction coefficients from amino acid sequence data, *Anal. Biochem. 182*, 319-326.

24. Parkin, S. E., Chen, S., Ley, B. A., Mangravite, L., Edmondson, D. E., Huynh, B. H., and Bollinger, J. M., Jr. (1998) Electron injection through a specific pathway determines the outcome of oxygen activation at the diiron cluster in the F208Y mutant of *Escherichia coli* ribonucleotide reductase protein R2, *Biochemistry 37*, 1124-1130.

25. Bollinger, J. M., Jr., Tong, W. H., Ravi, N., Huynh, B. H., Edmondson, D. E., and Stubbe, J. (1994) Mechanism of assembly of the tyrosyl-diiron(III) cofactor of E. coli ribonucleotide reductase. 2. Kinetics of the excess Fe^{2+} reaction by optical, EPR, and Mössbauer spectroscopies, *J. Am. Chem. Soc. 116*, 8015-8023.

26. Ravi, N., Bollinger, J. M., Jr., Huynh, B. H., Edmondson, D. E., and Stubbe, J. (1994) Mechanism of assembly of the tyrosyl radical-diiron(III) cofactor of *E. coli* ribonucleotide reductase: 1. Mössbauer characterization of the diferric radical precursor., *J. Am. Chem. Soc. 116*, 8007-8014.

27. Krebs, C., Chen, S., Baldwin, J., Ley, B. A., Patel, U., Edmondson, D. E., Huynh, B. H., and Bollinger, J. M., Jr. (2000) Mechanism of rapid electron transfer during oxygen activation in the R2 subunit of *Escherichia coli* ribonucleotide reductase. 2. Evidence for and consequences of blocked electron transfer in the W48F variant, *J. Am. Chem. Soc. 122*, 12207-12219.

28. Yun, D., Krebs, C., Gupta, G. P., Iwig, D. F., Huynh, B. H., and Bollinger, J. M., Jr. (2002) Facile electron transfer during formation of cluster **X** and kinetic competence of **X** for tyrosyl radical production in protein R2 of ribonucleotide reductase from mouse, *Biochemistry 41*, 981-990.

29. Bollinger, J. M., Jr., Edmondson, D. E., Huynh, B. H., Filley, J., Norton, J. R., and Stubbe, J. (1991) Mechanism of assembly of the tyrosyl radical-dinuclear iron cluster cofactor of ribonucleotide reductase, *Science 253*, 292-298.

30. Sjöberg, B.-M., Reichard, P., Gräslund, A., and Ehrenberg, A. (1977) Nature of the free radical in ribonucleotide reductase from *Escherichia coli*., *J. Biol. Chem. 252*, 536-541.

31. Larsson, A., Karlsson, M., Sahlin, M., and Sjöberg, B.-M. (1988) Radical formation in the dimeric small subunit of ribonucleotide reductase requires only one tyrosine 122, *J. Biol. Chem. 263*, 17780-17784.

32. Baldwin, J., Krebs, C., Ley, B. A., Edmondson, D. E., Huynh, B. H., and Bollinger, J. M., Jr. (2000) Mechanism of rapid electron transfer during oxygen activation in the R2 subunit of *Escherichia coli* ribonucleotide reductase. 1. Evidence for a transient tryptophan radical, *J. Am. Chem. Soc. 122*, 12195-12206.

33. Bollinger, J. M., Jr., Chen, S., Parkin, S. E., Mangravite, L. M., Ley, B. A., Edmondson, D. E., and Huynh, B. H. (1997) Differential iron(II) affinity of the sites of the diiron cluster in R2 of *Escherichia coli* ribonucleotide reductase: tracking the individual sites through the O_2 activation sequence, *J. Am. Chem. Soc. 119*, 5976-5977.

34. Bollinger, J. M., Jr., Stubbe, J., Huynh, B. H., and Edmondson, D. E. (1991) Novel diferric radical intermediate responsible for tyrosyl radical formation in assembly of the cofactor of ribonucleotide reductase, *J. Am. Chem. Soc. 113*, 6289-6291.

35. Sturgeon, B. E., Burdi, D., Chen, S., Huynh, B. H., Edmondson, D. E., Stubbe, J., and Hoffman, B. M. (1996) Reconsideration of **X**, the diiron intermediate formed during cofactor assembly in *E. coli* ribonucleotide reductase, *J. Am. Chem. Soc. 118*, 7551-7557.

36. Bollinger, J. M., Jr., Krebs, C., Vicol, A., Chen, S., Ley, B. A., Edmondson, D. E., and Huynh, B. H. (1998) Engineering the diiron site of *Escherichia coli* ribonucleotide reductase protein R2 to accumulate an intermediate similar to Hperoxo, the putative peroxodiiron(III) complex from the methane monooxygenase catalytic cycle, *J. Am. Chem. Soc. 120*, 1094-1095.

37. Liu, K. E., Wang, D., Huynh, B. H., Edmondson, D. E., Salifoglou, A., and Lippard, S. J. (1994) Spectroscopic detection of intermediates in the reaction of dioxygen with the reduced methane monooxygenase/hydroxylase from *Methylococcus capsulatus* (Bath), *J. Am. Chem. Soc. 116*, 7465-7466.

38. Yun, D., García-Serres, R., Chicalese, B. M., An, Y. H., Huynh, B. H., and J. Martin Bollinger, J. (2005) A peroxodiiron(III) precursor to cluster **X** in assembly of the iron-radical cofactor of ribonucleotide reductase from mouse, manuscript in preparation.

39. Pierce, B. S., Elgren, T. E., and Hendrich, M. P. (2003) Mechanistic implications for the formation of the diiron cluster in ribonucleotide reductase by quantitative EPR spectroscopy, *J. Am. Chem. Soc. 125*, 8748-8759.

40. Kurtz, D. M. (1990) Oxo and hydroxo bridged diiron complexes: a chemical perspective on a biological unit., *Chemical Reviews 90*, 585-606.

41. Sahlin, M., Lassmann, G., Pötsch, S., Sjöberg, B.-M., and Gräslund, A. (1995) Transient free radicals in iron/oxygen reconstitution of mutant protein R2 Y122F. Possible participants in electron transfer chains in ribonucleotide reductase, *J. Biol. Chem. 270*, 12361-12372.

42. Katterle, B., Sahlin, M., Schmidt, P. P., Pötsch, S., Logan, D. T., Gräslund, A., and Sjöberg, B.-M. (1997) Kinetics of transient radicals in *Escherichia coli* ribonucleotide reductase. Formation of a new tyrosyl radical in mutant protein R2, *J. Biol. Chem. 272*, 10414-10421.

LANA SALEH

EDUCATION

1999-2005 The Pennsylvania State University
Ph.D. in Biochemistry, Molecular Biology, and Microbiology
Advisor: Joseph Martin Bollinger, Jr.
Thesis Title: Oxygen Activation and Electron Transfer in Class I Ribonucleotide Reductase.

1997-1999 The Youngstown State University
M.S. in Chemistry
Advisor: Jeffrey A. Smiley
Thesis Title: Orotidine 5'-Monophosphate Decarboxylase: Purification and Spectral Studies.

1993-1997 The American University of Beirut
B.S. in Chemistry

SELECTED PUBLICATIONS

1. **Saleh, L.**; Bollinger, J. M., Jr. (2005) Cation Mediation of Radical Transf between Trp48 and Tyr356 during O_2 Activation by Protein R2 of *Escherichia c* Ribonucleotide Reductase: Relevance to R1-R2 Radical Transfer in Nucleoti Reduction?, submitted.

2. Krebs, C.; Price, J. C.; Baldwin, J.; **Saleh, L.**; Green, M. T.; Bollinger, J. M., . (2005) Rapid Freeze-Quench ^{57}Fe Mössbauer Spectroscopy: Monitoring Changes an Iron-Containing Active Site during a Biochemical Reaction *Inorganic Chemistr* **44**, 742-747.

3. Skulan, A. J.; Brunold, T. C.; Baldwin, J.; **Saleh, L.**; Bollinger, J. M., J Solomon, E. I. (2004) Nature of the Peroxo Intermediate of the W48F/D84 Ribonucleotide Reductase Variant: Implications for O_2 Activation by Binuclear No Heme Iron Enzymes, *J. Am. Chem. Soc*., **126**, 8842-8855.

4. **Saleh, L.**; Kelch, B. A.; Pathickal, B. A.; Baldwin, J.; Bollinger, J. M., Jr. (200 Mediation by Indole Analogues of Electron Transfer during Oxygen Activation Variants of Protein R2 of *Escherichia coli* Ribonucleotide Reductase Lacking t Electron-Shuttling Tryptophan, *Biochemistry*, **48**, 5953-5964.

5. **Saleh, L.**; Krebs, C.; Ley, B. A; Naik, S., Huynh, B. H.; Bollinger, J. M., . (2004) Use of a Chemical Trigger for Electron Transfer to Elucidate the Nature the Precursor to Cluster **X** in Assembly of the Iron-Radical Cofactor of *Escherich coli* Ribonucleotide Reductase, *Biochemistry*, **48**, 5965-5975.

6. Wei, P.P.; Skulan, A. J.; Mitic, N.; Yang, Y. S.; **Saleh, L.**; Bollinger, J. M., J Solomon, E. I. (2004) Electronic and Spectroscopic Studies of the Non-Her Reduced Binuclear Iron Sites of Two Ribonucleotide Reductase Varian Comparison to Reduced Methane Monooxygenase and Contributions to Reactivity, *J. Am. Chem. Soc*, **126**, 3777-3788.

7. Voegtli, W. C.; Sommerhalter, M; **Saleh, L.**; Baldwin, J; Bollinger, J. M., J Rosenzweig, A. C. (2003) Variable Coordination Geometries at the Diiron(II) Acti Site of Ribonucleotide Reductase R2, *J. Am. Chem. Soc*., **125**, 15822-15830.

8. Mitic, N.; **Saleh, L.**; Schenk, G.; Bollinger, J. M., Jr.; Solomon, E. I. (200 Rapid-Freeze-Quench Magnetic Circular Dichroism of Intermediate **X** Ribonucleotide Reductase: New Structural Insight, *J. Am. Chem. Soc*., **125**, 1120 11201.

HONORS

Alumni Association Dissertation Award 2004
Dr. Eugene D. Scudder Graduate Student Teaching Award 1998
The American University of Beirut Scholarship 1995-1997
The United Nations Scholarship 1993-1997